NASA CONTRACTOR REPORT

NASA CR-2553

FLEXIBLE ROTOR BALANCING BY THE INFLUENCE COEFFICIENT METHOD - MULTIPLE CRITICAL SPEEDS WITH RIGID OR FLEXIBLE SUPPORTS

Juergen M. Tessarzik

Prepared by
MECHANICAL TECHNOLOGY INCORPORATED
Latham, N.Y. 12110
for Lewis Research Center

NATIONAL AERONAUTICS AND SPACE ADMINISTRATION • WASHINGTON, D.C. • AUGUST 1975

1. Report No. NASA CR-2553	2. Government Accession No.	3. Recipient's Catalog No.
4. Title and Subtitle FLEXIBLE ROTOR BALANCING BY THE INFLUENCE COEFFICIENT METHOD - MULTIPLE CRITICAL SPEEDS WITH RIGID OR FLEXIBLE SUPPORTS		5. Report Date AUGUST 1975 6. Performing Organization Code
7. Author(s) Juergen M. Tessarzik		8. Performing Organization Report No. MTI-75TR3 10. Work Unit No.
9. Performing Organization Name and Address Mechanical Technology Incorporated 968 Albany-Shaker Road Latham, New York 12110		11. Contract or Grant No. NAS 3-14420 13. Type of Report and Period Covered Contractor Report
12. Sponsoring Agency Name and Address National Aeronautics and Space Administration Washington, D.C. 20546		14. Sponsoring Agency Code

15. Supplementary Notes
Final Report. Project Manager, David P. Fleming, Fluid System Components Division, NASA Lewis Research Center, Cleveland, Ohio

16. Abstract

Experimental tests were conducted to further demonstrate the ability of the influence coefficient method to achieve precise balance of flexible rotors of virtually any design for operation through virtually any speed range. Four distinct practical aspects of flexible-rotor balancing were investigated in the present work:

1. Balancing for operation through multiple bending critical speeds
2. Balancing of rotors mounted in both rigid and flexible bearing supports, the latter having significantly different stiffnesses in the horizontal and vertical directions so as to cause severe ellipticity in the vibration orbits
3. Balancing of rotors with various amounts of measured vibration response information (e.g., numbers of vibration data sets and numbers and types of vibration sensors) and with different numbers of correction planes
4. Balancing of rotors with different (though arbitrary) initial unbalance configurations

Tests were made on a laboratory quality machine having a 122 cm (48 in.) long rotor weighing 50 kg (110 lb) and covering a speed range up to 18 000 rpm. The balancing method was in every instance effective, practical, and economical and permitted safe rotor operation over the full speed range covering four rotor bending critical speeds. Improved correction weight removal methods for rotor balancing were investigated. Material removal from a rotating disk was demonstrated through application of a commercially available laser.

17. Key Words (Suggested by Author(s))	18. Distribution Statement
Flexible rotor balancing experiments Multiple bending critical speeds Computer methods Rotor balancing corrections with laser	Unclassified - unlimited

19. Security Classif. (of this report)	20. Security Classif. (of this page)	21. No. of Pages	22. Price*
Unclassified	Unclassified	129	$5.75

* For sale by the National Technical Information Service, Springfield, Virginia 22151

TABLE OF CONTENTS

TABLE OF CONTENTS (concluded)

SUMMARY

The current test program successfully extended the proven balancing capability of the Influence Coefficient Method to include four rotor system bending critical speeds in the operating speed range. Additional program accomplishments included verification of the balancing method on a rotor displaying noncircular orbits (due to dissimilar bearing support stiffnesses) and a rotor burdened with different initial unbalance distributions. Further, the efficiency of the balancing method with varying amounts of measured rotor response data was also evaluated. This was accomplished through the use of different numbers of displacement sensors located along the length of the rotor. The capability of the method to balance a flexible rotor using data obtained from accelerometers only, located on the bearing support housings, was also investigated (rigid bearing supports only).

The test rotor was 122 cm (48 in.) long and weighed 50 kg (110 lb). It carried five discs, and was deliberately designed to accentuate the bending mode shape as it occurred at the fourth critical speed. The rotor was operated at speeds up to 18,000 rpm. The first system bending critical speed occurred at 4,360 rpm and the fourth at 10,960 rpm. The bearings were located near the rotor nodal points associated with these critical speeds. Consequently, low bearing damping forces were transmitted to the rotor and substantial rotor orbits were experienced at those critical speeds. Little amplitude buildup was observed at the second and third critical speeds.

For the case where significant unbalances were initially added to the rotor in an in-line, in-phase configuration (single axial plane, weights all on same side of shaft center line) a relationship between the number of displacement sensors used for balancing and the number of trial weight runs could be observed. With seven displacement sensors employed, only three trial weight runs were required for acceptable rotor operation through four bending critical speeds. Reduction in the number of sensors down to two (one sensor located next to each journal bearing) increased the number of required trial weight runs to four, with noticeably poorer end results than were obtained for seven sensors.

Substitution of two accelerometers, located on the journal bearing housings, led to an initial improvement of rotor balance, but only to the point where the bearing forces were reduced below the measurement sensitivity of the accelerometers. This came about through a shift in rotor balance that very nearly aligned the nodal points with the journal bearing centers, thus reducing the forces measured at the accelerometers, but nevertheless increasing rotor deflection amplitudes at nearly all rotor displacement measurement stations. For this case, two accelerometers at these locations are simply inadequate to describe the complete nature of the rotor vibrations.

The introduction of flexible bearing supports with dissimilar stiffnesses in the vertical and horizontal directions produced considerable change in

rotor behavior. The orbits of the unbalanced rotor were predominantly elliptical, with the major axis of the ellipse horizontal. Balancing for passage through the first bending critical speed proved to be much easier than on the rigidly-supported rotor; only a single trial weight run (in four balancing planes) was required. Balancing for passage through the fourth critical speed required one or two more trial weight runs. Experiments further indicated that balancing of the flexibly-supported rotor was slightly more efficient with data obtained from four displacement sensors measuring rotor vertical motion, rather than from four measuring horizontal motion.

The extensive application of the balancing procedure again confirmed the value of such features as computationally-subtracted rotor out-of-roundness at the displacement-measured stations, and the freedom to employ trial weights of different sizes at different angular locations for each of the trial weight planes. The balancing method, as well as the instrumentation developed for its implementation, has now reached a proven level of capability which should recommend it to commercial users.

Through a separate investigation of current laser capabilities in the area of metal removal, the groundwork for further advances in rotor balancing has been laid. It was found that a commercially available laser can remove metal from rotating discs at rates suitable for non-stop balancing of rotors in the weight range typically represented by high-speed rotors. Controlled material removal from a rotating steel disc was demonstrated at various rotor speeds up to 3000 rpm.

INTRODUCTION

The information presented in this report, together with that to be found in earlier references [1-4]*, describes a series of studies designed to probe the capabilities and limits of the Influence Coefficient Method for balancing flexible rotors. The test results, observations, discussions and conclusions are therefore expected to be most useful to the engineer concerned with questions of general applicability of this method to classes of rotor-bearing systems, as opposed to the reader who may wish to obtain a better balance on a specific rotor. The latter individual may wish to refer to one of the application-oriented references [5-11] for more detailed guidance on particular configurations.

There is now in existence a rapidly-expanding body of technical literature describing an immensely successful method for the balancing of flexible rotors. This method, based upon linear influence-coefficient deflection theory, is generally referred to as the Influence Coefficient Method. The theory of this method was presented by Goodman in 1963 [12].

Beginning in 1969 under NASA sponsorship, an adoption of this theory to flexible rotor balancing was examined analytically by Rieger [13] and experimentally by Tessarzik [1, 2]. References [1, 2] described in detail the Exact Point-Speed Procedure, which is computationally the simplest application of the Influence Coefficient Method to flexible rotor balancing. References [1, 2] also presented experimental results where a fluid-film bearing supported rotor was balanced for safe (and slow) passage through the third (first flexural) bending critical speed. An experimental comparison of balancing effectiveness provided by the Exact Point-Speed and the Least Squares Balancing Procedures was made in [3] and [4]. Results of that investigation indicated nearly equal proficiency for both procedures for all test cases. However, testing was limited to rotor balancing through one bending critical speed. If a rotor is to be balanced for passage through more than one bending critical speed, the Least Squares Procedure is preferred because it accepts relatively large amounts of experimentally obtained balancing data. The procedure uses minimization of the squares of the residual amplitudes when the balancing data fed into the program exceeds the square matrix limitation of the basic mass-eccentricity equation used to find the rotor balance correction weights. A square matrix is "full" when e.g., on a rotor equipped with four displacement sensors, four balancing planes are selected for the placement of correction weights and trial weight data is obtained at one rotor speed. If data is to be acquired at more than one rotor speed (as is necessary when balancing for more than one bending critical speed) either the number of correction planes or the number of probes would have to be reduced if the Exact Point-Speed Procedure were to be used. This would constitute a serious obstacle to effective and efficient balancing. A description of the Least Squares Procedure is given by Lund in [14] and [15].

*Numbers in brackets designate References at end of report.

Other applications of the Least Squares Procedure to the balancing of flexible rotors have been reported by Tonnesen [16, 17], Badgley [5-7], Rieger and Badgley [8], and Badgley and Rieger [9]. An application of the procedure to the balancing of gas turbine engine simulator hardware is reported in [10].

The balancing experiments described in this report were set up to give conclusive evidence of the effectiveness of the influence coefficient method under adverse conditions which might be encountered in the balancing of production rotors. Essentially, four distinct aspects of practical flexible-rotor balancing were investigated:

1. Balancing through multiple bending critical speeds.

2. Balancing of rotors in rigid and flexible bearing supports.

3. Balancing of rotors with maximum and minimum trial weight response information, (number of trial weight data sets; displacement and acceleration sensors).

4. Balancing of rotors with different (though arbitrary) initial unbalance configurations.

The computer programs used for the successful balancing of the test rotor described in this report, as well as the analysis upon which the computer programs are based, were written by Dr. Jorgen Lund, consultant to MTI. The laser investigation was carried out by Mark S. Darlow, of MTI.

FLEXIBLE ROTOR BALANCING TEST APPARATUS

The basic mechanical apparatus had originally been designed and built for sensitive rotor unbalance response measurements, and was recently used for flexible rotor balancing experiments (References 1, 2, 3, 4). The rotor that was originally part of this test rig had been designed for operation through three critical speeds, with the first two essentially rigid body criticals. For the experiments described herein, a new rotor with much greater flexibility was designed and built. This rotor has four bending critical speeds within the operating speed limits of the bearing and drive system, with the first critical occurring at about 4400 rpm. The rotor was specifically designed to exhibit pronounced bending at the first and the fourth critical speeds.

Test Rotor Configuration

The test rotor, shown in Figure 1, was nearly 122 cm (48 in.) long and weighed 50 kg (110 lb). The two end discs of 5 kg (11 lb) each, and the largest disc 6.8 kg (15 lb) (second from left in Figure 1) were shrunk onto the shaft. All discs had outside diameters of 151 mm (5.95 in.). The basic journal bearing diameter was 63.5 mm (2.5 in.) and the small-diameter sections on the shaft, which were designed to facilitate rotor bending in the mode shape of the fourth critical speed were 38 mm (1.5 in.).

Each disc was equipped on one face with a row of axial, tapped holes intended for the placement of trial weights and the subsequent addition of correction weights. The tapped holes, 10 degrees apart, were at a 66.7 mm (2.625 in.) radius from the center of the shaft. On their back sides, the three shrunk-on discs contained additional sets of four holes 90 degrees apart for the placement of relatively large unbalance weights. The hole patterns were in line in all five discs.

One of the end discs was equipped on its outer face with a 6.3 mm (0.25 in.) wide reflective foil annulus extending over 180 degrees circumferentially and at a 5 cm (2 in.) radius from the shaft center. The other half of the annulus was painted dull black. The circumferential mid-point position on the reflective strip was the reference point on the rotor from which the angles for maximum dynamic displacement at the other rotor stations were measured (phase angles).

Test Rotor Support Bearings

The test rotor was radially supported by two identical tilting-pad type journal bearings, shown in Figures 2 and 3. The distance between bearings was 783 mm (30.837 in.). Each of the bearings consisted of four radially rigid pads [6]*, with each pad extending over an 80 degree arc and with a pivot position of 44 degrees (55 percent) from the leading edge. The pivot configuration was that of a fixed sphere (integral with the pivot [8]) in

*In this section, numbers in brackets refer to detail part numbers in Figure 2.

contact with a cylindrical surface. The ball-in-cylinder pivot geometry allowed the pad to tilt in both the pitch and roll directions. Thus, it permitted the pads to track both translatory and conical shaft motions. The latter capability is particularly useful in a test machine, because it allows the experimenter greater latitude in setting the maximum permissible orbits without fear of contact between the shaft and the edges of the pads.

Pad length in the axial direction was 63.5 mm (2.5 in.) and the radial clearance between each pad (at the pivot location) and the shaft was 0.062 mm (0.0025 in.). The pads were assembled in the bearing with a preload of 0.3 (the radial pivot clearance was set at 70 percent of the difference between the ground-in radius in the pad and the shaft radius). (Calculated journal bearing fluid-film radial stiffness as a function of rotor speed is presented and discussed below). Horizontal and vertical radial stiffnesses are identical for the bearings, which were oriented in the load-between-pivots configuration.

The lubricating fluid for the journal bearing was Dow Corning 200, with a kinematic viscosity of 0.65 cs at 25°C (77°F). The bearings were operated in a flooded condition with a maximum temperature rise of 5.5°C (10°F).

Axial positioning of the test rotor was provided by two externally-pressurized air-lubricated thrust bearings located on opposing sides of the two smaller rotor center masses. Each thrust bearing consisted of four rigidly mounted pads with an outer diameter of 114 mm (4.5 in.), an inner diameter of 70 mm (2.75 in.) and an angular arc of 60 degrees. The axial clearance in the thrust bearing was approximately 0.25 mm (0.010 in.). Locations of the thrust bearings are indicated in Figure 4, and in Section B-B of Figure 2.

For the flexible rotor balance tests reported herein, two test rotor-bearing support system configurations were used. In its original configuration, the test rotor had a rigid bearing support structure (items 12 and 13 in Figure 2). After modification, the pivot support ring [6] was reduced in diameter by approximately 3 mm (1/8 in.), and held in a concentric position relative to the housing [7] by four axial rods which were anchored in the adjacent seal housings on either side of the bearing support main housing. (See Figure 5). All four of the axial support rods were of rectangular cross-section, with the horizontal dimensions smaller (as seen in the installed position on the test rig) than the vertical dimension. This arrangement resulted in a bearing support stiffness that was lower in the horizontal than in the vertical direction. Consequently, elliptical rotor orbits were observed.

Figure 6 shows a series of rotor orbit photographs at six proximity probe stations along the length of the rotor. These photos were taken at three rotor speeds below the first critical speed, with the initial heavy rotor unbalance arranged in an in-line, alternating-phase configuration. With two of the four unbalance weights moved through 180° in their respective planes, so that the resultant unbalance configuration corresponded to the in-line, in-phase arrangement, rotor orbits were recorded as shown in Figure 7. Comparison of rotor orbit sizes in Figures 6 and 7 indicates a much more pronounced response of the rotor at the first critical speed to

the in-line, in-phase unbalance arrangement than to the in-line, alternating-phase configuration. The latter was specifically selected to produce a severe response of the rotor in the mode of the fourth critical speed.

The stiffness of each bearing support was approximately 3.15 x 10^7 N/m (180,000 lb/in.) in the vertical direction (Y-axis) and approximately 2.62 x 10^7 N/m (150,000 lb/in.) in the horizontal direction (X-axis). The unequal stiffness in the two directions produces rotor orbits (relative to the fixed machine casing) that are elliptical, and causes each critical speed to exhibit separate maximum amplitudes in the vertical and horizontal directions, separated in frequency by the ratio of the square root of their respective stiffnesses (1:1.2). Individual bearing support stiffness (four flexures) had been determined experimentally by monitoring the assembled journal bearing support housing on a vibration table and scanning the vibration input frequency until the vertical and horizontal resonances of the assembly had been found. The stiffnesses of the flexure assemblies in the vertical and horizontal directions were then calculated based upon the respective resonance frequencies and the known mass of the journal bearing support ring.

Mechanical Features of the Apparatus

The test machine (Figures 4 and 8) was mounted on a structural steel base weighing approximately 1455 kg (3200 lb). The base was isolated from the floor by rubber pads. (These details of the base assembly are mentioned here only for reasons of documentation. There is no inherent limitation of the Least Squares Balancing procedure relative to the type of machinery to be balanced.) Bolted to the top plate of the base was an aluminum jig plate [1]* to which were fastened the individual housings [2 and 3] for the journal and thrust bearings, and the proximity probe holders [4] which held capacitance probes [5] used to measure motions of the end masses [6]. Motions of the large center mass [7] were measured with capacitance probes [8] mounted in a guard housing [9]. Additional capacitance probes [10] were located next to each journal bearing and above each of the shaft-integral discs [probes 11 and 12]. Also mounted to the same plate was the electric drive motor [13].

The journal bearing housings [2] were equipped with seal rings [14] on both sides. Each of these rings had a clearance seal adjacent to the bearing housing with an outboard annular scavenging cavity. Outside the scavenging cavity was a labyrinth seal to restrict entry of air into the cavity. Bearing fluid leaking into the cavity was pumped back into the sump by two separate electrically-driven pumps. A positive-displacement pump driven by an air motor forced the bearing fluid through a water-cooled heat exchanger and back into the journal bearing housings. Journal bearing supply pressure was controlled to ensure a flooded condition. Journal bearing temperature was measured by thermocouples welded to the backs of the two lower pads in each bearing.

The drive motor [13] was a 30-hp, 30,000-rpm, 600-Hz, 600-volt electric

*In this section, numbers in brackets refer to detail part numbers in Fig. 4.

motor, powered from a variable-frequency generator set. The test rotor was coupled to the drive motor by a crowned spline coupling [15]. The teeth on the shaft part of the coupling were crowned so that the coupling could accommodate up to 0.76 mm (0.030 in.) radial misalignment between the axes of the motor and the test shaft without shaft restraint.

Instrumentation

The instrumentation required to run the test machine consisted of pressure gages indicating thrust bearing air supply pressure, journal bearing fluid supply pressure, drive motor bearing air-mist lubrication pressure, thermocouples indicating journal bearing pad and bearing fluid temperature, and a speed counter for shaft rotational speed. To assure safe rotor operation under heavy unbalance loads, vertical and horizontal capacitance-type proximity probes (with 2.5 mm (0.10 in.) range) were installed in seven locations along the rotor axis for orbit indications. These orbits were monitored during test runs through oscilloscope observation. The speed counter and capacitance probes were also used to acquire balancing data.

Additional instrumentation required for acquisition of balancing data consisted of two crystal accelerometers mounted on each of the journal bearing housings, and one optical probe for the identification of angular rotor positions (phase angles). The locations of the proximity probes along the rotor axis are shown in Figures 4, 22, and 37, among other figures.

A schematic of the complete data acquisition system as it was used for the flexible rotor balancing tests described in this report is shown in Figure 9.

An overall view of the test rig control hardware and data monitoring and acquisition instrumentation is given in Figure 10. In addition to the magnetic tape system which was used for the plotting of simultaneously-recorded rotor displacement amplitudes from various rotor stations, a paper printout system was used for faster and more accurate displacement probe readouts.

When the test rig was operated with rigid bearing supports, only the vertically-mounted capacitance probes were used for balancing purposes. The selection of the vertical plane instead of the horizontal plane for displacement measurements was an arbitrary decision. Since rotor orbits were generally observed to be circular, no particular significance was attached to this choice. For balancing tests conducted on the test rig with flexible bearing supports, vertical probes alone, horizontal probes alone, and combinations of both were selected as part of the experimental balancing process.

At this time, no fixed rule is available for specifying a priori the required number of measuring stations along the axis of the rotor for balancing by the procedures investigated. In fact, this topic received considerable study in the course of the herein-reported experiments. The maximum number of displacement sensors (capacitance-type probes) that could sensibly be installed on the test rig was seven. However, signals from all seven probe stations were not always used for the acquisition of trial weight data during balancing tests. Only for the first trial weight run in

each series was data from every station recorded so that different combinations of speeds and measuring stations could be selected, as desired, for computations of correction weight values.

An additional signal (commonly referred to as the reference signal) was used to relate a fixed angular position on the rotor (the equivalent of the commonly used 'mark') to the angular position at which maximum dynamic displacement occurred at each of the seven measurement stations for displacement measurements, or the two accelerometers for housing acceleration measurements.

General Analysis of the Rotor-Bearing System

A basic understanding of the dynamic response characteristics of a particular rotor to be balanced can be extremely valuable with respect to selection of both balancing planes and measurement stations. Critical speed calculations, and associated undamped mode shapes, will identify the number of criticals within or close to the operating speed range of the rotor, as well as the degree of "flexibility" of the rotor over the speed range. The mode shape plots can greatly assist in the selection of balance planes, both number and location.

As a matter of practical preparation for the balancing process, the locations of the proximity probes along the rotor axis should be at other than the shaft nodal points as they occur in the vicinity of the balancing speeds. Should the probes be at or near the nodal points, the low amplitude readings obtained may be a source of error in the calculation.

Similar comments apply to the locations selected for balancing planes. Highest balancing effectiveness will in general be obtained through the location of the balancing planes at non-nodal positions along the rotor for the rotor speeds of interest (including the effects of damping). This is because unbalances located at such non-nodal positions are most effective in producing large amplitudes. Quite obviously, the closer the balancing planes are to the most important unbalances, the better will be the result of the balancing procedure.

The following calculations were performed prior to the balancing tests. The first three apply to the test rotor on both types of bearing supports (rigid and flexible). The remaining three (calculated damped rotor amplitudes) apply to either the rigidly or the flexibly-supported rotor, as noted.

1. Journal bearing stiffness as a function of rotational speed for bearing preload factors of 0, 0.3, and 0.5, Figure 11. The test rig bearings were set up with a preload factor of 0.3. Because of bearing symmetry, horizontal and vertical stiffnesses were equal.

2. Rotor critical speeds as functions of bearing stiffness (curves marked 1st lateral, 2nd lateral, 3rd lateral, and 4th lateral, Figure 11). The second and third critical speeds effectively coincide at 5800 rpm.

3. Rotor undamped mode shapes at the calculated critical speeds for various bearing stiffnesses (Figure 12).

4. Damped rotor amplitudes as a function of speed at several stations along the test rotor with in-line, alternating-phase unbalance and rigid rotor bearing supports (Figure 13). The second and third critical speeds are effectively damped out.

5. Damped rotor amplitudes at the first through fourth lateral critical speeds with in-line, alternating-phase unbalance and rigid rotor bearing supports (Figure 14). The calculated rotor mode shapes are generally not planar.

6. Damped rotor amplitudes as a function of speed at several stations with flexibly-supported rotor bearings with in-line, alternating-phase unbalance, (Figure 15).

Sequence of Balancing Runs

The following aspects of flexible rotor balancing were investigated.

1. Multiple bending critical speeds. Balancing of a flexible rotor for safe and slow passage through more than one bending critical speed was the main objective of this investigation. Each balancing series was therefore continued until the initially-heavily-unbalanced rotor had been improved to the point of satisfactory operation through four bending critical speeds.

2. Rigid vs flexible supports. Rotors having both rigid and flexible bearing pedestals were throught to represent widely different applications of the balancing method. Consequently, the main body of experiments was repeated for both rigid and flexible bearing pedestals on the test rig.

3. Number and type of sensors. The quality and quantity of trial weight response information depends upon the number, location and type of sensors employed to record the response of the rotor-bearing system to trial weights during the balancing process. The same sensors are also used to determine the initial rotor condition, (i.e., the rotor response to the unbalance existing prior to balancing), and the rotor condition after balancing.

Information on rotor response can be maximized through installation along the axis of the rotor of many sensors which produce direct displacement readings between the rotor surface and the bearing support housing. Additional force or acceleration sensors which record the effect of the rotor vibrations upon the bearing supports, and thus upon the machine structure, may also be of value. A large number of sensors would be very informative, but would clearly be impractical because of space and cost requirements. On the other hand, the minimum number of sensors that will provide all essential information is difficult to determine beforehand unless computer-implemented response-balancing optimization studies are conducted.

The requirement for verification of satisfactory rotor operation may also have considerable bearing upon the number, type, and location of sensors. It is conceivable, for example, that a flexible rotor can be balanced for minimum bearing forces from information obtained from accelerometers on the bearing pedestal only, but that the same rotor could exhibit excessive

deformation at critical clearance locations (seals, etc). In such a case, displacement sensors in addition to, or instead of, force or acceleration sensors should be selected for the balancing operation. Successful balancing depends as much upon selection of sensor type and balancing criteria as upon the actual balance correction process.

The capability of the Influence Coefficient Balancing Method to balance the test rotor from information supplied by seven, four, and two displacement sensors or two accelerometers has therefore been extensively investigated for one initial unbalance configuration with both the rigid and flexible bearing supports.

4. Initial unbalance configuration. Two distinctly different initial rotor unbalance configurations were used in this balancing experiment. One initial unbalance configuration was designed to excite the first bending critical speed of the rotor (in-line, in-phase unbalance), and the other initial unbalance configuration was intended to produce especially severe rotor deflections at the fourth rotor bending critical speed (in-line, alternating-phase unbalance). Actually, for many rotors, the initial rotor unbalance configurations are of significance only in their relationship to the rotor mode shape of the first bending critical speed, particularly if bearing damping is relatively low for this mode. Once the rotor has been balanced for the first mode, the initial unbalance configuration has been altered significantly and it may no longer be possible to excite a higher critical rotor speed in the manner initially planned. For the test rotor the predominant number of balancing runs were made with the initial in-phase, in-line configuration. (Extensive tests with different initial unbalance configurations for balancing through one bending rotor initial speed were reported in References [1-4]. The initial, intentionally added unbalance to the test rotor was of equal magnitude for all balancing tests. It consisted of four individual unbalances of 26.7 gr-cm (0.371 oz-in.) each, which were positioned in four of the five rotor masses, as indicated in Figures 17, 25 or 39. In these pictures, the indicated angular position of all weights (45^{o}) is representative of the in-line, in-phase unbalance configuration. For the in-line, alternating-phase configuration, the second and fourth weights were moved angularly by 180^{o}. The positioning of the weights for the latter unbalance configuration is schematically indicated in Figures 6, and 13 through 15. However, in Figures 6, 13 and 14 the indicated magnitude of the unbalances is not identical to the unbalance used in the course of the experiments.

The flow chart in Figure 16 provides a guide to the test sequence and the documentation of the results in the form of rotor amplitude plots for the above four factors as they were investigated on the test rotor. Detailed examination of Figure 16 will reveal two additional variables which were not systematically investigated but nevertheless were touched upon in isolated instances. These were (1) number of balancing planes and (2) number of speeds at which data is taken.

The number of balancing or correction planes selected and the number of balancing speeds at which trial weight data is taken, are both discretionary variables for which only the lower limits seem obvious. The number of

balancing planes should, as a minimum, be equal to the number of critical speeds for which a rotor is to be balanced. (It may be advantageous or expeditious to select a larger number of balancing planes, but that depends largely upon the design of the particular rotor under consideration.) The test rotor has been balanced in four planes, with the exception of the very first balancing run (rigid pedestals, in-line, in-phase unbalance and seven displacement sensors), in which five balancing planes were used. Since the balancing process was generally just as successful with the number of balancing planes reduced to four, it was concluded that at least in the case of the test rotor the number of balancing planes need not exceed the number of bending critical speeds for successful balancing. (The question of the number of balancing planes had previously received some attention (e.g., Reference 1, page 24) where the selection of balancing planes at the ends of a rotor section that was very much stiffer than the rest of the rotor (the wide center mass) was not always a desirable choice. That was however a special case and should probably not be compared with rotors which have either a separate disc available for each balancing plane or which are of very nearly constant axial stiffness.)

The second variable involved the number of balancing speeds. There appears to be only one firm requirement for the selection of the number of balancing speeds at which trial weight data is to be taken for a flexible rotor. When balancing above the first bending critical speed, trial weight data taken at or near each of the preceding amplitude peaks associated with a bending critical speed must be included in the correction weight calculation. In the case of the test rotor, trial weight data obtained at the first bending critical speed had to be included in every balancing run that was aimed at reducing rotor amplitudes at the approach to the fourth critical. (The second and third critical speeds could safely be ignored when balancing for the fourth, because they were insufficiently exicted to produce sharp amplitude peaks.) The flow chart (Figure 16), indicates one test case where the result of ignoring the above rule has been investigated (Case 2b). (The rule that trial weight data from lower bending critical speeds exhibiting sharp amplitude peaks has to be included in all correction weight calculations was originally found in a paper study, [Reference 11] where a rotor of uniform cross-section was balanced for passage through multiple bending critical speeds.)

When the Least Squares Balancing Method is used, separate trial weight data runs may be required below each of the bending critical speeds, depending upon vibration amplitudes experienced. It is generally quite economical to take data at several speeds, because all that is necessary for each additional set of data is a set of simultaneous vibration readings at each selected speed. Therefore, the decision to use multiple speeds in balancing should be based upon the desired or required efficiency of the balancing improvement. Accuracy of the trial weight data, and particularly the absence of gross errors, is the key to rapid balance improvements. Gross errors may sometimes be diluted through the addition of better quality trial weight data taken at slightly different rotor speeds. On the other hand, it may be apparent from the observation of the balancing instrumentation that one particular rotor speed gives better (e.g., more stable) data than any other balancing speed considered. In that case, the single set of

data is preferable. In any case, the balancing engineer must take such details into consideration when designing his particular application.

The flow chart in Figure 16 indicates one case where a set of correction weights was calculated from data obtained at three rotational speeds and also from data obtained at two of these three speeds. The resultant rotor corrections were recorded for both of these cases for ready comparison (Cases 7a and 7b, Figures 78-81).

There are three more details in the balancing process which were not varied during these experiments, because they are outside the main line of investigation and could possibly have confused the interpretation of the results obtained when other variables were changed. These three items were:

1. All trial weight runs were performed with the trial weight placed first at the zero degree location and then, for a second run, 180 degrees away in the same plane. The purpose of this procedure is to obtain an improvement in experimental accuracy through vectorial averaging of the measurements. Attempts were not made to evaluate the need for this procedure with this test setup. This facet was investigated briefly in [3] where it was found that the second trial weight run generally increased the accuracy of the balance corrections. Obviously, the need for this increased effort will decrease with increases in the quality of measurements.

2. The effect that trial weights of different sizes might have had upon balancing effectiveness was not expressly studied in these experiments. It has already been concluded, as indicated in the foregoing discussion on the selection of balancing speed, that trial weight size selection cannot be completely arbitrary for a given rotor-bearing system. Within the limits provided by the Mechanical and Instrumental systems, the trial weight size was kept relatively low for convenience of operation. For reference, it may be noted that the typical trial weight was on the order of two to twelve percent of the total maximum deliberate unbalance weights added to the rotor. For test cases 1 through 5 a trial unbalance of 13.67 gr-cm (0.19 oz-in.) was used for the first trial weight run. This trial unbalance was also used for the second and third trial weight run of test case 5. For all other trial weight runs a smaller trial unbalance of 5.2 gr-cm (0.07 oz-in.) was used.

3. The balancing speed selected for trial weight runs was always as high as possible. The upper limit of the balancing speed was determined by the limit established for maximum rotor orbits and the size of the trial weight. After completion of the first balancing run, with correction weights inserted in the rotor, there usually also was an effective lower speed limit below which further trial weight runs could not be conducted. This is because rotor orbits (without the addition of the trial weight) frequently became too small at one or more rotor stations for reliable phase angle measurement. The selected balancing speeds are listed in Figure 16 for all test cases.

TEST RESULTS

Initial Rotor Condition Prior to All Tests

Prior to assembly of the test rig, in which the three discs were attached through heavy shrink fits to the shaft, all rotating components were individually balanced at low speeds in a commercial balancing machine. The shaft was dynamically balanced while rotating on solid supports at the bearing locations and the discs were balanced on short arbors. After assembly, the rotor was not sufficiently balanced to permit safe passage through the first critical speed. No further attempt was made to reduce initial rotor unbalance. Instead some fairly substantial unbalance weights were added to the rotor at several locations prior to each balancing series. (Safe passage has arbitrarily been defined as rotor orbits at nonbearing locations not exceeding 0.09 mm (0.0035 in.), and rotor orbits right next to journal bearing locations not exceeding approximately one-half of the available bearing clearance, or 0.062 mm (0.0025 in.) for the rigidly supported rotor. For the flexibly supported rotor, larger rotor orbits were allowed, even at the bearing stations (up to 0.075 mm (0.003 in.)). Rotor motion relative to the journal bearings was not measured in these setups.

First Test Case: Rotor With Rigid Bearing Pedestals; In-Line, In-Phase Unbalance; Seven Displacement Sensors

This test case was the first attempt to apply the Influence Coefficient Method to the balancing of a rotor for operation through more than one bending critical speed. The selection of the number of displacement sensors and balancing probes was conservative - all available balancing planes and probes were used. The relative locations of sensors, balancing planes and initial unbalance locations are shown in Figure 17, where the test rotor was photographed prior to installation in the test rig. For this test case, four unbalance weights of equal magnitude were placed in the rotor, one in each of four of the five rotor discs. On three discs, the unbalance weights were installed on the disc face opposite from the side where later trial and correction weights were placed.

The initial amplitudes for the speed range from 2,000 to 4,100 rpm are recorded as curves A in Figures 18 through 24, which represent amplitude data for probe stations 1 through 7. Only vertical amplitudes are shown, since rotor orbits were generally circular. All correction weight calculations were based upon vertical rotor amplitude measurements.

Test Results for Rotor With Rigid Pedestals; In-Line, In-Phase Unbalance; Seven Displacement Sensors

The most informative way to show rotor balance improvement is through graphic representation of rotor orbits over the operating speed range. Visual inspection of initial amplitudes obtained for the unbalanced rotor demonstrates quickly, by virtue of their magnitude and gradient over rotor speed, why passage through the first bending critical speed was not

attempted. (Passage through the first critical speed was not assumed to be impossible. Prior experience had shown, however, that the rotor would have hit a number of the displacement sensors, which were installed with 0.20 to 0.25 mm (0.008 to 0.010 in.) vertical offset. Excessive amplitudes might also have jeopardized the journal bearing seals and the journal bearings themselves, which could have easily been subject to surface damage had metal-to-metal contact occurred, because they were operating in a fluid with very poor lubricity.) Without a record for initial rotor amplitudes above the first critical speed, numerical evaluations of the effectiveness of the rotor balancing process becomes all but meaningless. Relying solely upon a graphical display of rotor amplitudes for the evaluation of rotor balance improvements not only avoids 'infinite' numerical improvement ratios above the first critical speed, but also precludes using 'average' amplitude numbers over speed ranges encompassing one or more sharp and possibly dangerous peaks.

Figures 18 through 24 contain the record of test rotor amplitude improvements as obtained from three consecutive balancing runs. Each figure represents amplitudes at one particular rotor station along the length of the rotor. When evaluating rotor improvement after a particular balancing run, it may be necessary to consult all of the identically lettered curves in the full set of seven figures, because occasionally the large amplitude at just one rotor station determined the maximum safe rotor operating speed.

Inspection of Figures 18 through 24 shows with utmost clarity the progression and success of the flexible-rotor balancing method applied to the test rotor. After the first balancing run, for which trial weight data was obtained at 3315 rpm, rotor amplitudes below the first bending critical speed improved to the point where the rotor could pass slowly through the critical speed and proceed until amplitudes increased again on the approach to the fourth critical speed, which, if reached, would produce peak amplitudes at approximately 11,000 rpm. The results of the first balancing run are shown as curves B in Figures 18 through 24.

Rotor amplitudes depicted as curves C in Figures 18 through 24 resulted from a repeat balancing run below the first critical speed, with trial weight data now taken at the slightly higher balancing speed of 4265 rpm as compared to 3315 rpm for the first run. The increase in balancing speed reflects the improvement of rotor balance; the fact that no trial weight data was taken above the first critical speed reflects the necessity of passing through the first critical with trial weights in place, which would have caused amplitudes exceeding the arbitrarily preset safe amplitude limits. The second balancing run was very successful, reducing amplitudes at the first critical speed to very low levels and improving considerably amplitudes near the fourth critical speed.

The third and last balancing run, for which trial weight data was taken at 4395 rpm and 8885 rpm, reduced rotor amplitude levels to very acceptable operational values. The results are shown as curves D in Figures 18 through 24. There is no off-hand reason why amplitudes could not have been reduced further, had it been so desired.

Second Test Case: Rotor With Rigid Pedestals; In-Line, In-Phase Unbalance; Four Displacement Sensors

For the second test case the balancing conditions were made more difficult through omission of one balancing plane and three displacement sensors. Omission of the fifth balancing plane was not expected to create too difficult a situation, because the remaining four planes were well distributed on the rotor, at or near locations of maximum rotor deflections pertaining to the fourth critical speed. The omission of three adjacent displacement sensors from three of the five rotor masses was a more drastic step, taken in order to approach somewhat more closely the number of sensors available in general machinery configurations. The locations relative to the rotor of balancing planes, displacement sensors and initial unbalance for the second test case are shown in Figure 25.

Test Results for Rotor With Rigid Pedestals; In-Line, In-Phase Unbalance; Four Displacement Sensors

The results for the second test case were highly successful and most encouraging, proving the ability of the balancing method to be effective under less than ideal conditions. Representing the initial unbalance rotor condition, curves A in Figures 26 through 32 are identical to those in Figures 18 through 24. Based upon trial weight data obtained at 3315 rpm for the first test case, but with all information obtained from the three center probes (rotor stations 2, 4 and 5) and from balancing plane 4 omitted, correction weights were calculated and placed in balancing planes 1, 2, 3 and 5. The resultant rotor amplitude improvements are shown as curves B in Figures 26 through 32. Improvements in rotor balance were significant, however they were not sufficient to allow safe passage through the first bending critical speed.

The results of a second and third balancing run, with data taken at 4225 rpm for the former and at 4295 and 8885 rpm for the latter are shown as curves C and D respectively in Figures 26 through 32. Both show very good improvement in rotor balance with final results comparable to those obtained for the first test case. Since fully acceptable results of comparable quality were achieved with an identical number of balancing runs, it can be concluded that neither omission of the fifth balancing plane, nor that of three displacement sensors, was detrimental to efficient balancing.

As part of the second test case, another aspect of the Least Squares Balancing Method was checked out: the requirement that trial weight data taken at or near lower critical speeds be included in the correction weight calculations when balancing for higher critical speeds. The last set of correction weights that had resulted in rotor amplitudes 'D' in Figures 26 through 32 was removed from the rotor and a new set of weights installed which was based only upon half of the previously used data, namely the data acquired at 8885 rpm only. Rotor amplitudes were then recorded which had much higher values at the first critical speed. They are shown in Figures 33 through 38 for six of the seven rotor stations and should be compared with curves D in Figures 26 through 32. The case for including data taken at lower critical speeds is apparent.

Third Test Case: Rotor With Rigid Pedestals; In-Line, In-Phase Unbalance; Two Displacement Sensors

Following the successful nature of the second test case, two more displacement sensors were eliminated from the data-taking process for balancing, leaving only two sensors. Both remaining sensors were located inboard of each of the two journal bearings. The same four correction planes were used as in the second test case (see Figure 39).

Test Results for Rotor With Rigid Pedestals; In-Line, In-Phase Unbalance; Two Displacement Sensors

The results of the third test case are shown as curves B through E in Figures 40 through 46 for the seven stations along the test rotor. It is quite obvious now, that balancing the test rotor with just two sensors, located near the nodal points of the mode shape at the first critical speed, is not the best approach. Three balancing runs were required to bring the rotor past the first critical speed and the result of balancing at the fourth critical speed was not as good as those previously achieved with either four or seven sensors. Nevertheless, balancing proved to be possible under these adverse conditions, and that is felt to be a remarkable achievement.

Inspection of Figures 40 through 46 clearly shows the insufficiency of the two-probe data available for the calculation of correction weights. There is no longer a steady progression towards better rotor balance at all rotor stations. At three rotor stations, amplitudes were generally higher after the first correction, and improvement after each balancing run was erratic when viewed for all measurement stations. Vibration amplitudes at those stations at which trial weight data was acquired (No. 2 and 6) generally did show a consistent improvement with each balancing run, however.

Fourth Test Case: Rotor With Rigid Pedestals; In-Line, In-Phase Unbalance; Two Acceleration Sensors

The switchover from radial displacement sensors to acceleration sensors located on the bearing pedestals is a significant step in the direction of meeting the restrictive sensor accessability limitations encountered in actual production machinery. In the preceding third test case, the rotor was balanced using data obtained by two displacement sensors located adjacent to each of the bearing housings. The substitution of accelerometers mounted on each of the bearing housings (see Figure 47) was, therefore, expected to provide a direct measure of the degradation of information obtained about rotor behavior when bearing transmitted forces (as recorded by the accelerometers) are substituted for rotor displacements as balancing criteria.

Again, the first set of calculated correction weights was based upon data recorded during the very first trial weight run, from which each of the first correction weight sets in the preceding three test cases was obtained. (All previously installed correction weights were, of course, again removed from the rotor prior to installation of the first correction weight set calculated from accelerometer data.)

The second trial weight data run was conducted at the reduced rotor speed of 3200 rpm (versus 3315 rpm for the original data run) because it appeared that larger and steadier accelerometer signals could be obtained at this speed. For the third and last trial weight run, rotor speeds of 2650, 2980, and 3400 rpm were selected. It was obvious, however, from visual observation of the data monitoring oscilloscope screens that the vibration data at each of these speeds was of poor quality in this last run. Correction weight sample calculations confirmed this and therefore no balancing was performed based on the third trial weight data run.

Test Results for Rotor With Rigid Pedestals; In-Line, In-Phase Unbalance; Two Accleration Sensors

Balancing of the test rotor with rotor vibration data obtained exclusively from accelerometers located on the bearing housings produced unexpected results, which at first glance appeared to be contradictory. It was found that the amount of unbalance in the rotor was apparently substantially reduced (at least to the point where accelerometer signals became too small to be discernible by the available instrumentation) but at the same time the "corrected" rotor showed amplitude increases at all stations where rotor displacements were monitored (Figures 48 and 49, curves B). To ascertain the validity of these experimental results, rotor response calculations were made, simulating the initial unbalanced rotor condition and the "improved" condition after balancing from accelerometer data. The calculations confirmed the experimental results, illuminating an excellent example of an undesirable result which can occur in flexible rotor balancing when the location of the vibration sensors happens to coincide with the nodal points on the rotor for the particular rotor speed at which balancing is attempted. Under such conditions, the sensors used are inadequate to describe the complete nature of the rotor vibration, and the balancing process is falsely concluded to be successful. Additional sensors of course immediately correct this erroneous conclusion.

Figure 50 shows calculated mode shapes for the test rotor at 3000 and 4000 rpm, assuming unbalance of identical magnitude and location as was placed in the rotor prior to the balancing tests. (Some discrepancy between calculated and measured values, perhaps up to 20 percent, must be allowed due to the unknown amount of residual unbalance present in the rotor prior to the placement of the intentional in-line, in-phase unbalance.) The calculated mode shapes in Figure 50 show an increasing rotor displacement amplitude between 3000 and 4000 rpm, which is the speed range in which the first set of trial weight data is taken. (Below 3000 rpm, rotor amplitudes are too small for accurate data acquisition, and above 4000 rpm amplitudes would be too large due to the close vicinity of the first critical speed.) Accelerations of the bearing housings due to the rotor vibrations under the influence of the initial unbalance were successfully recorded and used for the calculation of the first set of correction weights. The criterion for successful data acquisition is that recorded phase angles between the acceleration signal and the reference signal (Fotonic sensor signal) do not vary substantially with time (at constant rotor speed). (In this context "substantial" phase angle variation means variations of $\pm$ 30° or more, which do seem to occur whenever the data signal begins to slip below the threshold of instrumentation sensitivity.) The usual criterion for

successful correction weight calculation is that the addition to the rotor of the calculated correction weights will result in reduced amplitudes, at least at the balancing speed.

For the test case where a known heavy unbalance has been intentionally added to the rotor, a preview of the effectiveness of the calculated correction weights may be obtained by comparing the unbalance weight vectors with the correction weight vectors for angular location and magnitude. This is, of course, only a very approximate comparison when unbalance and correction weights are not located in identical axial rotor planes, as is the case for this test rotor. Nevertheless, Figure 51 clearly indicates that the first set of corrections, obtained with accelerometer data only, resulted in a substantial reduction of the initial rotor unbalance.

The full significance of the effect of the first unbalance reduction becomes apparent only from inspection of Figure 50(b), where a new set of rotor mode shapes is shown. This set was calculated with inclusion of the correction weight determined for the actual test rotor. The new unbalance configuration in the rotor causes the nodal points to shift towards the midpoint of the rotor so that they will almost exactly coincide with the (axial) bearing center lines in the speed range in which trial weight data has to be taken. With rotor amplitudes reduced nearly to zero at the bearing location, bearing displacements and accelerations diminish, making further balancing with accelerometer data alone impossible. Actually, this condition was reached after a second successful trial weight run, which resulted in slightly improved rotor amplitudes at all rotor stations (over the results of the first trial weight run) (Figure 48 and 49 curves C). The actual test also showed a slight increase in rotor amplitudes at those measuring stations where amplitudes should have decreased slightly according to the response calculations.

The most important conclusion that may be drawn from this test series is that sensor locations at the nodal points of the rotor must be avoided, particularly when the number of sensors does not exceed the number of nodal points encountered in the rotor at the highest critical speed to be balanced for. There is no reason to assume that the same problem would not be encountered with displacement probes instead of accelerometers. In the particular case of this test rotor, two displacement probes mounted directly next to the bearing housings (third test case) worked quite well – probably for the simple reason that the nodal points never shifted far enough towards the center of the rotor to coincide exactly with the probe locations.

Fifth Test Case: Rotor With Rigid Pedestals; In-Line, Alternating-Phase Unbalance; Four Displacement Sensors

When a rotor has completed its manufacturing cycle, the built-in unbalance is of unknown magnitude and location. The severity of dynamic rotor response is known to vary not only with the magnitude of the unbalance (at any given rotor speed) but also with the axial and radial location of the unbalance. Depending upon the mode shape of the rotor elastic axis, even an in-plane circumferential shift of a particular unbalance by 180° may cause a large change in rotor amplitudes. For a rotor which is to operate

over a speed range encompassing more than one bending mode shape (critical speed), there is therefore no unique "most severe" unbalance combination. Deliberate addition of "initial" unbalance to a rotor for test purposes should, therefore, include suitable variations in the unbalance distribution to cover the most severe combinations at each of the critical speeds that are to be encountered.

For the test rotor two unbalance arrangements were used: the in-line, in-phase configuration of equal weights attached to each disc; and a second arrangement where every second weight was rotated by 180^{o} to give an in-line, alternating-phase configuration. This latter configuration accentuates rotor deflections at the fourth critical speed, because each unbalance weight is located at a point of maximum deflection of the rotor for that mode.

This section contains the balancing results obtained for the test rotor intentionally unbalanced with an in-line, alternating-phase weight configuration. Four displacement sensors were used to record rotor amplitudes and phase angles for the calculation of correction weights, which were applied in four axial rotor planes. This set of intermediate conditions was chosen for a fair comparison of the results obtained with this unbalance configuration and the in-line, in-phase configuration examined previously (see Figures 26 through 32). (Four measuring probes and four correction planes were determined to be a reasonable balancing configuration in the previous section, while seven probes and five planes were determined to provide ample information for "easy" balancing and two measuring probes and four trial weight planes resulted in "difficult" balancing.)

Test Results for Rotor With Rigid Pedestals; In-Line, Alternating-Phase Unbalance; Four Displacement Sensors

The test results for this case are shown in Figures 52 through 57. Comparison of these figures with those obtained under identical conditions but with an in-line, in-phase unbalance configuration (Figures 26 through 32) indicates a slightly reduced efficiency in rotor orbit reductions. Three, instead of two, trial weight runs were now required before the rotor exhibited small (less than 0.25 mm (0.001 in.)) orbits at the first critical speed. Interestingly, balancing of the test rotor for passage through the fourth critical speed still required only one additional trial weight run. There thus appeared to be no "left-over" effect above the first critical speed from an initial unbalance arrangement which had been designed to excite strongly the mode shape of the fourth critical speed. Nominally this balancing test case required the same number of trial weight runs (four) as were previously necessary to complete the balancing with only two probes and the unbalance initially arranged in an in-line, in-phase configuration. However, inspection of rotor amplitudes as they were monitored and recorded after each successive balancing run clearly indicates a much more orderly progression in the balancing improvement when readings from four probes were used for correction weight calculations, than when data from only two probes were used.

Sixth Test Case: Rotor With Flexible Bearing Pedestals; In-Line, In-Phase Unbalance

The introduction of flexibility into the journal bearing supports produced some very noticeable changes in the observed rotor orbits, as seen from the rigid machine bed. (See Figures 6 and 7.) The changes in observed rotor behavior were due exclusively to the flexures, since journal bearing clearances (bearing-pad to shaft) were left undisturbed when the change-over was made. For this test case the initial rotor unbalance distribution was again arranged in the in-line, in-phase configuration. Displacement sensors located in four rotor axial planes were used (Figure 25). The rotor was balanced for operation over the complete speed range through four critical speeds with data obtained from four vertical probes.

The effectiveness of the first trial weight run was additionally tested with correction weights calculated from data obtained through only the four horizontal displacement sensors, and also from data obtained simultaneously through both the four vertical and the four horizontal probes. The selection of four sensor locations along the rotor was based upon the results of the investigation conducted with the rotor on rigid supports (test cases one through three) where balancing effectiveness was examined as a function of the number of sensor locations. Four sensor planes were found to make the most efficient use of the data acquisition and computation effort for this test rotor.

Test Results for Rotor With Flexible Bearing Pedestals; In-Line, In-Phase Unbalance

The test results from this test case as well as from the succeeding case, when the initial rotor unbalance was arranged in an in-line, alternating-phase configuration, differed significantly in one respect from all experimental results obtained previously when the rotor had been equipped with rigidly supported journal bearings. Only one series of trial weight runs was required to achieve satisfactory rotor balance for passage through the first system critical speed. For this test case, only one additional trial weight run was required (with trial weight data taken at 4200 and 9300 rpm) to reduce rotor amplitudes to sufficiently low levels over the full speed range, including safe and slow passage through the fourth critical speed. The results of this balancing effort are shown in Figures 58 through 62. In each figure, curve A designates rotor amplitudes as they were recorded for the unbalanced rotor, curve B shows the result of the first trial weight run and curve C indicates the final result of two trial weight runs. Inspection of curves B and C clearly reveals the effect exerted by the dissimilar stiffnesses of the journal bearing support flexures. The rotor system now experiences two separate resonances, with the resonance in the horizontal direction occurring at approximately 4300 rpm and the vertical resonance at approximately 4900 rpm. Trial weight data taken for the purpose of suppressing the first critical speed was always taken at a rotor speed below where the first peak (horizontal resonance) occurred. However, when balancing for the fourth critical speed, no difference was observed in the results if first critical speed trial weight data was collected just below the horizontal resonance (4300 rpm) or the vertical resonance (4900 rpm).

After completion of the balancing run which had brought the rotor into a state of balance permitting operation over the full speed range (up to 15,000 rpm) including passage through the fourth critical speed, all correction weights were removed and a new set of correction weights was added. These new weights had been calculated from data obtained from the four horizontal displacement probes located in the same rotor axial location as the corresponding vertical probes. The trial weight data for those probes had been obtained at the same time as the data for the vertical probes. The results of this correction are shown as curves C in Figures 63 through 67.

The balancing process was not continued further with these weights in place. Instead, after the curve C runs had been completed, the weights were removed and a new set was installed which had been calculated based upon response data recorded by both the vertical and the horizontal probes (eight probes in all). The results for this third run are shown as curves D in Figures 63 through 67. Curves A and B are identical to those shown in Figures 58 through 62 and represent the original, unbalanced rotor condition and the result of the first correction based upon data from vertical probes only, respectively. Inspection of Figures 63 through 67 indicates that best results were obtained from the set of vertical probes, while the lowest ranking is assigned to rotor correction from the combination data set of vertical and horizontal probes.

Seventh Test Case: Rotor With Flexible Bearing Pedestals; In-Line, Alternating-Phase Unbalance

After removal of all previously applied correction weights, two of the unbalance weights were moved by 180^{o} in their respective rotor planes to create an arrangement of intentionally added in-line, alternating-phase unbalances in the rotor. This unbalance arrangement, as well as the location of the four displacement sensor planes used for this test case, was identical to that investigated for the Fifth Test Case. The test conditions for the Fifth and the Seventh Test Cases differ therefore only in the addition of journal bearing support flexures to the latter.

The sequence followed in the execution of test runs for this test case is shown in Figure 16. Inspection of Figure 16 reveals that in this test case the rotor was balanced in three sequences for operation through all four critical speeds: twice with data obtained from four vertical probes (cases 7a and b, and 7e), and once with data from four horizontal probes (case 7f). In addition, three subexperiments (cases 7b - 7d) were performed in response to questions that arose in the course of the experiments.

The first balancing sequence (7a) started with a trial weight run at 3330 rpm, at which balancing data was acquired for four vertical probes and correction weights were calculated which permitted rotor passage through the first critical speed. This was followed by two additional trial weight runs, which achieved satisfactory rotor balance for passage through the fourth critical speed (cases 7a and 7b). Two of the three subexperiments (7c and 7d) were based upon the completed first balancing run where data had been obtained at 3330 rpm with four vertical probes and a second

trial weight run where data had been obtained at 4590 and 8800 rpm for the full complement of six vertical and four horizontal probes. In the first subexperiment (7c), data from the six vertical probes was used to calculate a set of correction weights. In the second subexperiment (7d) correction weights were calculated from the four horizontal probes instead. The results obtained from either the four vertical probes (7a), or six vertical probes (7c) or four horizontal probes (7d) are compared in Figures 73 through 77. The third subexperiment (Case 7b) was based upon two completed balancing runs of the first test sequence. At the third trial weight run, data was acquired at three speeds (4200, 9600 and 10,600 rpm). In Case 7a the data from all three speeds was used for the calculation of correction weights, while for Case 7b the data taken at the third speed was omitted from the input to the correction weight calculations.

The second test sequence (Case 7e, Figures 82 through 85) is essentially a repeat of the first sequence, where the uncorrected rotor was completely balanced for passage through all four bending critical speeds using data obtained through the same four vertical probes used previously, but with only two trial weight runs.

Test Results for Rotor With Flexible Bearing Pedestals, In-Line, Alternating-Phase Unbalance

For the first test sequence of the Seventh Test Case (7a and b, Figures 68 through 72), a total of three trial weight runs was required to achieve passage through the fourth critical speed. This was the only instance this test rotor required two trial weight runs to improve performance between the first and fourth critical speeds to the point where safe passage through the fourth critical speed was possible.

Data for the final trial weight run, which formed the basis for the final correction in this first test sequence, had been acquired at three rotor speeds: 4200, 9600 and 10,600 rpm (Test Case 7a).

An alternate set of correction weights was later calculated from data obtained at the two lower rotor speeds only (Test Case 7b). When this second set of weights was substituted for the one previously installed, a new, but slightly inferior set of rotor response curves was obtained. For comparison, the two sets of resultant rotor amplitude curves are plotted on Figures 78 through 81. Curves D_3 which are identical to curves D in Figures 68 through 72 represent rotor amplitudes obtained by balancing with data from three rotor speeds. Curves D_2 are their counterparts, obtained after balancing based upon data from two speeds only. Curves C, which depict the condition of the rotor prior to either one of these two balancing runs, are also identical to curves C in Figures 68 through 72.

Before proceeding to the second test sequence (Case 7e), the results of two additional subexperiments are briefly noted (Figures 73 through 77).

Pursuing further the difference in results (from Case 6) obtained for vertical and horizontal probes, additional trial weight data (six vertical

and four horizontal probes) was taken at 4590 and 8800 rpm for the test sequence which had been initiated with a trial weight run at 3330 rpm. Each of these three different sets of correction weights were in turn installed in the rotor and the corresponding rotor responses recorded.

For comparison, the results are plotted in Figures 73 through 77. Curves B, which are identical to curves B in Figures 68 through 72, indicate the starting condition for the second correction run. Curves C, D and E indicate results obtained from four vertical, six vertical, and four horizontal probes, respectively. Curves E (from the horizontal probes) indicate the poorest overall rotor performance (highest rotor amplitudes in the speed range between 10,000 and 11,000 rpm).

No clear-cut superiority can be ascribed to either the four or the six vertical probe case. This finding contradicts any expectation of superior results from utilization of six probes. Such an expectation could be based, for example, upon the observation that rotor amplitudes at the two additional rotor stations (No. 3 and 4, Figure 7) were often higher than at any of the four other rotor stations from which trial weight data was collected.

The second test sequence (Test Case 7e) in this test case developed from the desire to ascertain the need for two trial weight runs for the rotor to be able to operate through the fourth bending critical speed after having passed the first critical speed. An effort was made to optimize the effectiveness of the first and second sets of trial weight data by pushing the balancing speeds closer to the limit of safe rotor operation, without reduction of trial weight size. The results of the first trial weight run (cases 7c and 7f) did not indicate any apparent success of that strategy as far as rotor amplitudes at the first critical speed are concerned. Those were generally much higher than those observed for the first balancing sequence in this test case, where the first set of trial weight data was obtained at 3330 rpm (Test Case 7a). However, above the first critical speed, amplitudes increased now much less rapidly (compare curves B in Figures 82 through 85 with curves B in Figures 68 through 72). Consequently, the second data collection speed in the second trial weight run was now increased from 8800 rpm to 9800 rpm and the rotor was very successfully balanced with two trial weight runs (see curves C in Figures 82 through 85). However, when using the data from the four horizontal probes (Test Case 7f), the results were not quite the same. The first trial weight run yielded large reductions in rotor amplitude at the first critical speed, but rapidly increasing rotor amplitudes existed above the first critical (curves B, Figures 86 through 90). Consequently, the second balancing speed of the second trial weight run had to be reduced to 8800 rpm. The resultant rotor balance from the second trial weight run with data from horizontal probes was only barely acceptable. A third trial weight run would have been required if rotor amplitudes were to be brought down to previously achieved low levels, particularly at the resonance locations. Comparing the overall results of the first and the second balancing sequence from this test case, it is concluded that balancing of the flexibly-supported test rotor with an initial in-line, alternating-phase unbalance for operation above the first and through the fourth critical speed proved slightly more difficult than

under any other test condition investigated. This is the third indication (see also results of previous test cases 6a, 6b and 7a and 7d) that balancing of this rotor (on flexible bearing supports) proved less successful from data obtained by the horizontal probes than by the vertical probes. The explanation may possibly lie in the observed rotor motion at the second probe (journal bearing opposite from drive end) which was almost exclusively in the vertical direction, when the rotor was initially unbalanced by an in-line, alternating-phase unbalance (see Figure 6).

In the course of the second test sequence in this test case a subexperiment (not shown in Figure 16) was performed which emphasizes the desirability to include rotor out-of-roundness values at the measurement stations in all calculations of balancing correction weights. Rotor out-of-roundness of 0.0075 mm (0.0003 in.) T.I.R. at the drive-end disc was inadvertently omitted from the calculations for the first set of correction weights based upon trial weight data taken at 3750 rpm from vertical probes only. As shown in Figures 91 through 95, curves B, an appreciable deterioration of rotor balance was observed in the vicinity of the fourth critical speed when rotor out-of-roundness was not taken into account at only one of the four measurement stations. However, improvement of rotor balance at the fourth critical speed through the inclusion of rotor out-of-roundness values did result in somewhat higher amplitudes at the first critical speed than had existed after the correction which neglected out-of-roundness (see curves C in Figure 91 through 95).

DYNAMIC ROTOR CHARACTERISTICS IN POLAR COORDINATES

For balancing purposes the dynamic behavior of a rotor can be adequately described by three parameters: rotor amplitude, rotor phase angle and rotor speed. In this report, the description of rotor phase angle in relation to either rotor speed or amplitude has, so far, been omitted, mostly because of space limitations. The complete description of rotor behavior through separate amplitude and phase angle plots over the full rotor speed range is not commonly provided in rotor balancing work, because most balancing is done at one particular speed. Instead, combined amplitude-phase angle information is generally sought in the form of rotor displacement or bearing force vectors at discrete balancing speeds. (This is ultimately the information which is used in all balancing processes for the calculation of correction weights for the unbalanced rotor.)

The spatial deformation of an unbalanced, flexible rotor is most difficult to visualize from rotor amplitude and phase angle plots alone. For this purpose, a combination of rotor amplitude plots in the form of rotor orbit pictures (as presented in Figures 6 and 7) and superimposed phase angle information is generally preferred as the basic information from which deflected rotor shapes at various speeds may be inferred. The obvious drawback of this approach is the noncontinuous nature of the descriptive process between rotor speed points, and the fact that amplitude and phase angle information have to be acquired separately.

Recently, electronic instrumentation has been developed to overcome these drawbacks. With the aid of such instrumentation, a speed-continuous plot of rotor amplitudes and phase angles may be obtained in polar coordinates. Such a plot depicts the rotor displacement vector loci as seen by the particular displacement sensor, with an angular reference provided by a separate reference sensor which records a known angular location on the rotor (the equivalent of the traditional 'mark' on the rotor, which appears as a sharp spike on time-base oscilloscope pictures of rotor amplitudes).

For the special case of a rotor that moves in circular orbits relative to the measurement base, a vector loci plot may be produced from just one displacement sensor at each rotor axial measurement location, and each sensor may have an arbitrary, but known angular location relative to the reference sensor. For the general case of noncircular rotor orbits, two sensors in each measurement plane, preferably separated angularly by 90 degrees, should be used. The plots from the two probes (here called "vertical" and "horizontal"), may be quite different from each other and rotor spatial relationships are now much harder to visualize. Nevertheless, such plots provide the operator of rotating machinery with easily monitored information on the behavior of his machine. With experience, complete response patterns may be recognizable from such data. Examples of such patterns for the test rotor are presented and discussed in the next section.

Polar Amplitude Plots for Test Rotor

During the course of the balancing experiments performed on the test rotor with flexible bearing supports, a newly developed multichannel tracking filter became available from the manufacturer on a try-out basis. This multichannel instrument provides not only the filtered amplitude of the data signal, but also the sine and cosine components of the signal, thus eliminating the need for a separate phase meter. (A separate reference signal for phase angle measurements is, of course, required.) When the values of the sine and cosine components are plotted as the x and y components on polar coordinates, the vector loci for the processed amplitude signal are found.

Some of the test rotor response data that had previously been recorded on magnetic tape for balancing purposes were reprocessed for the purpose of plotting unbalance vector loci. After plotting just a few cases of the test rotor in different unbalance conditions (various states of balance), some well-known and easily recognizable patterns in rotor response became apparent. The most easily recognizable response pattern is that of rotor passage through a critical speed. The increase and decrease of rotor amplitude and the change in phase angle by about 180 degrees associated with passage through a critical speed produce a distinct, nearly circular loop on the polar plot. Between criticals, continual growth in rotor amplitude with no perceptable change in phase angle shows as straight outward-bound lines. There are many more distinguishable features in these plots (such as small loops, angular oscillations, etc.) that might yield some interesting information, if analyzed.

The potential of the polar amplitude plot to give a reflection of the unbalance configuration present in an unbalance rotor is indicated in Figures 96 and 97, where the test rotor amplitude projections as seen by the vertical and horizontal displacement probes are shown plotted in polar coordinates. In Figure 96 the rotor was in the unbalanced condition, with the unbalance arranged in an in-line, in-phase configuration, in an angular position 45 degrees ahead of the zero mark on the rotor. The reference probe, which was used for the phase angle measurement between the zero mark on the rotor and the maximum dynamic displacement of the rotor, was located in the same angular position as the vertical probe. There has been no correction made in Figure 96 or any of the subsequent figures for this fact, therefore, the angles as determined by the horizontal probes include a lag of 90 degrees. Keeping this in mind, a striking similarity between the amplitude projections of the vertical and horizontal probes and between those of the vertical and horizontal probes among themselves, is evident. Partially, this similarity is the result of at least approximately circular rotor orbits (see Figure 7 for rotor orbit photograph for the initially unbalanced rotor with in-line, in-phase unbalance) and the nearly cylindrical motion into which the particular unbalance configuration is forcing the rotor at low speeds.

When two of the intentional unbalance weights in the test rotor were moved to create an in-line, alternating-phase unbalance configuration, drastically different rotor amplitude vector loci were recorded (Figure 97). The vertical rotor amplitude vector locations still exhibit some orderly arrangement, while their horizontal counterparts no longer seem to follow a recognizable pattern. The amplitudes at the maximum rotor speed (which correspond to the end points of each probe signal trace) have been indicated by arrows with their appropriate probe designations. It is important to remember, that those arrows designate the projections of the signals from the vertical and horizontal probes and the phase angle thus shown is the angle between the maximum projected vertical or horizontal probe signal amplitude and the reference signal. The spatial deflection of the rotor cannot be seen in the arrangement of the amplitude vectors of either the vertical or horizontal projections alone. To facilitate comparative study, the rotor orbits associated with the amplitude vectors as recorded at the maximum rotor speed (4550 rpm) are also shown in Figure 97.

Examination of the orbits associated with the amplitude vector locations clearly shows a very complicated set of rotor motions as recorded by the full set of displacement sensors arranged along the length of the rotor. It seems astonishing then, that the balancing process applied to the flexibly-supported rotor with either the in-line, in-phase or the in-line, alternating-phase unbalance configuration, was equally successful with only the slightest hint of the complications that should have been expected from an examination of Figures 96 and 97. (The balancing results associated with these two unbalance configurations were shown in Figures 58 through 62 for the in-line, in-phase case and in Figures 82 through 85 for the in-line, alternating-phase configuration.)

A second set of amplitude vector loci for the rotor initially unbalanced by an in-line, in-phase unbalance configuration is shown in Figure 98. However, in this case the rotor had already been balanced for passage through

the first critical speed, but not yet well enough balanced for passage through the fourth critical speed. The amplitude vector location traces in Figure 98 display the typical large, almost circular loop indicative of the phase angle shift at the passage through the critical speed and the straight-line tails, which indicate increasing amplitudes between critical speeds, at minimal phase angle changes.

In Figure 98 the amplitudes associated with the passage through the first critical speed (diameter of large loops) are quite large, and do not represent a well-balanced rotor (see also curves B, Figures 58 through 62 for the corresponding amplitude versus rotor speed curves).

A much smaller loop in Figure 99 indicated a better balanced rotor at the first critical speed, where the rotor was initially unbalanced by an in-line, alternating-phase unbalance configuration. For clarity, in Figure 99 the traces from only the two probes at a single rotor location (Station 3) are shown. The remaining traces were very similar, with the orientation of the "tails" divided between the same angular orientation as shown, and approximately 180 degrees away.

The final stage of rotor balance for the rotor with the initial in-line, in-phase unbalance and the initial in-line, alternating-phase unbalance is indicated by the amplitude vector locations at Station 3, in Figures 100 and 101, respectively. Both sets of traces are now virtually indistinguishable, with double loops indicating passage through two bending critical speeds and acceptably small peak amplitudes. In Figure 101, rotor speeds are indicated at various points on the amplitude curves. The spacing of these speed markers makes it abundantly clear that by far the largest part of these curves (almost all of the loops) is produced during a very limited part of the rotor speed curve, namely at the passage through the critical speeds.

THE USE OF A LASER FOR MATERIAL REMOVAL DURING ROTOR BALANCING OPERATIONS

Mass balancing of a rotor generally requires that material be either added to or removed from the rotor in one or more axial planes. Ordinarily, this is accomplished by either insertion of precisely weighed screws or weights into previously prepared holes or slots, or the removal of material from the rotor at predetermined locations by standard machining methods, such as hand grinding or drilling. Material may also be removed from the rotor by a laser.

The application of a laser for this purpose is not a new idea. Known applications of lasers include the single-plane balancing of small gyros and other similar small rotors [18, 19]. In these applications, unbalances are detected and located, and a laser is used for removing material in a more or less trial-and-error fashion. However, for the present application the intent is to use a laser to improve the speed, efficiency and flexibility of a multiplane balancing technique which has already been proved to be extremely effective.

There are several important advantages to using a laser for material removal in rotor balancing. The most important of these advantages is that the material can be removed while the rotor is spinning at its normal balancing speed. This eliminates the necessity of stopping the rotor to add or remove material after each balancing run, and then starting the rotor up again for the next balancing run. A large amount of time may be saved especially when dealing with high inertia rotors, or those that require temperature stabilization. Another related advantage to using a laser is that it would allow a rotor to be balanced inside its normal housing without disassembly. For example, a turbine engine rotor could be balanced while operating in its normal configuration in the engine. Ports need merely to be designed into the engine housing in the balancing planes, into which lenses or adjustable focus lens tubes may be inserted in order to converge the laser beam on the surface from which material is to be removed. In such a manner, the turbine rotor may be balanced to a much finer degree than it could outside of the engine. In addition, the rotor may be rebalanced whenever and wherever necessary after simply reconnecting the instrumentation and re-inserting the lenses. In this way, the rotor may be rebalanced while the engine is still in its normal operating location, be it in a power plant, on an airplane wing or almost anywhere. Of course, there are innumerable other cases in which this is a distinct advantage besides turbine engines.

A third advantage to using a laser is that the time required to remove the necessary amount of material would amount to only a few seconds or at most a few minutes. This is much less than the time required to remove a similar amount of material using standard machining methods.

Laser Capability

A search was made for the type of laser best suited to the turbine-engine rotor application. This laser would have to be capable of producing short duration, high-energy pulses at a reasonably high repetition rate. It would have to have a well-defined time lag between triggering and firing. In addition, it would have to be portable, of reasonable cost, and with minimum maintenance. The type of laser most nearly fitting this description is a neodymium-doped laser with glass as the host material. The major drawback of this type of laser is the inherent difficulty of cooling glass, which creates a practical limit on energy density and repetition rate. However, both are still sufficiently high to be acceptable. This type of laser is presently in widespread use for drilling and welding steel and similar materials. Therefore, its applicability to material removal is well established.

Experimental Tests

In order to demonstrate the feasibility and effectiveness of laser material removal for balancing, a test was carried out in which a laser was used to remove material from a rotating disc, 15.2 cm (6 in.) in diameter, and also from static samples. On the rotating disc, a target consisting of one black and one reflective semicircle was placed on the bottom of each disc and a Fotonic™ Sensor was used to trigger the laser so that the location of material removal could be controlled.

The entire test apparatus, including the laser head and power supply, is shown in Figure 102. The laser used in the tests was a "Laser Incorporated" Model 11 laser driller. The laser pulse duration was 800 microseconds with an output energy of 25 joules at the operating point, which was maintained throughout the experiment. This laser is capable of delivering up to one pulse per second. In the rotating disc part of the experiment, the total optical path was about 140 centimeters, laser to disc surface, and near field imaging was used, exclusively, throughout the experiment. Under actual operating conditions, the pulse duration could be reduced to as little as 300 microseconds. Shorter pulse duration becomes more important when higher rotor speeds are encountered.

The disc was irradiated as described in Table I. The major purpose of this series of tests was to determine the relationship between rotor speed and the length of the slot where material was removed. It is noted that proportionality could not be established. This is because the laser does not deliver an equal amount of energy throughout each pulse, but rather there is a well-defined reduction in energy toward the end of the pulse. Consequently, as the rotor speed is increased and the arc length of the disc exposed to the laser slot increases, the energy density is decreased until the energy being delivered at the end of the pulse does not reach the vaporization threshold of the material. However, this does not necessarily mean that higher rotor speeds result in less material being removed. Actually, it is entirely possible that more material is removed at higher rotor speeds because a longer slot does not need to be as deep to remove as much material. Since the laser beam goes increasingly more out of

Table 1

Length Of Laser-Removed Material Slot As A Function Of Disc Speed
(10 Pulses At 25 Joules Per Pulse; Spot Size (Slot Width), 0.5 mm)

Disc RPM	Slot Length
750	9 mm
1000	10 mm
1250	11 mm
1500	11 mm
2000	12 mm
3000	13 mm

Table 2

Characteristics Of Laser Material Removal Tests
(Laser Energy, 25 Joules Per Pulse)

Test No.	Disc RPM	Lens	Spot Size	Number Of Pulses
1	1500	10 diopter	.5 mm	95
2	1500	8 diopter	.66 mm	95
3	1500	8 diopter	.66 mm	95
4	1500	8 diopter	.66 mm	47
5	1500	3.75 diopter	2.06 mm	50
6	1500	6.5 diopter	.86 mm	95
7	1500	6.5 diopter	.86 mm	32
8	3000	6.5 diopter	.86 mm	95
9	500	6.5 diopter	.86 mm	32
10	1500	6.5 diopter	.86 mm	32
11*	1500	6.5 diopter	.86 mm	32

*For this test only, material was removed from shiny (lathe turned) surface.

focus, and consequently becomes less efficient, as the slot gets deeper, a long shallow slot may produce more material removal provided the amount of energy delivered per unit area does not drop below the vaporization threshold of the rotor material. By inspection of the disc, it could be seen that the quantity of material (estimated 150 mg) removed at different test speeds was roughly the same. Therefore, at least for the range of speeds examined, rotor speed is apparently not a critical factor in material removal. In addition, higher speeds will probably be accompanied by smaller rotor diameters, thus reducing the surface velocity.

For the experiments almost the entire edge of the disc was coated with machine blue. The purpose was to improve the absorption of the surface, thereby improving the efficiency of the metal removal process. The machine blue edge of the disc was irradiated as described by tests 1 - 10 in Table II. Several of these slots are shown in the photograph in Figure 103. For comparison, the portion of the edge of the disc which was not coated with machine blue was irradiated in test 11, under the same conditions as test 10. The resulting slot, which does not appear to be significantly longer than those on the blue areas, is shown in Figure 104. Shown in the same photograph are three holes created by static irradiation of the disc. Figure 105 shows the disc with several series of pulses at slightly different axial locations. The purpose of this test was to increase the width of the slot, thereby increasing the surface area being irradiated. In this way, more material can be removed without having to readjust the focus of the laser beam in order to remove material inside the slot. Similarly, several slots can be cut which are completely axially separated. This would probably be even more effective than widening a single slot because in a single slot gradually being widened, molten or vaporized material seems to reattach itself to the lowest points of the previously cut indentation. An overall view of the disc after irradiation is shown in the photograph in Figure 106. Figure 106 also shows the Fotonic Sensor target on the face of the disc.

Static laser drilling tests were conducted to compare laser driling efficiency for different materials. Several static samples were irradiated with ten pulses with an 800 microsecond pulse duration at 25 joules output. The samples included bars of low carbon steel (which is the material the discs are made of), and SAE 4140 stainless steel, which is a common rotor shaft and disc material. Approximately fifteen to twenty milligrams of material were removed from each sample. This demonstrates that the results obtained above are, at least in a qualitative way, applicable to a large number of rotor shafts.

Further experimentation in laser drilling of rotating surfaces is necessary in order to develop a more quantitative understanding of the effects of several parameters on the removal of material. These parameters include, but are not limited to, rotor speed, rotor material, surface finish and color of rotor, rotor environment, laser power, pulse duration, pulse repetition rate, lens size, location and arrangement. In addition, a detailed study is needed to determine whether the material removed will create any problems, especially inside an operating engine. It is probable that the material would be either vaporized or burned and carried

away from the rotor by the operating mechanism (i.e., combustible gases, air, or steam).

In summary, it has been shown experimentally that a laser can remove quantities of material of the order of 150 milligrams from the edge of a six-inch diameter disc rotating at speeds up to 3000 rpm in well under two minutes. In addition, it is reasonable to believe that substantially larger quantities of material could be removed by simply readjusting the focus of the laser beams as the slot gets deeper, or by moving the laser beam slightly in the axial direction. The latter could be accomplished within reasonable limits by simply moving the laser head without having to alter the positions of the lenses. In any case, it appears that a laser is capable of removing sufficient quantities of material from a rotating surface to be useful in practical rotor balancing operations.

CONCLUSIONS

The experimental program documented in this report has shown that a lightly damped, flexible rotor can be balanced systematically and efficiently for operation through four bending critical speeds. The successful nature of the experimental work indicates that the influence coefficient balancing method should be equally applicable to rotors or shafts having more than four bending critical speeds in their operating speed ranges.

All balancing experiments reported here were performed on a 122 cm (48 in.) long rotor weighing 50 kg (110 lb), operating in the speed range up to 18,000 rpm. The rotor was supported with liquid-lubricated tilting-pad journal bearings having equal fluid-film stiffnesses in the vertical and horizontal directions. With journal bearing housings rigidly bolted to the machine bed, the rotor was successfully balanced from data obtained from displacement probes located at a number of locations along the rotor axis. Balancing was also conducted with accelerometers only, mounted on the two journal bearing housings. This balancing resulted in a significant reduction of bearing housing vibrations, which was, however, achieved at the expense of generally higher rotor displacements elsewhere. In this case, the balancing effort appears to have shifted rotor nodal points towards the bearing locations. Under such dynamic conditions, the bearing housing sensors alone are inadequate to describe the complete nature of rotor vibration. An additional sensor of course immediately corrects this problem.

The absolute number of displacement sensors used for balancing was not found to be critical. The rotor was successfully balanced for operation through all four bending critical speeds with two, four and seven displacement sensors. It must be noted, however, that for the two sensor case, the displacement sensors were located adjacent to the journal bearings and sufficiently far away from rotor nodal points for meaningful recording of rotor vibrations. The balancing efficiency increased markedly when the number of displacement sensors was increased from two to four, but showed insignificant gains with the increase from four to seven sensors. When only two sensors were used, a total of four trial weight runs were needed to achieve satisfactory rotor balance, while a total of three runs each sufficed for balancing with four and seven probes.

Four correction planes were found satisfactory to balance for operation through four bending critical speeds; the addition of a fifth correction plane, located in the fifth rotor disc, did not noticeably improve balancing efficiency.

The addition of flexure bars with unequal stiffnesses in two mutually perpendicular directions to the support structure of the journal bearings caused a significant change in the observed response of the rotor to intentionally-added unbalances. Rotor orbits became generally elliptical, with the major axis of the ellipse oriented horizontally (in alignment

with the 'soft' direction of the support flexures). At the first bending critical speed, a double peak was observed in the amplitude resonance (separated in frequency proportional to the square root of the support flexure stiffnesses in the vertical and horizontal directions). Balancing of the flexibly-supported rotor proved to be even more effective, with most of the gain in efficiency obtained at the first critical speed. Balancing for passage through the fourth critical speed appeared to be slightly more difficult in certain cases. The use of vertical probes (recording generally smaller signals than the horizontal probes) appeared to be slightly more advantageous. An increase in the number of sensors above four offered no advantage.

The effect of two different unbalance configurations upon balancing was investigated on the rigidly-as well as the flexibly-supported rotor: an in-line, in-phase configuration where nearly equal unbalance weights were arranged in identical angular locations on the rotor (on the same side of the rotor center line), and an in-line, alternating-phase arrangement where every second weight had been moved by 180 degrees in its own plane.

The in-line, alternating-phase arrangement produced much more diverse types of rotor orbits when applied to the flexibly-supported rotor, but did not affect balancing at all. In the rigidly-supported rotor, the in-line, alternating-phase unbalance arrangement did not produce a noticeable change in orbital response, but nevertheless seemed to cause an increase in the required balancing effort from three trial weight runs previously required for the in-line, in-phase unbalance configuration, to four trial weight runs.

In the test rotor, balancing corrections were accomplished through addition of weighed setscrews in predrilled holes. As an alternative means of providing rotor balancing corrections, a laser drilling process was briefly investigated. Available laser metal removal systems were found to be capable of metal removal from a spinning rotor at rates suitable for balancing of rotors in the small to medium weight range. Electronic control of a laser for automatic balance weight correction has been demonstrated on a rotating steel disc.

REFERENCES

1. Tessarzik, J.M., "Flexible Rotor Balancing by the Exact Point-Speed Influence Coefficient Method," MTI Technical Report No. MTI-70TR59, NASA Contractor Report CR-72774, prepared for NASA-Lewis Research Center under Contract No. NAS3-13473, October 1970.

2. Tessarzik, J.M., Badgley, R.H., and Anderson, W.J., "Flexible Rotor Balancing by the Exact Point-Speed Influence Coefficient Method," Journal of Engineering for Industry, ASME Trans., Series B, Vol. 94, No. 1, February 1972, p 148.

3. Tessarzik, J.M., "Flexible Rotor Balancing by the Influence Coefficient Method: Part 1 - Evaluation of the Exact Point-Speed and Least Squares Procedures," MTI Technical Report No. MTI-72TR32, NASA Contractor Report CR-121107, prepared for NASA-Lewis Research Center under Contract No. NAS3-14420, July 1972.

4. Tessarzik, J.M., and Badgley, R.H., "Experimental Evaluation of the Exact Point-Speed and Least-Squares Procedures for Flexible Rotor Balancing by the Influence Coefficient Method," Journal of Engineering for Industry, ASME Trans., Series B, Vol. 96, No. 2, May 1974, pp 633 - 643.

5. Badgley, R.H., "The Potential Impact of Multiplane-Multispeed Balancing on Gas Turbine Production and Overhaul Costs," ASME Paper No. 74-GT-96, presented at the ASME Gas Turbine Conference and Products Show, Zurich, Switzerland, April 2, 1974.

6. Badgley, R.H., "Recent Developments in Multiplane-Multispeed Balancing of Flexible Rotors in the United States," presented at the Symposium on Dynamics of Rotors, IUTAM, Lyngby, Denmark, August 12, 1974.

7. Badgley, R.H., "Implications of Multiplane-Multispeed Balancing for Future Turbine Engine Design and Cost," Paper presented at the 1974 Aerospace Engineering & Manufacturing Meeting of the Society of Automotive Engineers, September 30 - October 4, 1974, San Diego, California.

8. Rieger, N.F., and Badgley, R.H., "Flexible Rotor Balancing of a High-Speed Gas Turbine Engine," SAE Paper No. 720741, presented at SAE National Combined Farm, Construction & Industrial Machinery and Power Plant Meeting, Milwaukee, Wisconsin, September 11-14, 1972.

9. Badgley, R.H., and Rieger, N.F., "The Effects of Multiplane Balancing on Flexible Rotor Whirl Amplitudes," SAE Paper No. 730102, presented at SAE International Automotive Engineering Congress, Detroit, Michigan, January 8-12, 1973.

10. Cundiff, R.A., Badgley, R.H., and Reddecliff, J., "Design, Manufacture, and Operation of a Dynamic Simulator for Testing Advanced Small Gas Turbine Engine Components," paper presented at the Symposium on Propulsion System Structural Integration and Engine Integrity, Monterey, California, September 6, 1974.

11. Badgley, R.H., and Tessarzik, J.M., "Balancing of High Speed Interconnect Shafting for Operation Above Multiple Bending Critical Speeds," AHS Paper No. 873, presented at the 30th Annual National Forum of the American Helicopter Society, Washington, D.C., May 1974.

12. Goodman, T.P., "A Least-Squares Method for Computing Balance Corrections," Journal of Engineering for Industry, Trans. ASME, Series B, Vol. 86, No. 3, August 1964, pp 273-279.

13. Rieger, N.F., "Balancing High-Speed Rotors to Reduce Vibration Levels," paper presented at ASME Design Conference, Chicago, May 11, 1972.

14. Lund, J.W., and Tonnesen, J., "Experimental and Analytic Investigation of High-Speed Rotor Balancing - Phase I," Department of Machine Design Technical University of Denmark, Research Report No. FR-8, Project No. FP-4, December 1970.

15. Lund, J.W., and Tonnesen, J., "Analysis and Experiments on Multiplane Balancing of Flexible Rotors," Journal of Engineering for Industry, ASME Trans., Series B, Vol. 94, No. 1, February 1972, p 233.

16. Tonnesen, J., "Experimental Investigation of High-Speed Rotor Balancing," Department of Machine Design Technical University of Denmark, Research Report No. FR-9, December 1972.

17. Tonnesen, J., "Further Experiments on Balancing of a High-Speed Flexible Rotor," Journal of Engineering for Industry, ASME Trans., Series B, Vol. 96, No. 2, May 1974, pp 431-440.

18. "Proposed Method of Rotary Dynamic Balancing by Laser," Technical Support Package, Brief 67-10452, Technology Utilization Office, Marshall Space Flight Center, Alabama.

19. Damon, W.E., "Research on Laser Balancing of Rotating Turbine Components," AFML-TR-69-206, Wright-Patterson Air Force Base, Ohio, 1969.

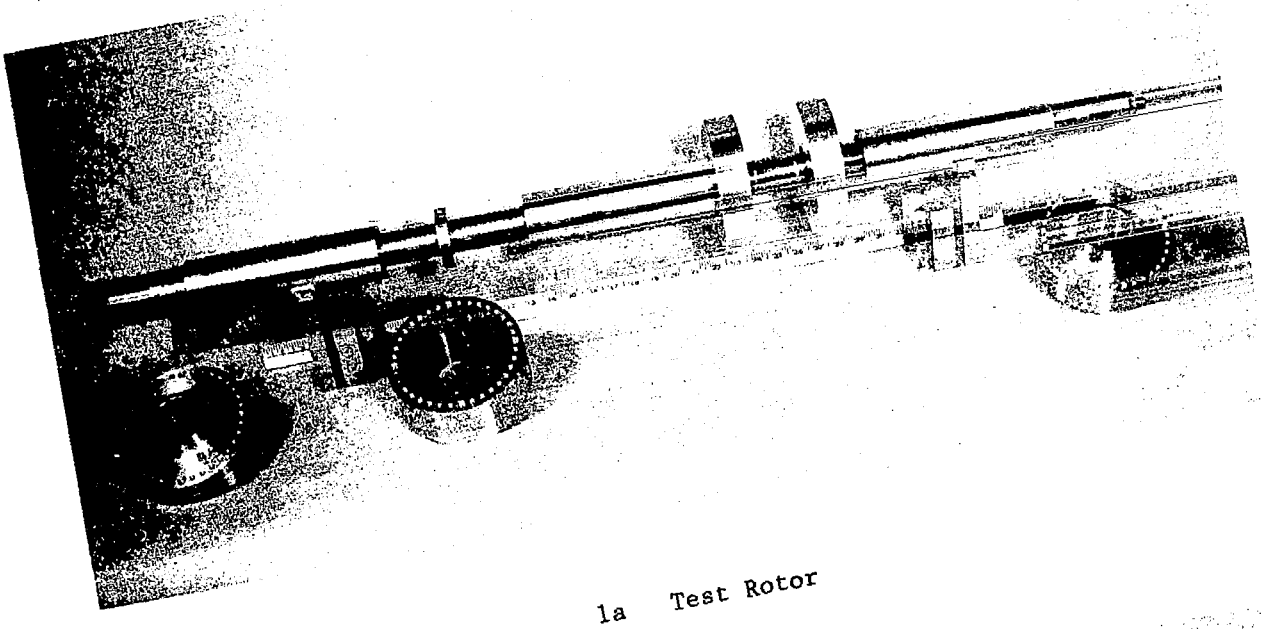

1a Test Rotor

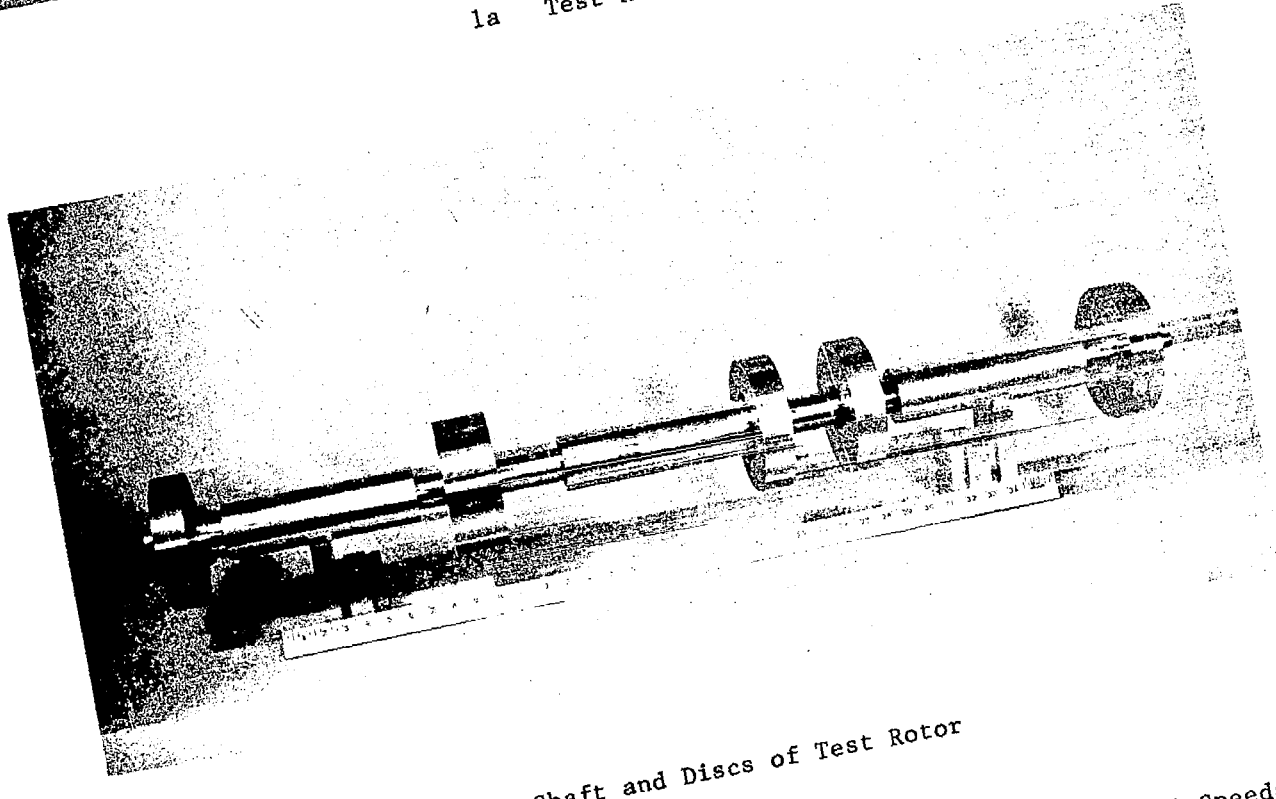

1b Shaft and Discs of Test Rotor

Fig. 1 Test Rotor Designed For Operation Through Four Bending Critical Speeds I
Demonstration of High-Speed Multiplane Flexible-Rotor Balancing System

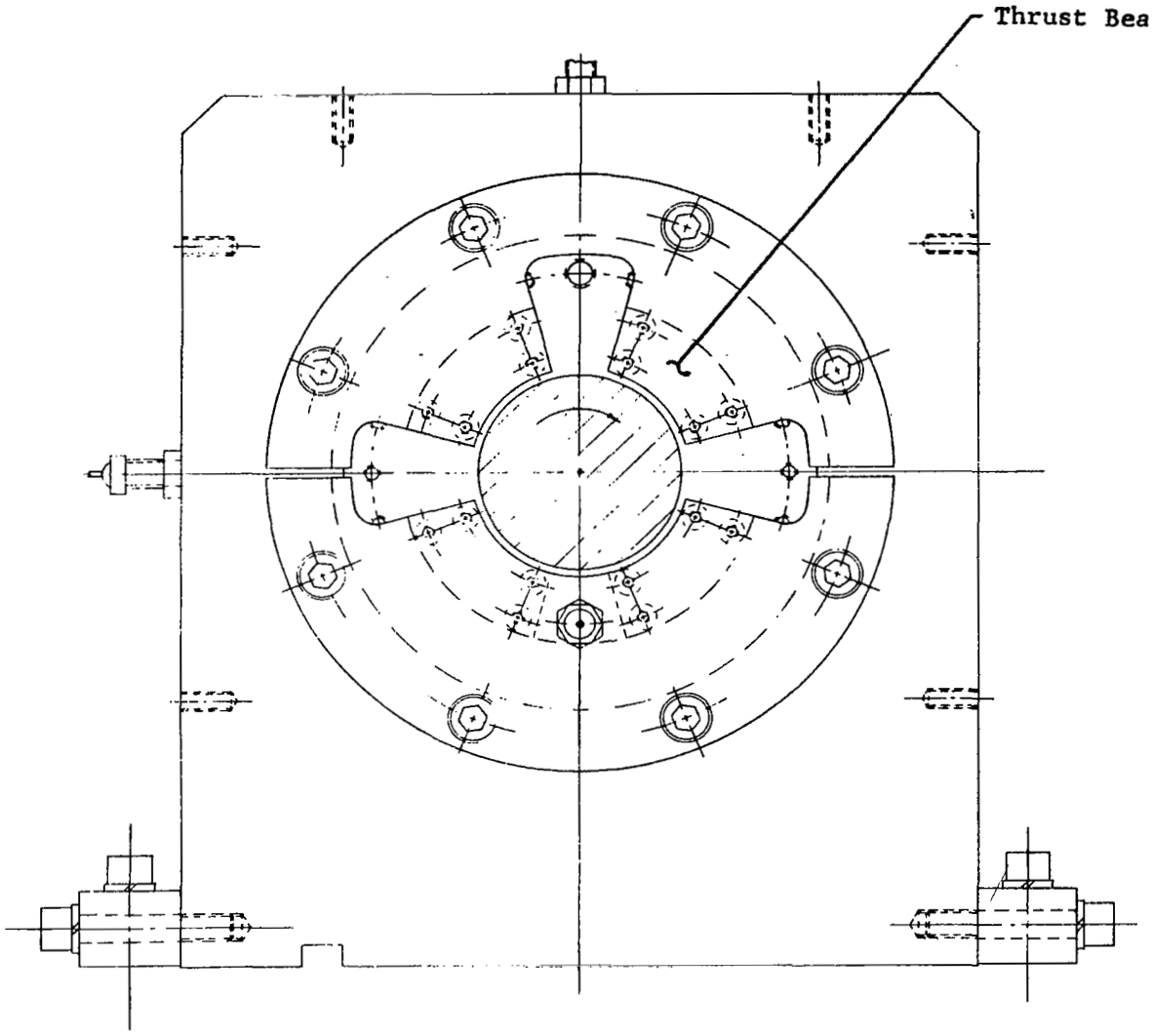

Section B-B
(From Fig. 4)

Fig. 2a Thrust Bearing Assembly Drawing of Flexible Rotor Test Rig with Rigid Bearing Pedestals

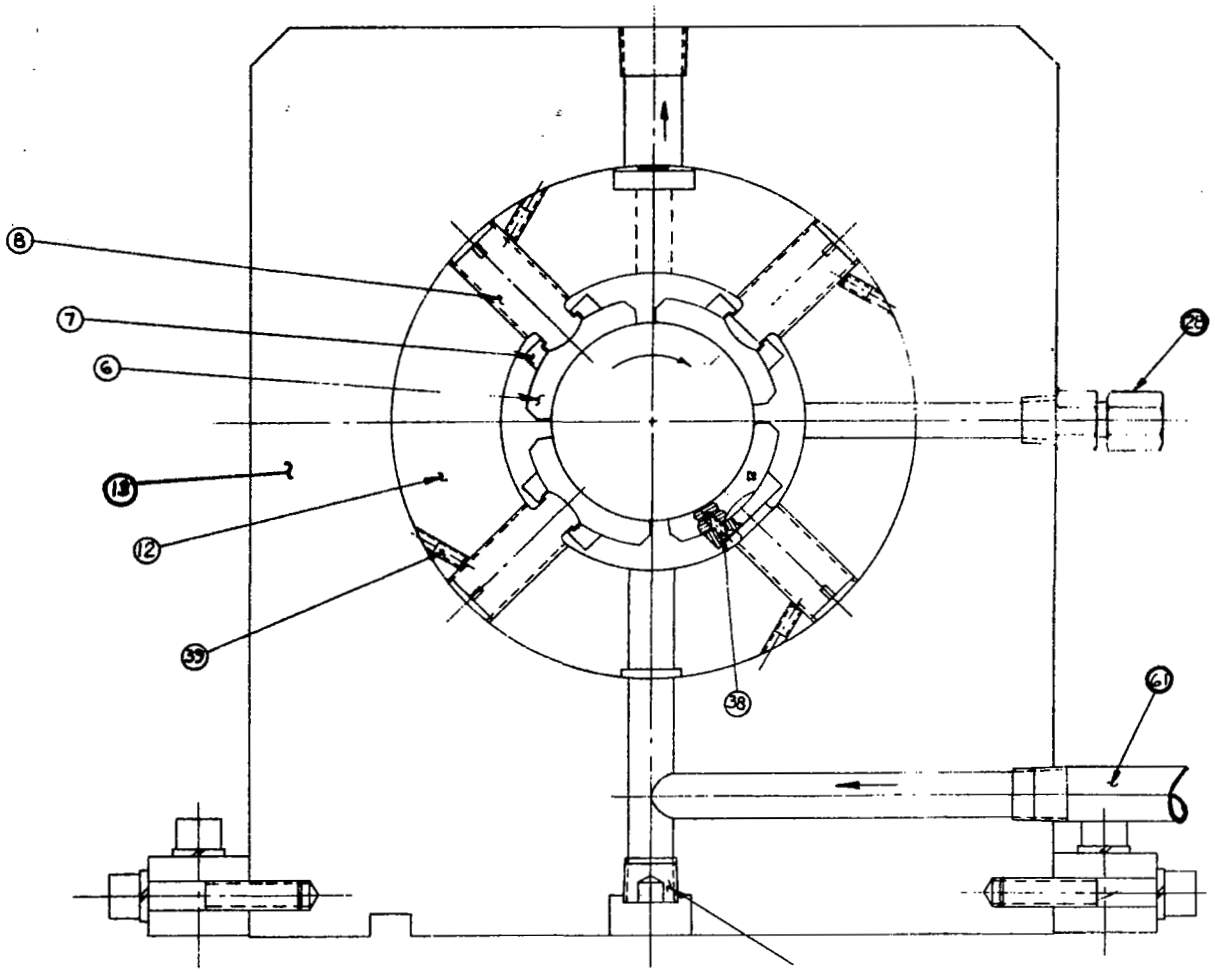

Section C-C
(From Fig. 4)

Fig. 2b Journal Bearing Assembly Drawing of Flexible Rotor Test Rig with Rigid Bearing Pedestals

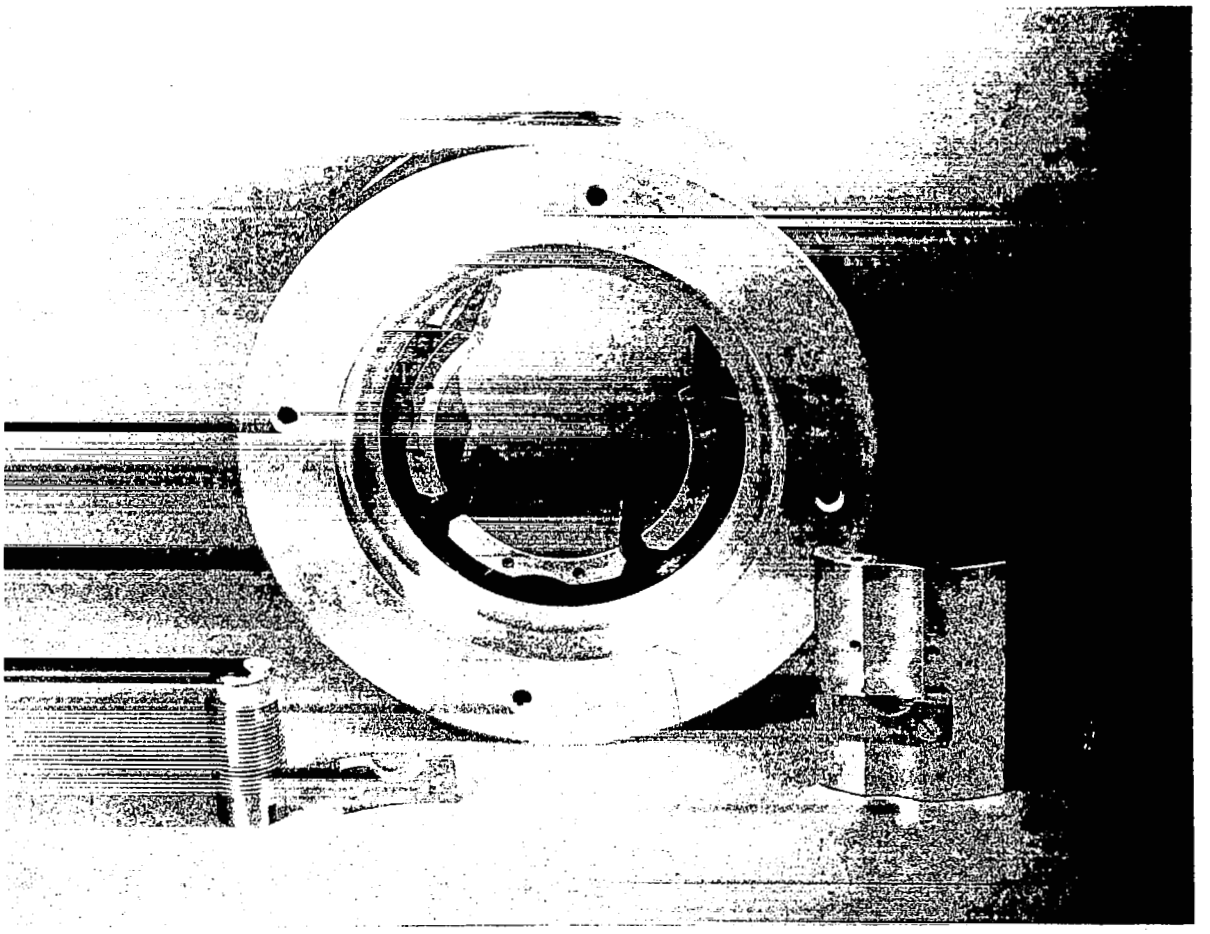

Fig. 3 Tilting-Pad Journal Bearing for Test Rig Rotor

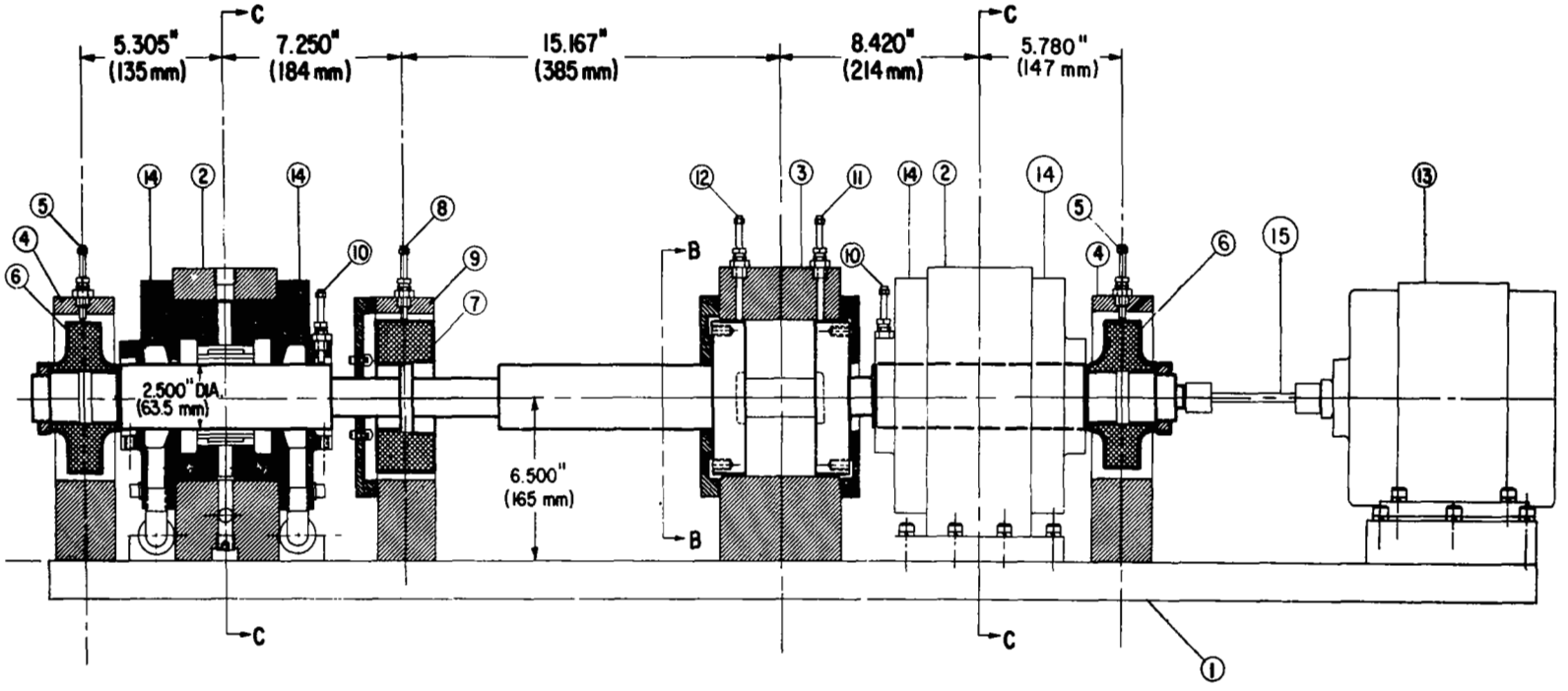

Fig. 4 Assembly Drawing of Flexible-Rotor Test Rig
(Rigid Bearing Supports Shown)

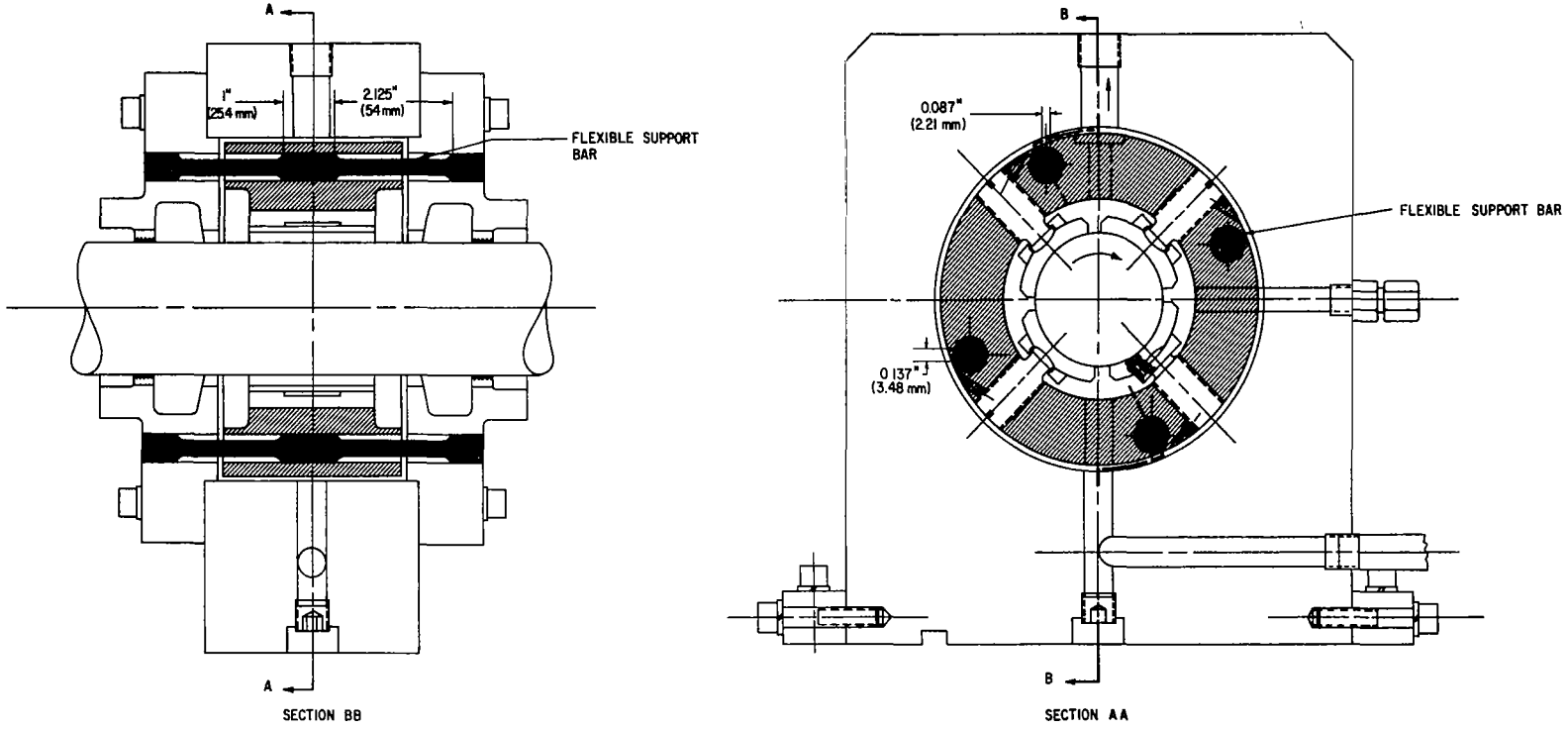

Fig. 5 Flexibly-Mounted Journal Bearing Support Structure

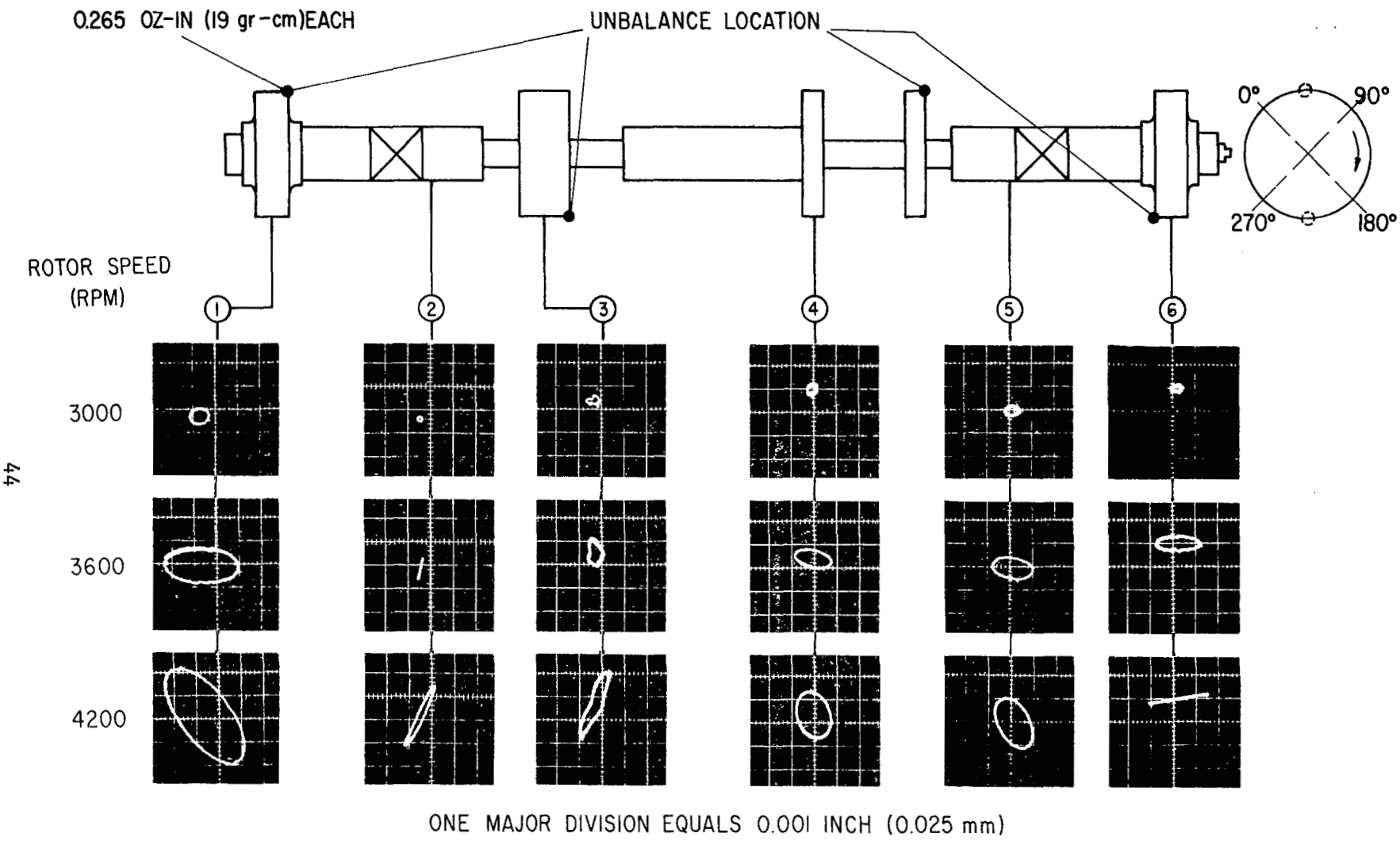

Fig. 6 Test Rotor Orbits at Subcritical Rotor Speeds (Rotor With Initial In-Line, Alternating-Phase Unbalance)

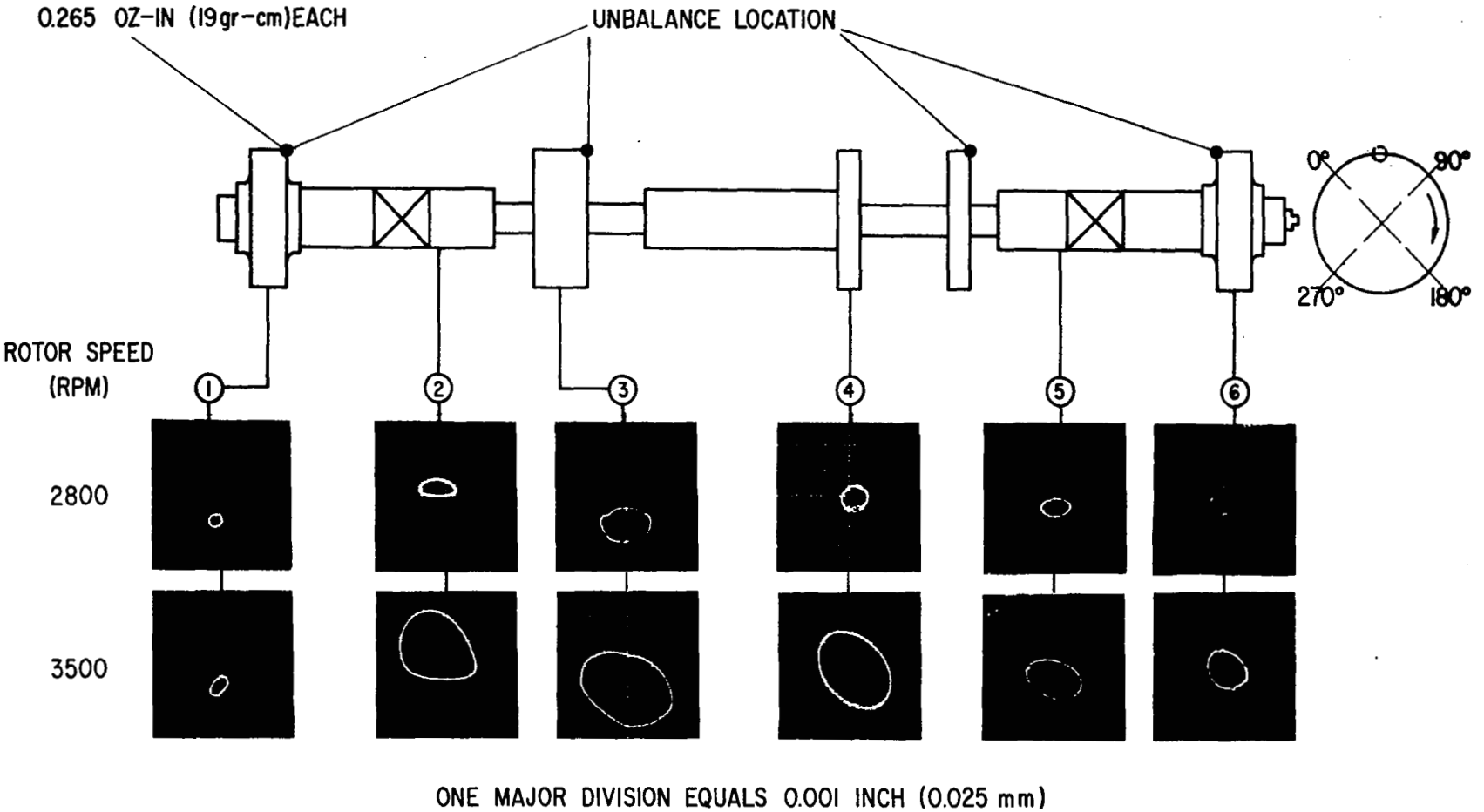

Fig. 7 Test Rotor Orbits at Subcritical Rotor Speeds (Rotor With Initial In-Line, In-Phase Unbalance)

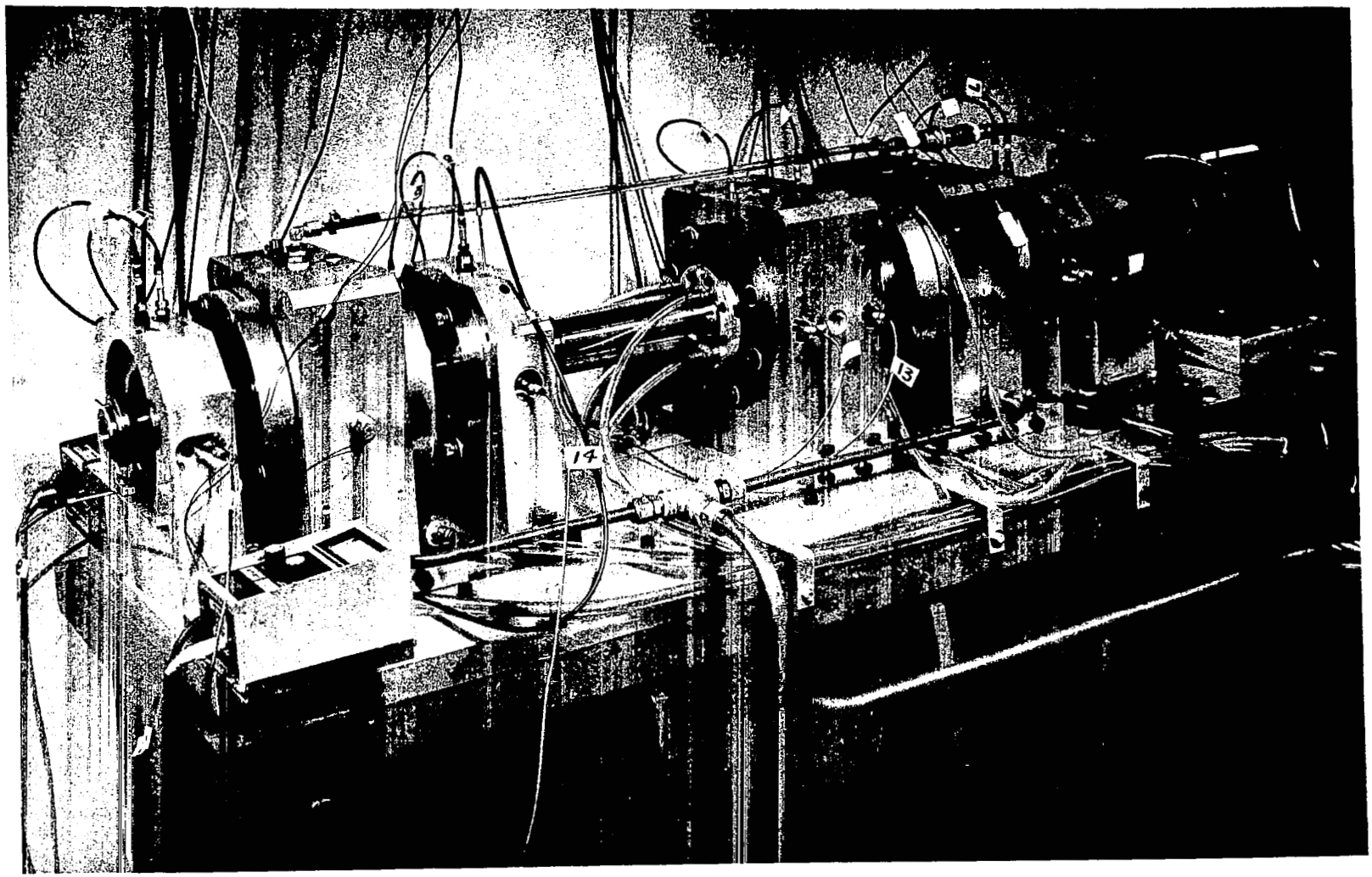

Fig. 8 Test Rig Assembly Used for Demonstration of High-Speed Multiplane Flexible-Rotor Balancing System

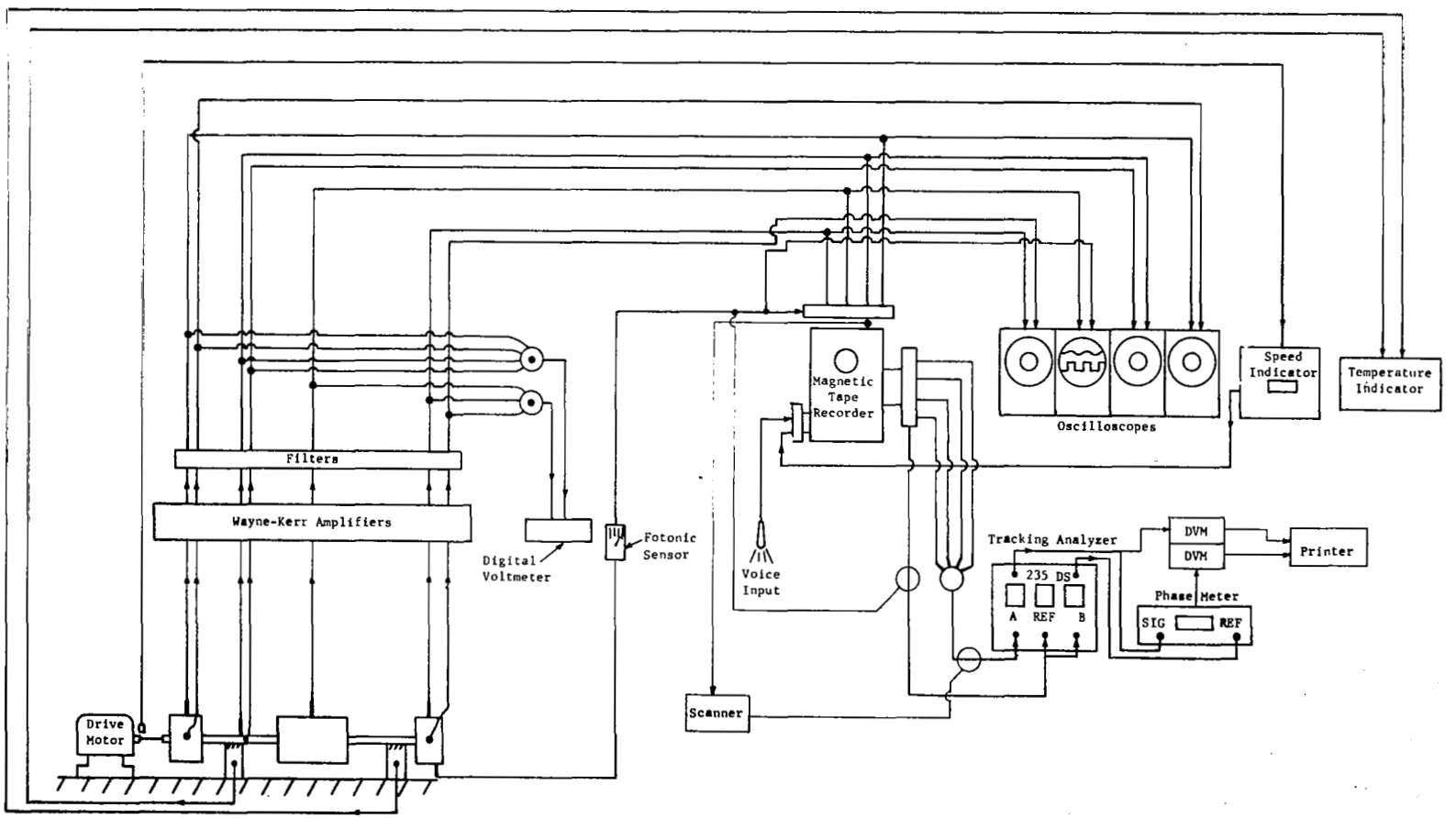

Fig. 9 Schematic of Flexible-Rotor Balancing Instrumentation

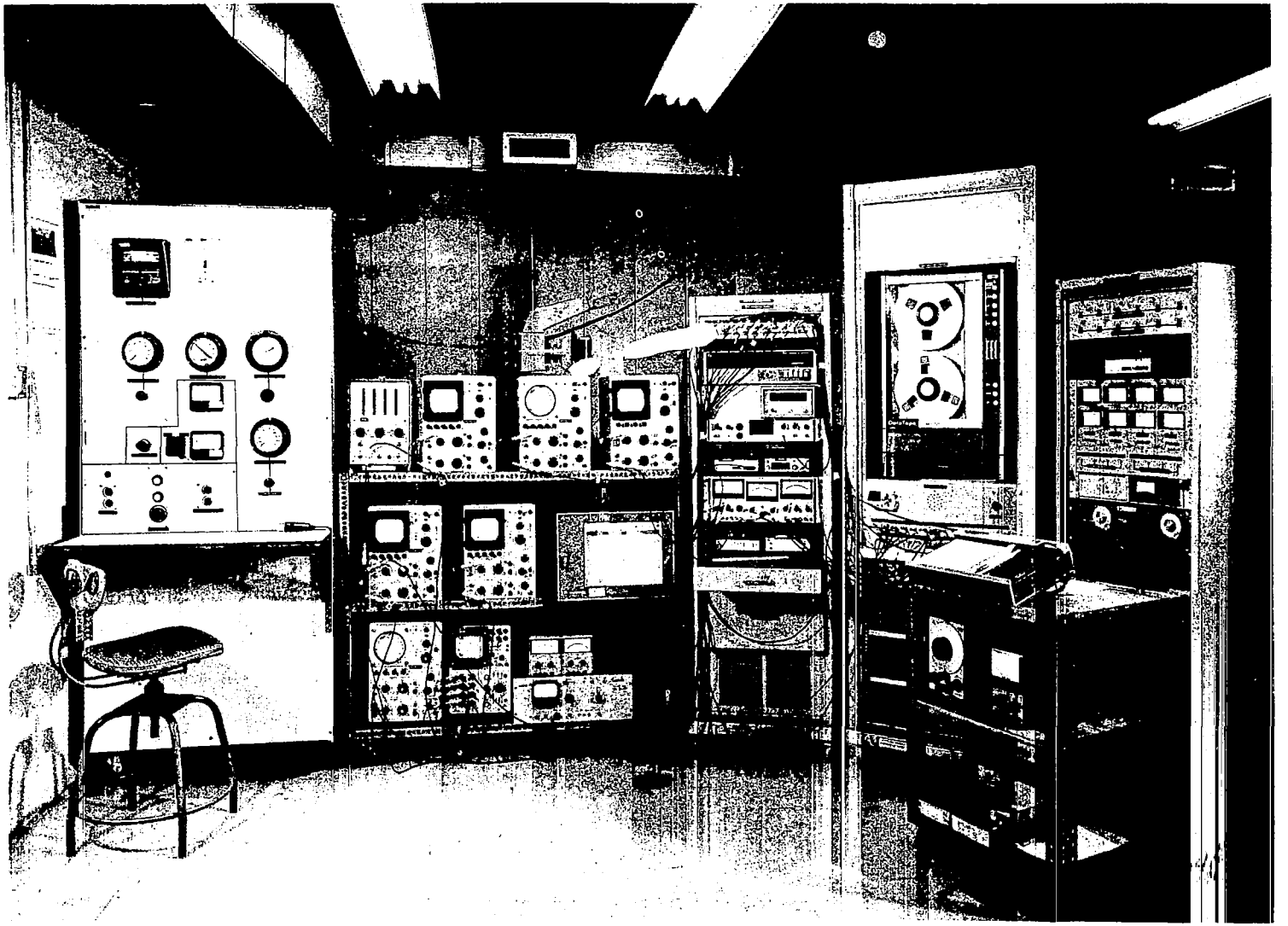

Fig. 10 Test Rig Control Hardware and Data Monitoring and Acquisition Instrumentation Used During High-Speed Multiplane Flexible-Rotor Balancing Tests

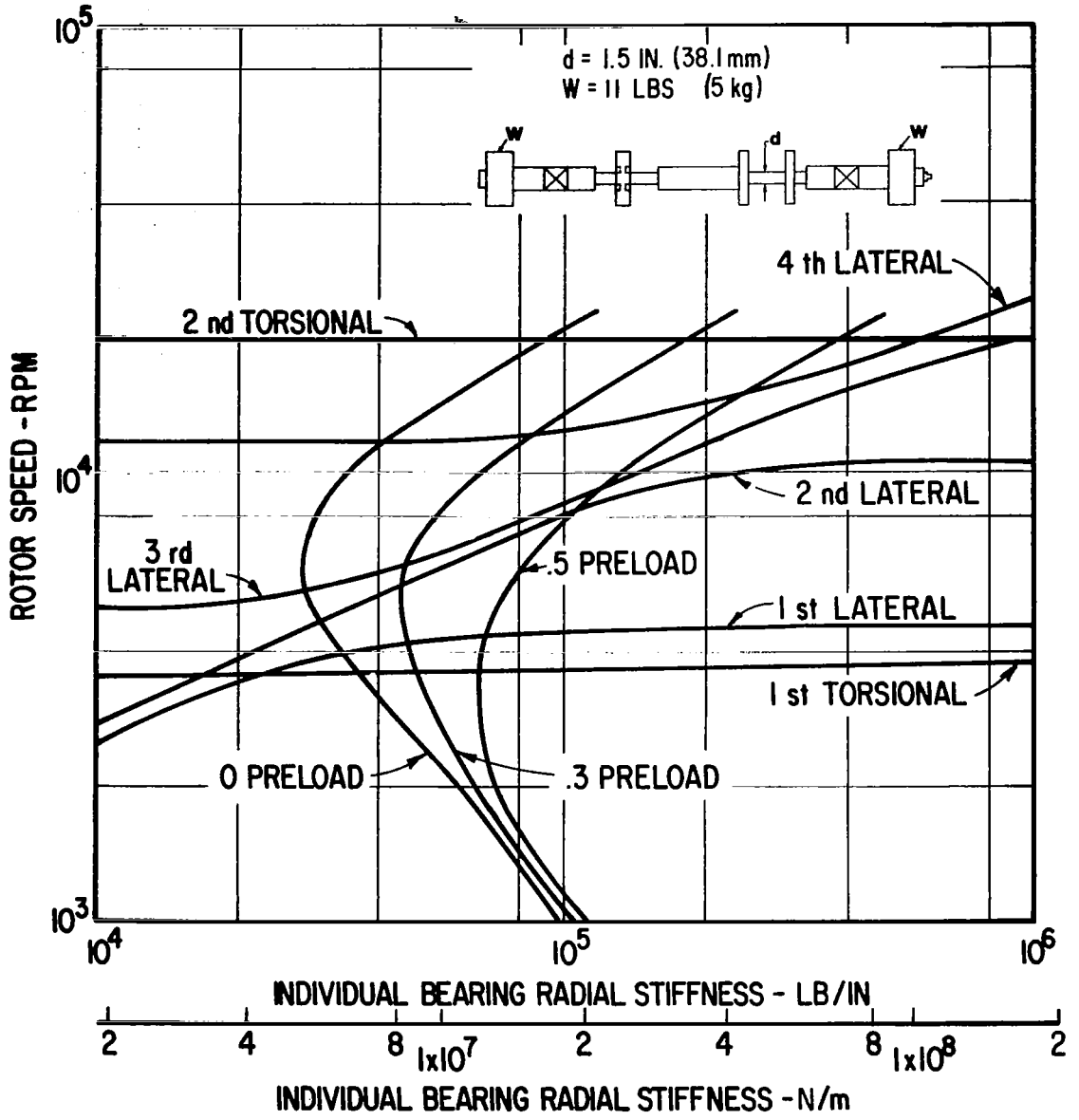

Fig. 11 Calculated Critical Speed Map and Bearing Stiffnesses for Shaft-Bearing System Used During High-Speed Multiplane Flexible Rotor Balancing Tests

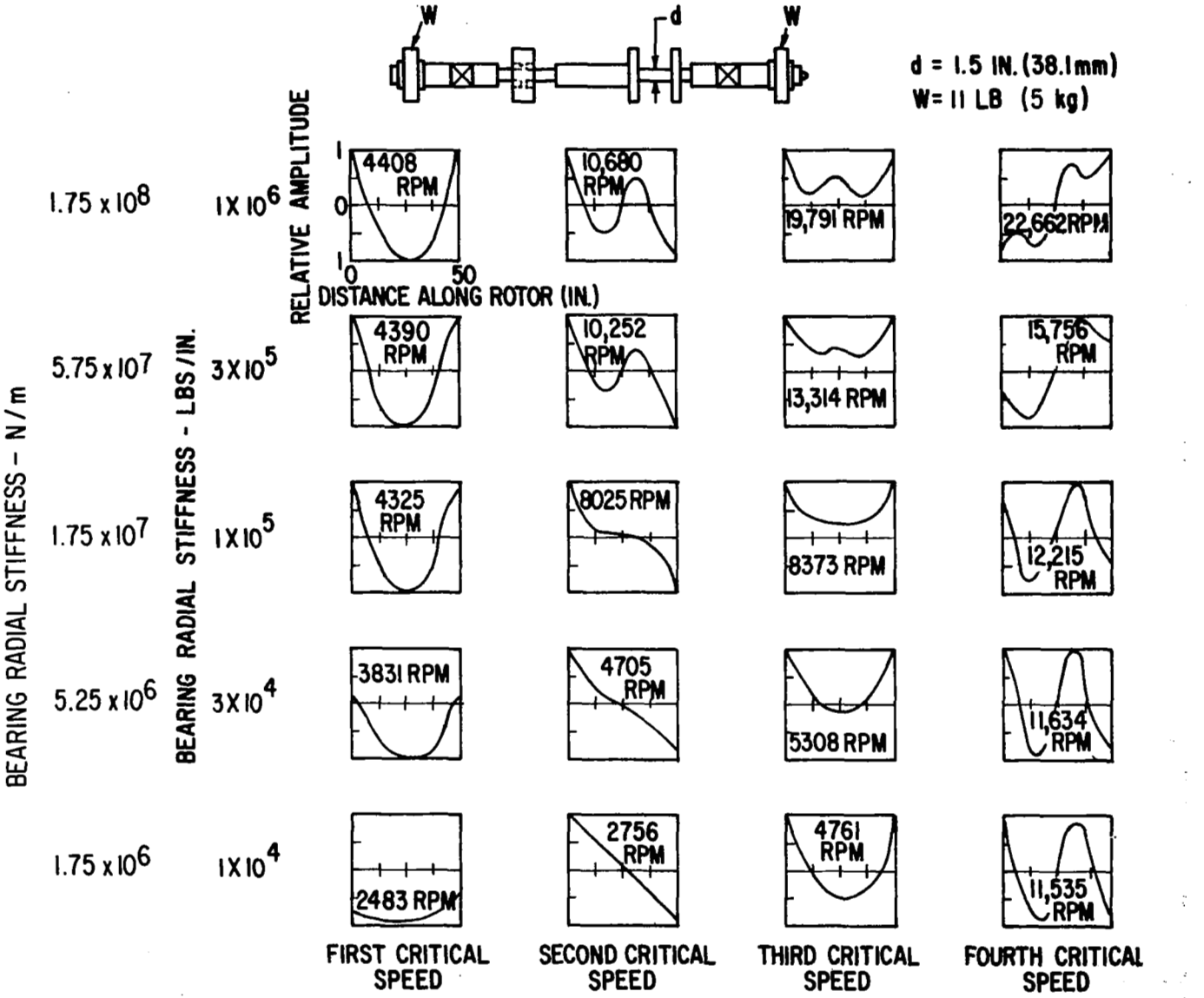

Fig. 12 Calculated Undamped Mode Shapes For Flexible-Rotor Test Rig

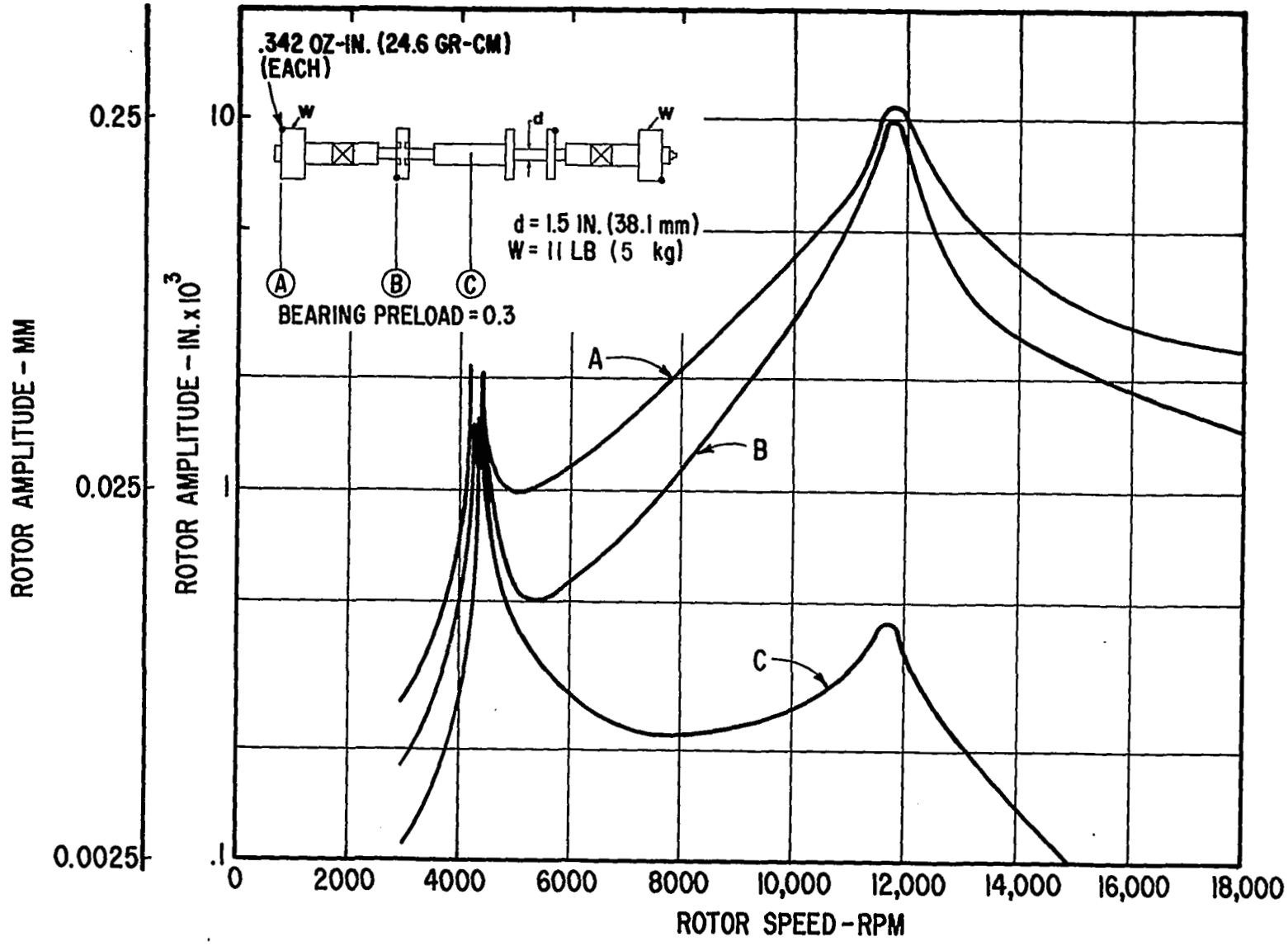

Fig. 13 Calculated Damped Rotor Amplitudes (Peak) at Stations A, B, and C With In-Line, Alternating-Phase Unbalance

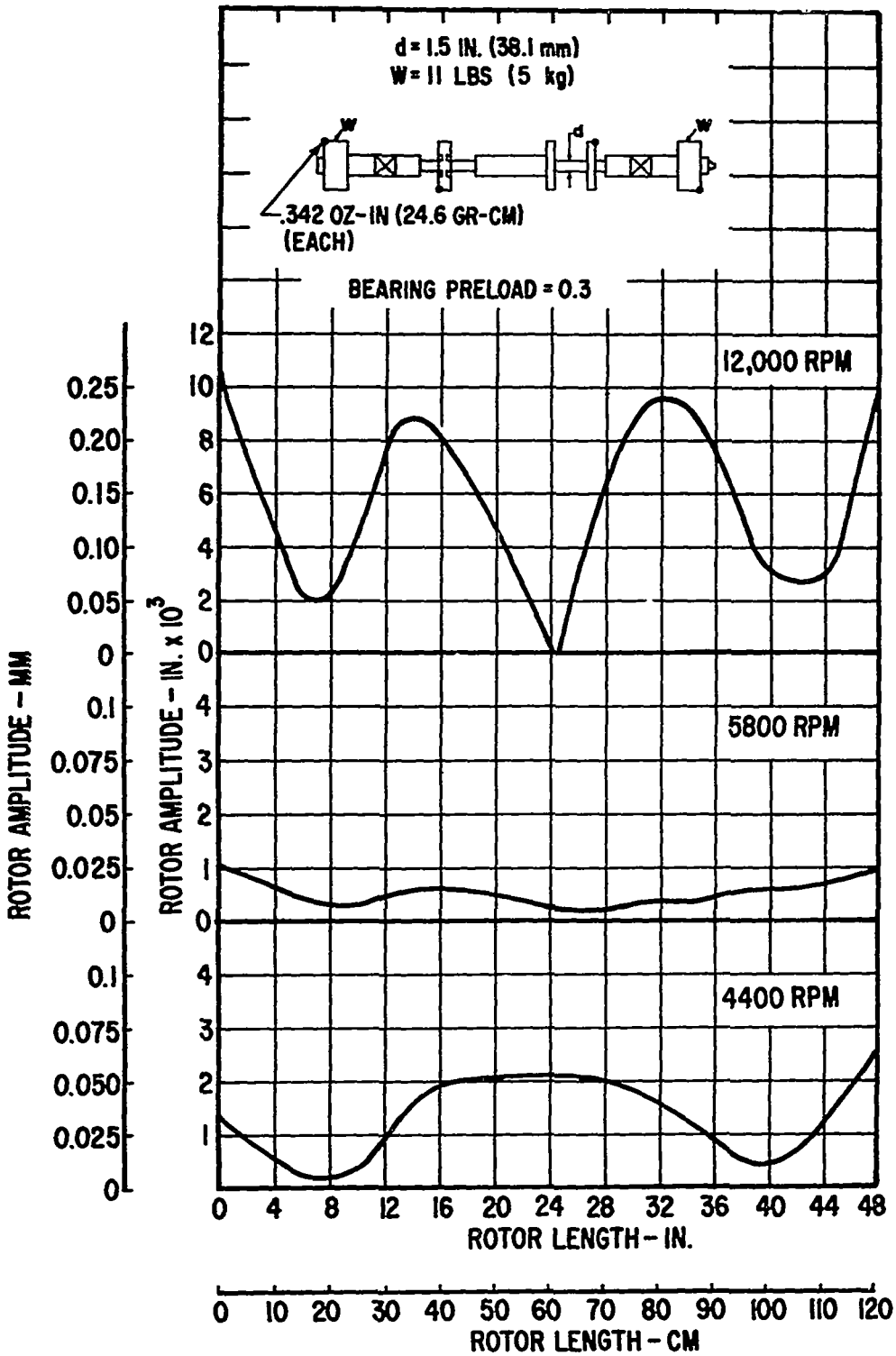

Fig. 14 Calculated Damped Rotor Amplitudes at the First, Third and Fourth Lateral Critical Speeds With In-Line, Alternating-Phase Unbalance and Rigid Bearing Supports

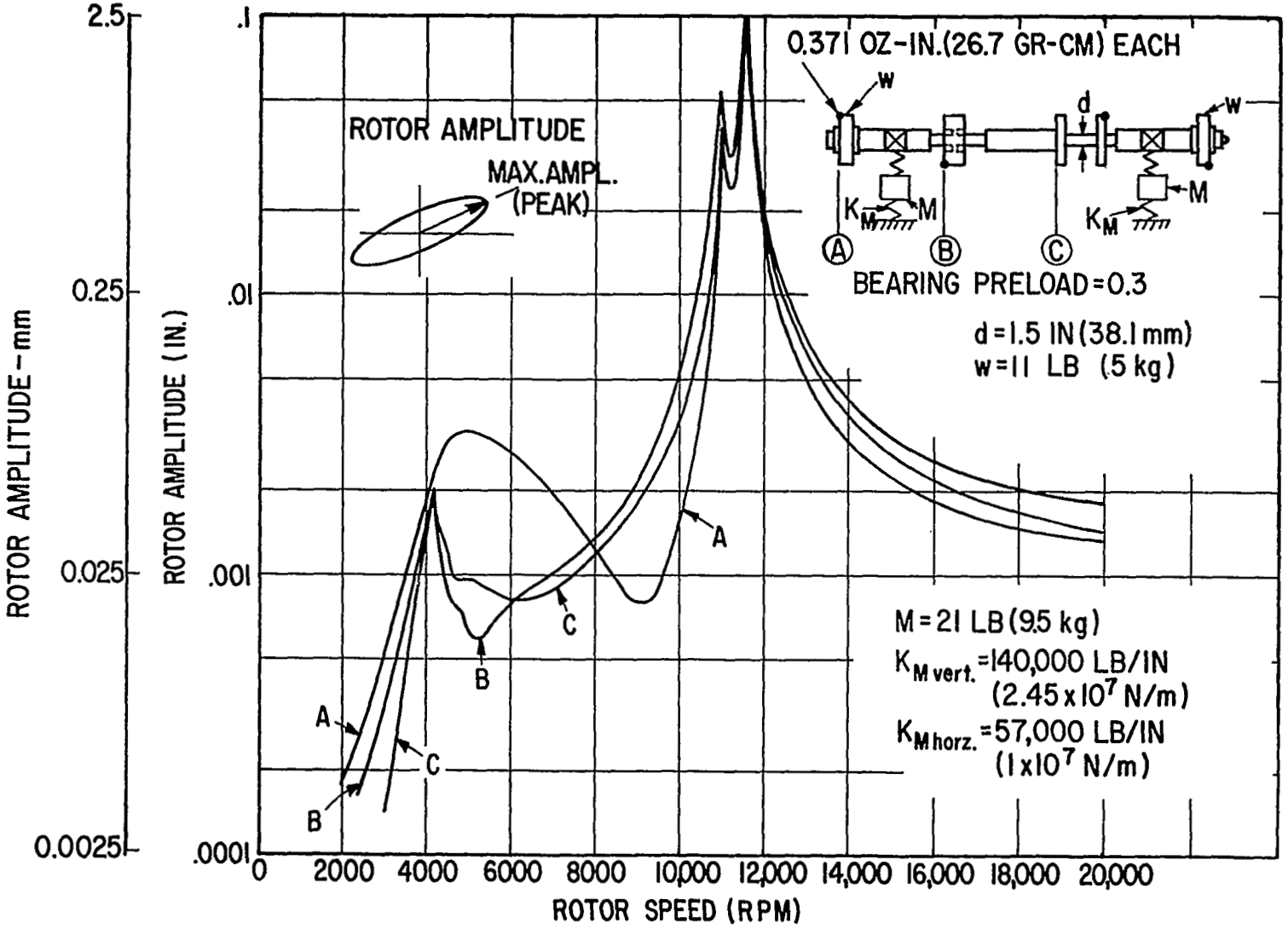

Fig. 15 Calculated Maximum Damped Rotor Amplitudes (Peak) at Stations A, B, and C With In-Line, Alternating-Phase Unbalance and Flexible Bearing Supports

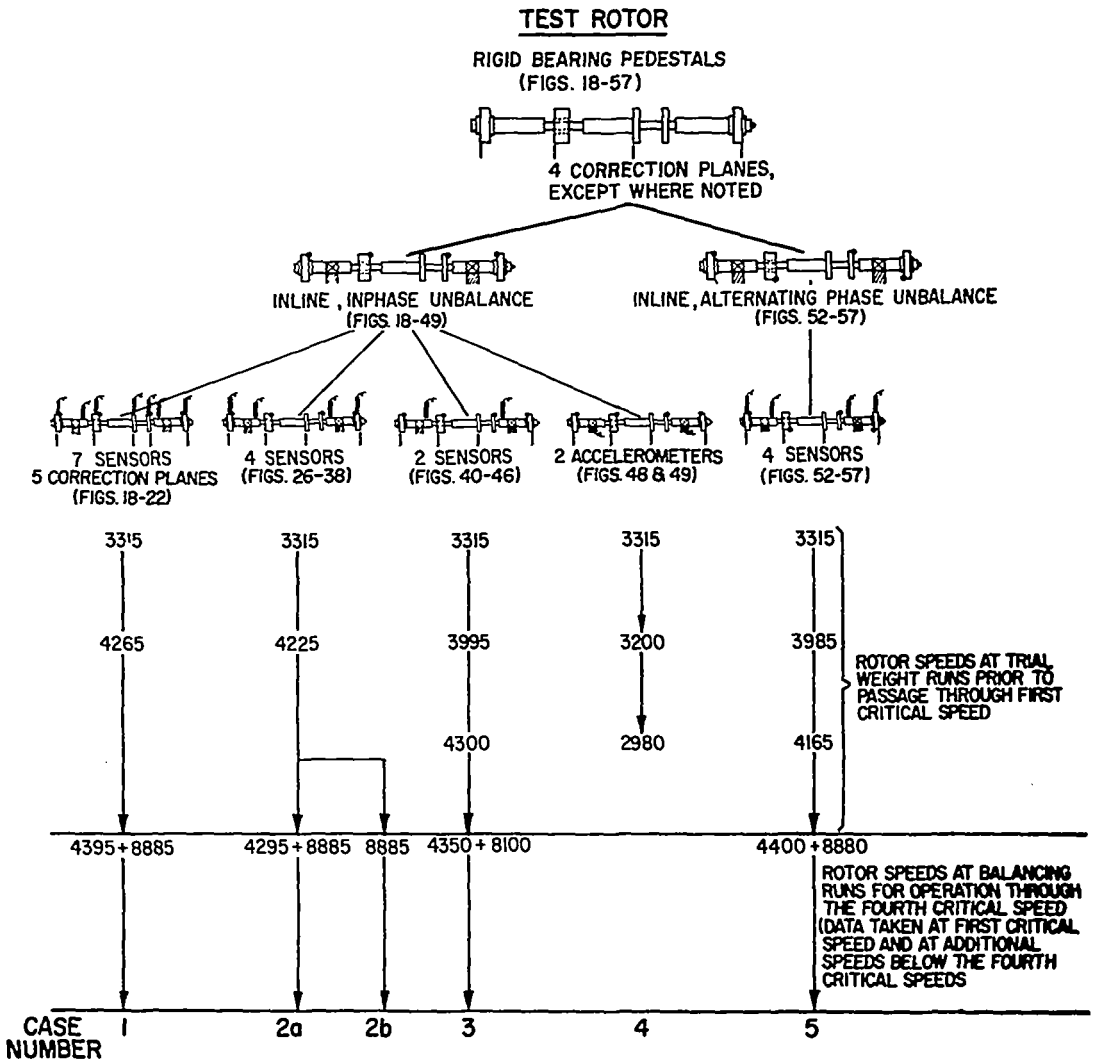

Fig. 16 Test Plan Schematic for Flexible-Rotor Balancing Tests

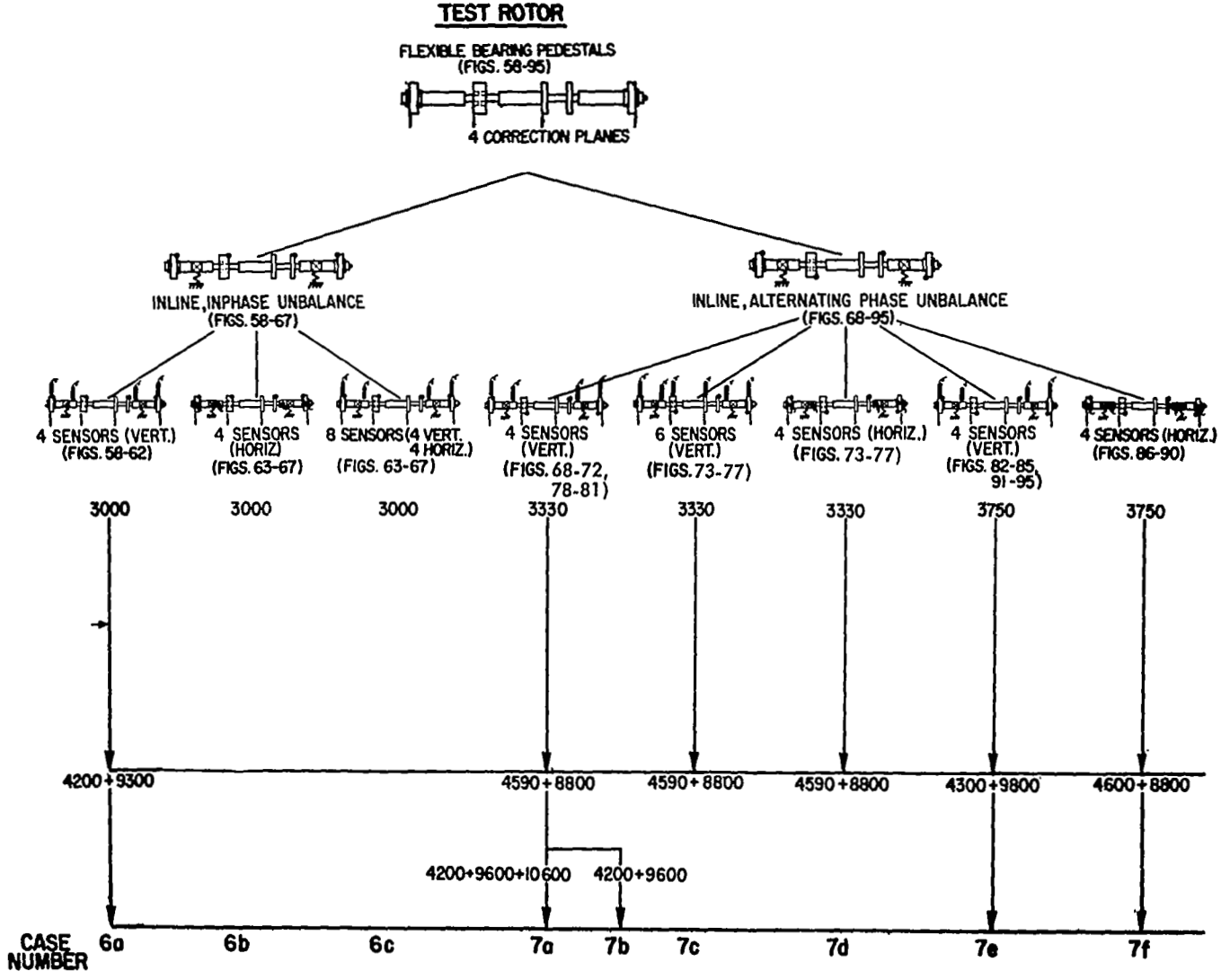

Figure 16 (Continued)

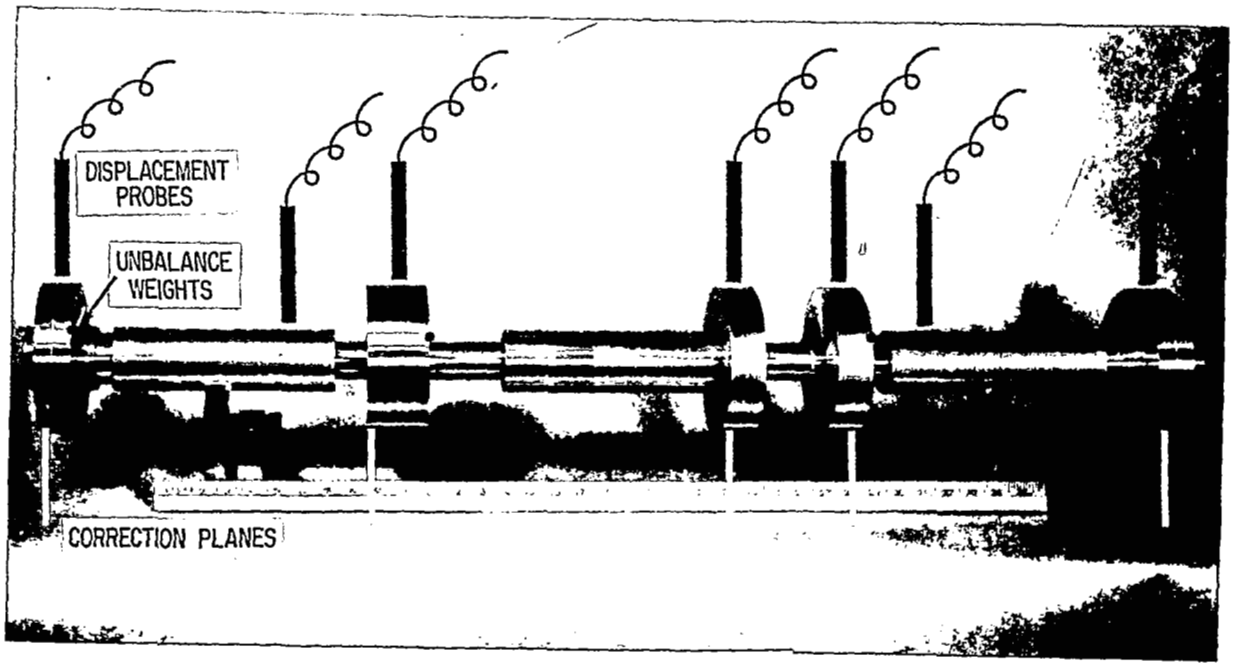

Fig. 17 Shaft-Disc Assembly for Operation Through Four Flexible Critical Speeds, Shown With Location of Seven Displacement Probe Sensors, Five Correction Planes and In-Line, In-Phase Initial Unbalance Location

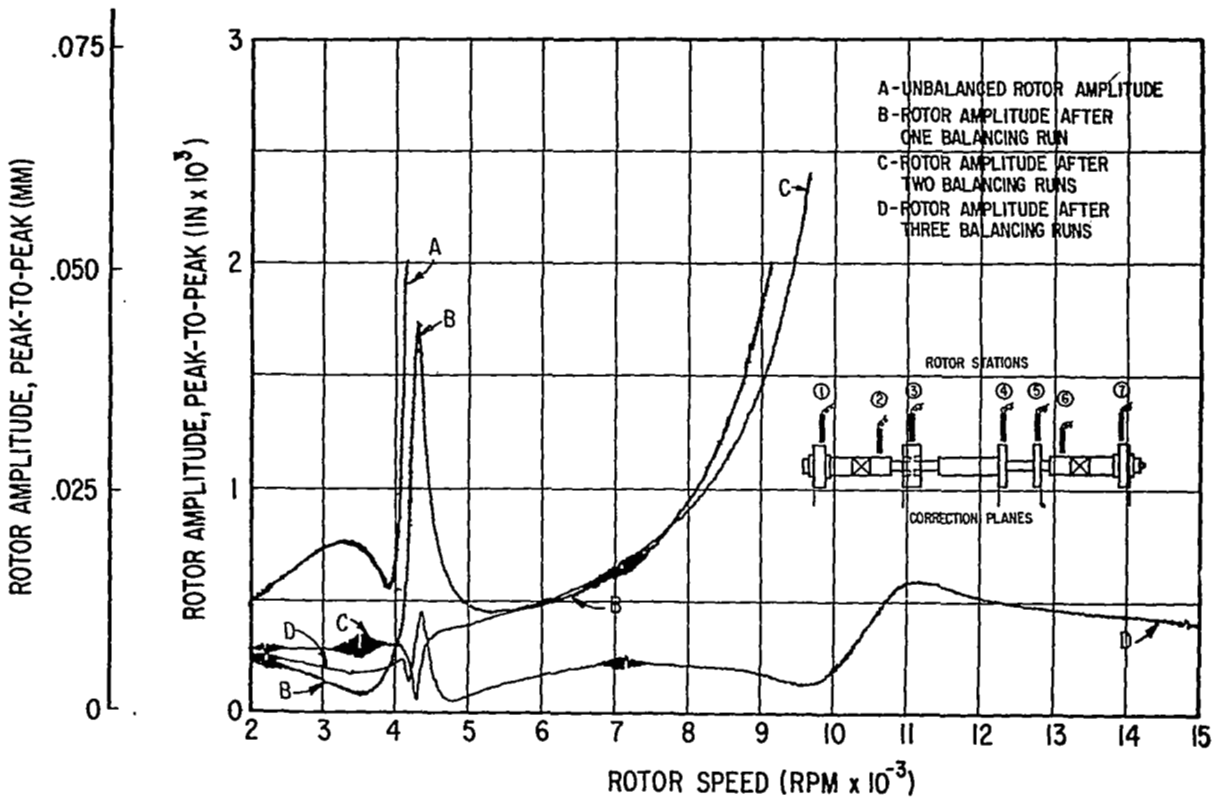

Fig. 18 Vertical Rotor Amplitudes at Station 1 – Initial Condition (In-Line, In-Phase Unbalance) and After Three Consecutive Balancing Runs by the Least Squares Procedure (Seven Probes)

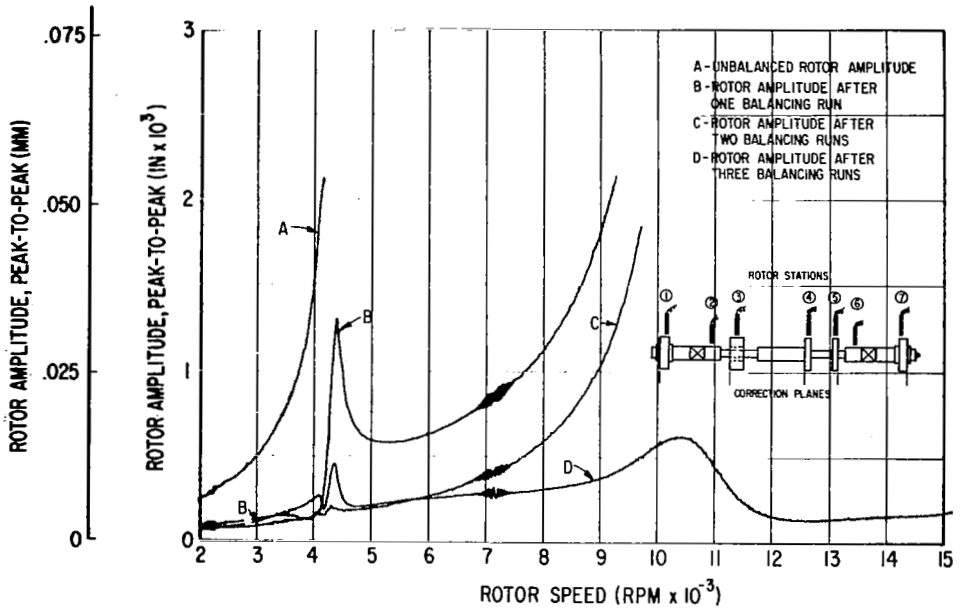

Fig. 19 Vertical Rotor Amplitudes at Station 2 — Initial Condition (In-Line, In-Phase Unbalance) and After Three Consecutive Balancing Runs by the Least Squares Procedure (Seven Probes)

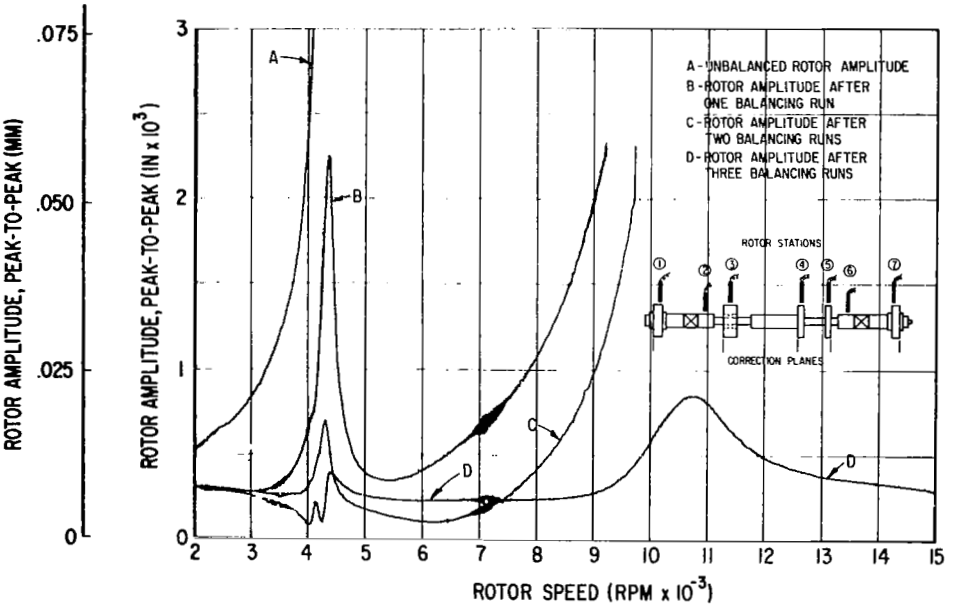

Fig. 20 Vertical Rotor Amplitudes at Station 3 — Initial Condition (In-Line, In-Phase Unbalance) and After Three Consecutive Balancing Runs by the Least Squares Procedure (Seven Probes)

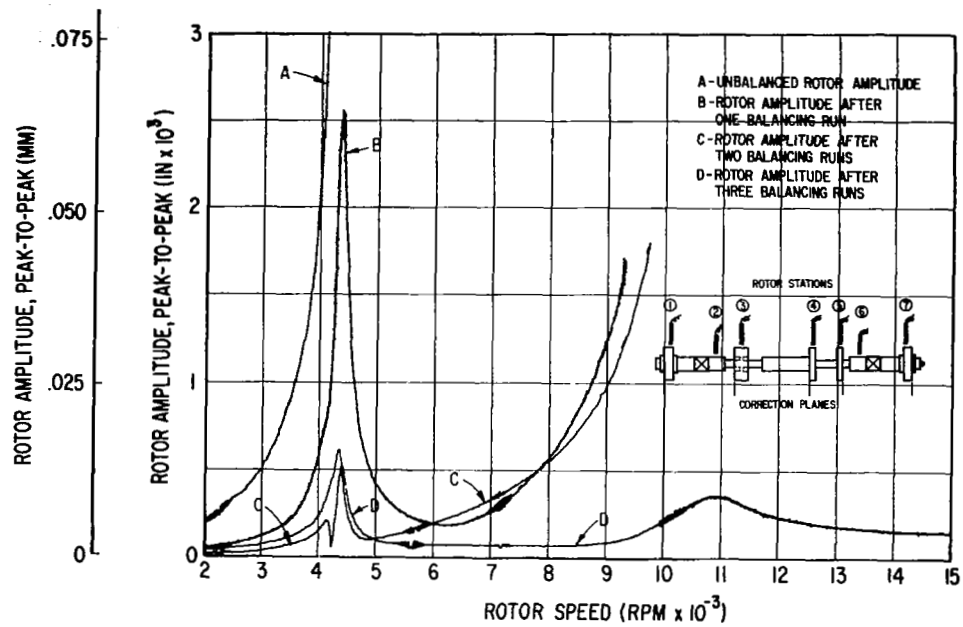

Fig. 21 Vertical Rotor Amplitudes at Station 4 — Initial Condition (In-Line, In-Phase Unbalance) and After Three Consecutive Balancing Runs by the Least Squares Procedure (Seven Probes)

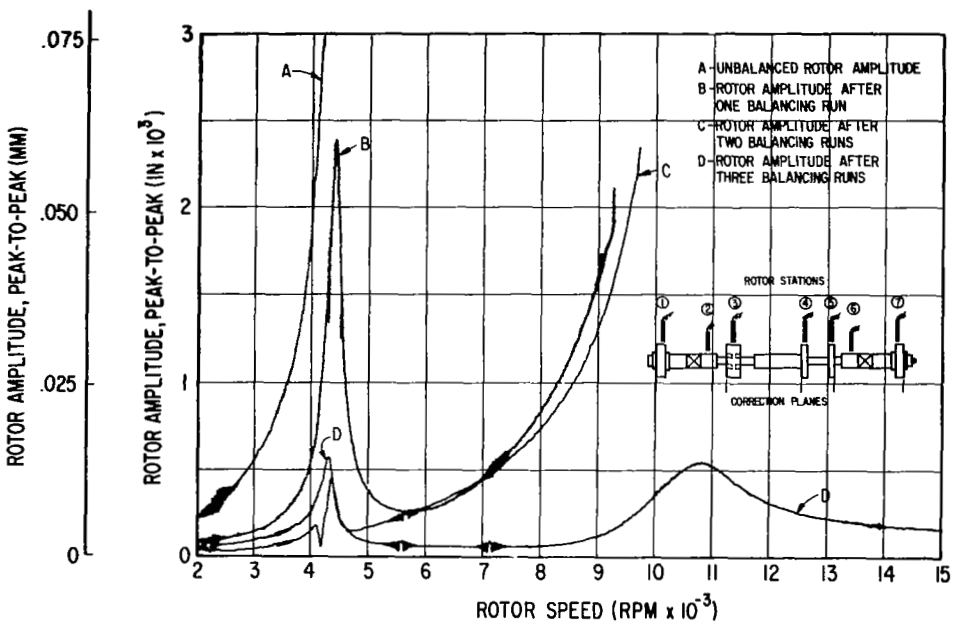

Fig. 22 Vertical Rotor Amplitudes at Station 5 — Initial Condition (In-Line, In-Phase Unbalance) and After Three Consecutive Balancing Runs by the Least Squares Procedure (Seven Probes)

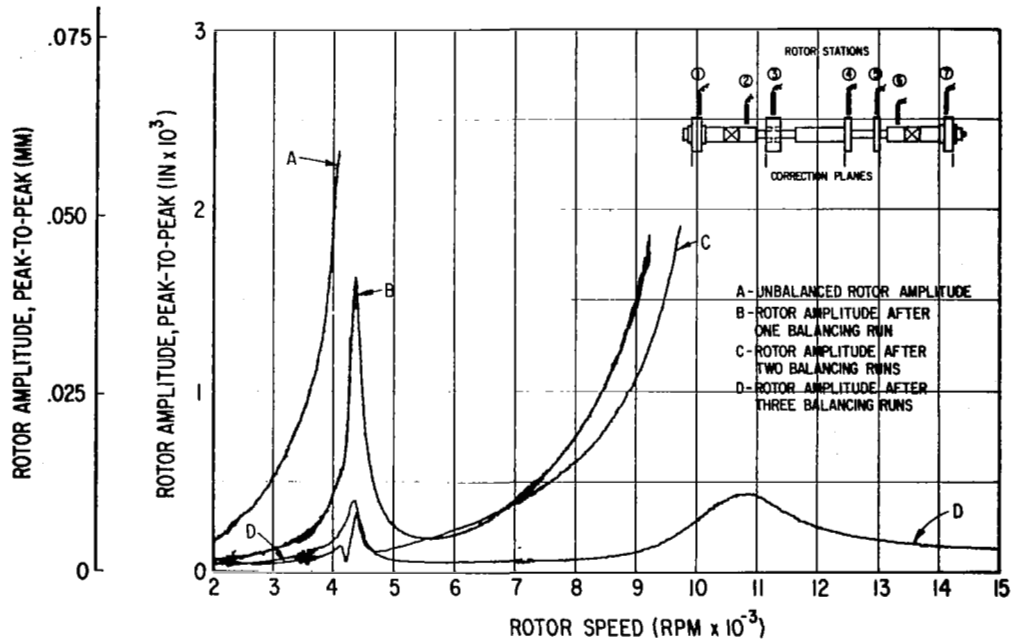

Fig. 23 Vertical Rotor Amplitudes at Station 6 — Initial Condition (In-Line, In-Phase Unbalance) and After Three Consecutive Balancing Runs by the Least Squares Procedure (Seven Probes)

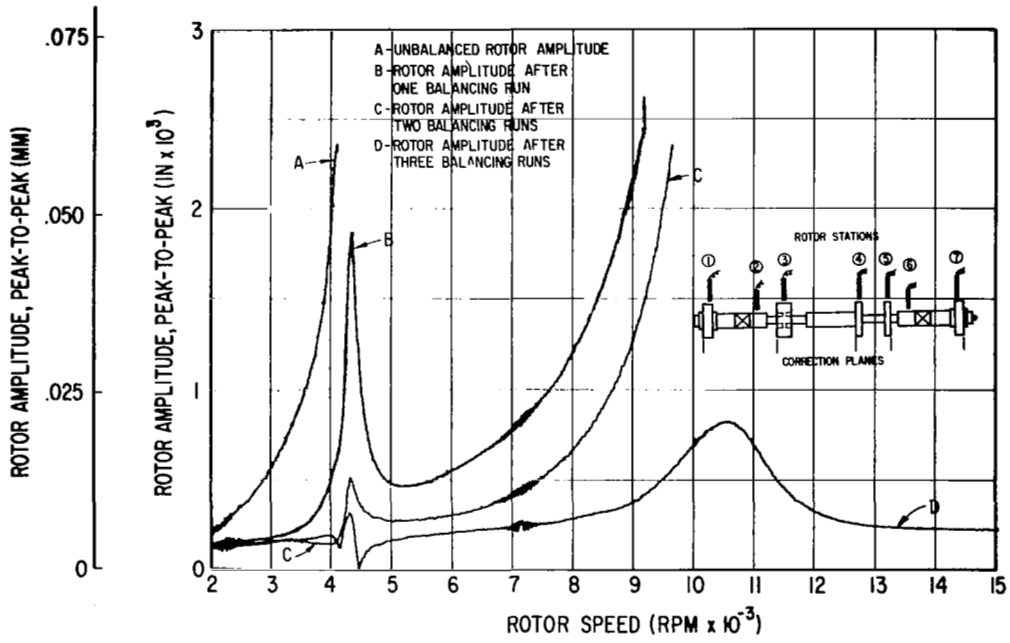

Fig. 24 Vertical Rotor Amplitudes at Station 7 — Initial Condition (In-Line, In-Phase Unbalance) and After Three Consecutive Balancing Runs by the Least Squares Procedure (Seven Probes)

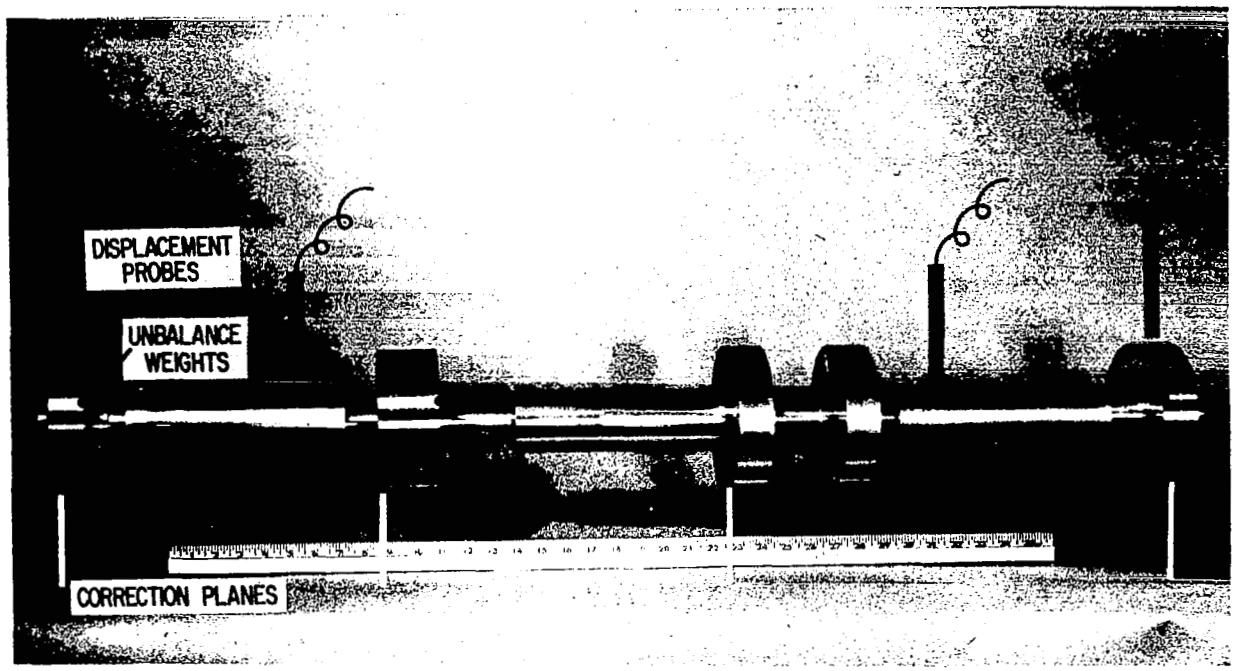

Fig. 25 Shaft-Disc Assembly For Operation Through Four Flexible Critical Speeds, Shown With Location of Four Displacement Probe Sensors, Four Correction Planes and In-Line, In-Phase Initial Unbalance Location

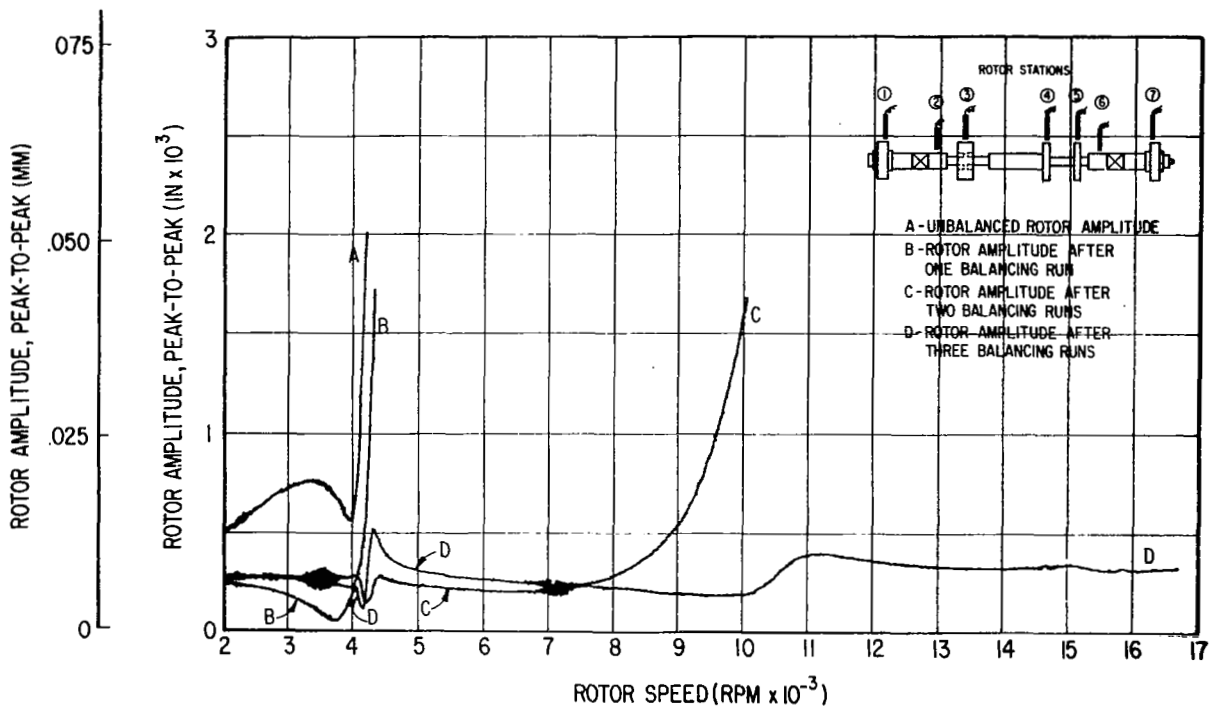

Fig. 26 Vertical Rotor Amplitudes at Station 1 — Initial Condition (In-Line, In-Phase Unbalance) and After Three Consecutive Balancing Runs by the Least Squares Procedure (Four Probes)

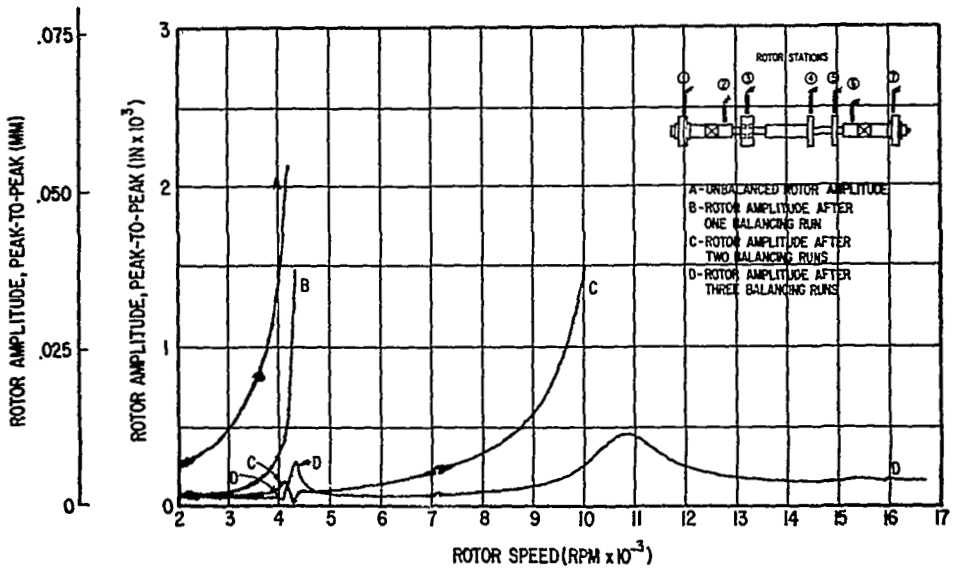

Fig. 27 Vertical Rotor Amplitudes at Station 2 — Initial Condition (In-Line, In-Phase Unbalance) and After Three Consecutive Balancing Runs by the Least Squares Procedure (Four Probes)

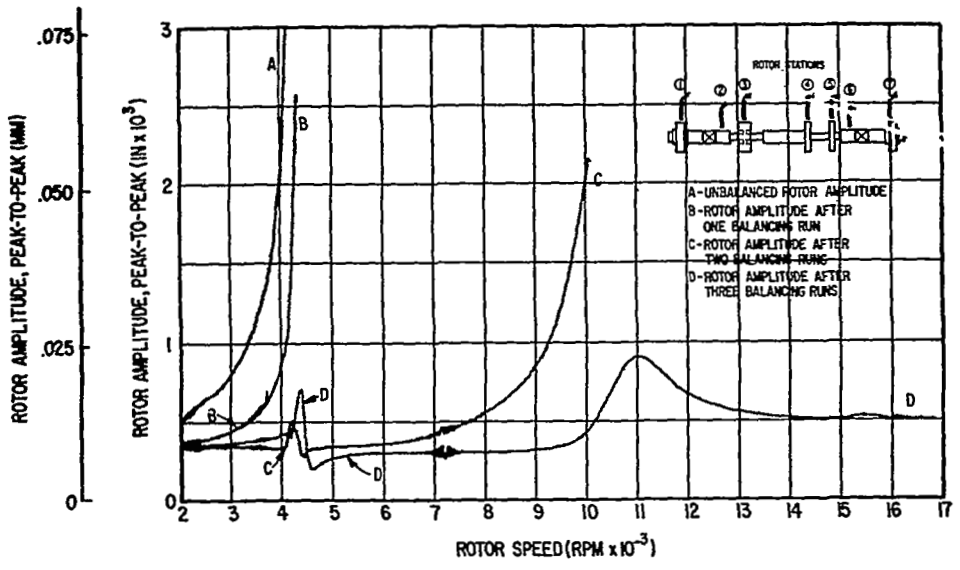

Fig. 28 Vertical Rotor Amplitudes at Station 3 — Initial Condition (In-Line, In-Phase Unbalance) and After Three Consecutive Balancing Runs by the Least Squares Procedure (Four Probes)

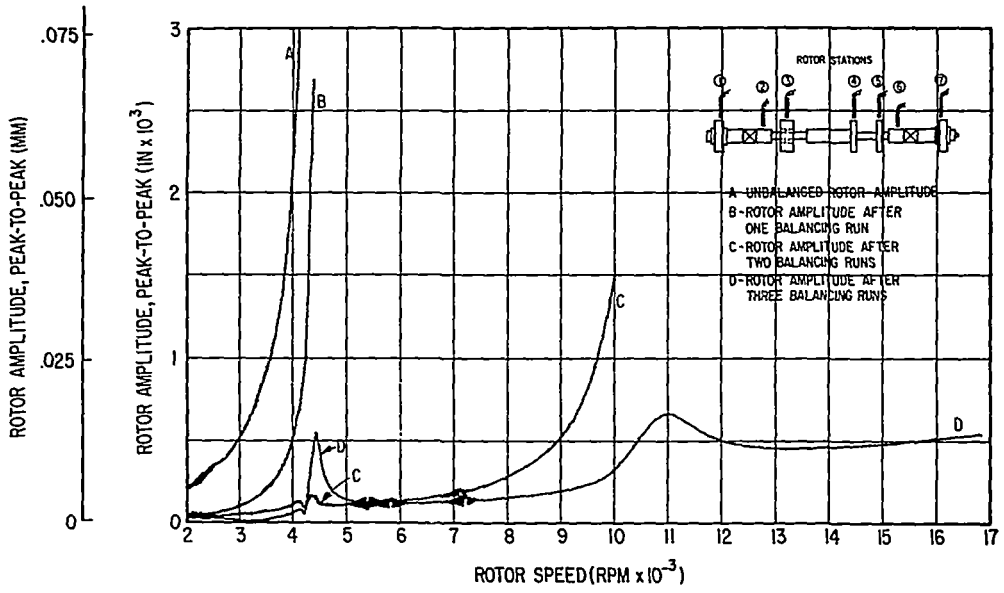

Fig. 29 Vertical Rotor Amplitudes at Station 4 – Initial Condition (In-Line, In-Phase Unbalance) and After Three Consecutive Balancing Runs by the Least Squares Procedure (Four Probes)

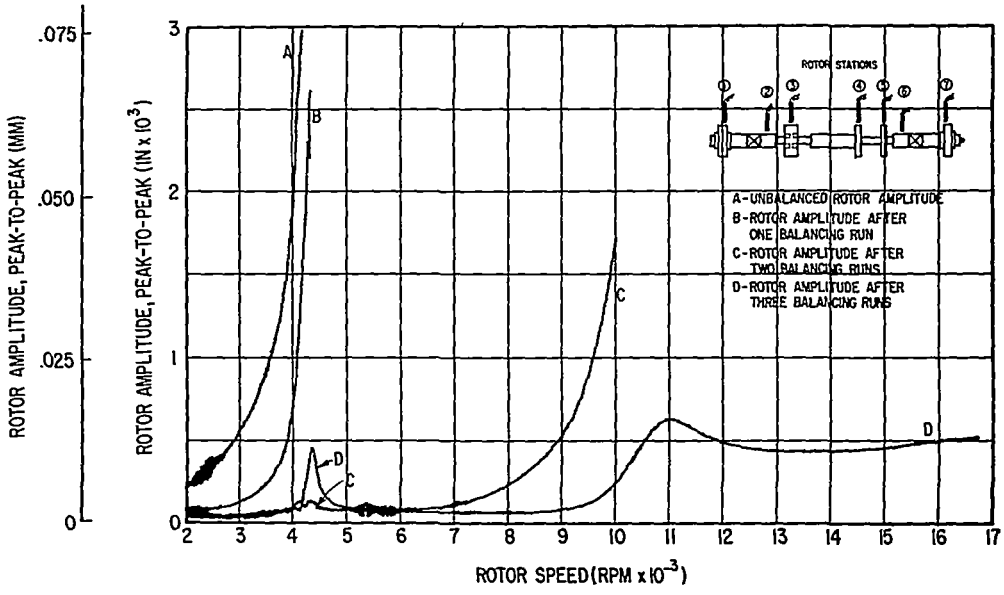

Fig. 30 Vertical Rotor Amplitudes at Station 5 – Initial Condition (In-Line, In-Phase Unbalance) and After Three Consecutive Balancing Runs by the Least Squares Procedure (Four Probes)

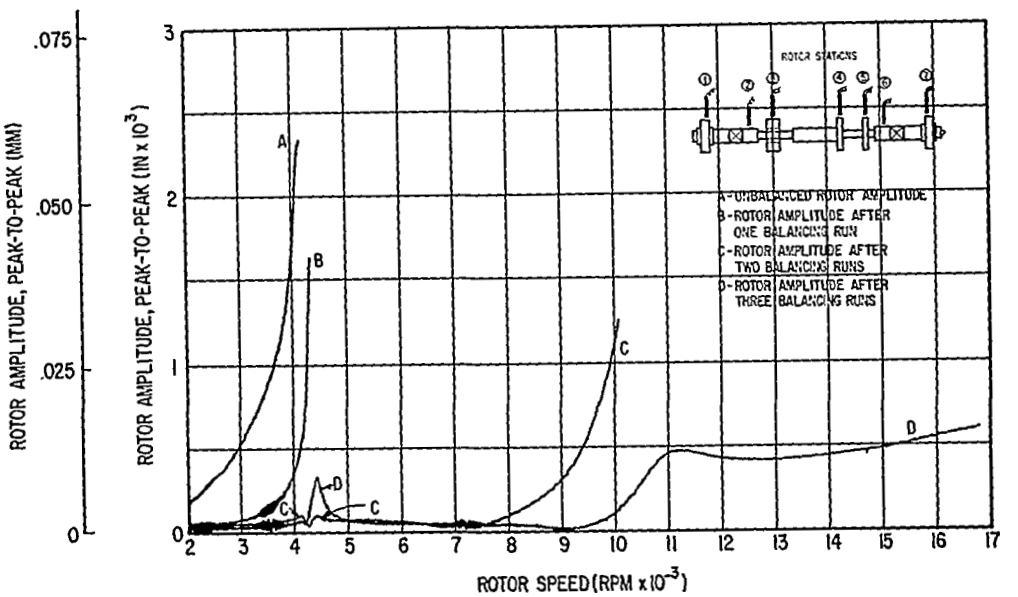

Fig. 31 Vertical Rotor Amplitudes at Station 6 — Initial Condition (In-Line, In-Phase Unbalance) and After Three Consecutive Balancing Runs by the Least Squares Procedure (Four Probes)

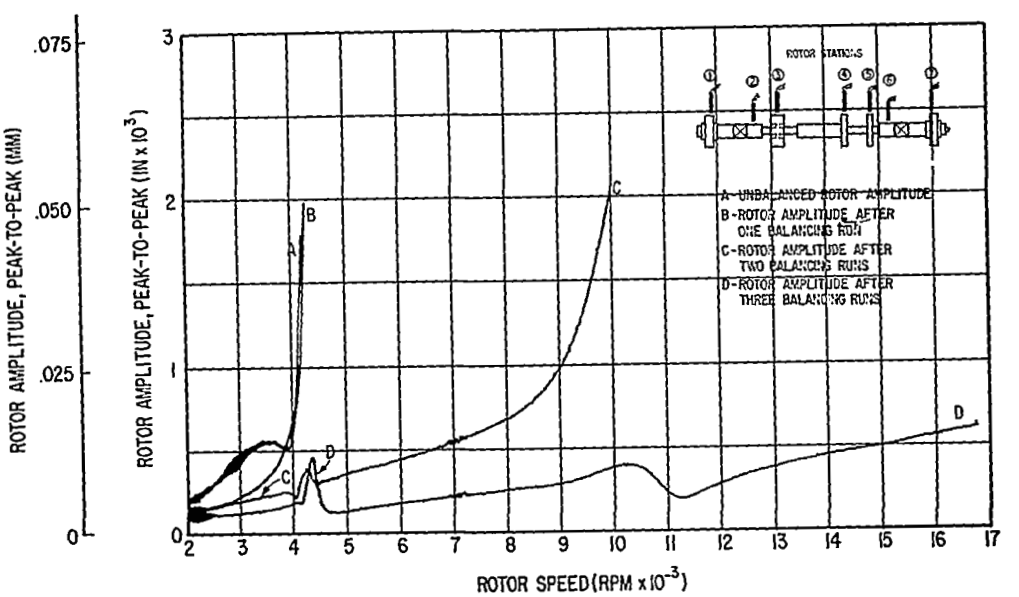

Fig. 32 Vertical Rotor Amplitudes at Station 7 — Initial Condition (In-Line, In-Phase Unbalance) and After Three Consecutive Balancing Runs by the Least Squares Procedure (Four Probes)

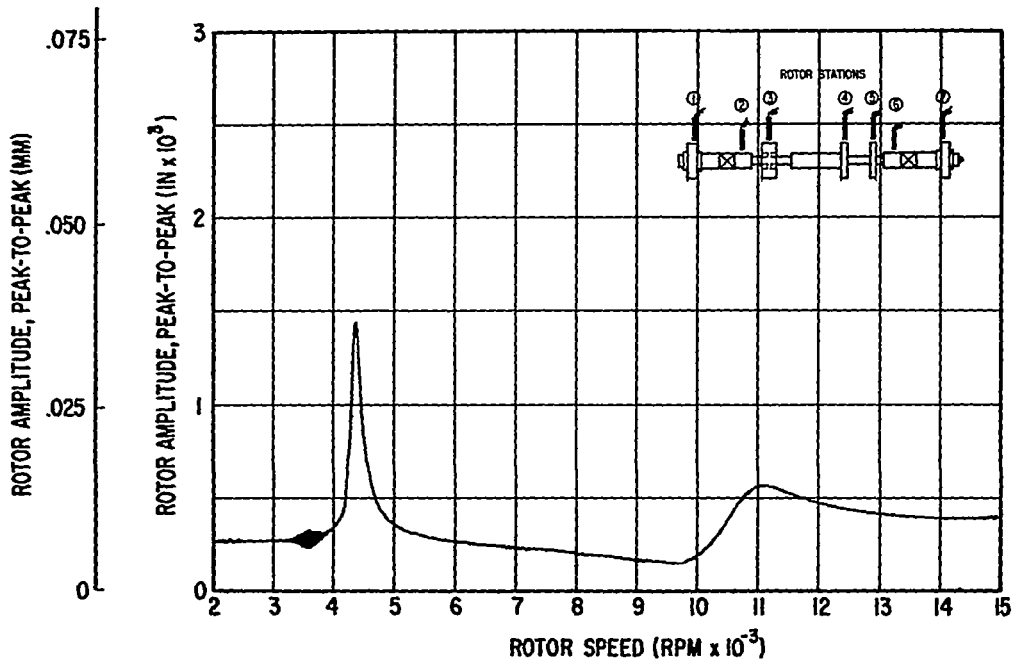

Fig. 33 Vertical Rotor Amplitudes at Station 1 — After Three Consecutive Balancing Runs With Trial Weight Data for Final Run Acquired at 8885 RPM Only (In-Line, In-Phase Initial Unbalance Condition)

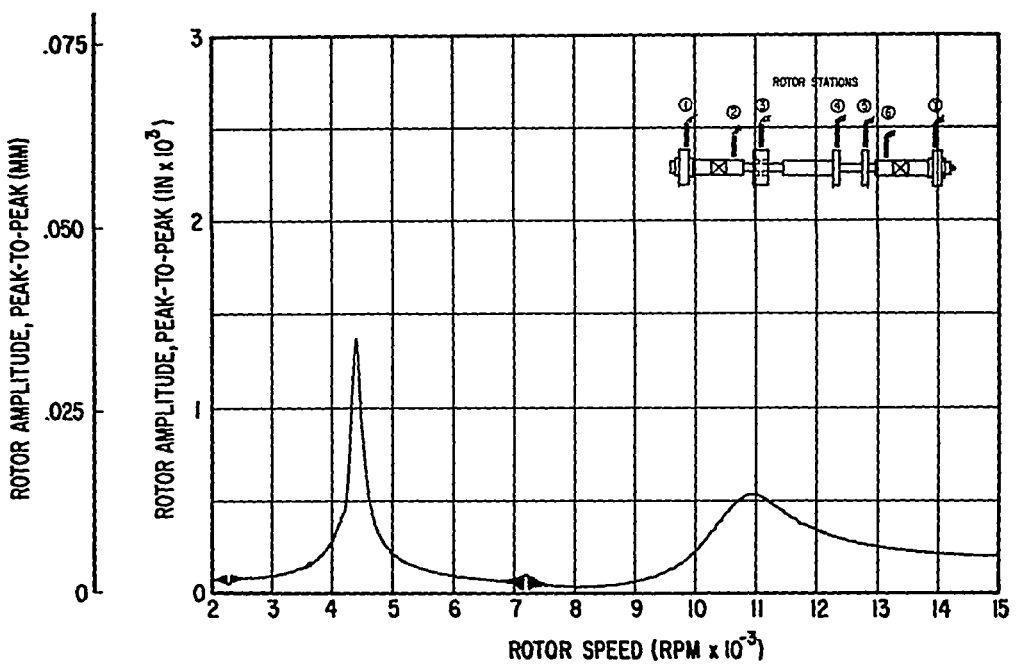

Fig. 34 Vertical Rotor Amplitudes at Station 2 — After Three Consecutive Balancing Runs With Trial Weight Data for Final Run Acquired at 8885 RPM Only (In-Line, In-Phase Initial Unbalance Condition)

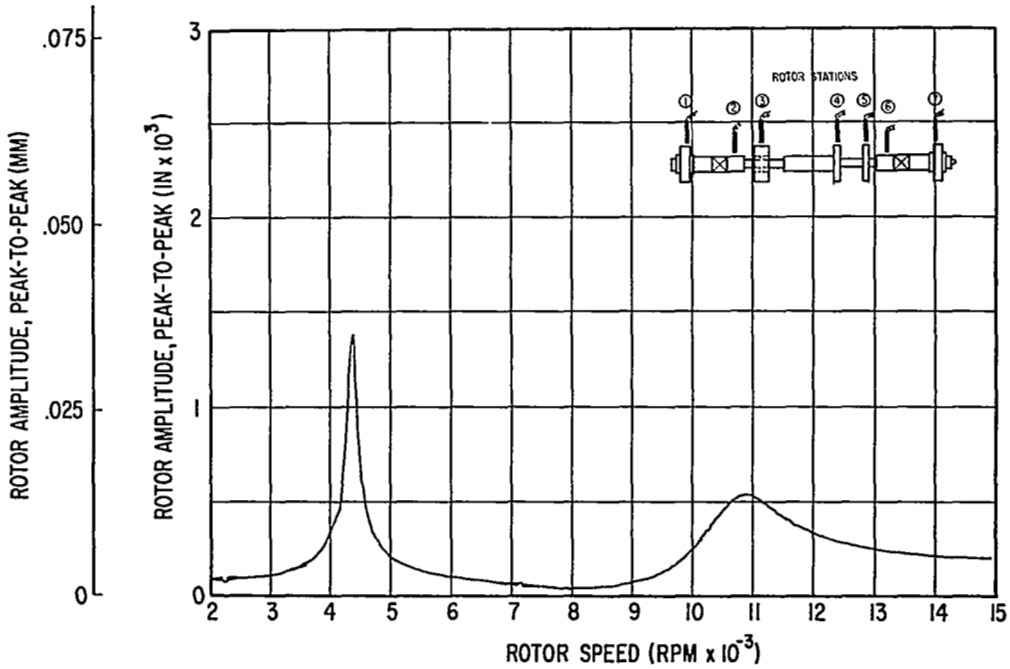

Fig. 35 Vertical Rotor Amplitudes at Station 3 — After Three Consecutive Balancing Runs With Trial Weight Data for Final Run Acquired at 8885 RPM Only (In-Line, In-Phase Initial Unbalance Condition)

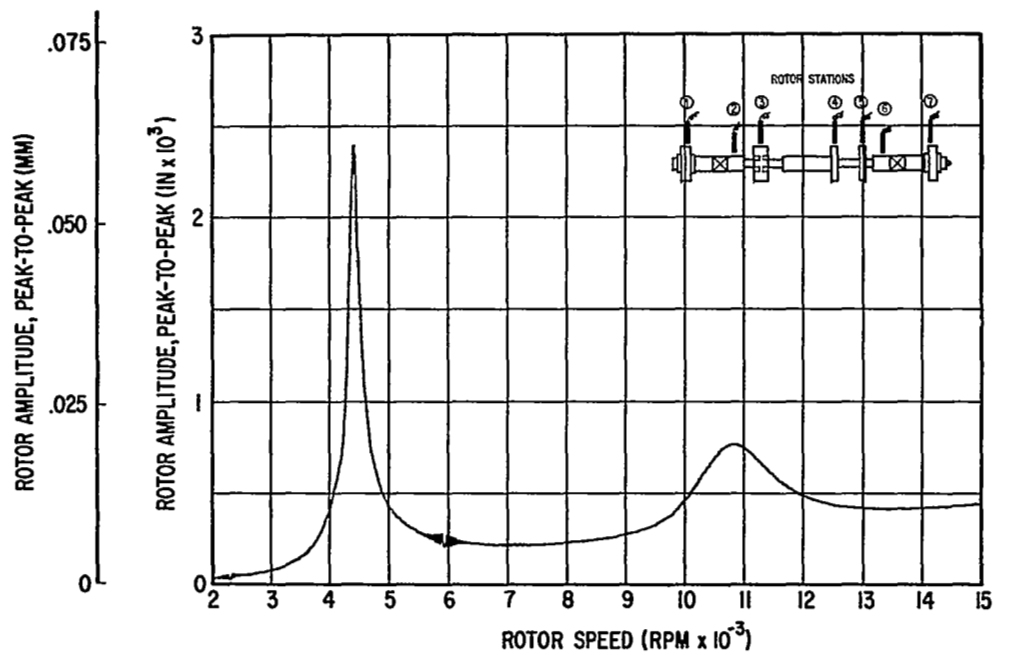

Fig. 36 Vertical Rotor Amplitudes at Station 4 — After Three Consecutive Balancing Runs With Trial Weight Data for Final Run Acquired at 8885 RPM Only (In-Line, In-Phase Initial Unbalance Condition)

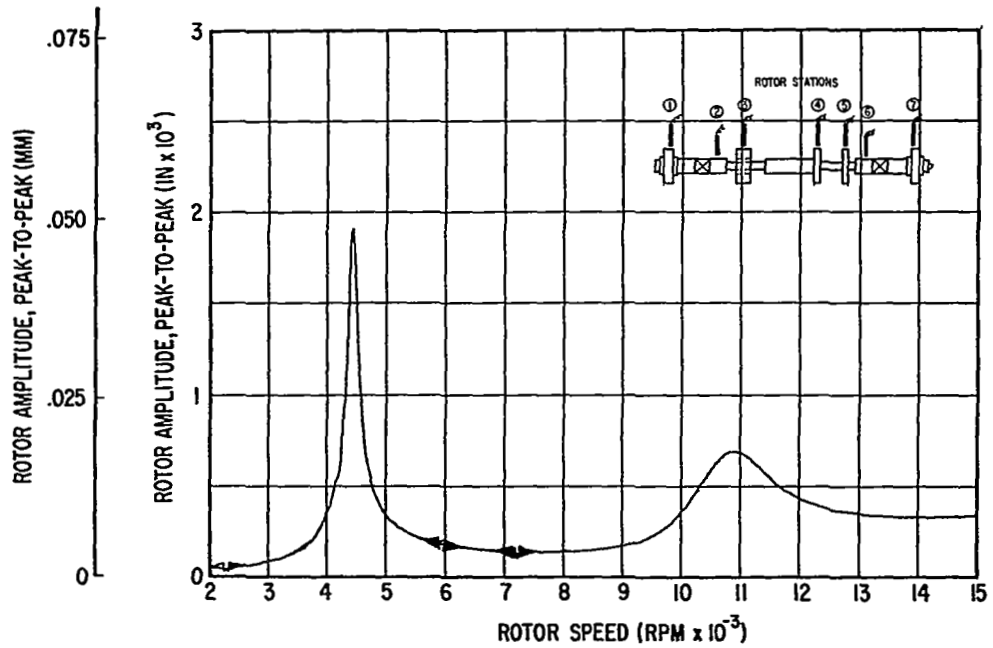

Fig. 37 Vertical Rotor Amplitudes at Station 5 — After Three Consecutive Balancing Runs With Trial Weight Data for Final Run Acquired at 8885 RPM Only (In-Line, In-Phase Initial Unbalance Condition)

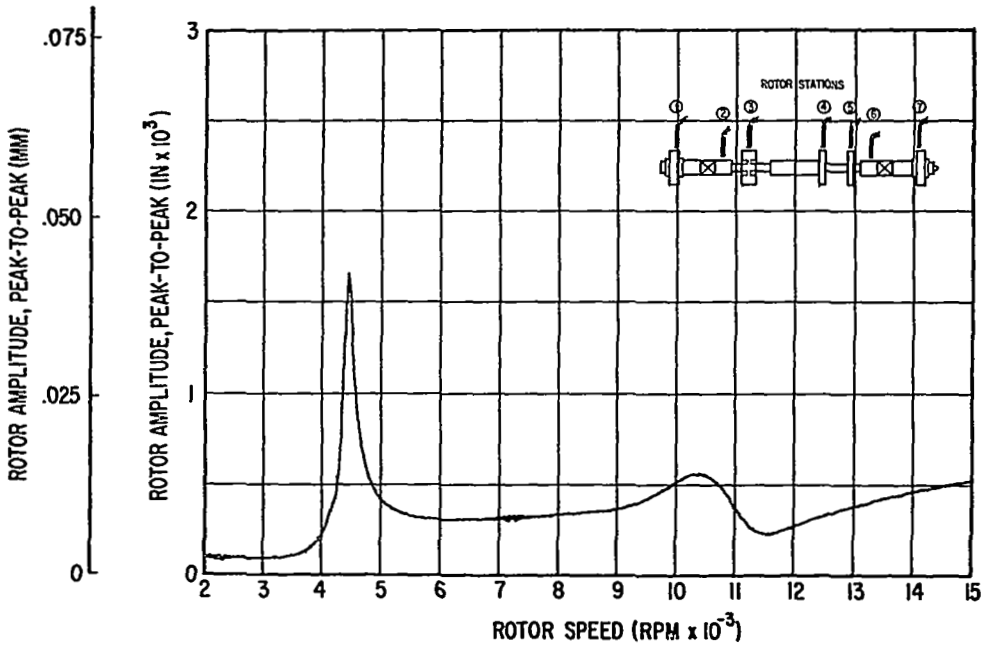

Fig. 38 Vertical Rotor Amplitudes at Station 7 — After Three Consecutive Balancing Runs With Trial Weight Data for Final Run Acquired at 8885 RPM Only (In-Line, In-Phase Initial Unbalance Condition)

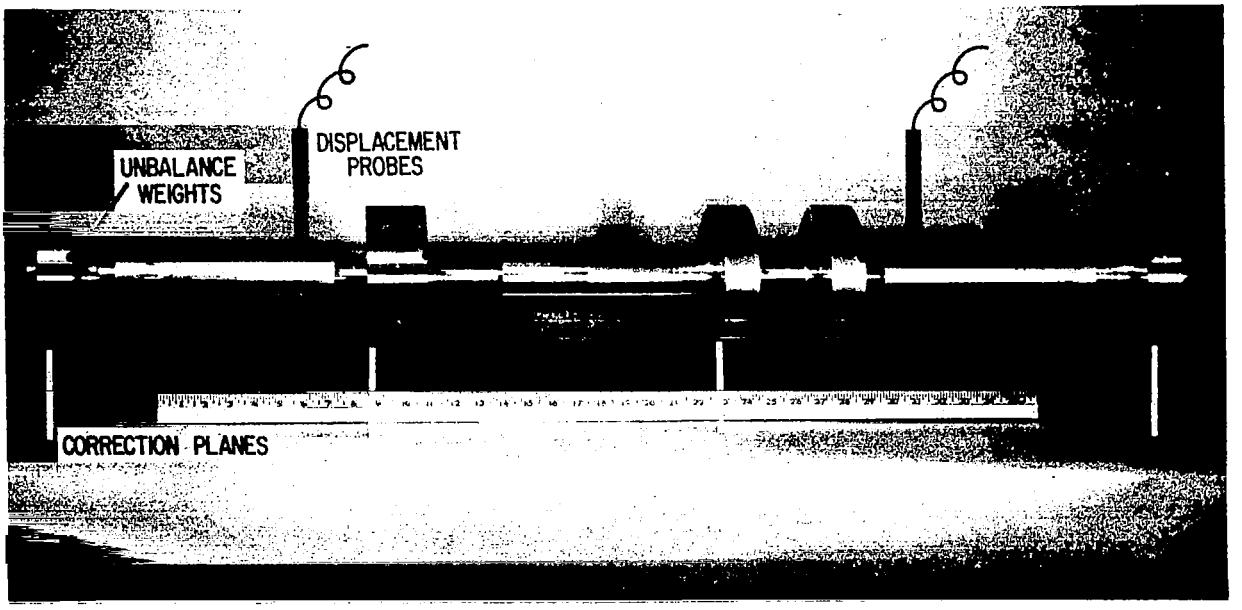

Fig. 39 Shaft-Disc Assembly For Operation Through Four Flexible Critical Speeds, Shown With Location of Two Displacement Probe Sensors, Four Correction Planes and In-Line, In-Phase Initial Unbalance Location

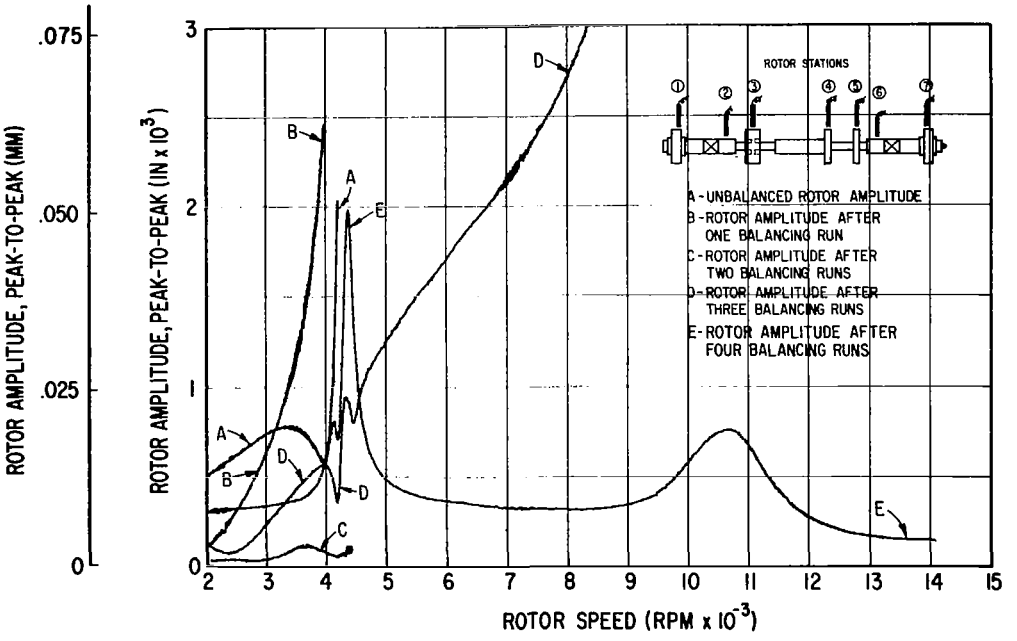

Fig. 40 Vertical Rotor Amplitudes at Station 1 — Initial Condition (In-Line, In-Phase Unbalance) and After Four Consecutive Balancing Runs by the Least Squares Procedure (Two Probes)

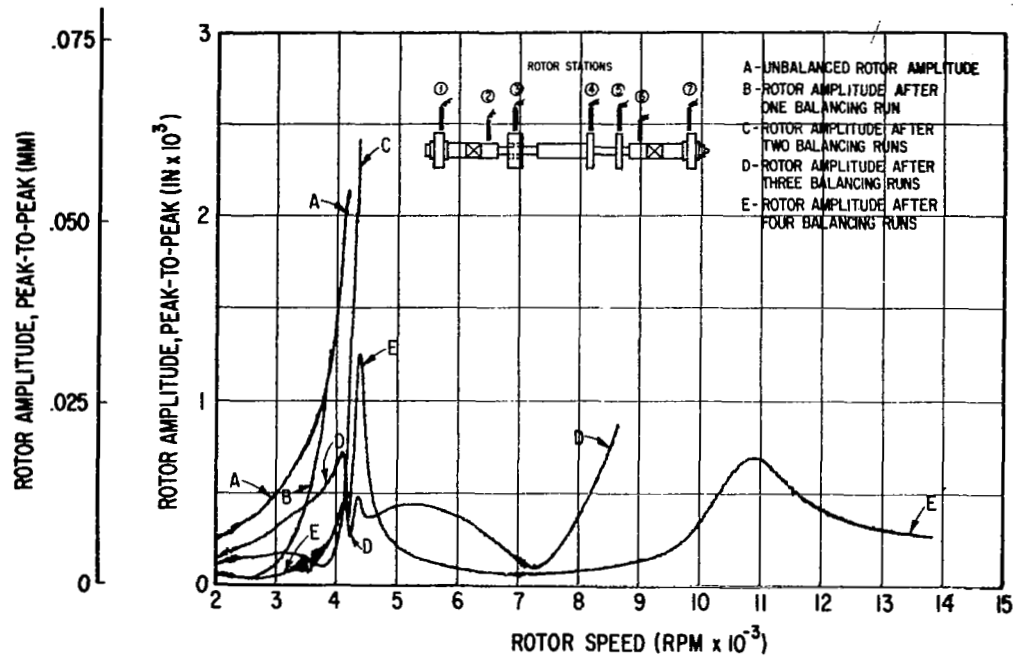

Fig. 41 Vertical Rotor Amplitudes at Station 2 – Initial Condition (In-Line, In-Phase Unbalance) and After Four Consecutive Balancing Runs by the Least Squares Procedure (Two Probes)

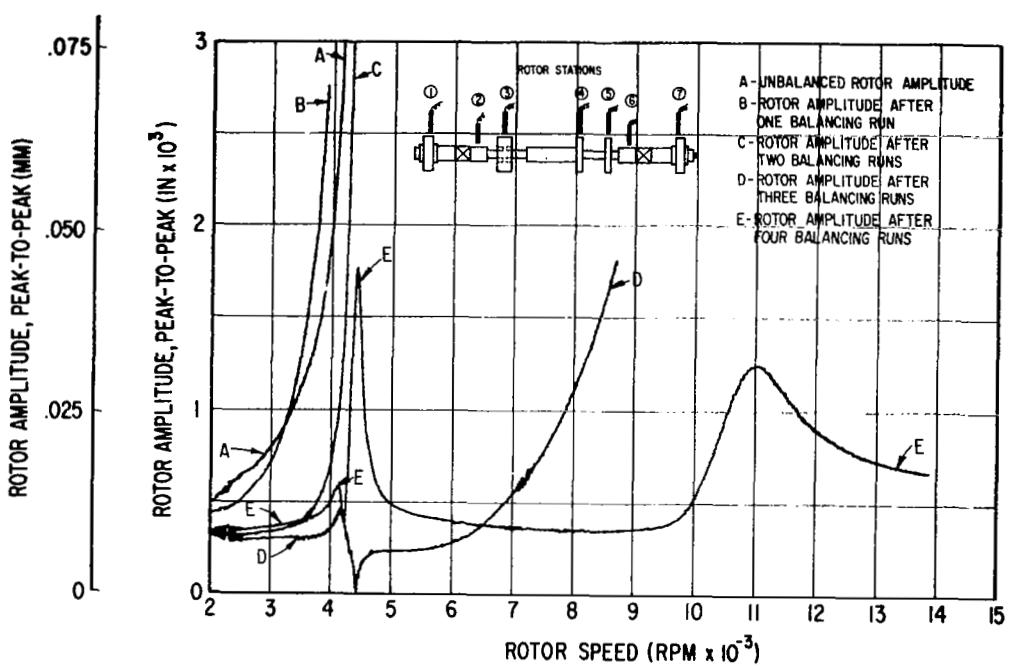

Fig. 42 Vertical Rotor Amplitudes at Station 3 – Initial Condition (In-Line, In-Phase Unbalance) and After Three Consecutive Balancing Runs by the Least Squares Procedure (Two Probes)

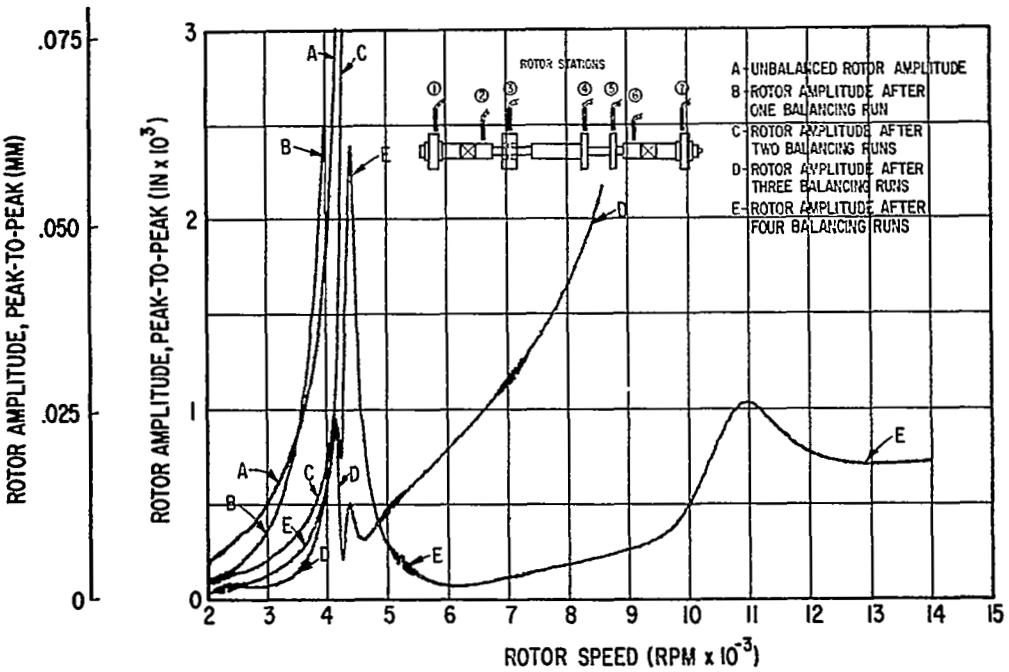

Fig. 43 Vertical Rotor Amplitudes at Station 4 — Initial Condition (In-Line, In-Phase Unbalance) and After Four Consecutive Balancing Runs by the Least Squares Procedure (Two Probes)

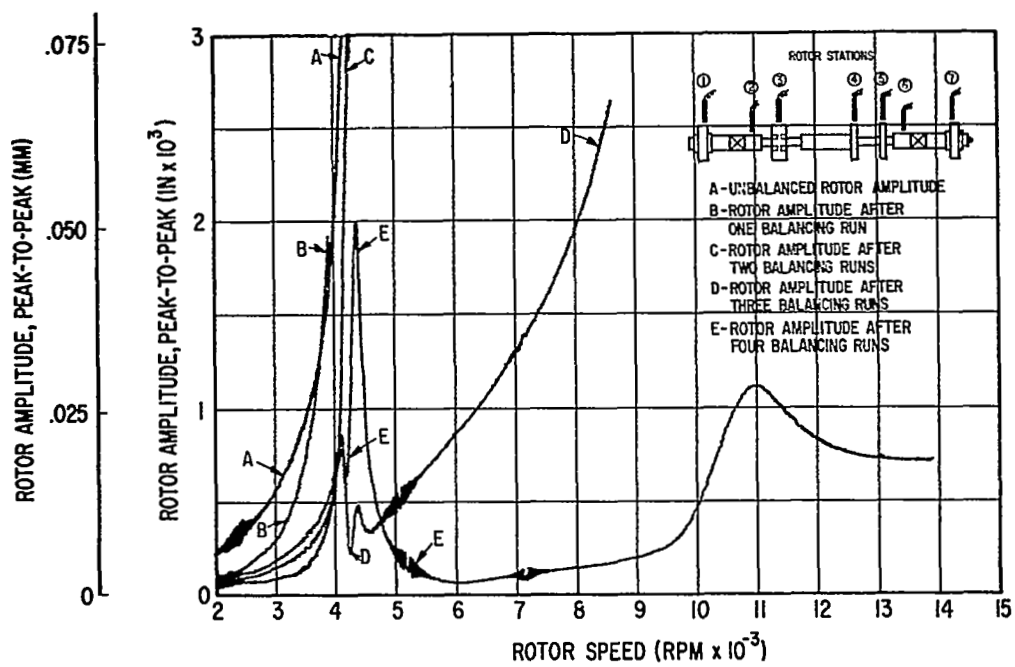

Fig. 44 Vertical Rotor Amplitudes at Station 5 — Initial Condition (In-Line, In-Phase Unbalance) and After Four Consecutive Balancing Runs by the Least Squares Procedure (Two Probes)

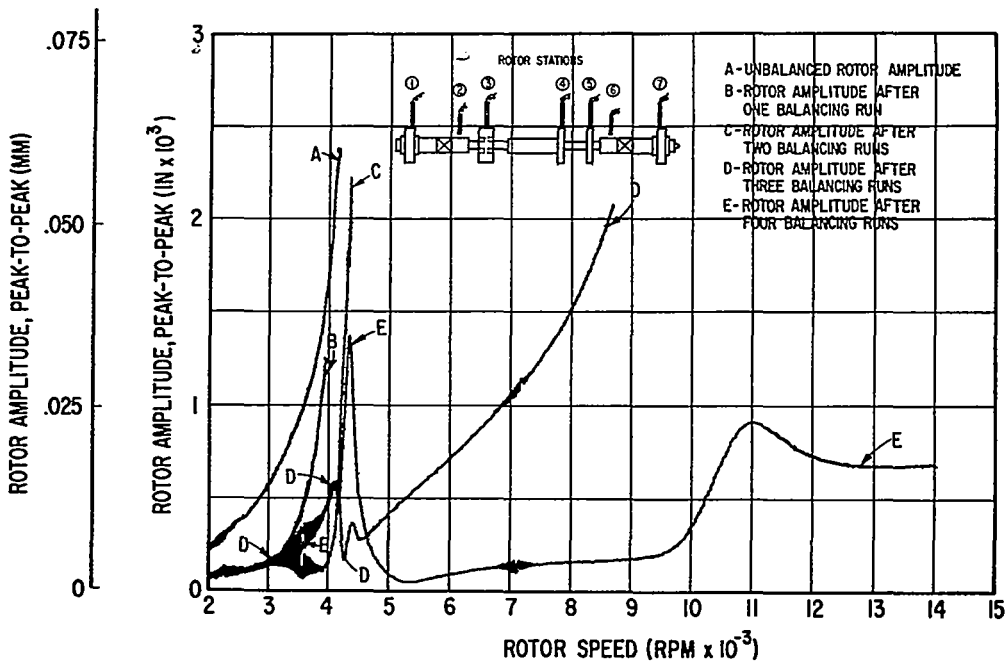

Fig. 45 Vertical Rotor Amplitudes at Station 6 — Initial Condition (In-Line, In-Phase Unbalance) and After Four Consecutive Balancing Runs by the Least Squares Procedure (Two Probes)

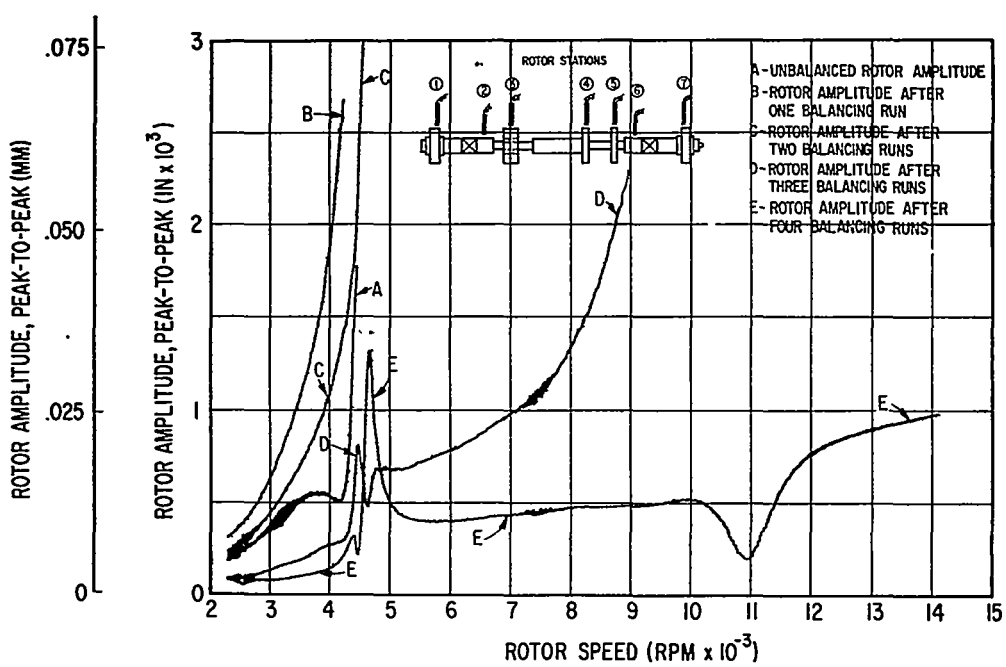

Fig. 46 Vertical Rotor Amplitudes at Station 7 — Initial Condition (In-Line, In-Phase Unbalance) and After Four Consecutive Balancing Runs by the Least Squares Procedure (Two Probes)

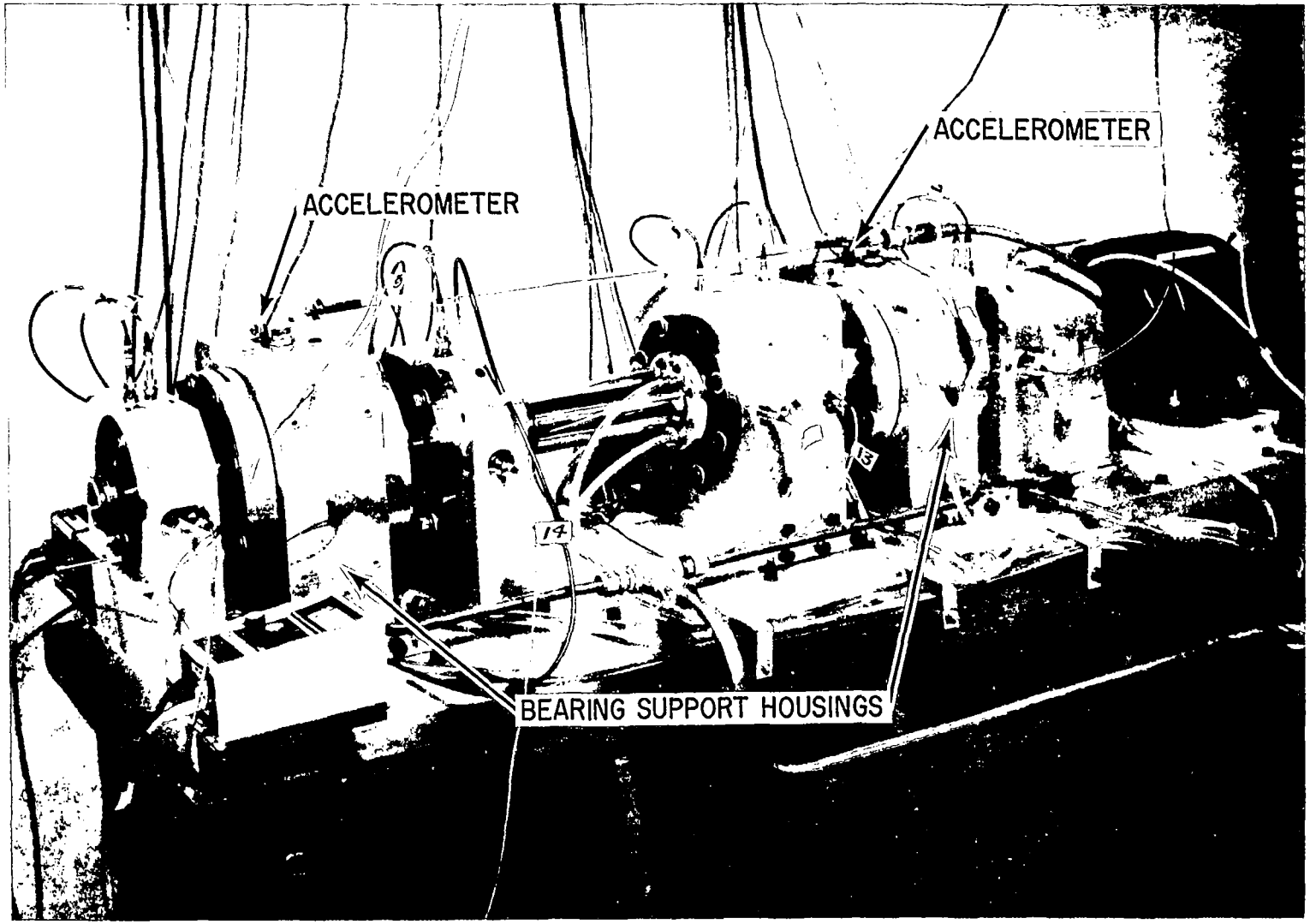

Fig. 47 Test Rig For High-Speed Multiplane Flexible-Rotor Balancing With Accelerometers on Bearing Support Housings

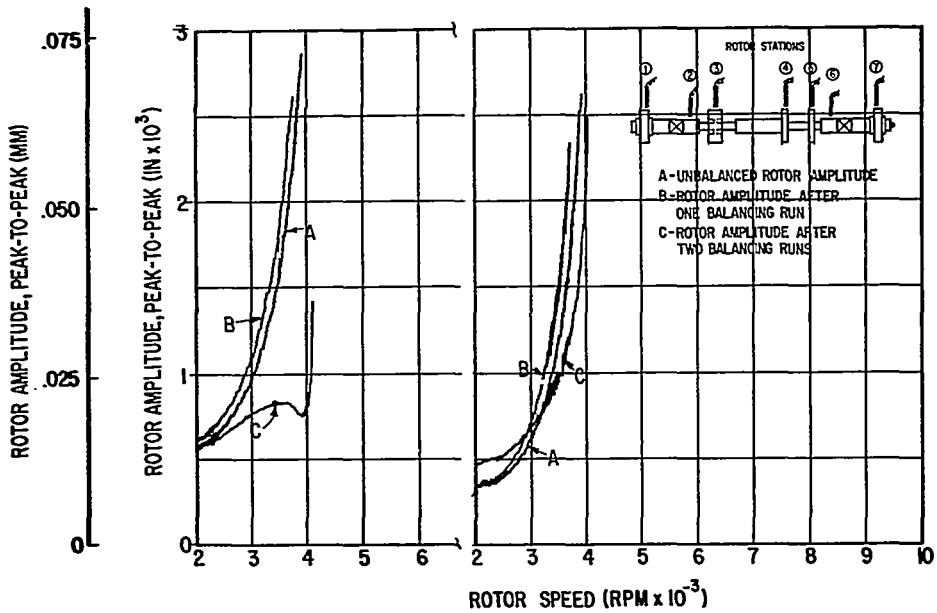

Fig. 48 Vertical Rotor Amplitudes at Stations 1 and 3 — Initial Condition (In-Line, In-Phase Unbalance) and After Two Consecutive Balancing Runs by the Least Squares Procedure (Two Accelerometers on Journal Bearing Housings)

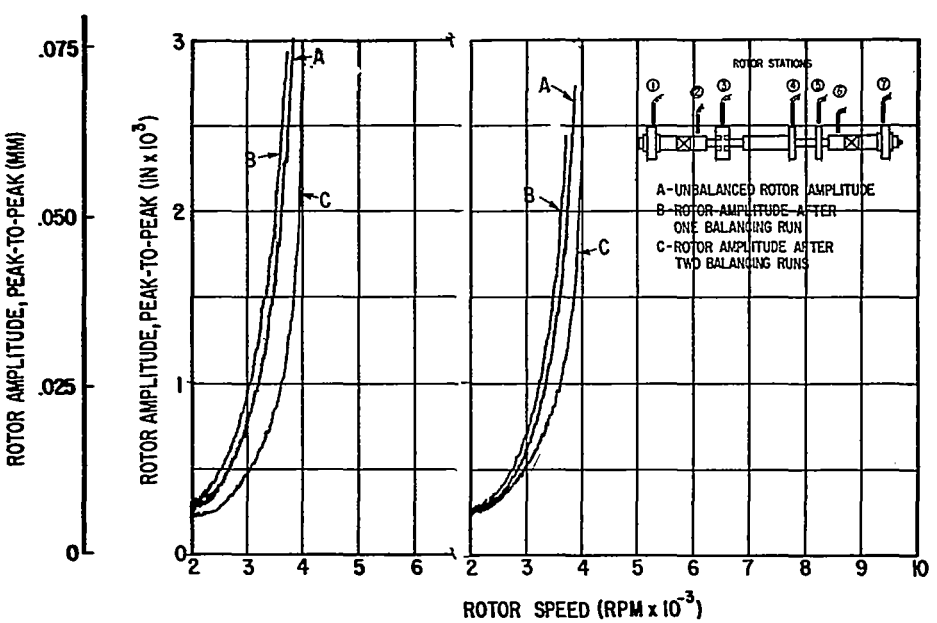

Fig. 49 Vertical Rotor Amplitudes at Stations 4 and 5 — Initial Condition (In-Line, In-Phase Unbalance) and After Two Consecutive Balancing Runs by the Least Squares Procedure (Two Accelerometers on Journal Bearing Housings)

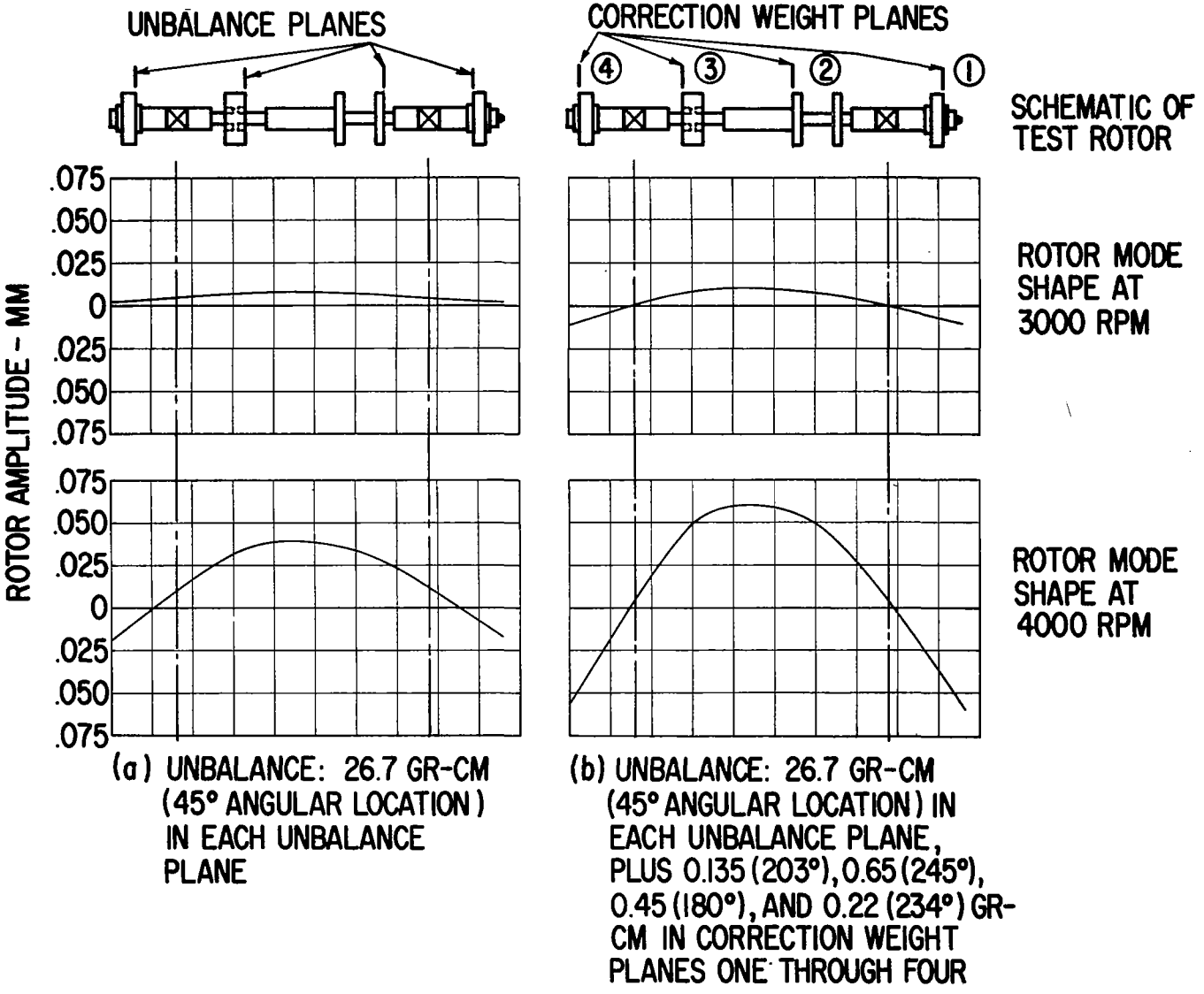

Fig. 50 Calculated Mode Shapes For Test Rotor With Initial In-Line, In-Phase Unbalance (a) And With First Set of Correction Weights Included (b)

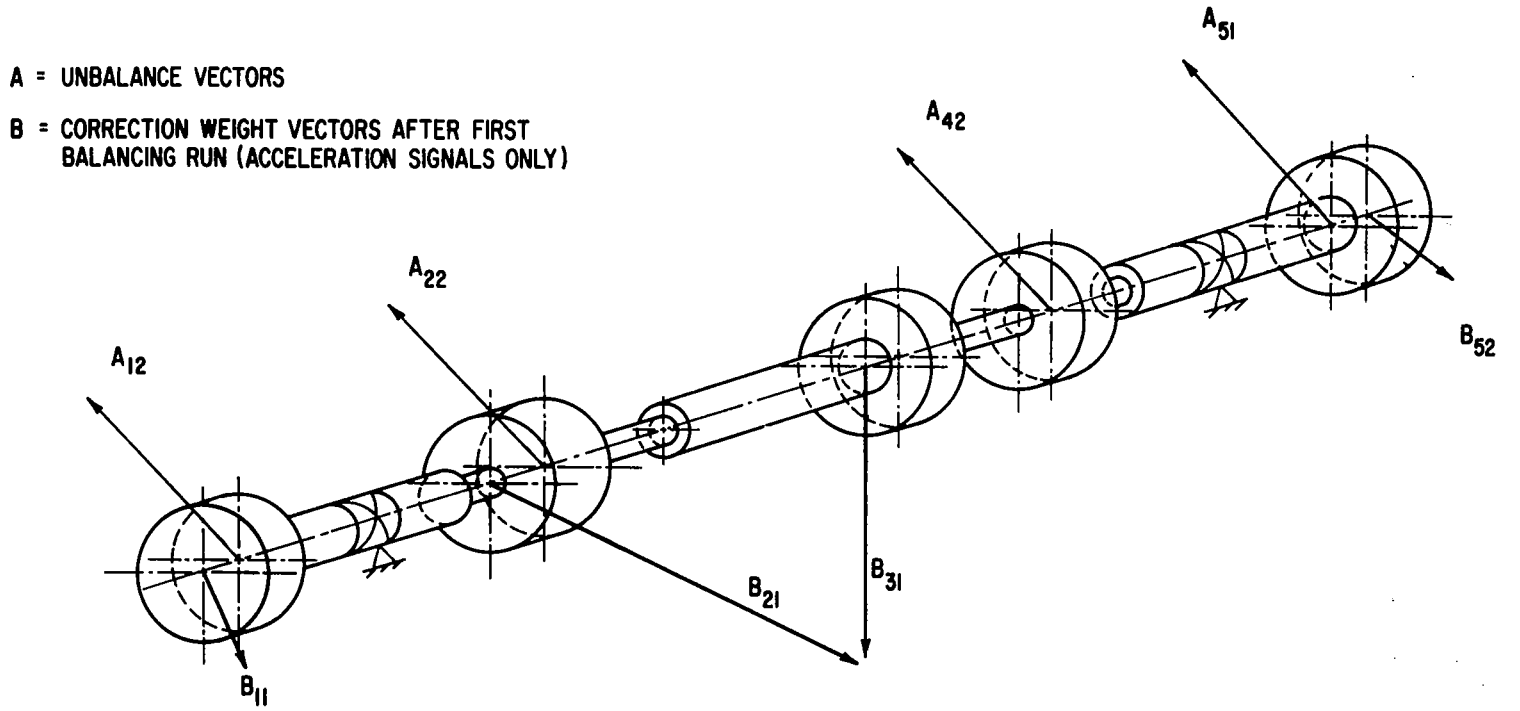

Fig. 51 Unbalance Vectors and Correction Weight Vectors For Test Rotor With In-Line, In-Phase Unbalance Condition

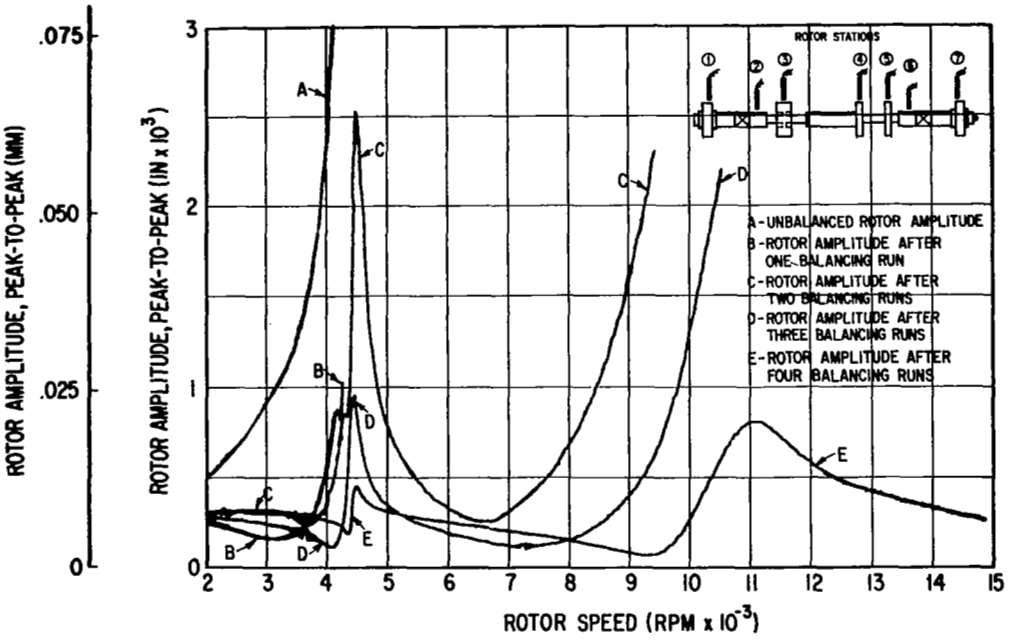

Fig. 52 Vertical Rotor Amplitudes at Station 1 — Initial Condition (In-Line, Alternating-Phase Unbalance) and After Four Consecutive Balancing Runs by the Least Squares Procedure (Four Probes)

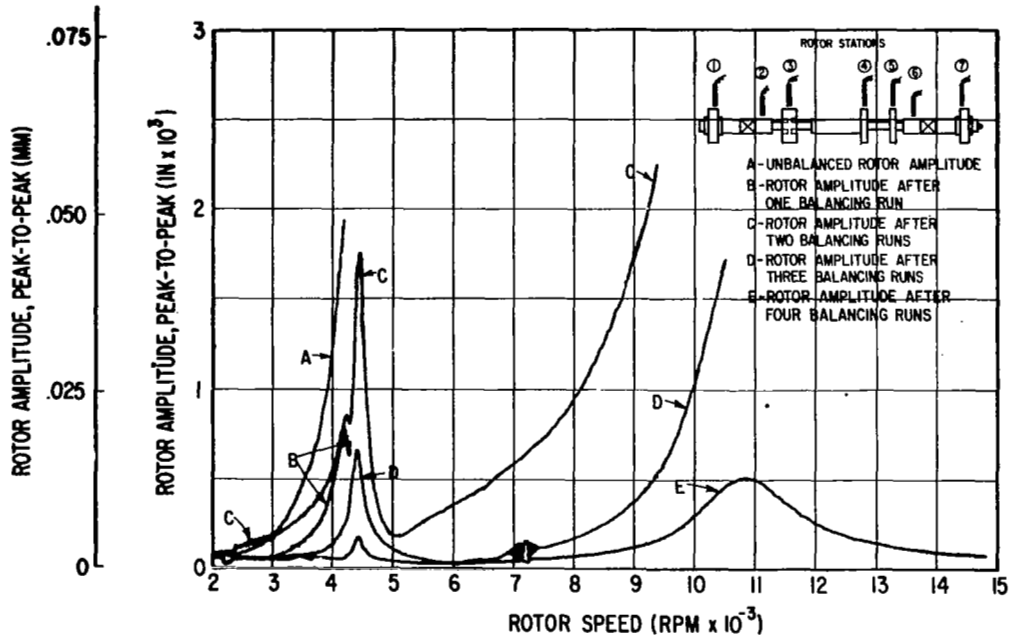

Fig. 53 Vertical Rotor Amplitudes at Station 2 — Initial Condition (In-Line, Alternating-Phase Unbalance) and After Four Consecutive Balancing Runs by the Least Squares Procedure (Four Probes)

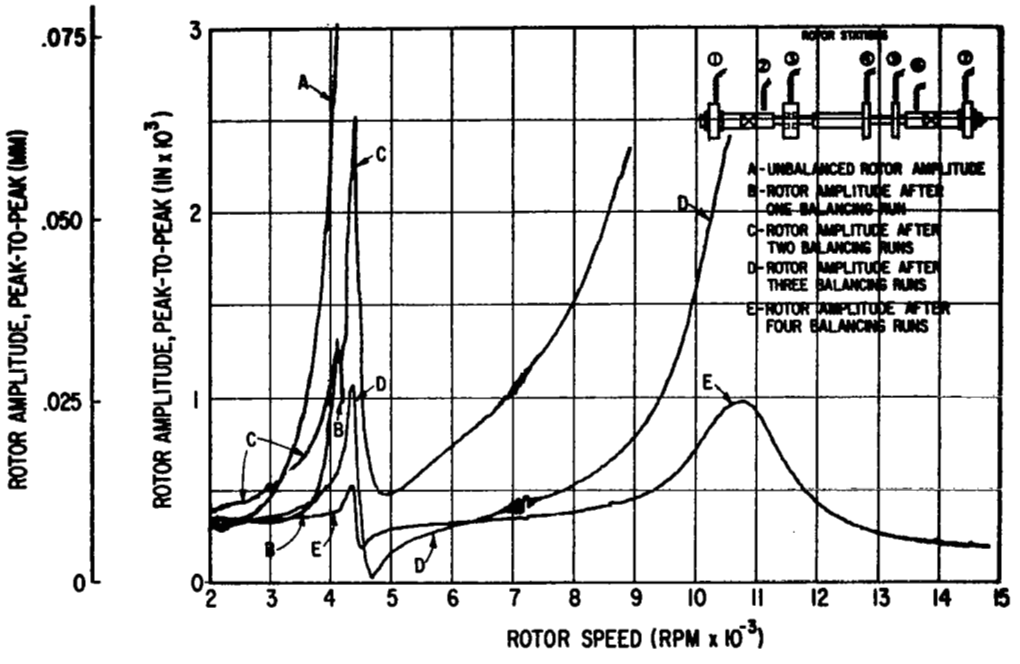

Fig. 54 Vertical Rotor Amplitudes at Station 3 – Initial Condition (In-Line, Alternating-Phase Unbalance) and After Four Consecutive Balancing Runs by the Least Squares Procedure (Four Probes)

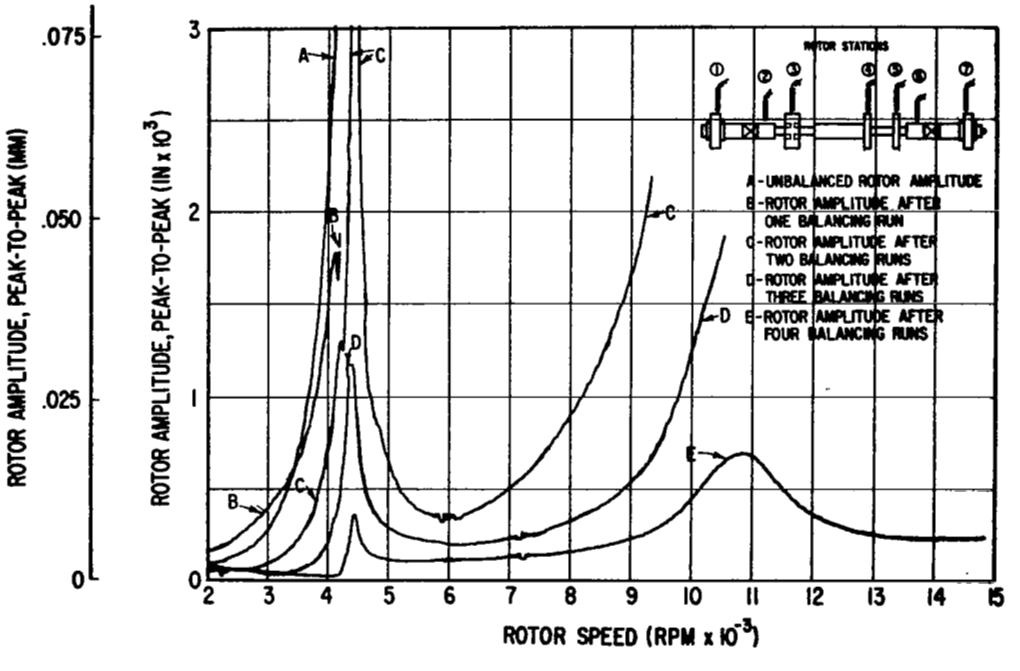

Fig. 55 Vertical Rotor Amplitudes at Station 4 – Initial Condition (In-Line, Alternating-Phase Unbalance) and After Four Consecutive Balancing Runs by the Least Squares Procedure (Four Probes)

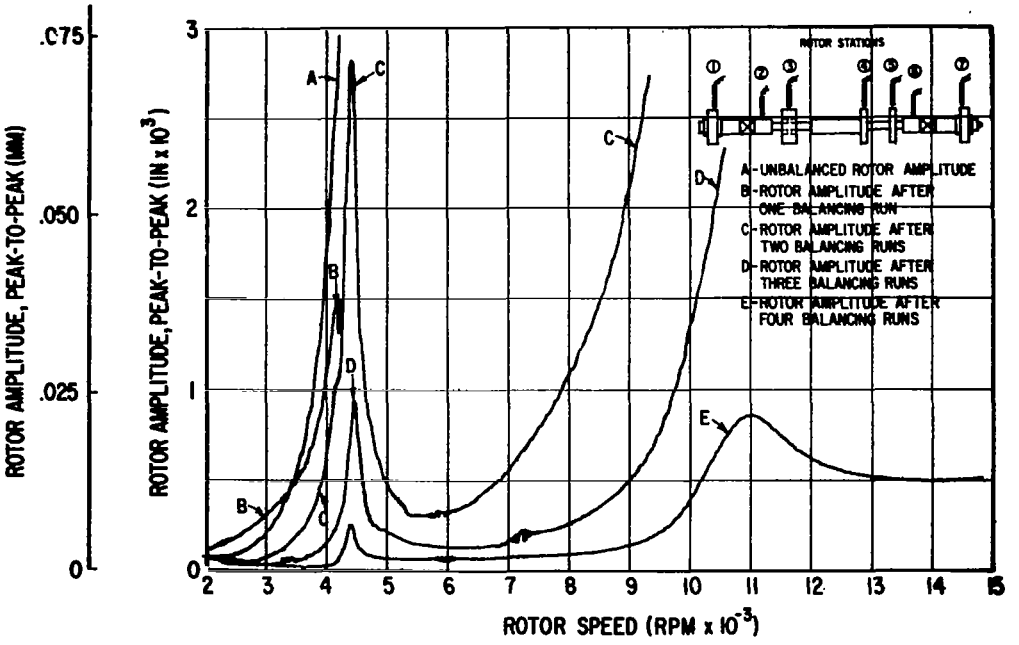

Fig. 56 Vertical Rotor Amplitudes at Station 5 — Initial Condition (In-Line, Alternating-Phase Unbalance) and After Four Consecutive Balancing Runs by the Least Squares Procedure (Four Probes)

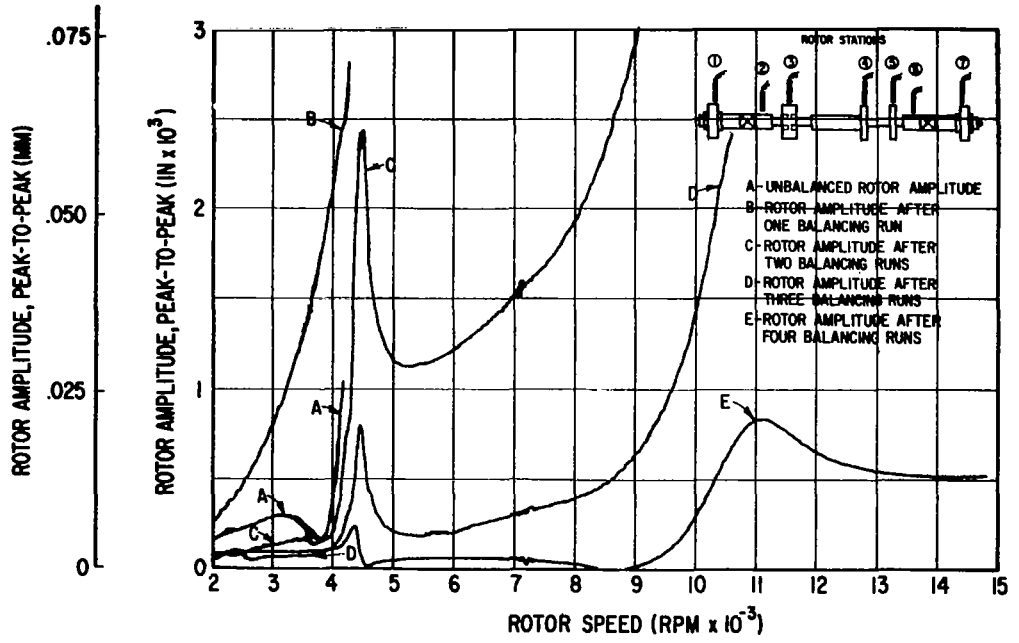

Fig. 57 Vertical Rotor Amplitudes at Station 7 — Initial Condition (In-Line, Alternating-Phase Unbalance) and After Four Consecutive Balancing Runs by the Least Squares Procedure (Four Probes)

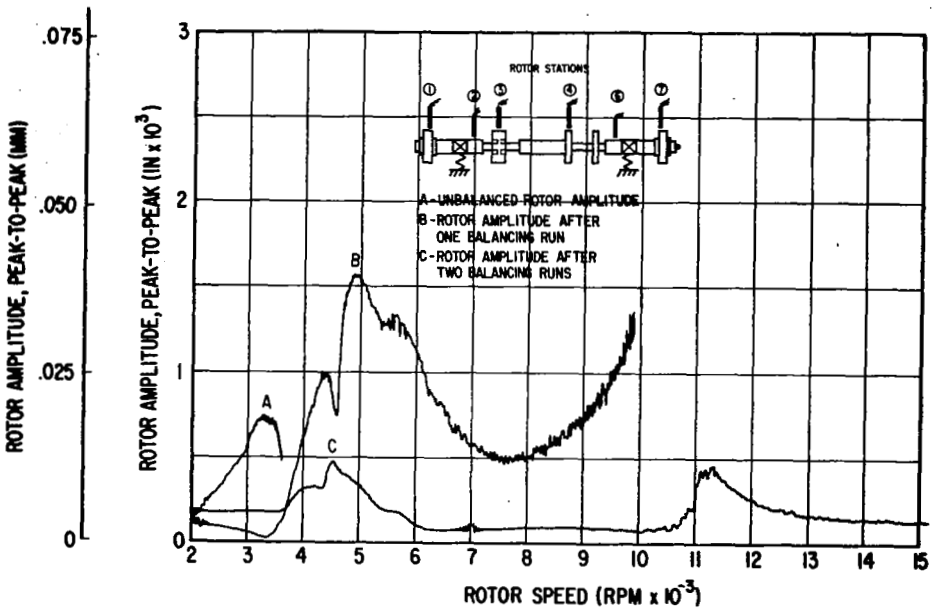

Fig. 58a Vertical Rotor Amplitudes

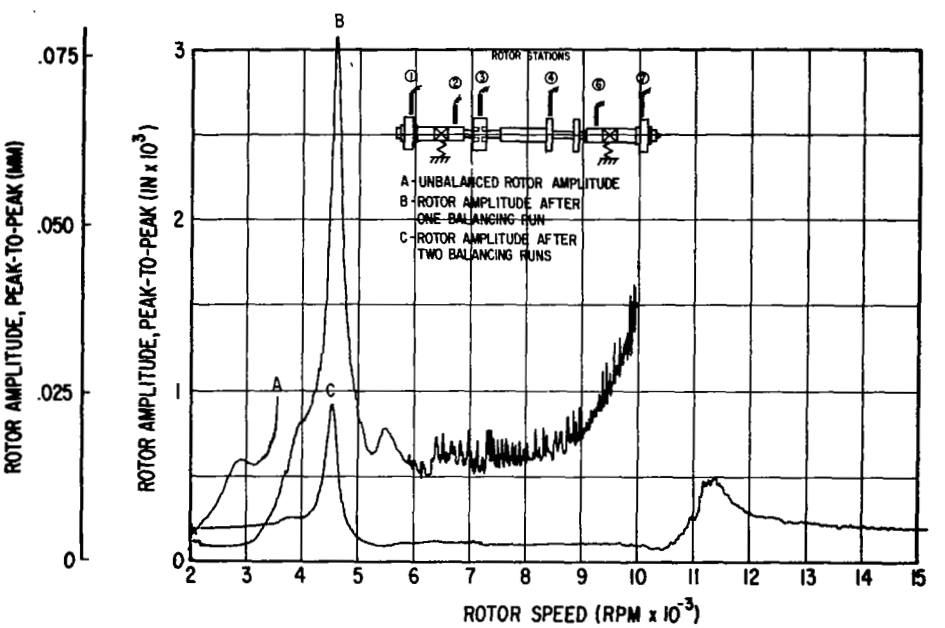

Fig. 58b Horizontal Rotor Amplitudes

Fig. 58 Vertical and Horizontal Rotor Amplitudes at Station 1 — Initial Condition (In-Line, In-Phase Unbalance) and After Two Consecutive Balancing Runs by the Least Squares Procedure (Four Probes)

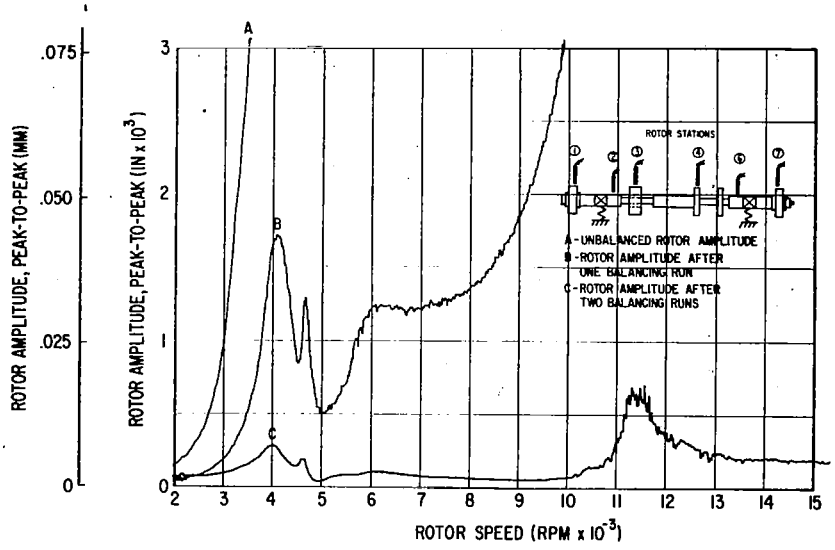

Fig. 59a Vertical Rotor Amplitudes

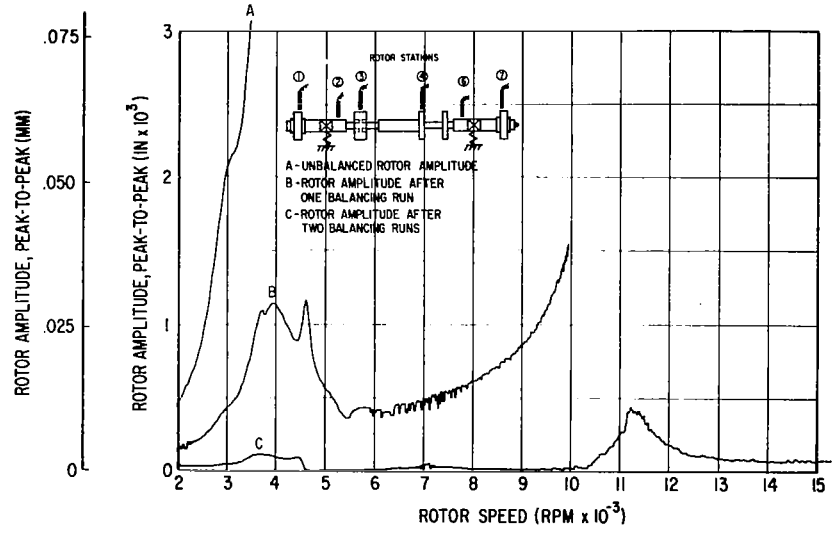

Fig. 59b Horizontal Rotor Amplitudes

Fig. 59 Vertical and Horizontal Rotor Amplitudes at Station 2 -- Initial Condition (In-Line, In-Phase Unbalance) and After Two Consecutive Balancing Runs by the Least Squares Procedure (Four Probes)

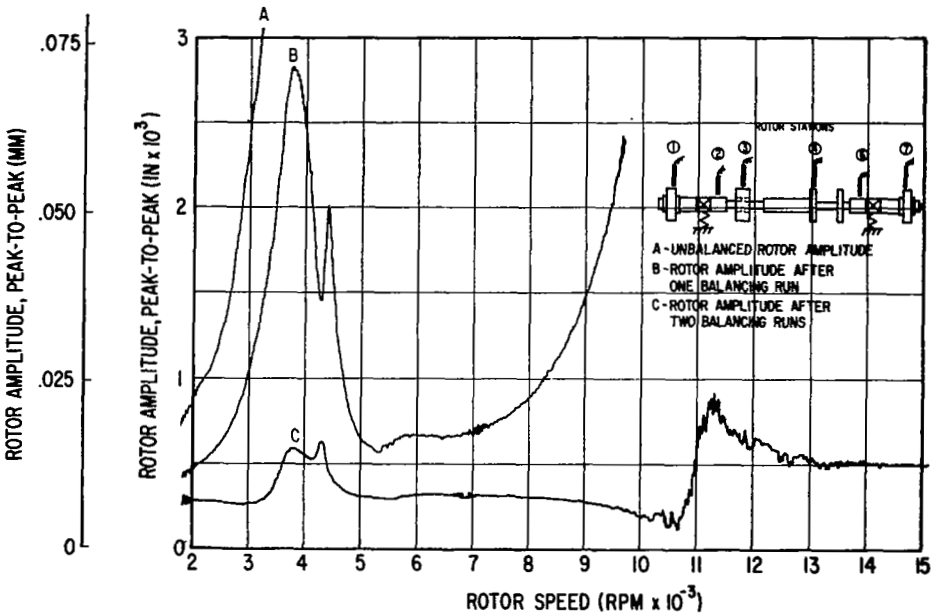

Fig. 60a Vertical Rotor Amplitudes

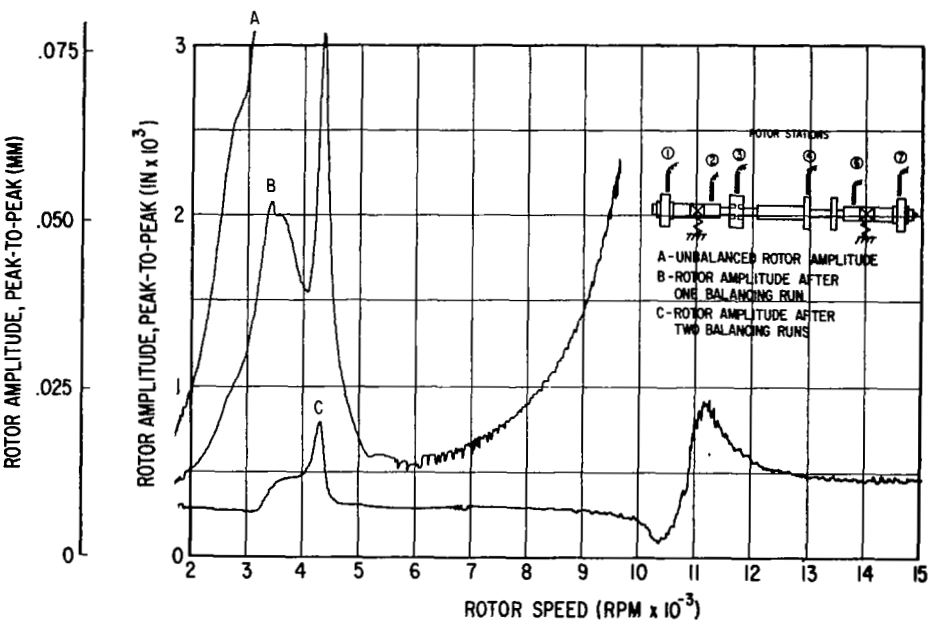

Fig. 60b Horizontal Rotor Amplitudes

Fig. 60 Vertical and Horizontal Rotor Amplitudes at Station 3 — Initial Condition (In-Line, In-Phase Unbalance) and After Two Consecutive Balancing Runs by the Least Squares Procedure (Four Probes)

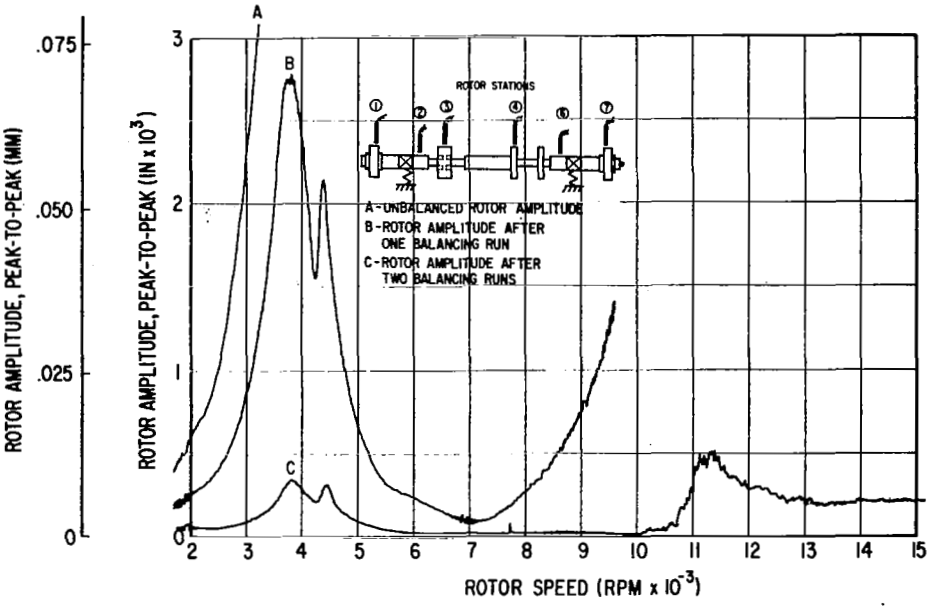

Fig. 61a Vertical Rotor Amplitudes

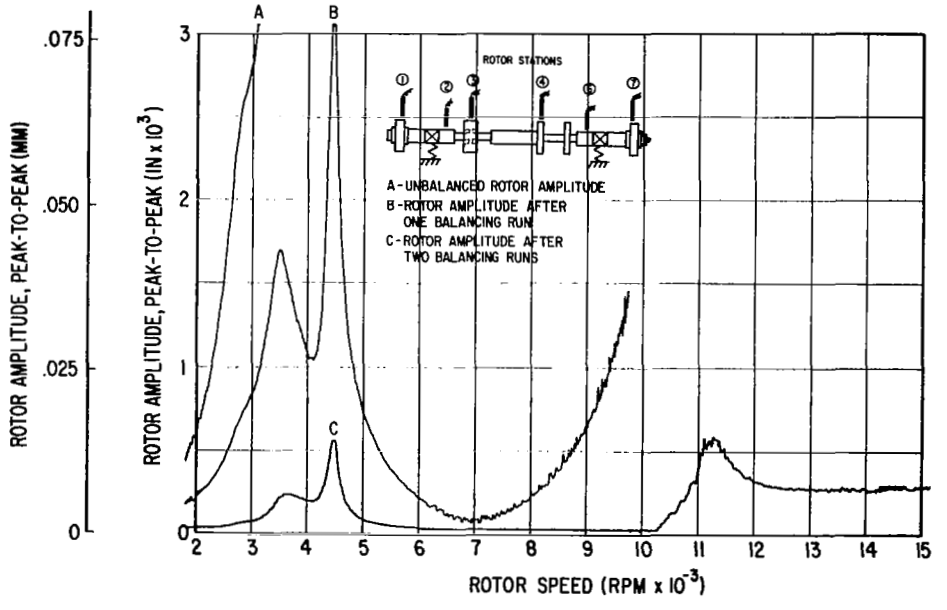

Fig. 61b Horizontal Rotor Amplitudes

Fig. 61 Vertical and Horizontal Rotor Amplitudes at Station 4 — Initial Condition (In-Line, In-Phase Unbalance) and After Two Consecutive Balancing Runs by the Least Squares Procedure (Four Probes)

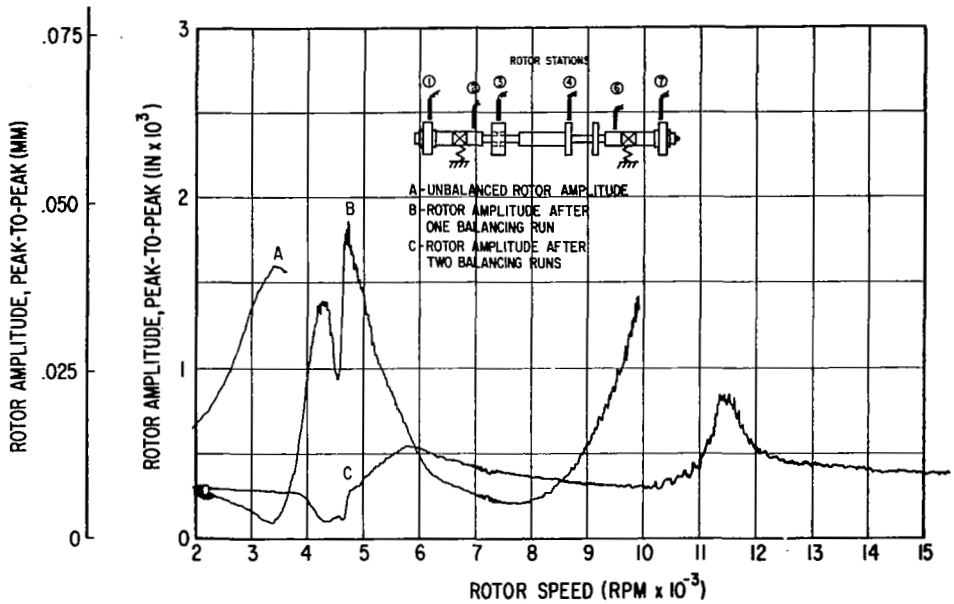

Fig. 62a Vertical Rotor Amplitudes

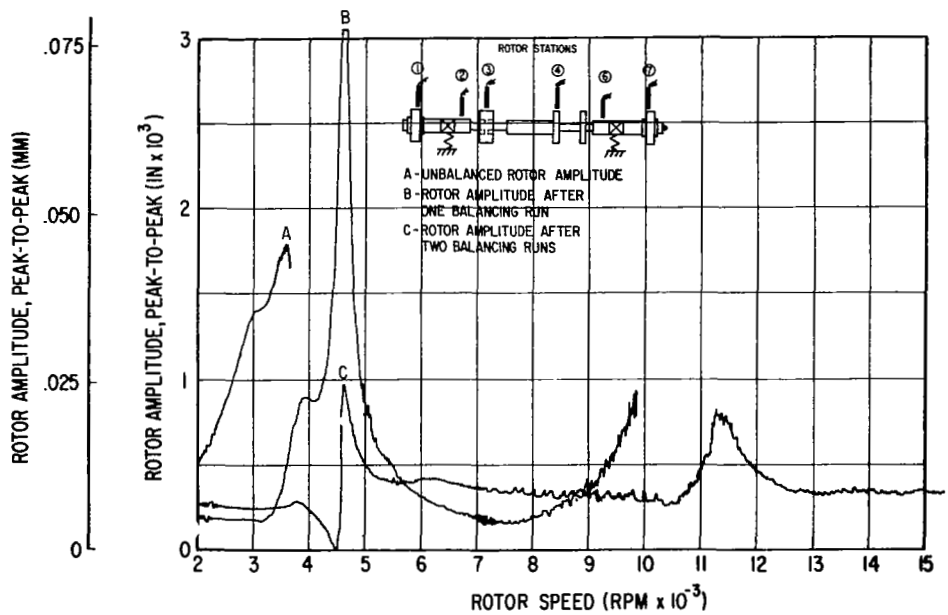

Fig. 62b Horizontal Rotor Amplitudes

Fig. 62 Vertical and Horizontal Rotor Amplitudes at Station 7 — Initial Condition (In-Line, In-Phase Unbalance) and After Two Consecutive Balancing Runs by the Least Squares Procedure (Four Probes)

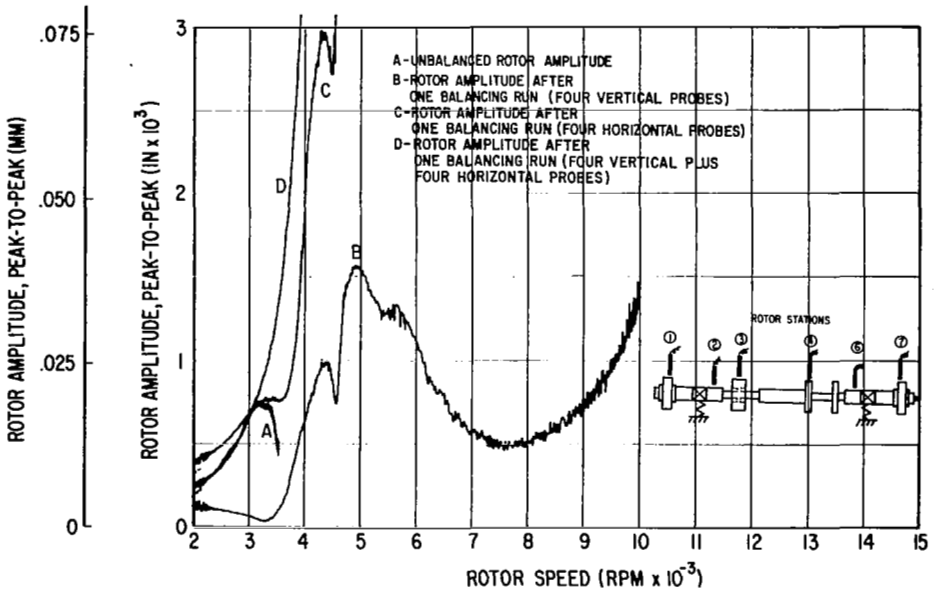

Fig. 63a Vertical Rotor Amplitudes

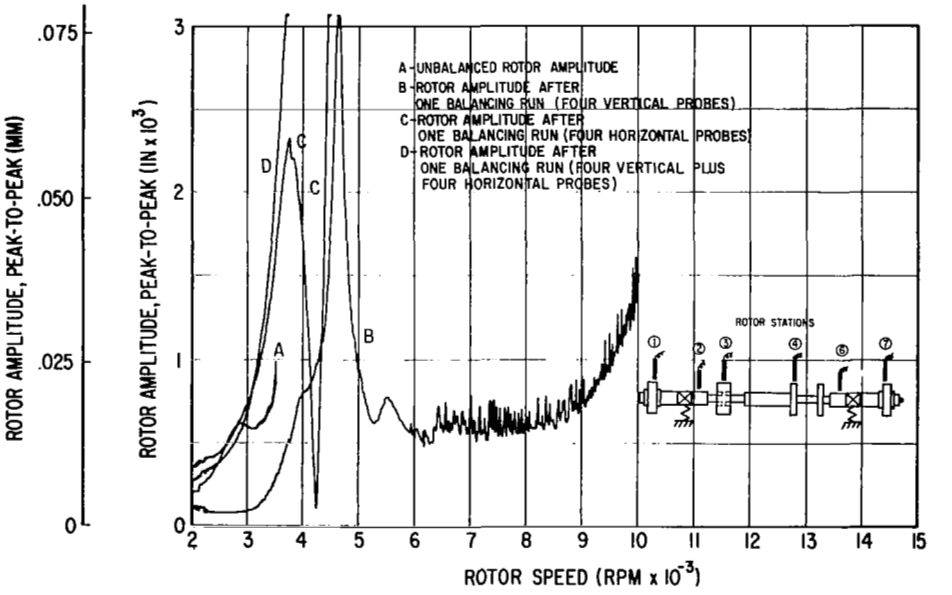

Fig. 63b Horizontal Rotor Amplitudes

Fig. 63 Vertical and Horizontal Rotor Amplitudes at Station 1 — Initial Condition (In-Line, In-Phase Unbalance) and After One Balancing Run by the Least Squares Procedure (Four Vertical Probes, or Four Horizontal Probes, or Four Vertical Plus Four Horizontal Probes)

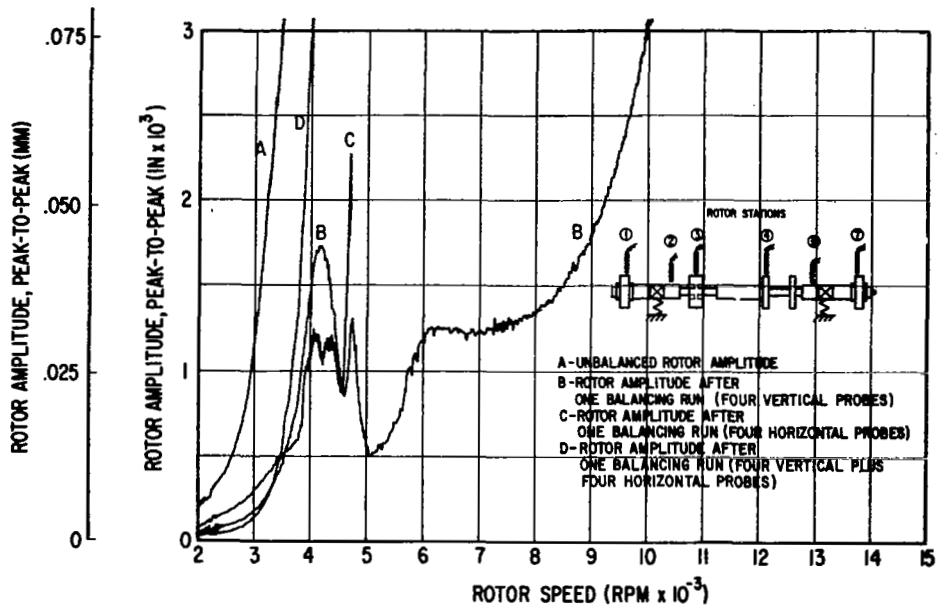

Fig. 64a Vertical Rotor Amplitudes

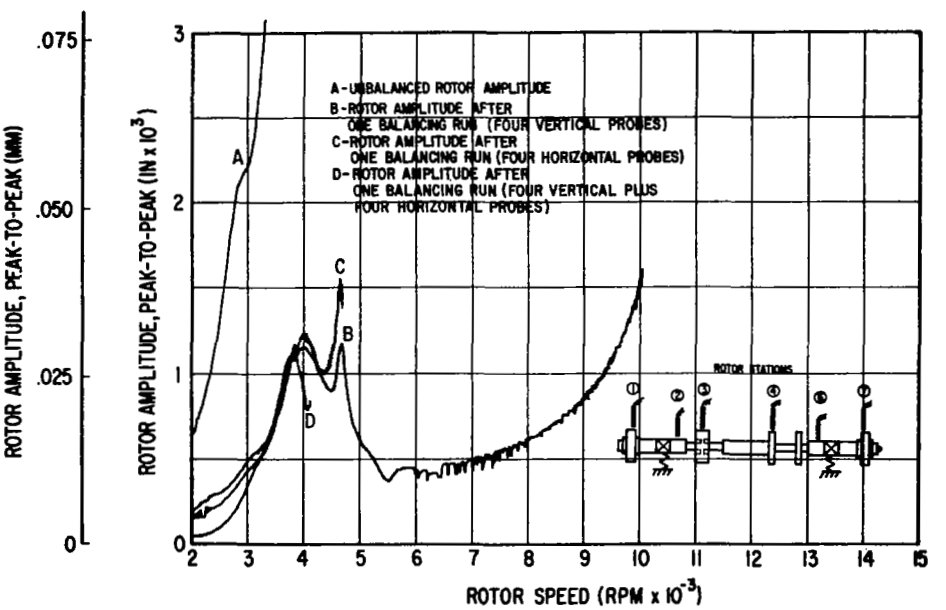

Fig. 64b Horizontal Rotor Amplitudes

Fig. 64 Vertical and Horizontal Rotor Amplitudes at Station 2 — Initial Condition (In-Line, In-Phase Unbalance) and After One Balancing Run by the Least Squares Procedure (Four Vertical Probes, or Four Horizontal Probes, or Four Vertical Plus Four Horizontal Probes)

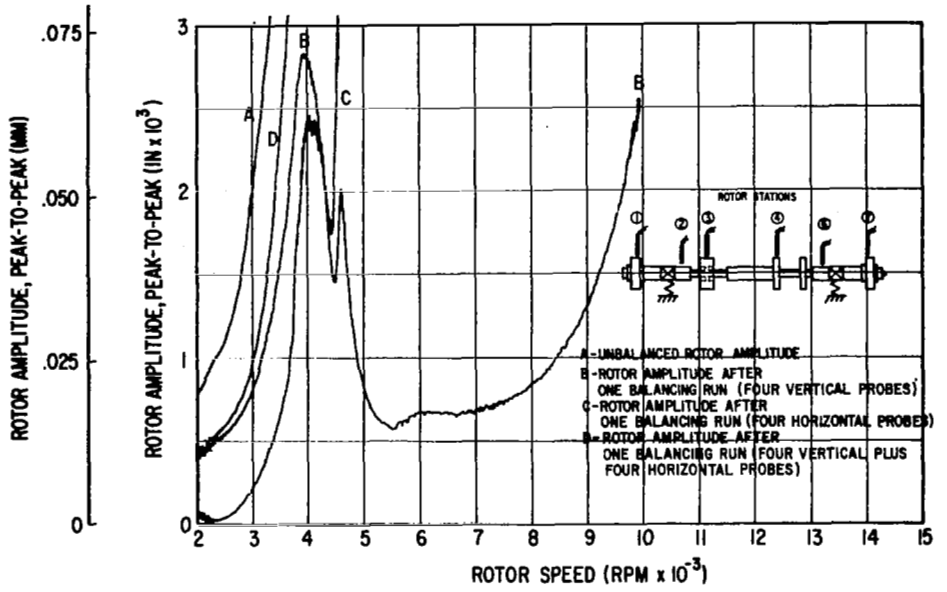

Fig. 65a Vertical Rotor Amplitudes

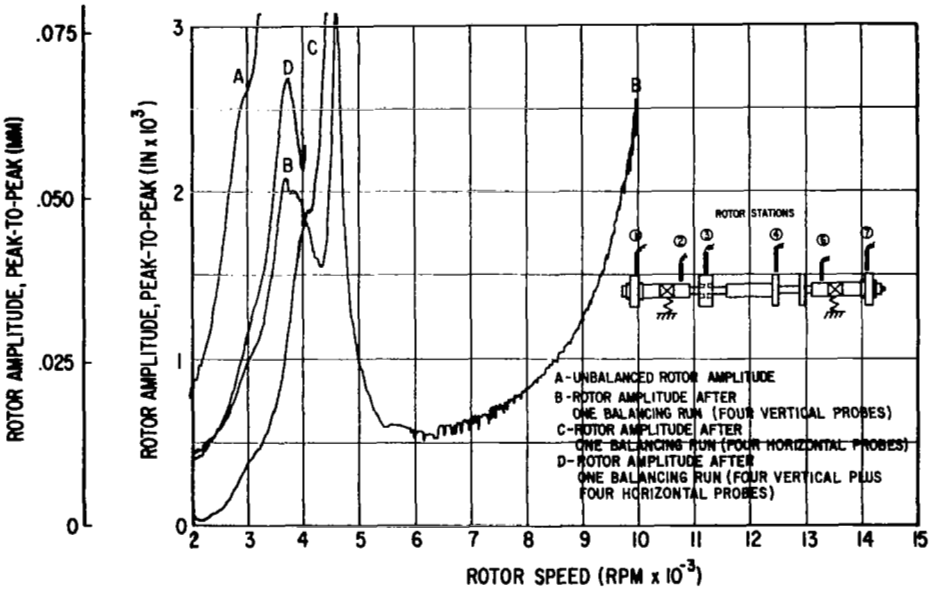

Fig. 65b Horizontal Rotor Amplitudes

Fig. 65 Vertical and Horizontal Rotor Amplitudes at Station 3 — Initial Condition (In-Line, In-Phase Unbalance) and After One Balancing Run by the Least Squares Procedure (Four Vertical Probes, or Four Horizontal Probes, or Four Vertical Plus Four Horizontal Probes)

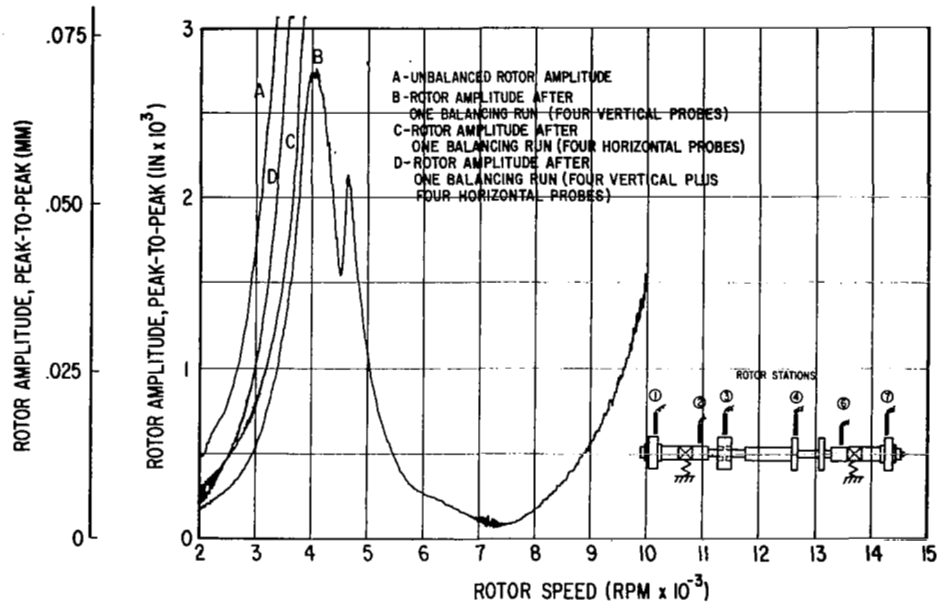

Fig. 66a Vertical Rotor Amplitudes

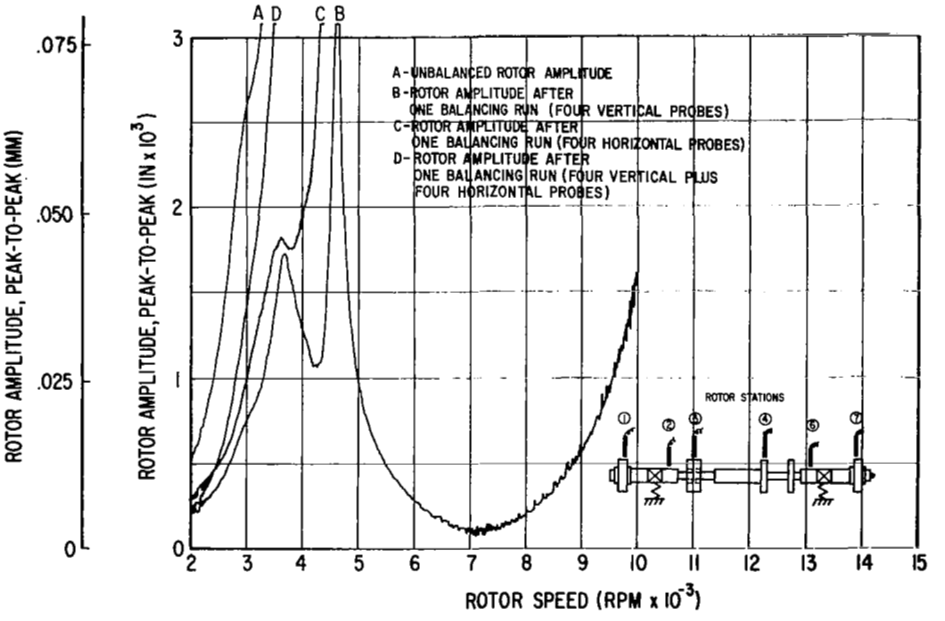

Fig. 66b Horizontal Rotor Amplitudes

Fig. 66 Vertical and Horizontal Rotor Amplitudes at Station 4 — Initial Condition (In-Line, In-Phase Unbalance) and After One Balancing Run by the Least Squares Procedure (Four Vertical Probes, or Four Horizontal Probes, or Four Vertical Plus Four Horizontal Probes)

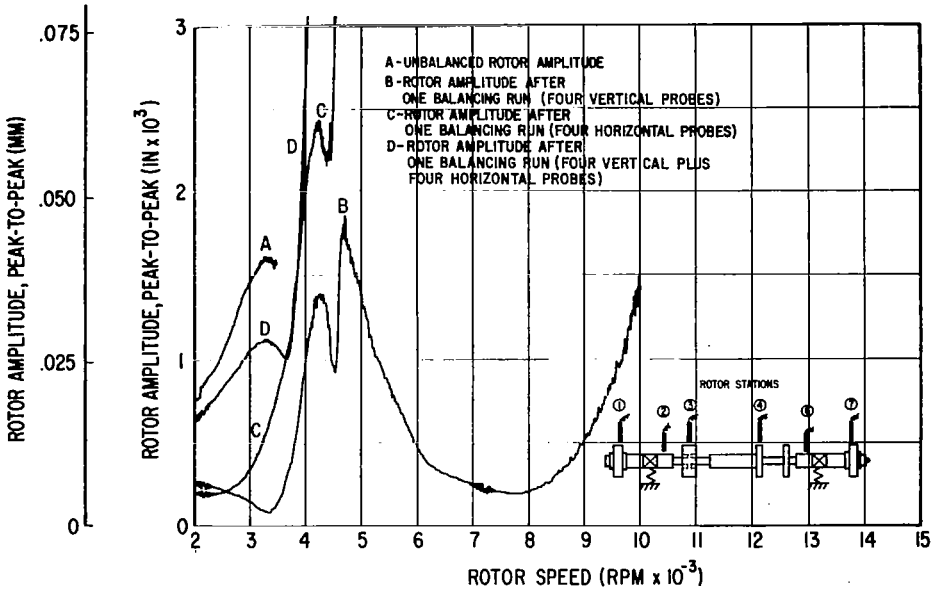

Fig. 67a Vertical Rotor Amplitudes

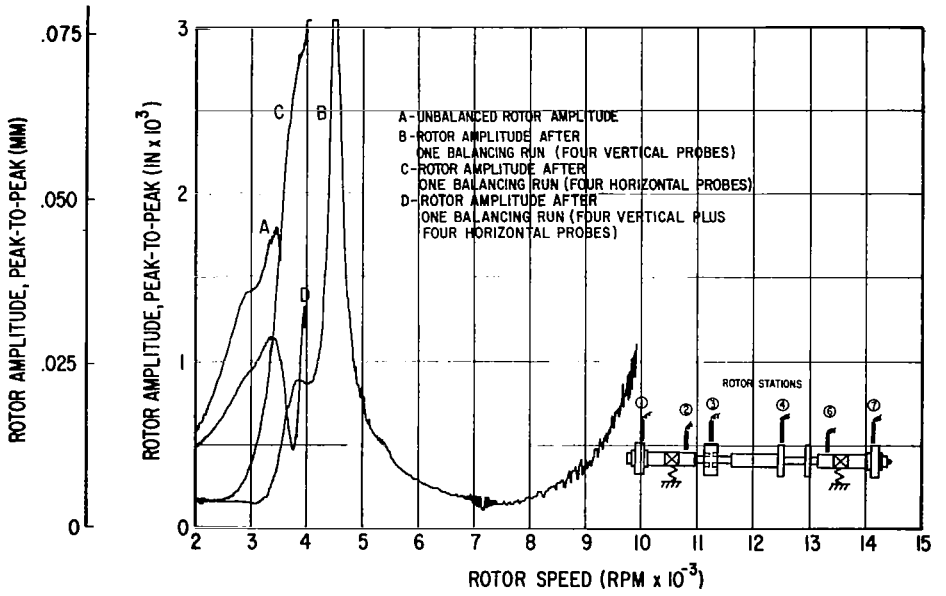

Fig. 67b Horizontal Rotor Amplitudes

Fig. 67 Vertical and Horizontal Rotor Amplitudes at Station 7 — Initial Condition (In-Line, In-Phase Unbalance) and After One Balancing Run by the Least Squares Procedure (Four Vertical Probes, or Four Horizontal Probes, or Four Vertical Plus Four Horizontal Probes)

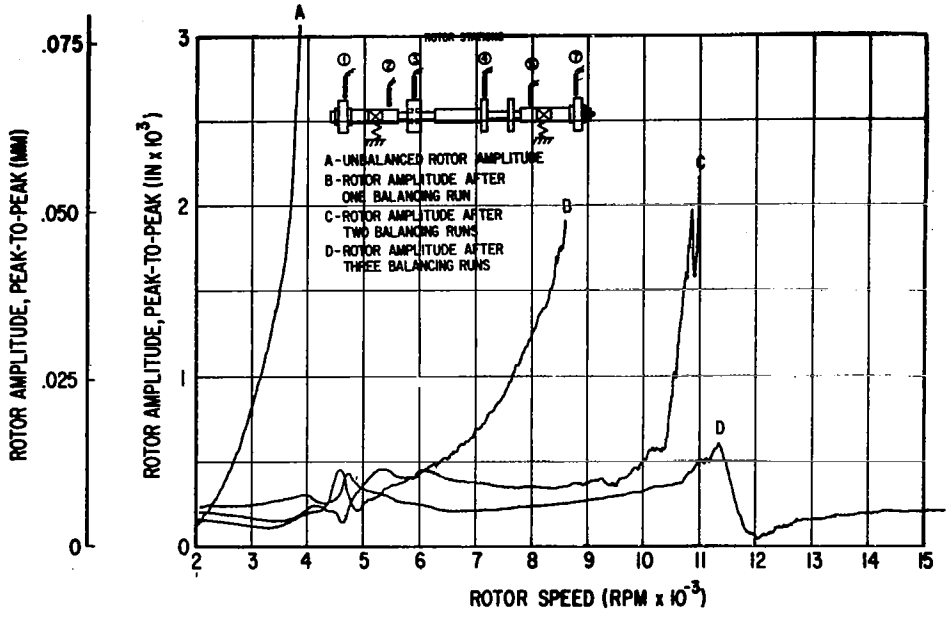

Fig. 68a Vertical Rotor Amplitudes

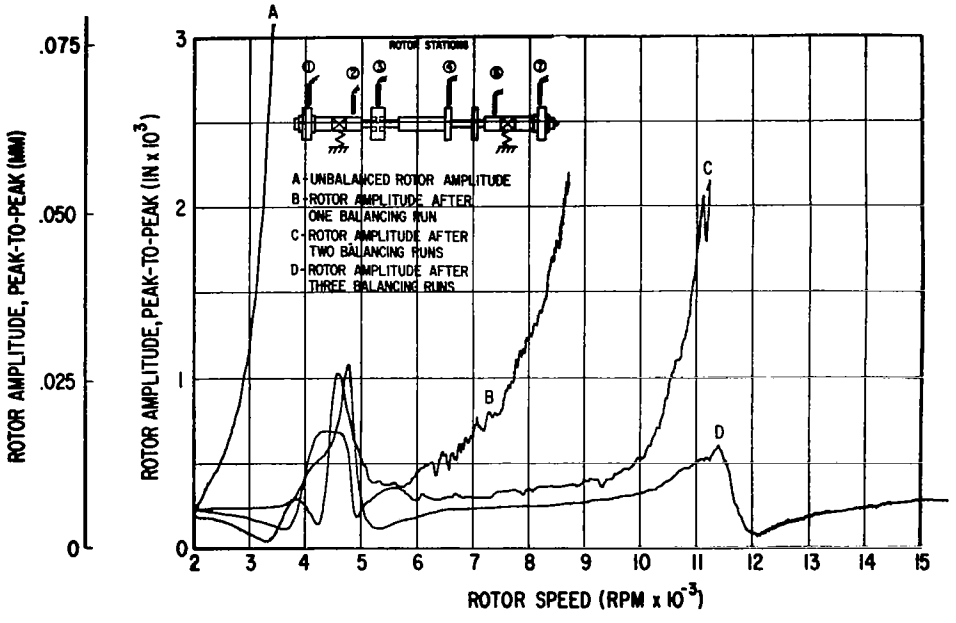

Fig. 68b Horizontal Rotor Amplitudes

Fig. 68 Vertical and Horizontal Rotor Amplitudes at Station 1 — Initial Condition (In-Line, Alternating-Phase Unbalance) and After Three Consecutive Balancing Runs by the Least Squares Procedure (Four Vertical Probes)

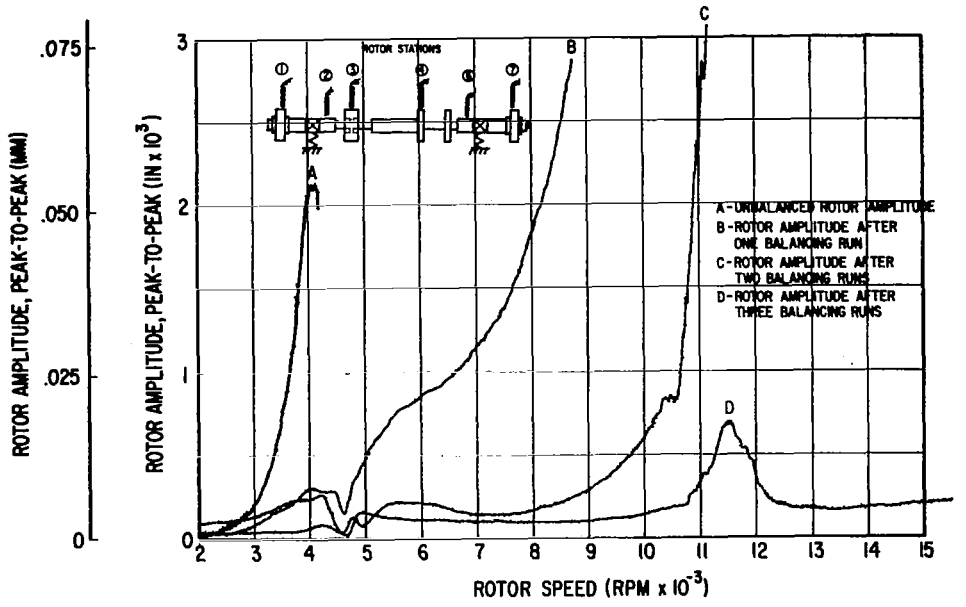

Fig. 69a Vertical Rotor Amplitudes

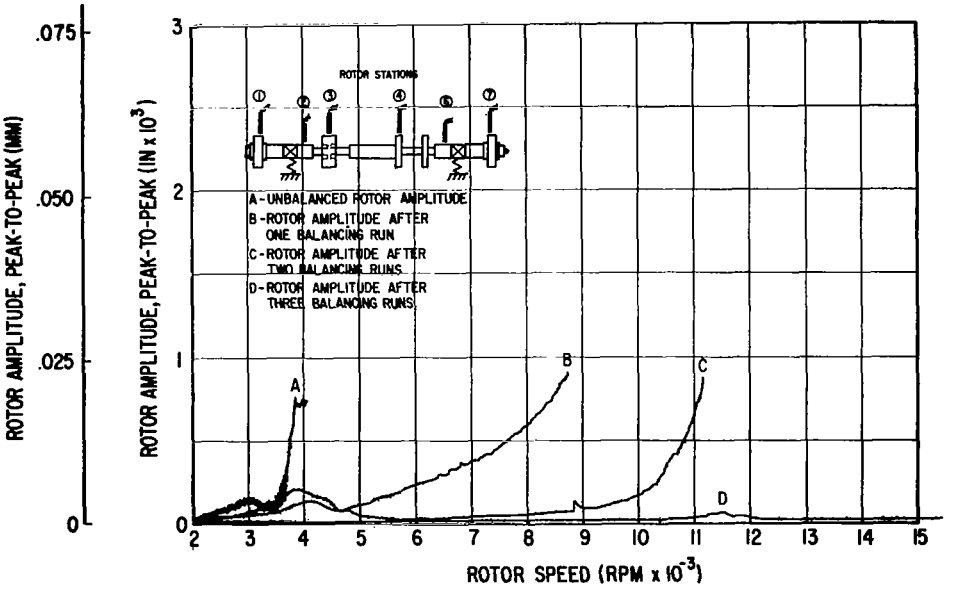

Fig. 69b Horizontal Rotor Amplitudes

Fig. 69 Vertical and Horizontal Rotor Amplitudes at Station 2 — Initial Condition (In-Line, Alternating-Phase Unbalance) and After Three Consecutive Balancing Runs by the Least Squares Procedure (Four Vertical Probes)

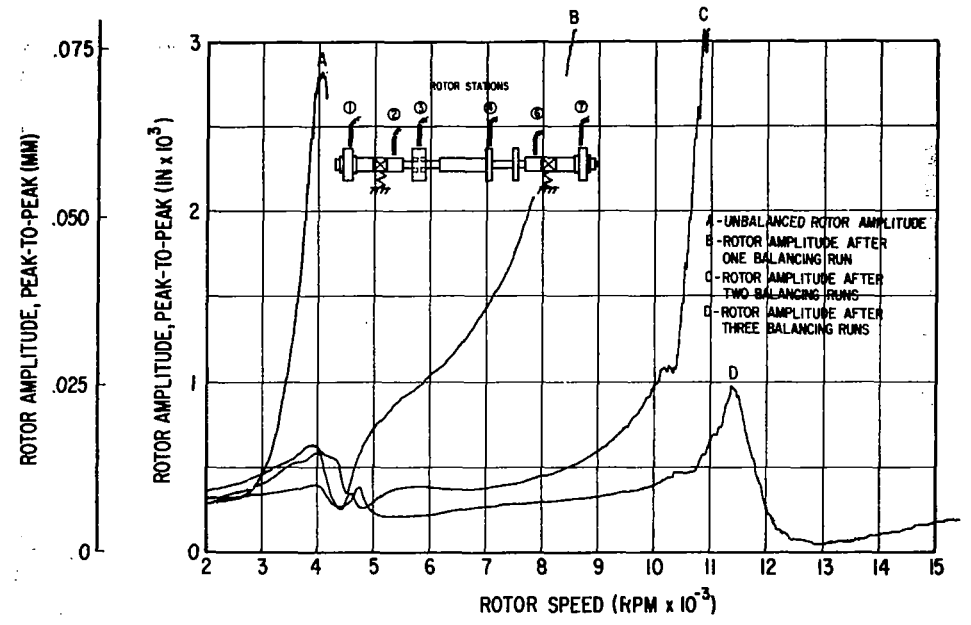

Fig. 70a Vertical Rotor Amplitudes

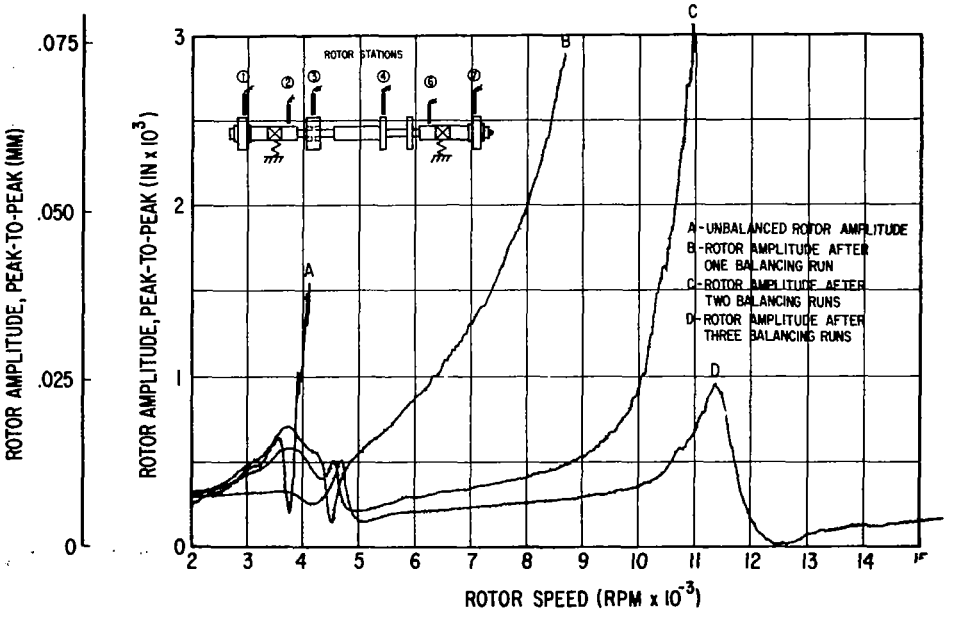

Fig. 70b Horizontal Rotor Amplitudes

Fig. 70 Vertical and Horizontal Rotor Amplitudes at Station 3 — Initial Condition (In-Line, Alternating-Phase Unbalance) and After Three Consecutive Balancing Runs by the Least Squares Procedure (Four Vertical Probes)

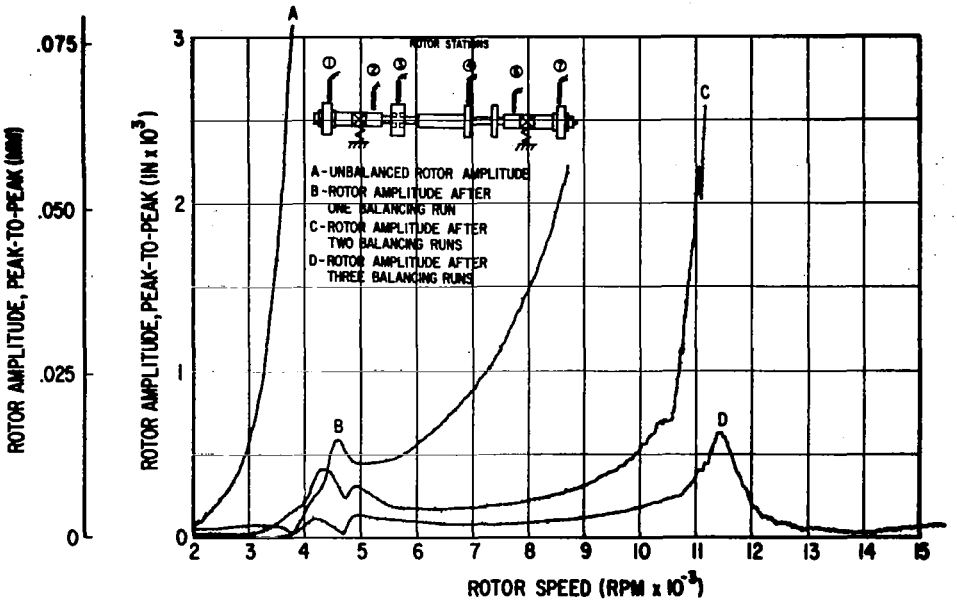

Fig. 71a Vertical Rotor Amplitudes

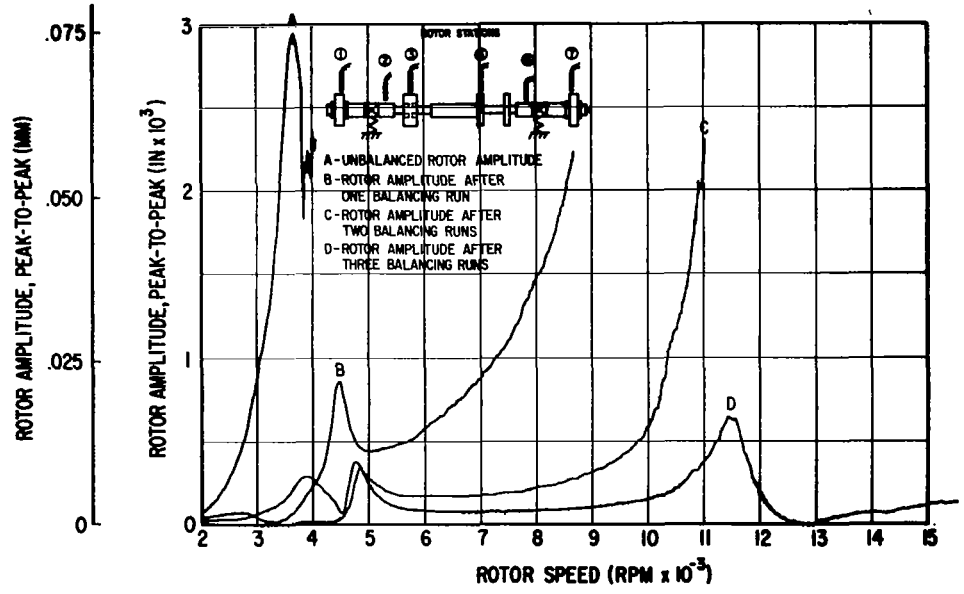

Fig. 71b Horizontal Rotor Amplitudes

Fig. 71 Vertical and Horizontal Rotor Amplitudes at Station 4 — Initial Condition (In-Line, Alternating-Phase Unbalance) and After Three Consecutive Balancing Runs by the Least Squares Procedure (Four Vertical Probes)

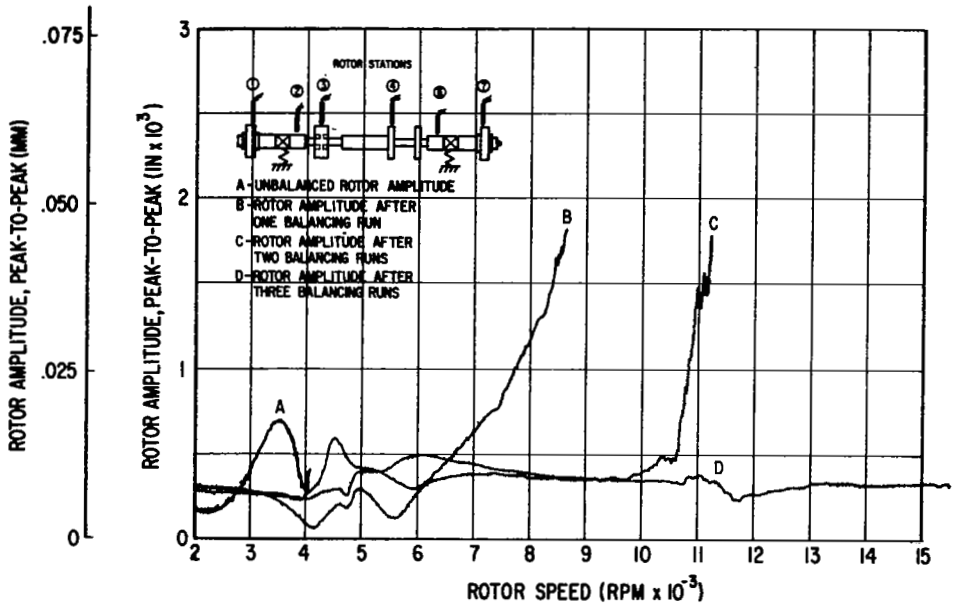

Fig. 72a Vertical Rotor Amplitudes

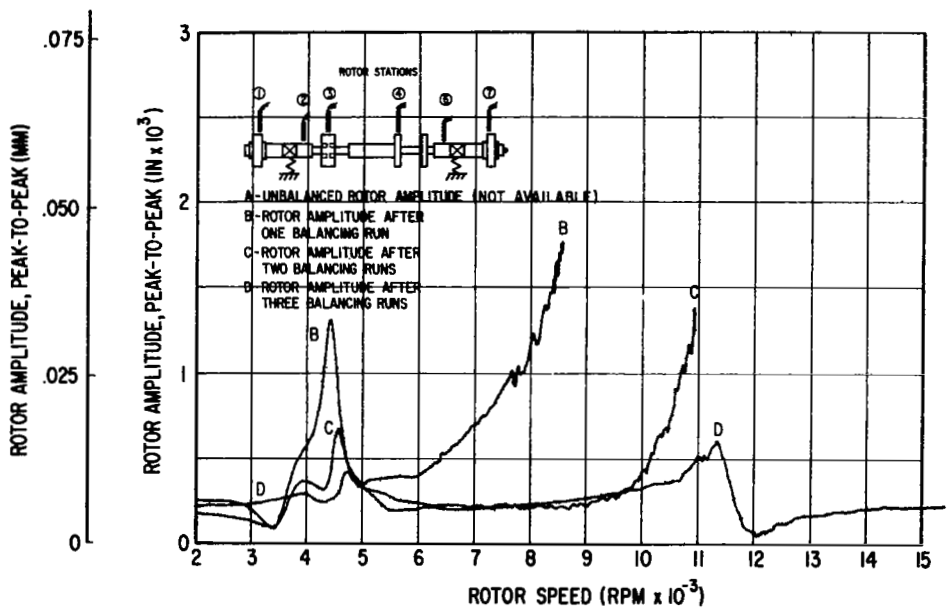

Fig. 72b Horizontal Rotor Amplitudes

Fig. 72 Vertical and Horizontal Rotor Amplitudes at Station 7 — Initial Condition (In-Line, Alternating-Phase Unbalance) and After Three Consecutive Balancing Runs by the Least Squares Procedure (Four Vertical Probes)

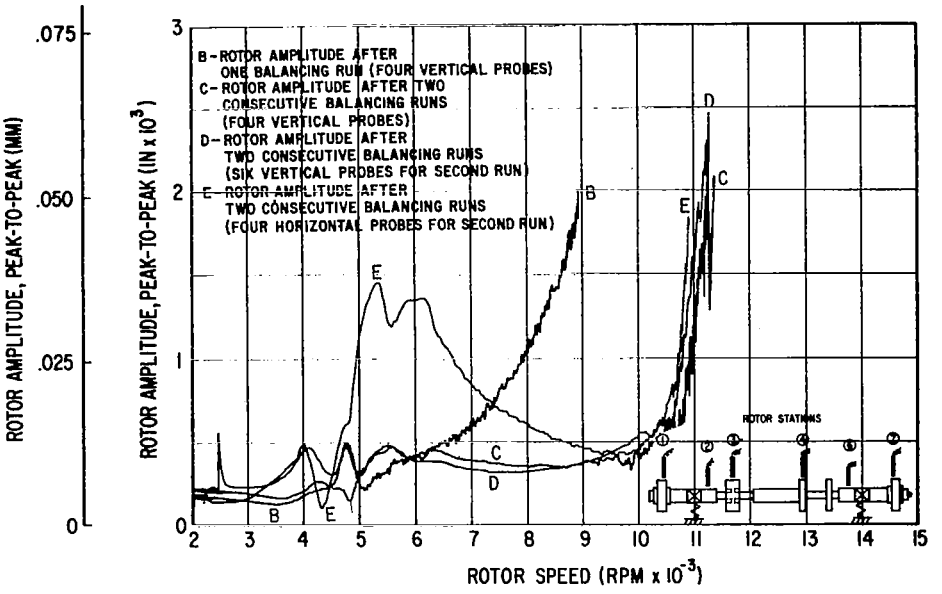

Fig. 73a Vertical Rotor Amplitudes

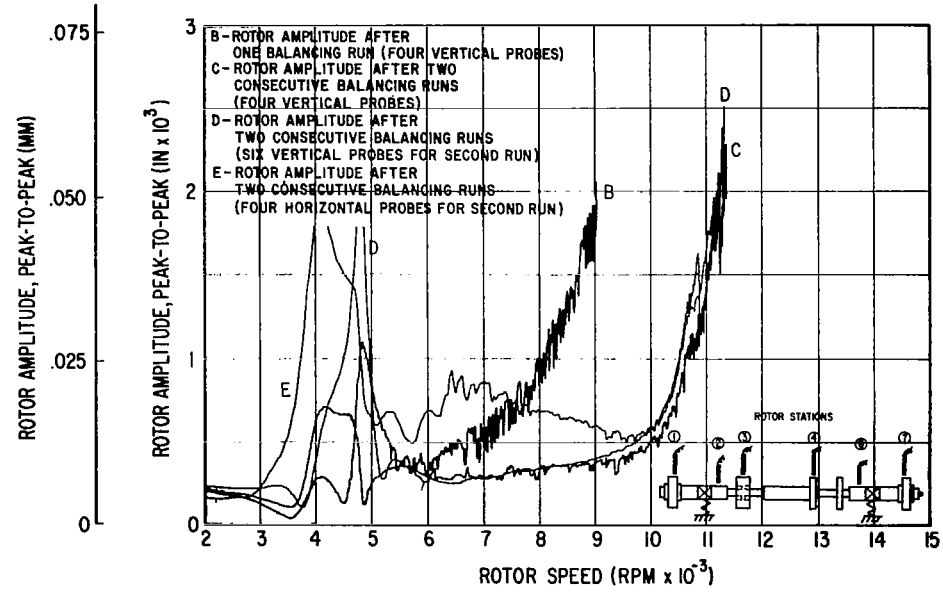

Fig. 73b Horizontal Rotor Amplitudes

Fig. 73 Vertical and Horizontal Rotor Amplitudes at Station 1 — (In-Line, Alternating-Phase Unbalance) After Two Consecutive Balancing Runs by the Least Squares Procedure (Four Vertical Probes at the First Run, and Either Four Vertical Probes, or Six Vertical Probes or Four Horizontal Probes at the Second Run)

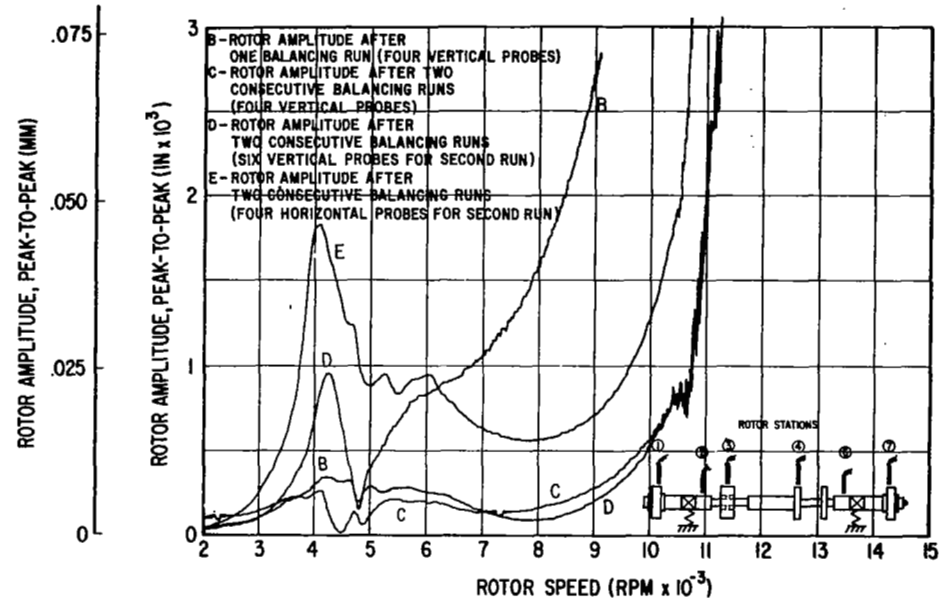

Fig. 74a Vertical Rotor Amplitudes

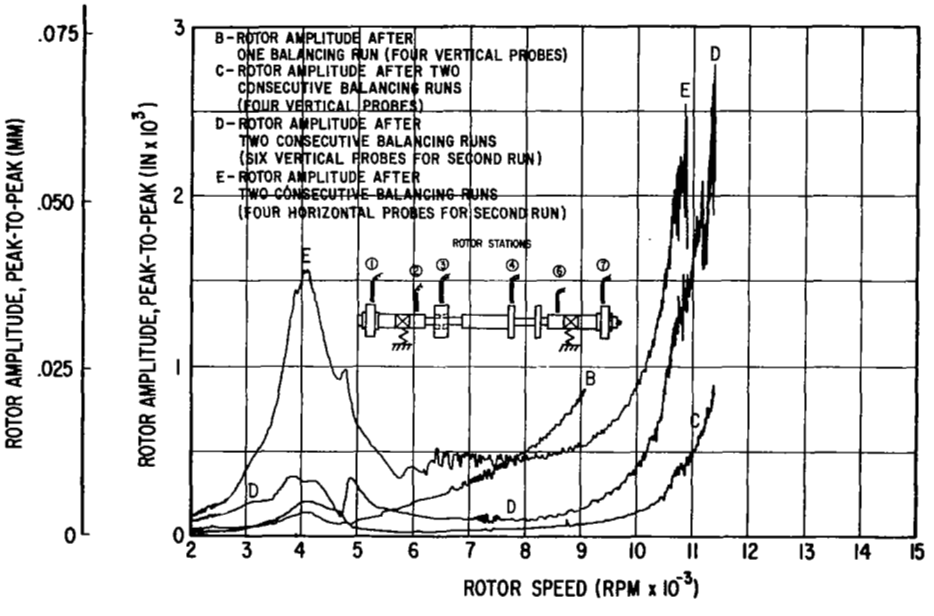

Fig. 74b Horizontal Rotor Amplitudes

Fig. 74 Vertical and Horizontal Rotor Amplitudes at Station 2 — (In-Line, Alternating-Phase Unbalance) After Two Consecutive Balancing Runs by the Least Squares Procedure (Four Vertical Probes at the First Run, and Either Four Vertical Probes, or Six Vertical Probes or Four Horizontal Probes at the Second Run)

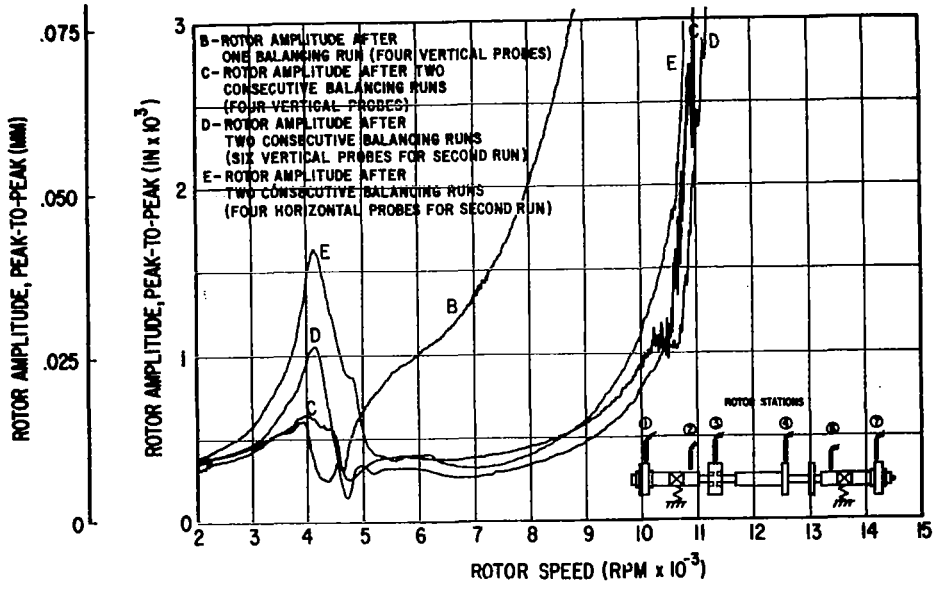

Fig. 75a Vertical Rotor Amplitudes

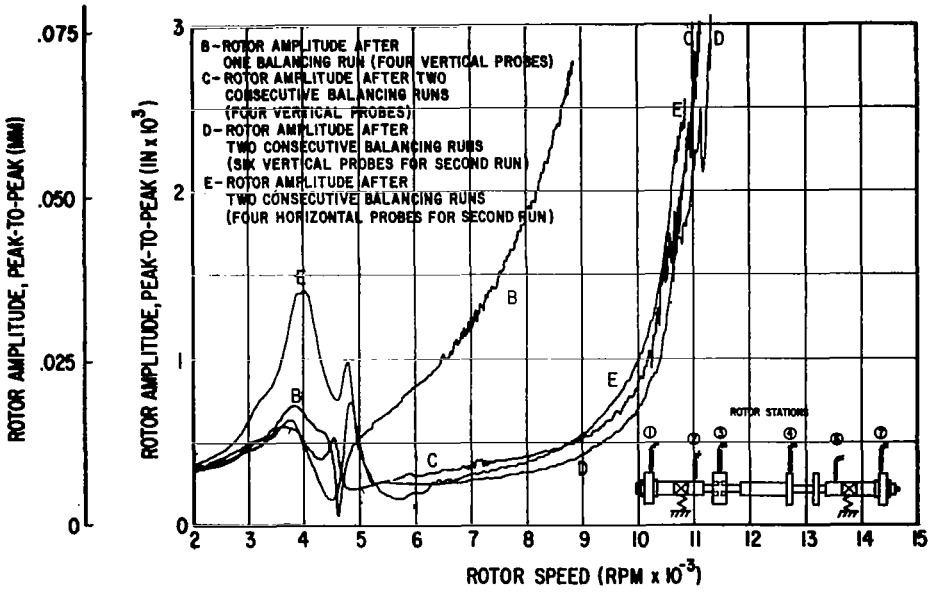

Fig. 75b Horizontal Rotor Amplitudes

Fig. 75 Vertical and Horizontal Rotor Amplitudes at Station 3 — (In-Line, Alternating-Phase Unbalance) After Two Consecutive Balancing Runs by the Least Squares Procedure (Four Vertical Probes at the First Run, and Either Four Vertical Probes, or Six Vertical Probes or Four Horizontal Probes at the Second Run)

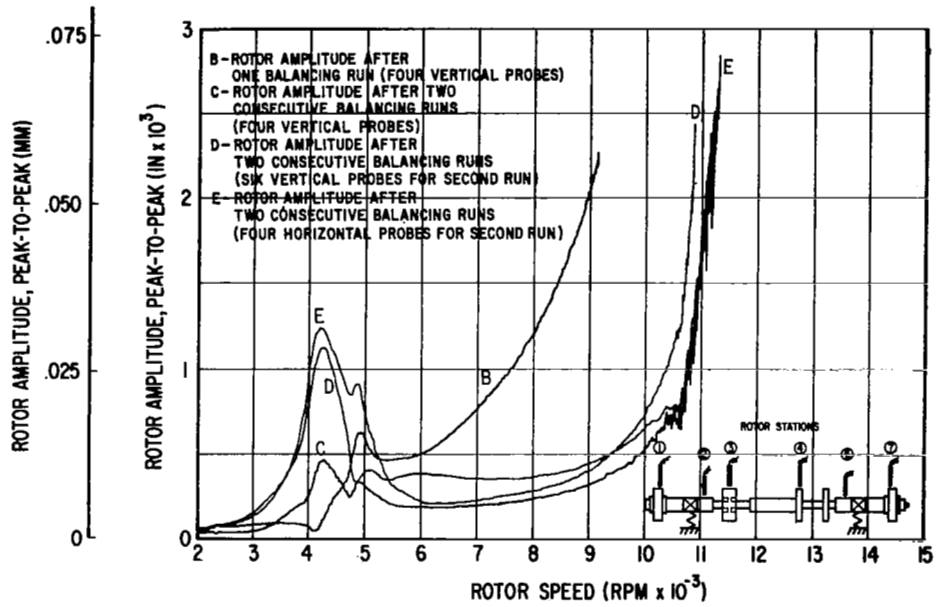

Fig. 76a Vertical Rotor Amplitudes

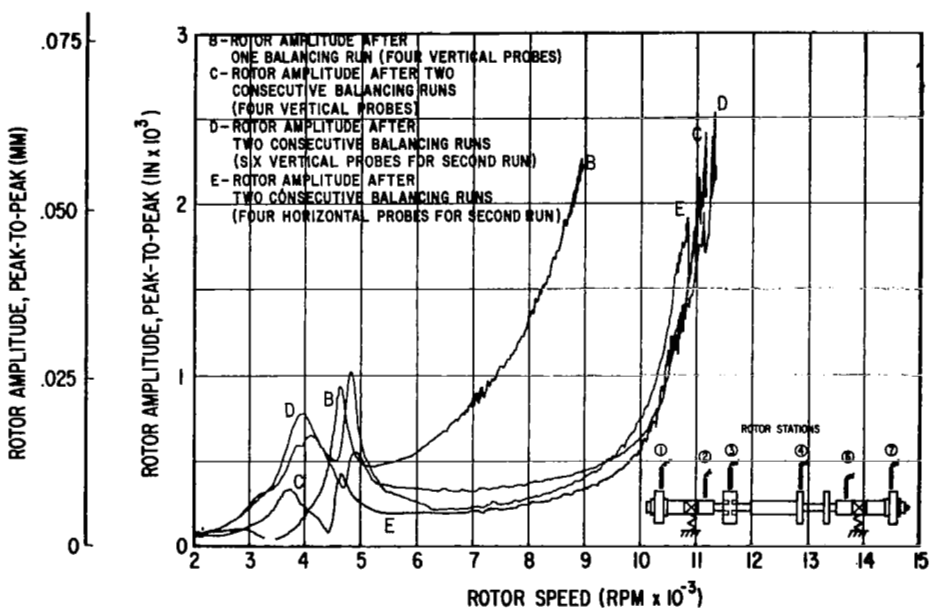

Fig. 76b Horizontal Rotor Amplitudes

Fig. 76 Vertical and Horizontal Rotor Amplitudes at Station 4 — (In-Line, Alternating-Phase Unbalance) After Two Consecutive Balancing Runs by the Least Squares Procedure (Four Vertical Probes at the First Run, and Either Four Vertical Probes, or Six Vertical Probes or Four Horizontal Probes at the Second Run)

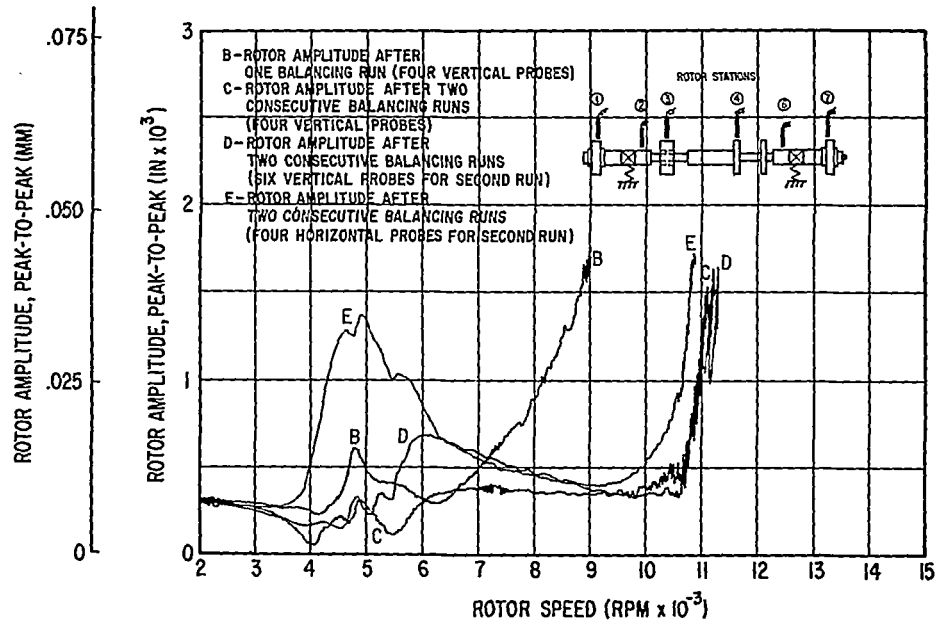

Fig. 77a Vertical Rotor Amplitudes

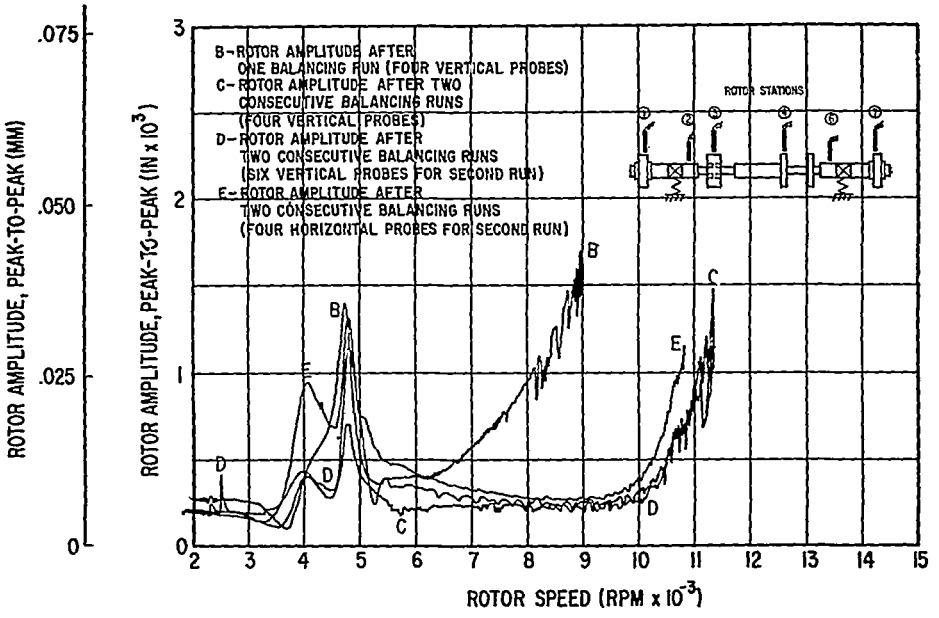

Fig. 77b Horizontal Rotor Amplitudes

Fig. 77 Vertical and Horizontal Rotor Amplitudes at Station 7 — (In-Line, Alternating-Phase Unbalance) After Two Consecutive Balancing Runs by the Least Squares Procedure (Four Vertical Probes at the First Run, and Either Four Vertical Probes, or Six Vertical Probes or Four Horizontal Probes at the Second Run)

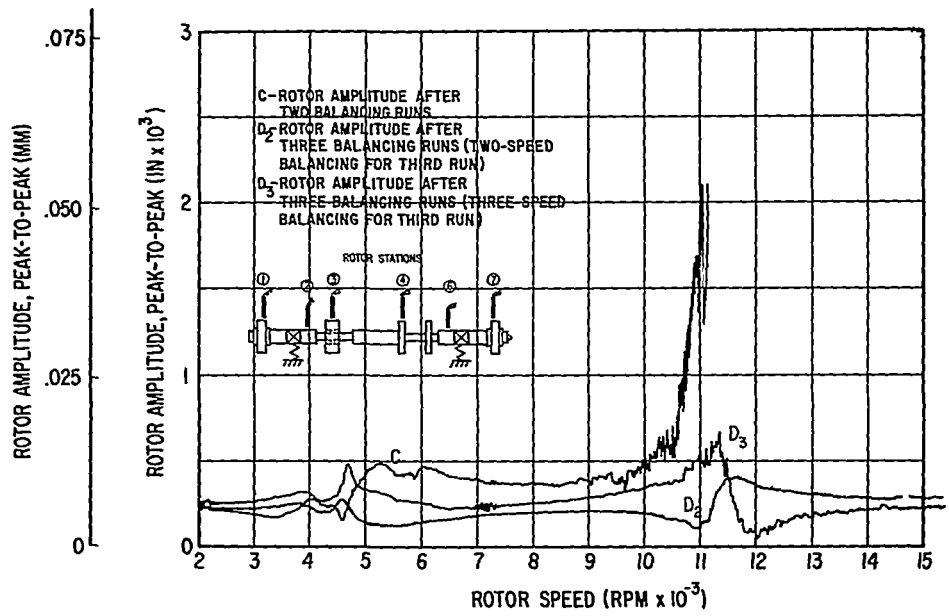

Fig. 78a Vertical Rotor Amplitudes

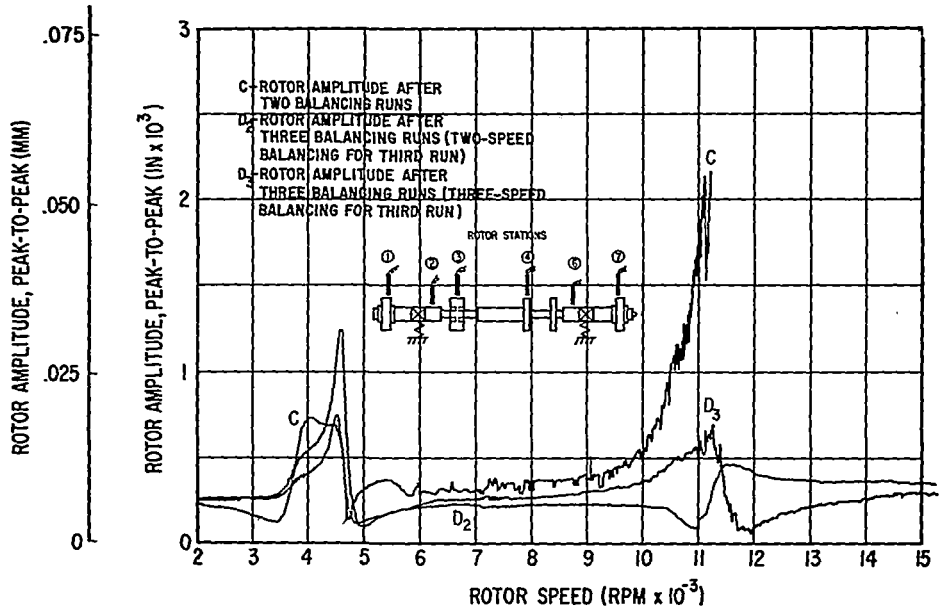

Fig. 78b Horizontal Rotor Amplitudes

Fig. 78 Vertical and Horizontal Rotor Amplitudes at Station 1 – (In-Line, Alternating-Phase Unbalance) After Two and Three Consecutive Balancing Runs by the Least Squares Procedure (Four Probes, Two Speeds and Four Probes, Three Speeds)

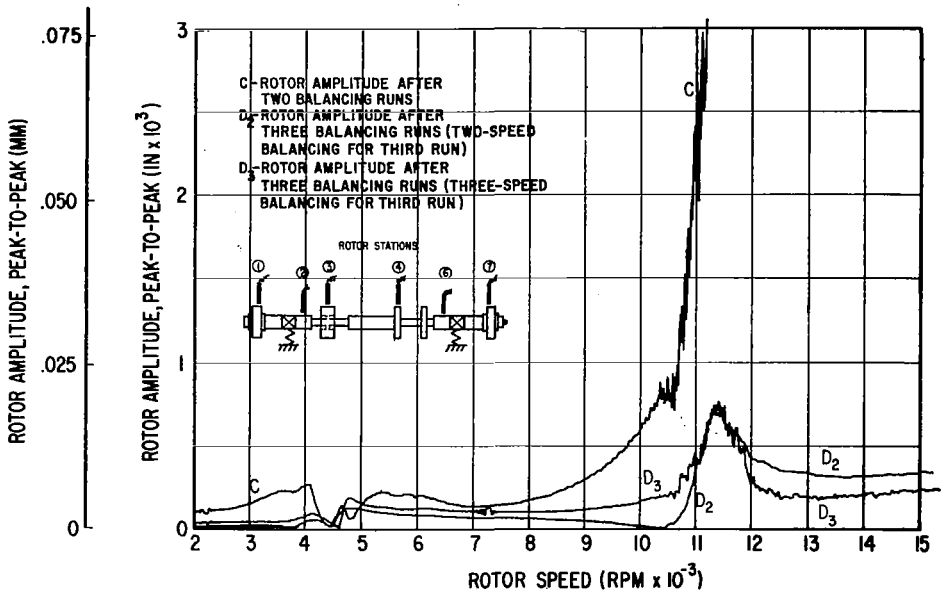

Fig. 79a Vertical Rotor Amplitudes

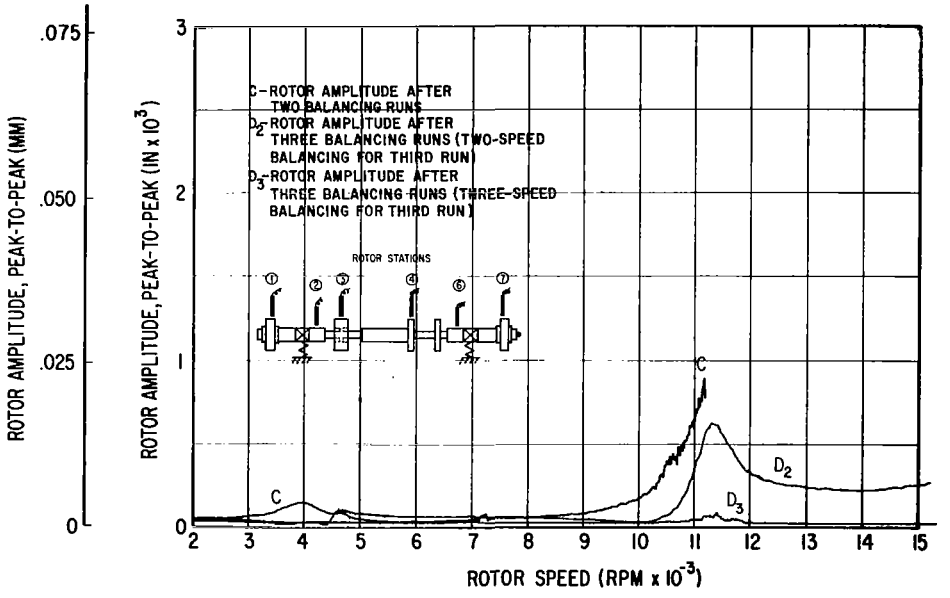

Fig. 79b Horizontal Rotor Amplitudes

Fig. 79 Vertical and Horizontal Rotor Amplitudes at Station 2 — (In-Line, Alternating-Phase Unbalance) After Two and Three Consecutive Balancing Runs by the Least Squares Procedure (Four Probes, Two Speeds and Four Probes, Three Speeds)

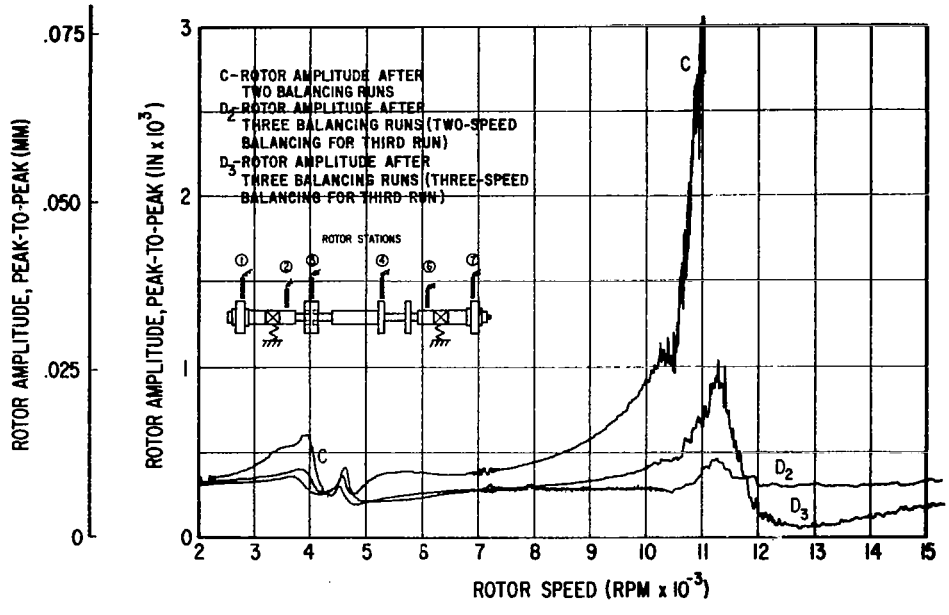

Fig. 80a Vertical Rotor Amplitudes

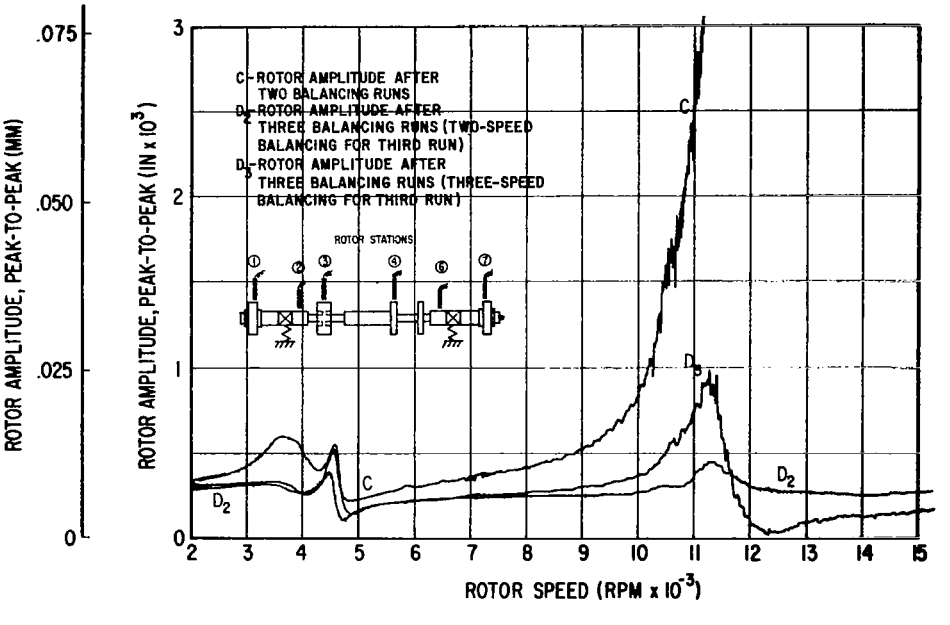

Fig. 80b Horizontal Rotor Amplitudes

Fig. 80 Vertical and Horizontal Rotor Amplitudes at Station 3 — (In-Line, Alternating-Phase Unbalance) After Two and Three Consecutive Balancing Runs by the Least Squares Procedure (Four Probes, Two Speeds and Four Probes, Three Speeds)

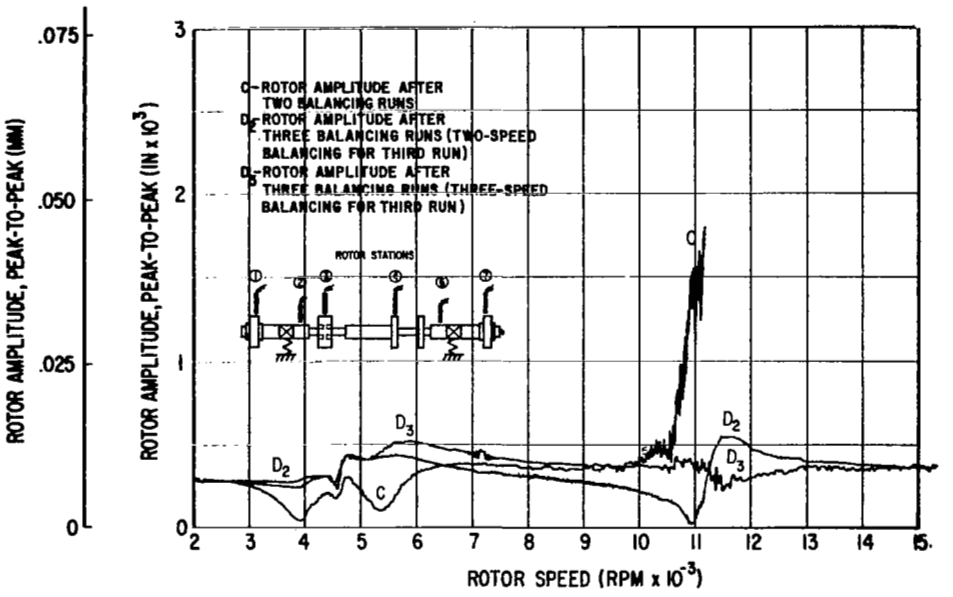

Fig. 81a Vertical Rotor Amplitudes

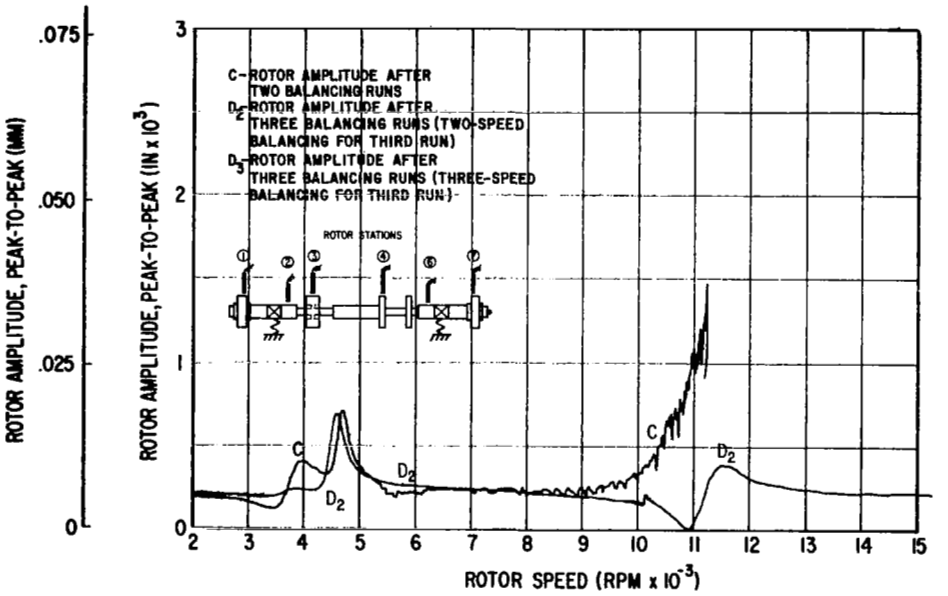

Fig. 81b Horizontal Rotor Amplitudes

Fig. 81 Vertical and Horizontal Rotor Amplitudes at Station 7 – (In-Line, Alternating-Phase Unbalance) After Two and Three Consecutive Balancing Runs by the Least Squares Procedure (Four Probes, Two Speeds and Four Probes, Three Speeds)

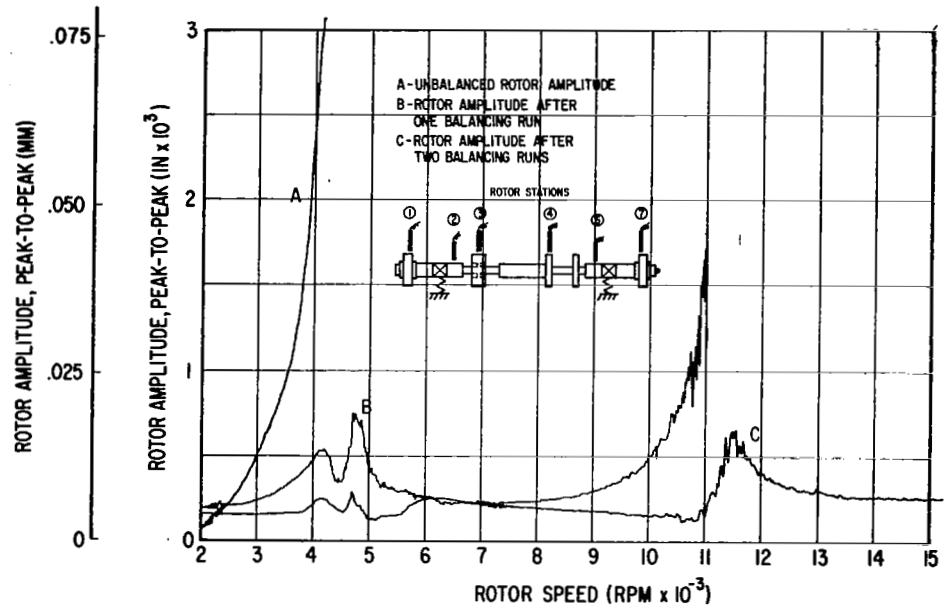

Fig. 82a Vertical Rotor Amplitudes

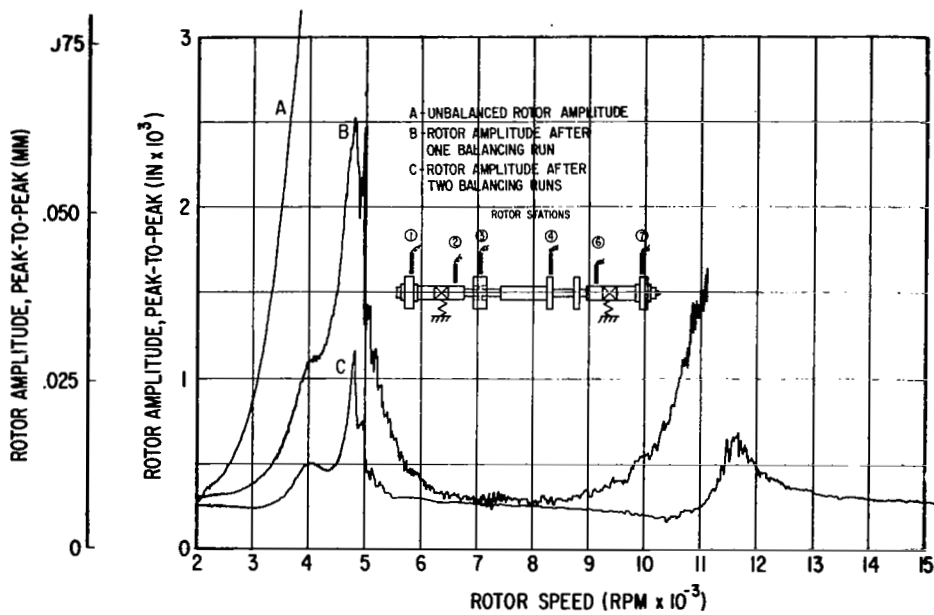

Fig. 82b Horizontal Rotor Amplitudes

Fig. 82 Vertical and Horizontal Rotor Amplitudes at Station 1 — Initial Condition (In-Line, Alternating-Phase Unbalance) and After Two Consecutive Balancing Runs by the Least Squares Procedure (Four Vertical Probes)

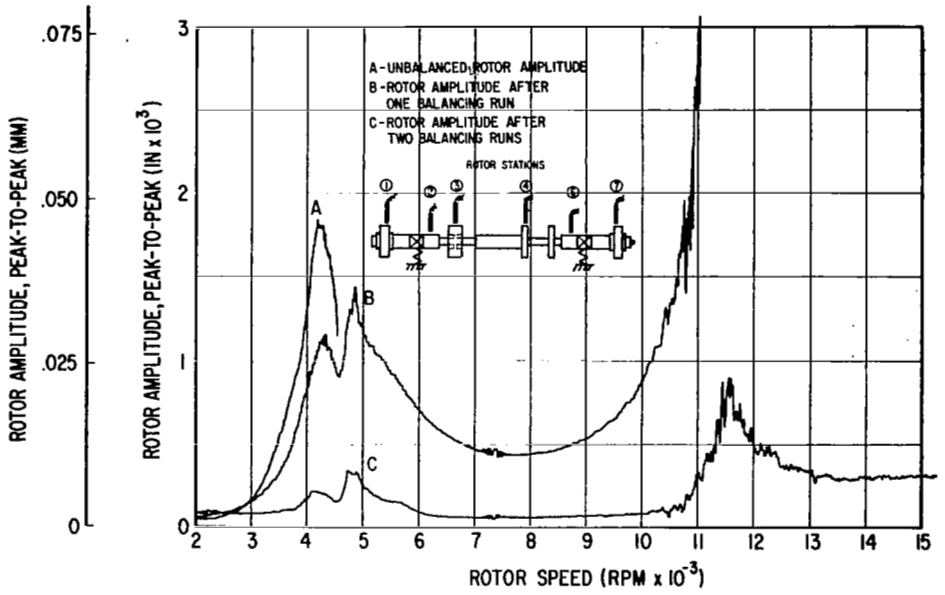

Fig. 83a Vertical Rotor Amplitudes

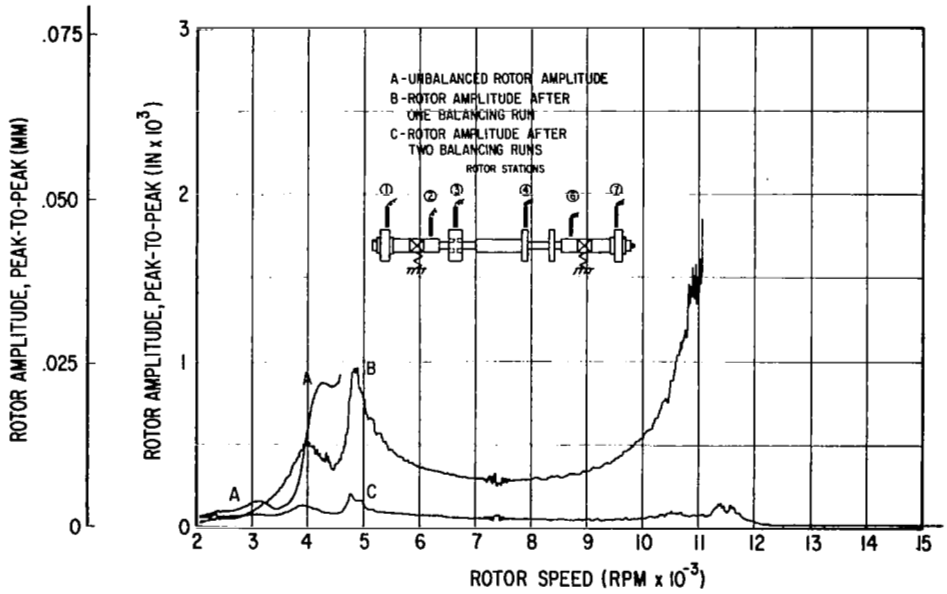

Fig. 83b Horizontal Rotor Amplitudes

Fig. 83 Vertical and Horizontal Rotor Amplitudes at Station 2 — Initial Condition (In-Line, Alternating-Phase Unbalance) and After Two Consecutive Balancing Runs by the Least Squares Procedure (Four Vertical Probes)

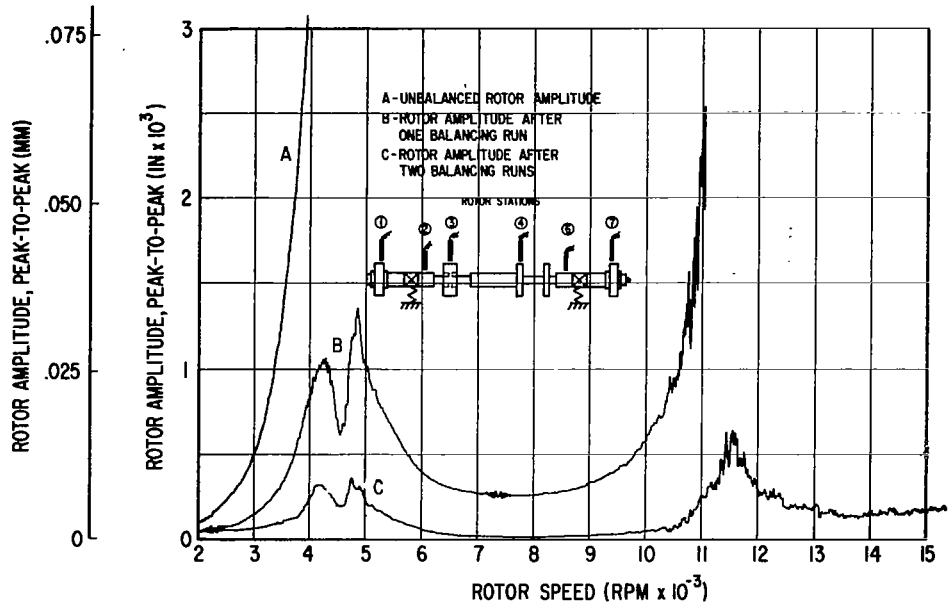

Fig. 84a Vertical Rotor Amplitudes

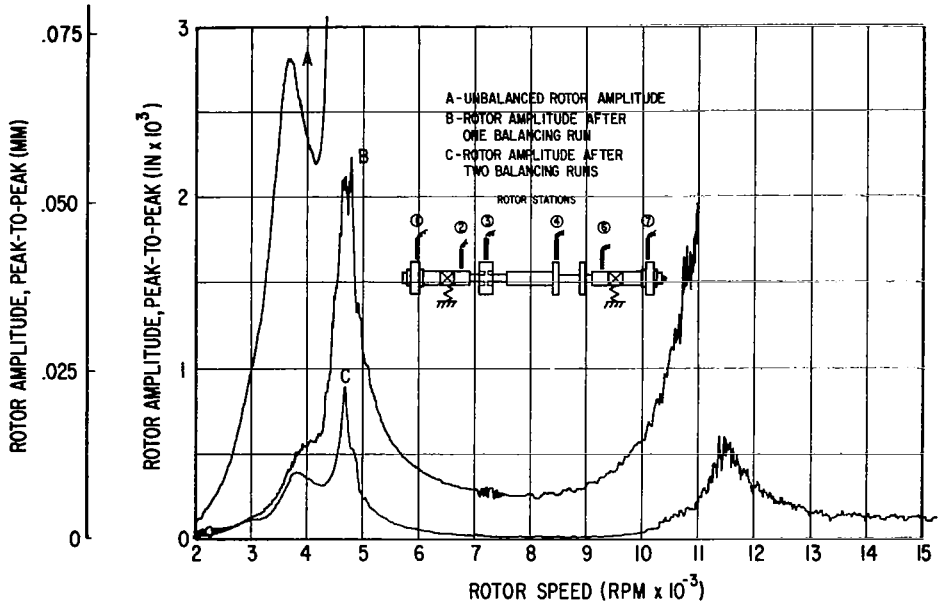

Fig. 84b Horizontal Rotor Amplitudes

Fig. 84 Vertical and Horizontal Rotor Amplitudes at Station 4 — Initial Condition (In-Line, Alternating-Phase Unbalance) and After Two Consecutive Balancing Runs by the Least Squares Procedure (Four Vertical Probes)

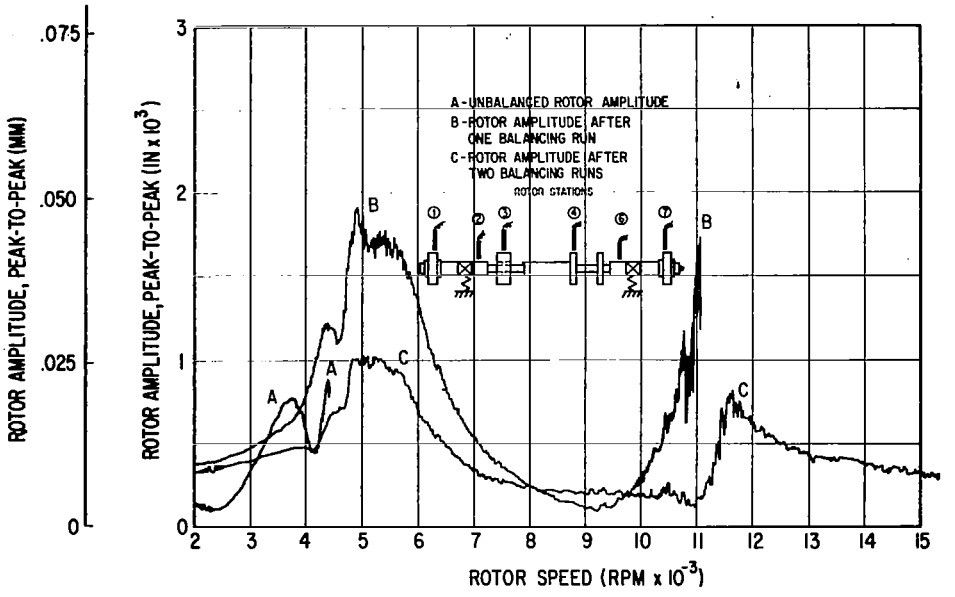

Fig. 85a Vertical Rotor Amplitudes

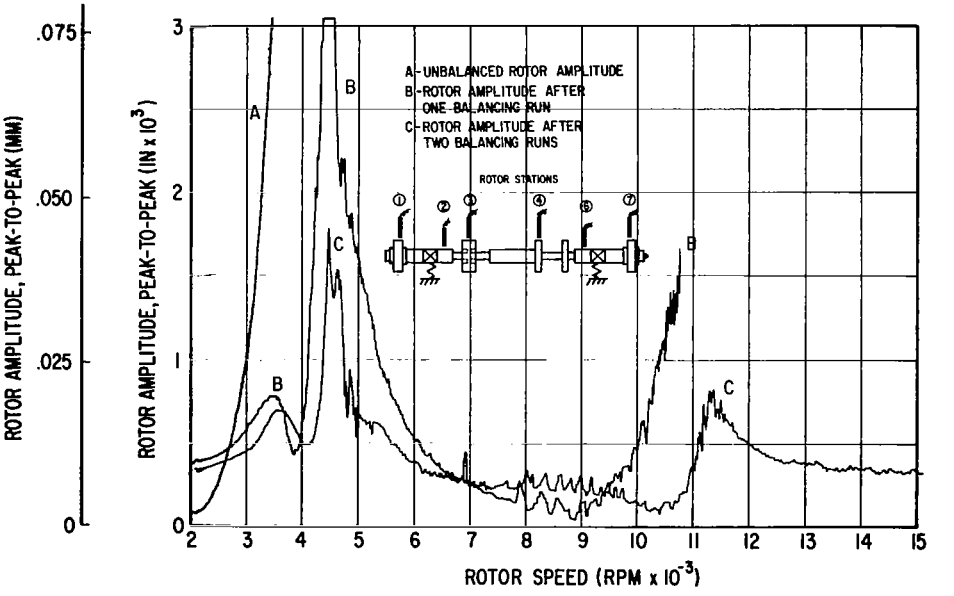

Fig. 85b Horizontal Rotor Amplitudes

Fig. 85 Vertical and Horizontal Rotor Amplitudes at Station 7 — Initial Condition (In-Line, Alternating-Phase Unbalance) and After Two Consecutive Balancing Runs by the Least Squares Procedure (Four Vertical Probes)

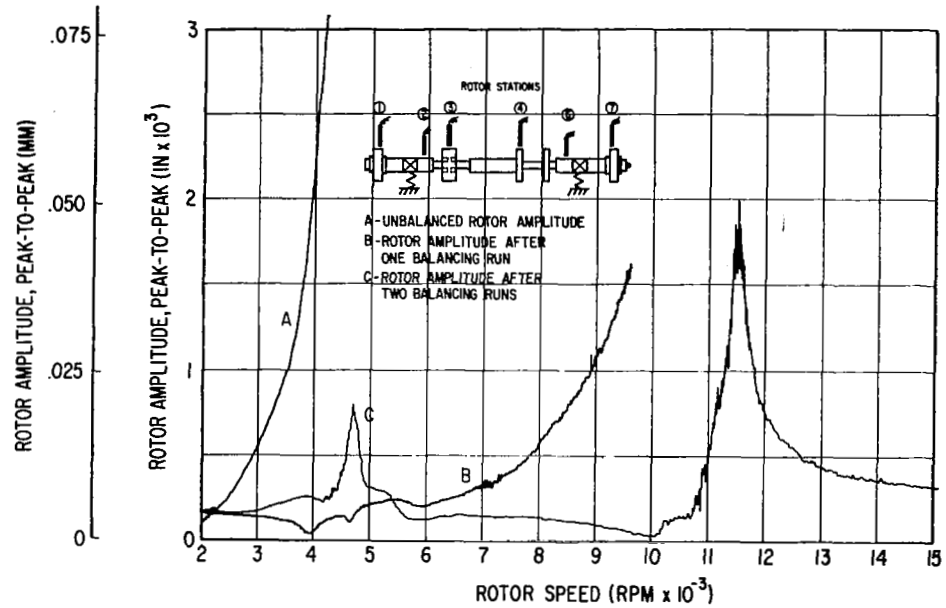

Fig. 86a Vertical Rotor Amplitudes

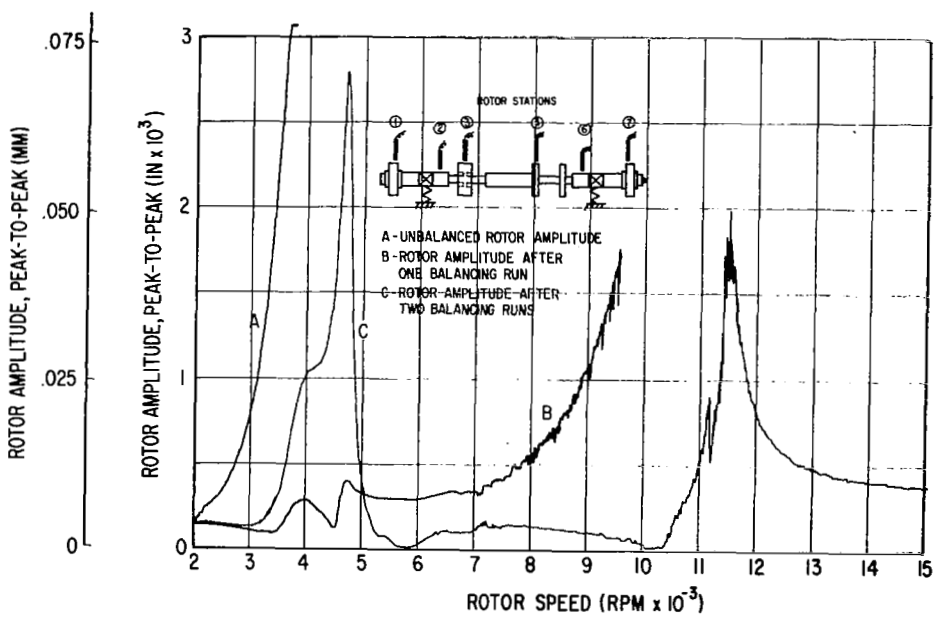

Fig. 86b Horizontal Rotor Amplitudes

Fig. 86 Vertical and Horizontal Rotor Amplitudes at Station 1 — Initial Condition (In-Line, Alternating-Phase Unbalance) and After Two Consecutive Balancing Runs by the Least Squares Procedure (Four Horizontal Probes)

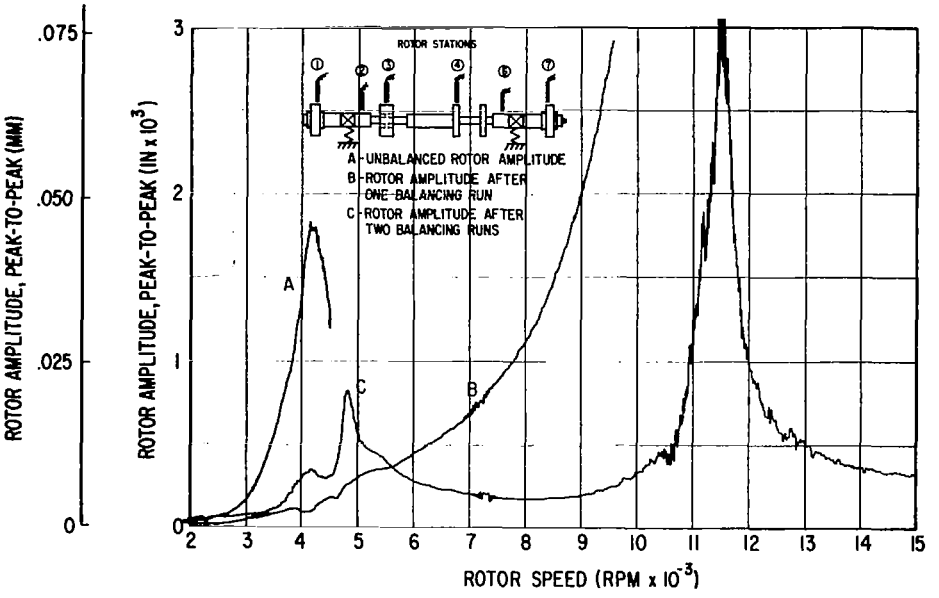

Fig. 87a Vertical Rotor Amplitudes

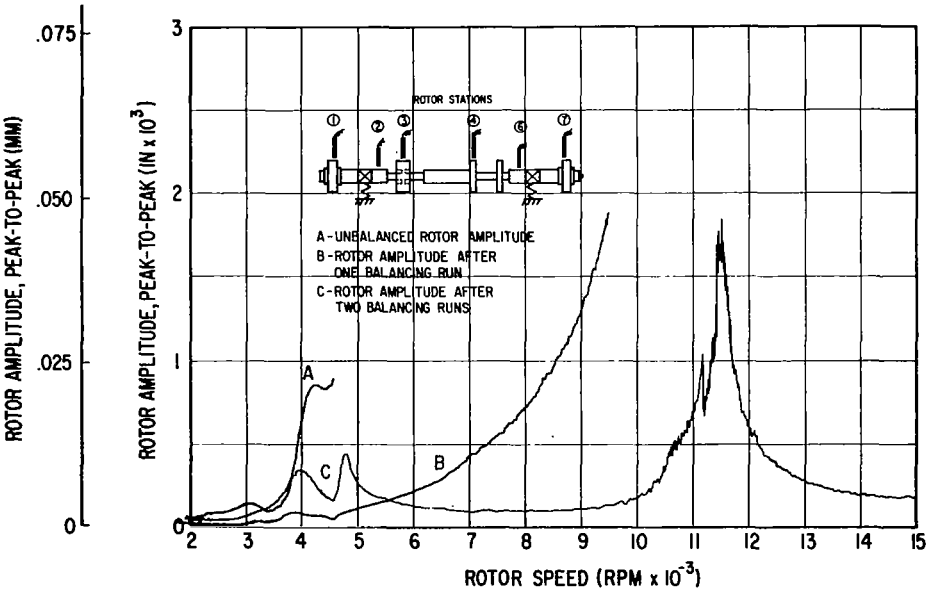

Fig. 87b Horizontal Rotor Amplitudes

Fig. 87 Vertical and Horizontal Rotor Amplitudes at Station 2 — Initial Condition (In-Line, Alternating-Phase Unbalance) and After Two Consecutive Balancing Runs by the Least Squares Procedure (Four Horizontal Probes)

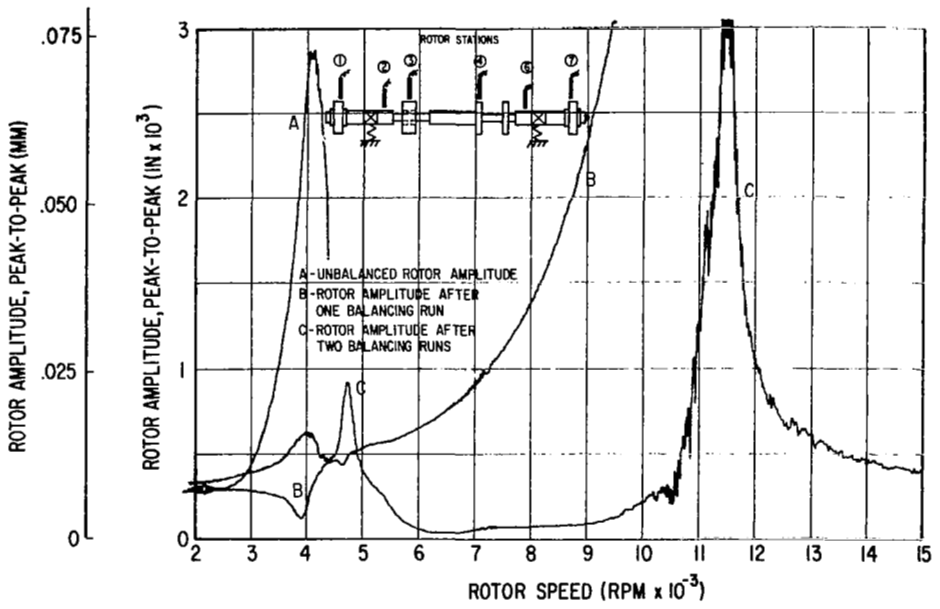

Fig. 88a Vertical Rotor Amplitudes

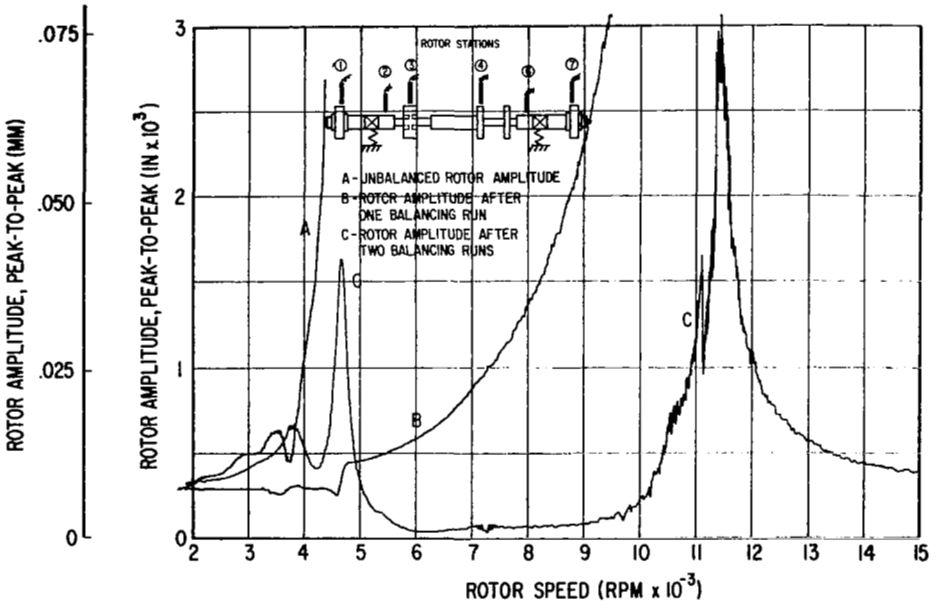

Fig. 88b Horizontal Rotor Amplitudes

Fig. 88 Vertical and Horizontal Rotor Amplitudes at Station 3 — Initial Condition (In-Line, Alternating-Phase Unbalance) and After Two Consecutive Balancing Runs by the Least Squares Procedure (Four Horizontal Probes)

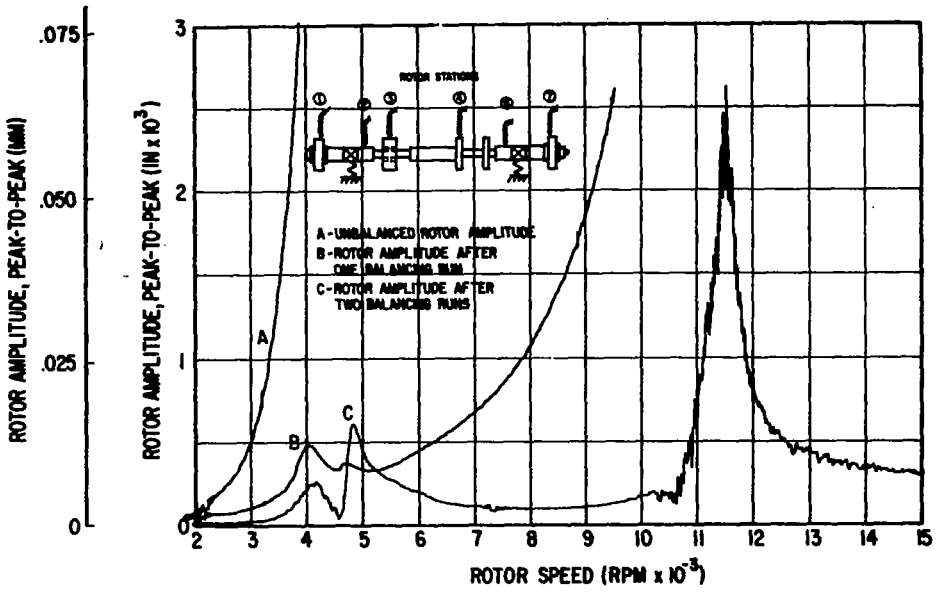

Fig. 89a Vertical Rotor Amplitudes

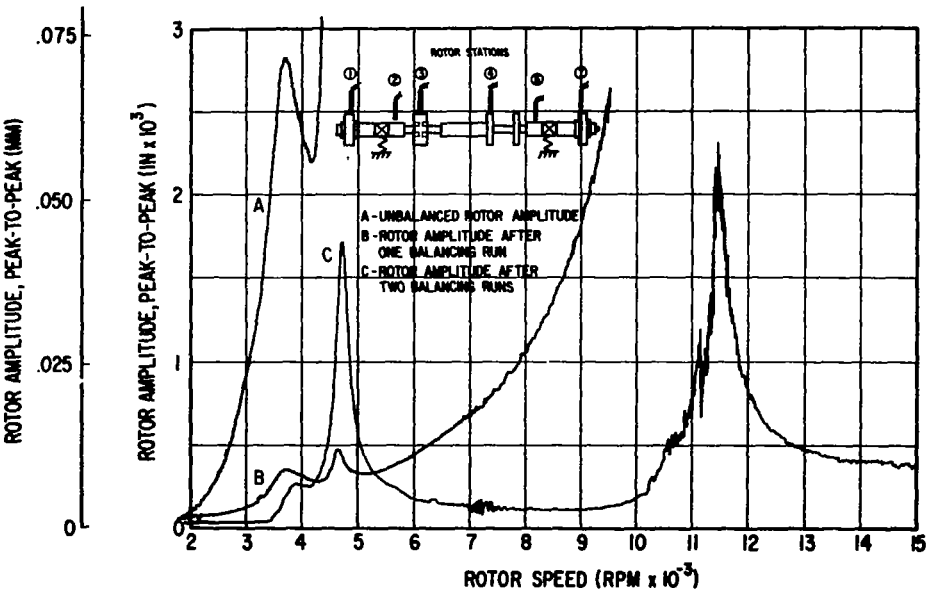

Fig. 89b Horizontal Rotor Amplitudes

Fig. 89 Vertical and Horizontal Rotor Amplitudes at Station 4 — Initial Condition (In-Line, Alternating-Phase Unbalance) and After Two Consecutive Balancing Runs by the Least Squares Procedure (Four Horizontal Probes)

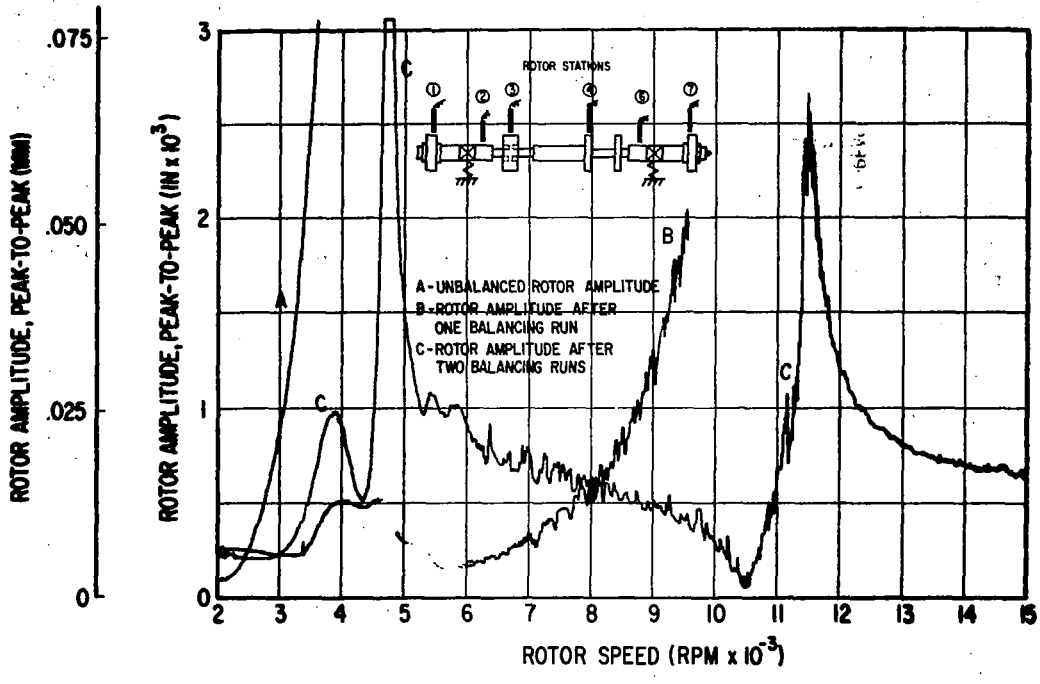

Fig. 90 Horizontal Rotor Amplitudes at Station 7 - Initial Condition (In-Line, Alternating-Phase Unbalance) and After Two Consecutive Balancing Runs by the Least Squares Procedure (Four Horizontal Probes)

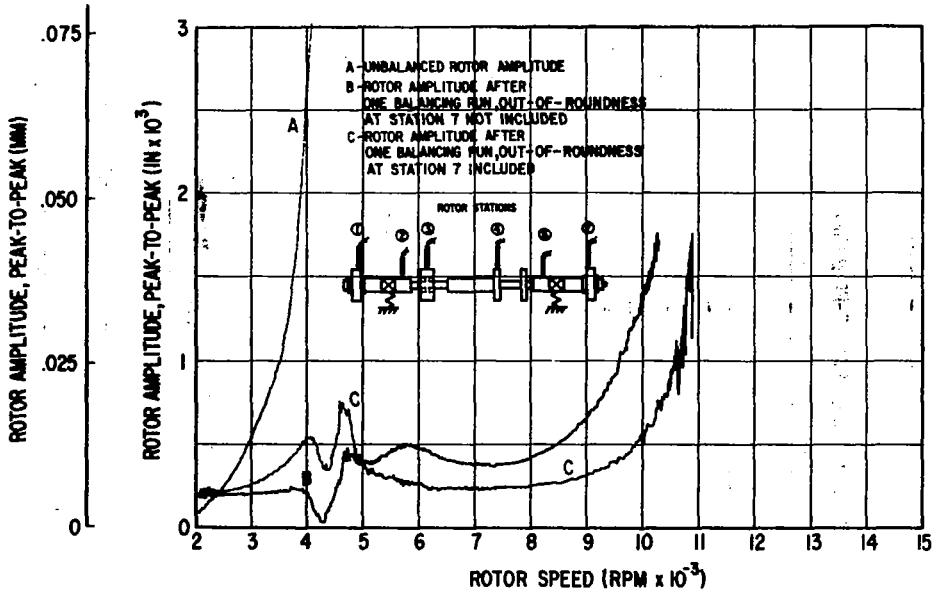

Fig. 91a Vertical Rotor Amplitudes

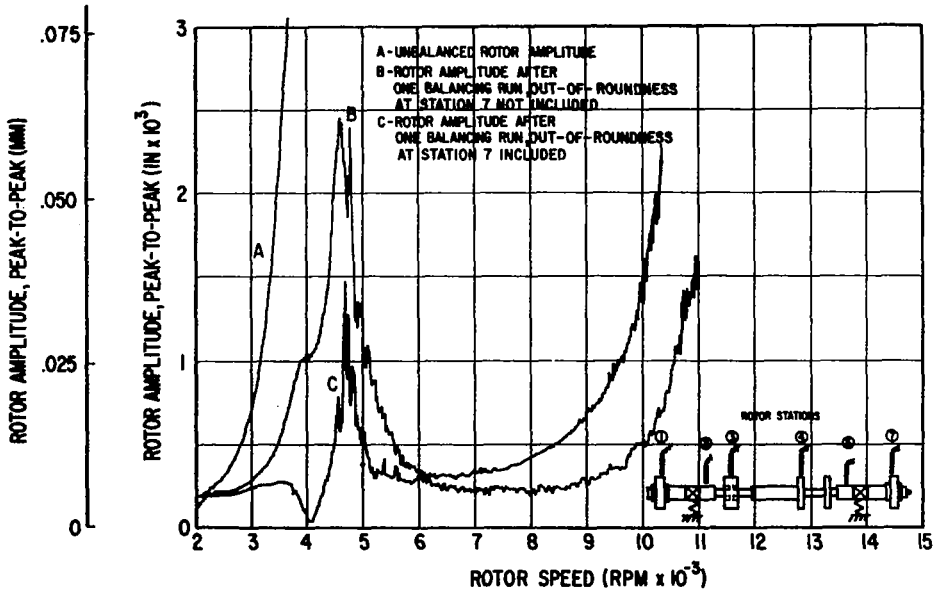

Fig. 91b Horizontal Rotor Amplitudes

Fig. 91 Vertical and Horizontal Rotor Amplitudes at Station 1 — Initial Condition (In-Line, Alternating-Phase Unbalance) and After One Balancing Run by the Least Squares Procedure (Four Vertical Probes With and Without Out-Of-Roundness at Station 7 Considered)

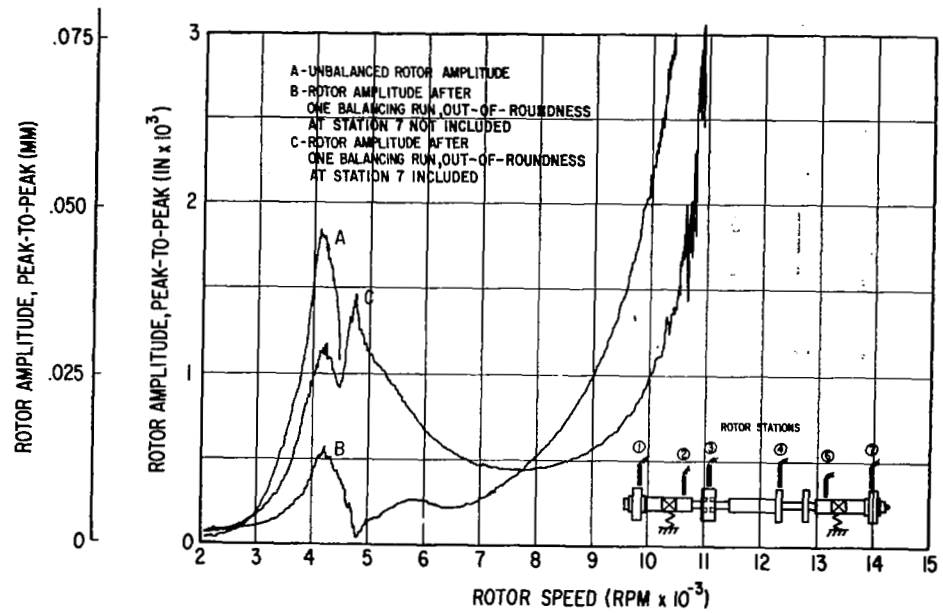

Fig. 92a Vertical Rotor Amplitudes

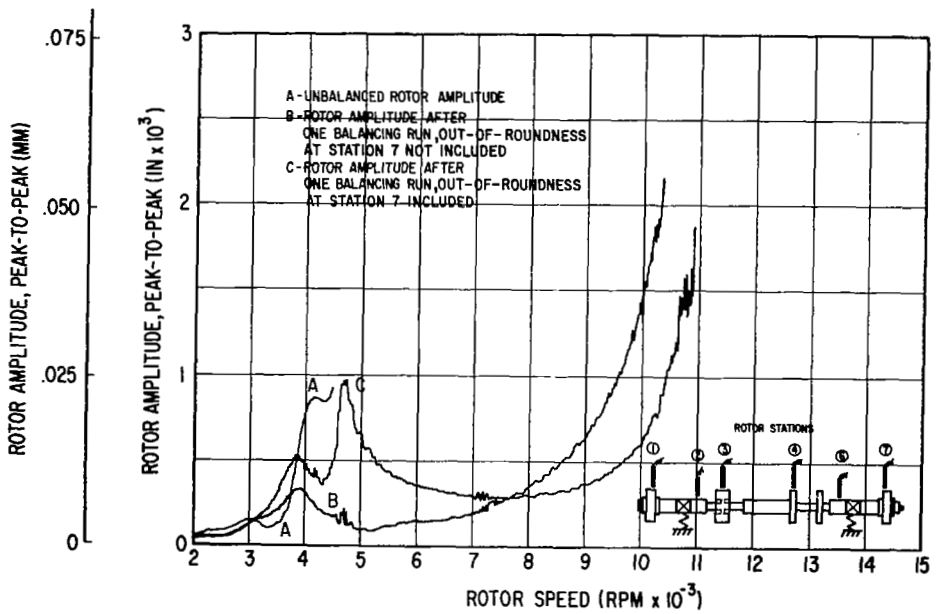

Fig. 92b Horizontal Rotor Amplitudes

Fig. 92 Vertical and Horizontal Rotor Amplitudes at Station 2 – Initial Condition (In-Line, Alternating-Phase Unbalance) and After One Balancing Run by the Least Squares Procedure (Four Vertical Probes With and Without Out-Of-Roundness at Station 7 Considered)

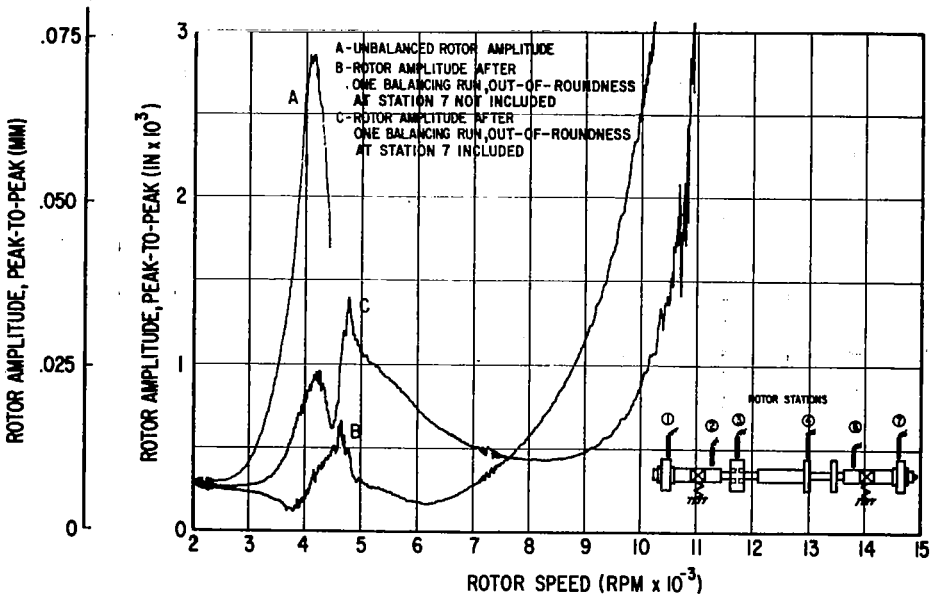

Fig. 93a Vertical Rotor Amplitudes

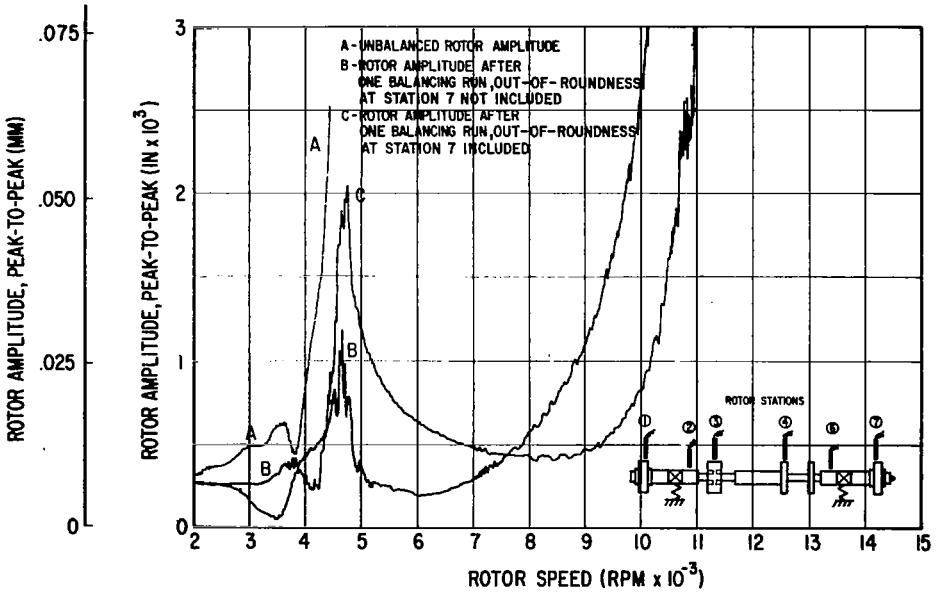

Fig. 93b Horizontal Rotor Amplitudes

Fig. 93 Vertical and Horizontal Rotor Amplitudes at Station 3 — Initial Condition (In-Line, Alternating-Phase Unbalance) and After One Balancing Run by the Least Squares Procedure (Four Vertical Probes With and Without Out-Of-Roundness at Station 7 Considered)

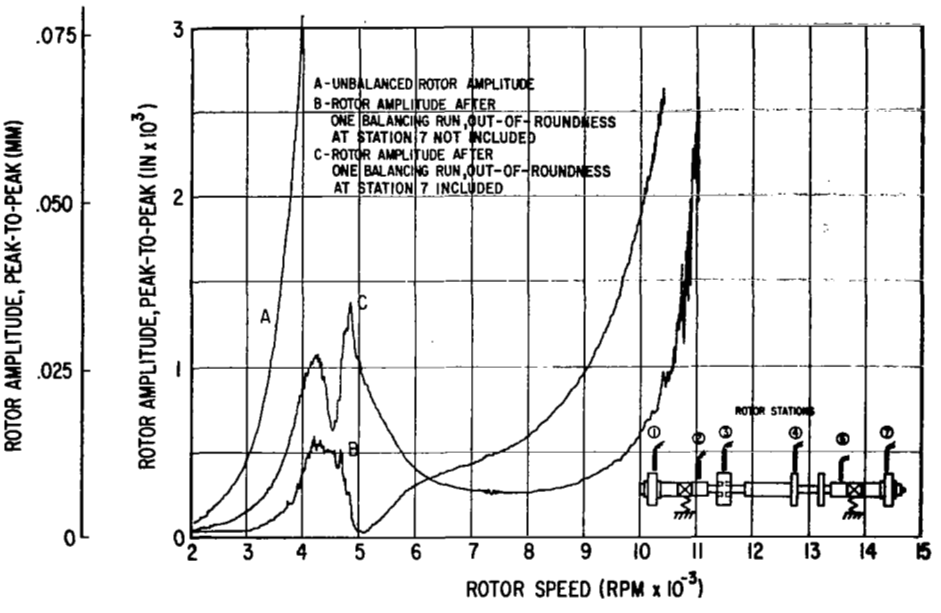

Fig. 94a Vertical Rotor Amplitudes

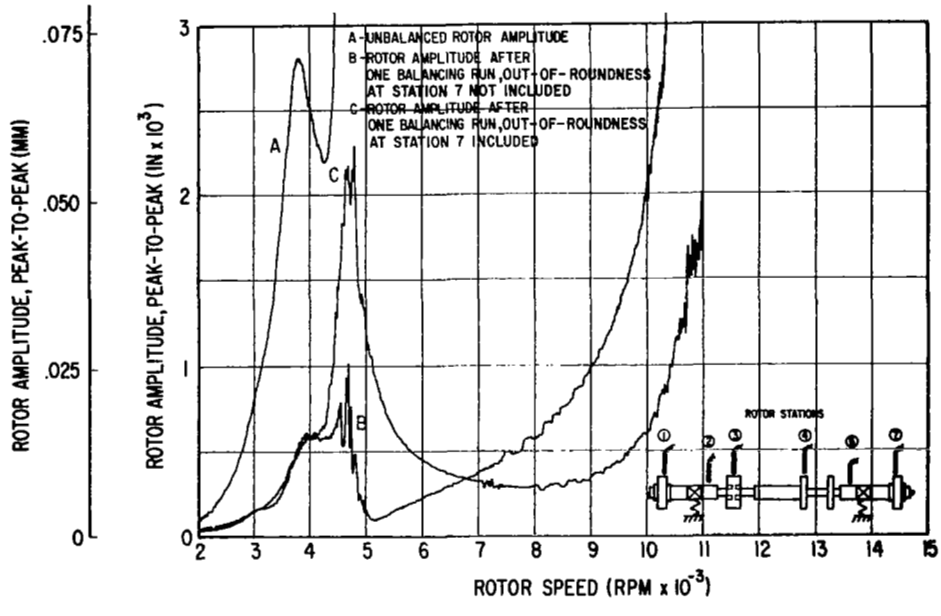

Fig. 94b Horizontal Rotor Amplitudes

Fig. 94 Vertical and Horizontal Rotor Amplitudes at Station 4 — Initial Condition (In-Line, Alternating-Phase Unbalance) and After One Balancing Run by the Least Squares Procedure (Four Vertical Probes With and Without Out-Of-Roundness at Station 7 Considered)

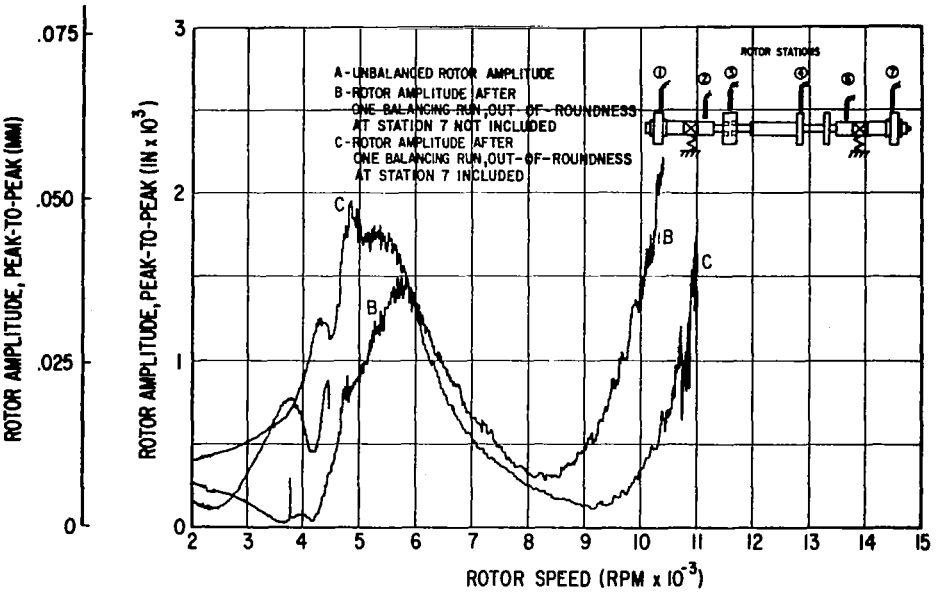

Fig. 95a Vertical Rotor Amplitudes

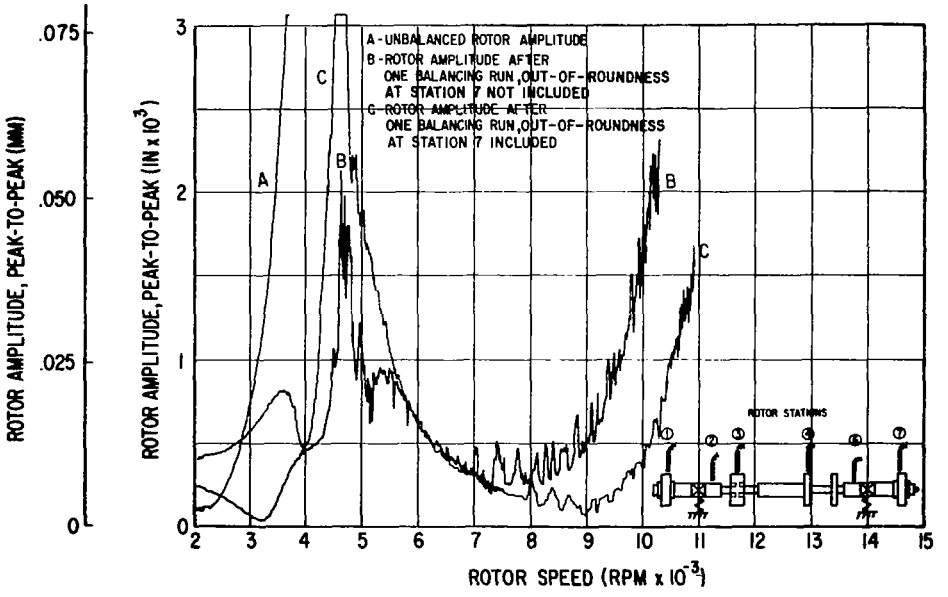

Fig. 95b Horizontal Rotor Ampltidues

Fig. 95 Vertical and Horizontal Rotor Amplitudes at Station 7 — Initial Condition (In-Line, Alternating-Phase Unbalance) and After One Balancing Run by the Least Squares Procedure (Four Vertical Probes With and Without Out-Of-Roundness at Station 7 Considered)

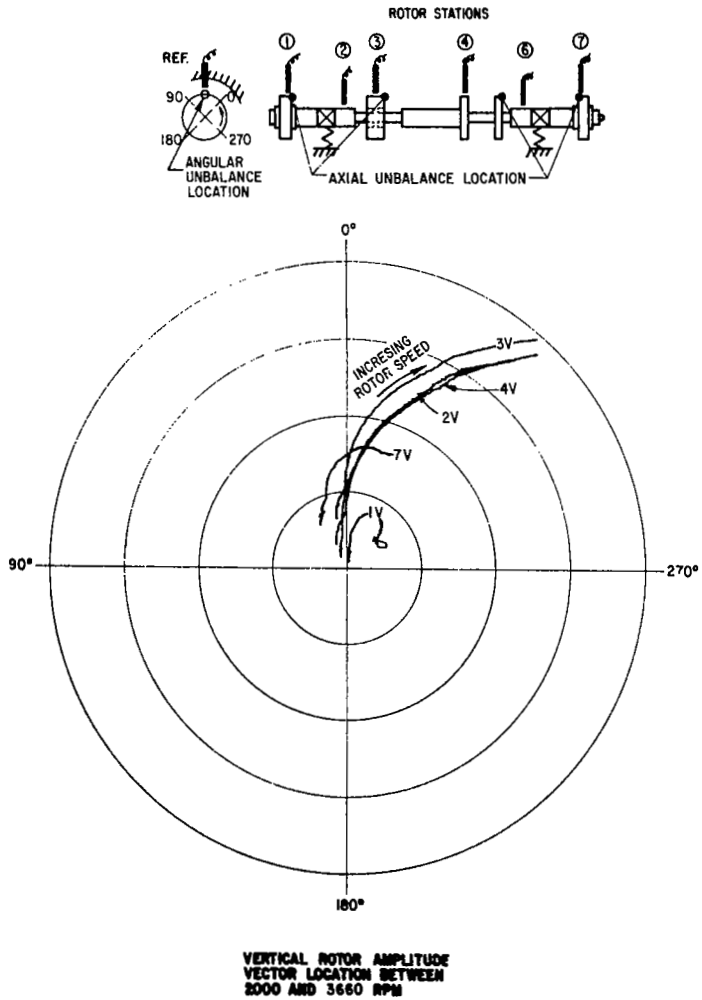

VERTICAL ROTOR AMPLITUDE VECTOR LOCATION BETWEEN 2000 AND 3660 RPM

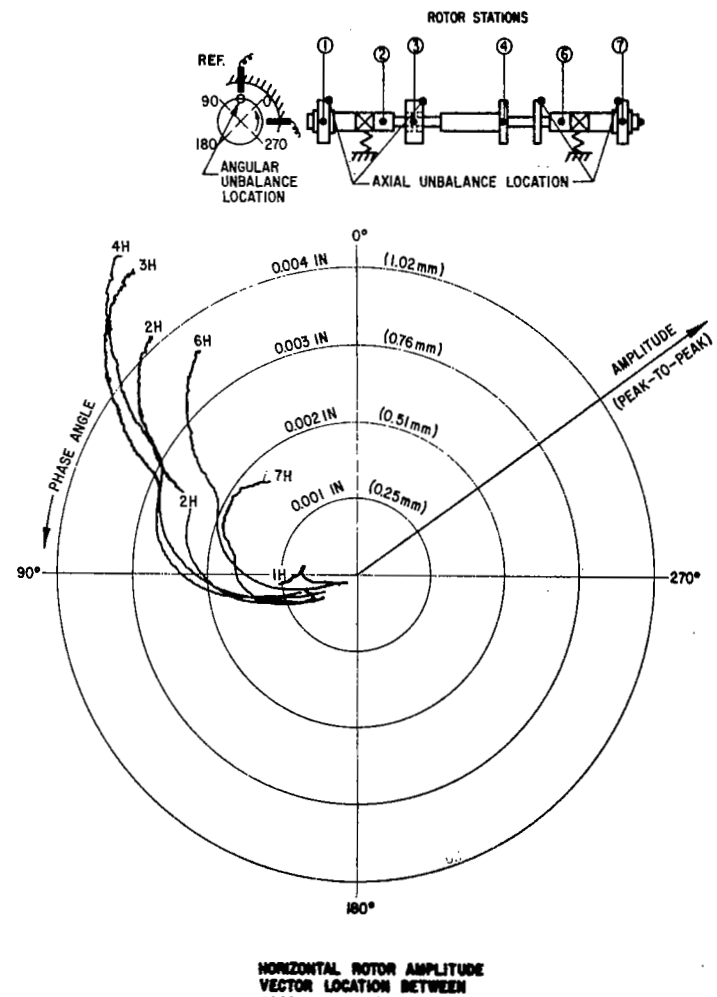

HORIZONTAL ROTOR AMPLITUDE VECTOR LOCATION BETWEEN 2000 AND 3660 RPM

Fig. 96 Vertical and Horizontal Amplitude Vector Locations For Flexibly-Supported Rotor (With In-Line, In-Phase Unbalance) at Subcritical Rotor Speeds

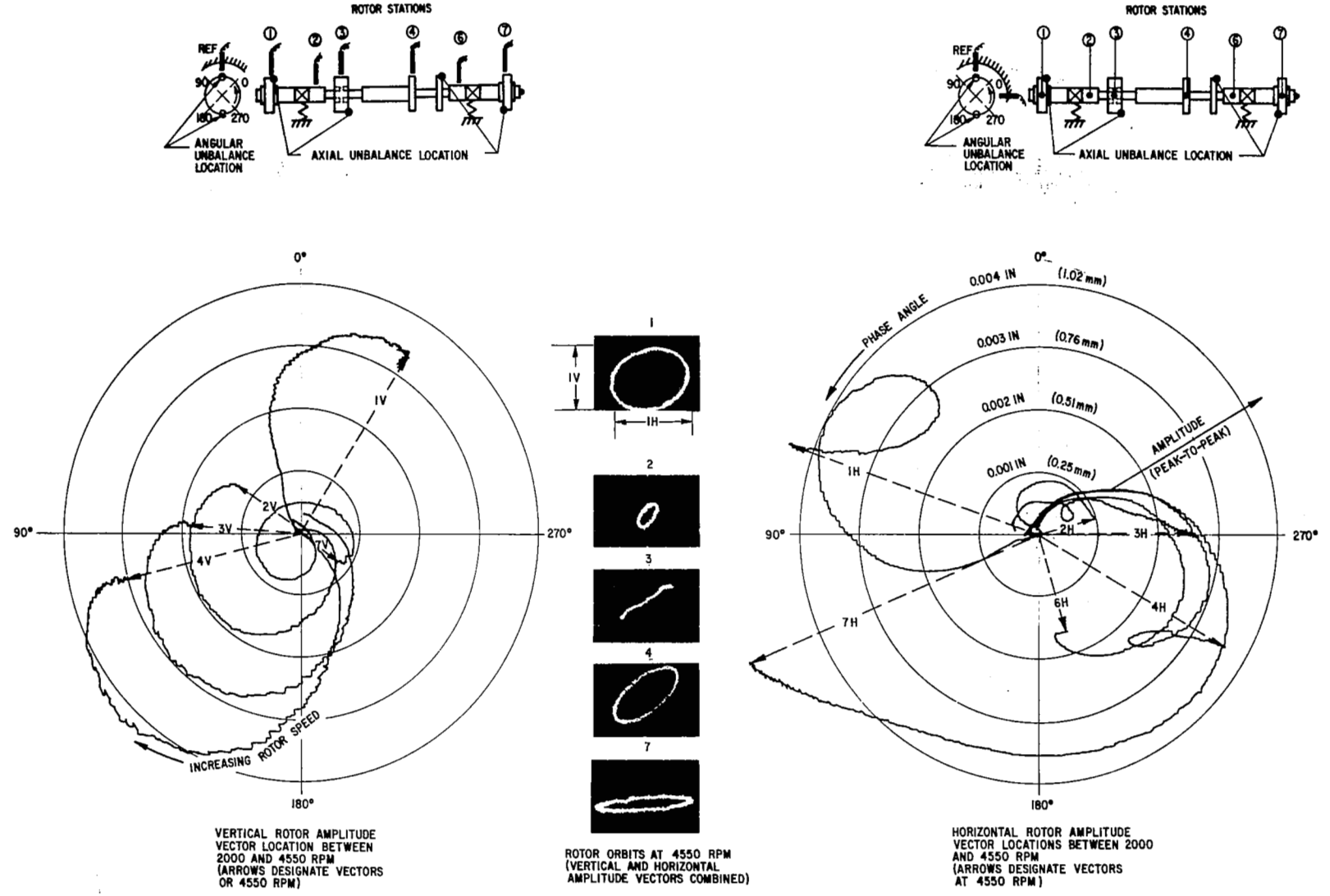

Fig. 97 Vertical and Horizontal Amplitude Vector Locations for Flexibly-Supported Rotor (With In-Line, Alternating-Phase Unbalance) at Subcritical Rotor Speeds

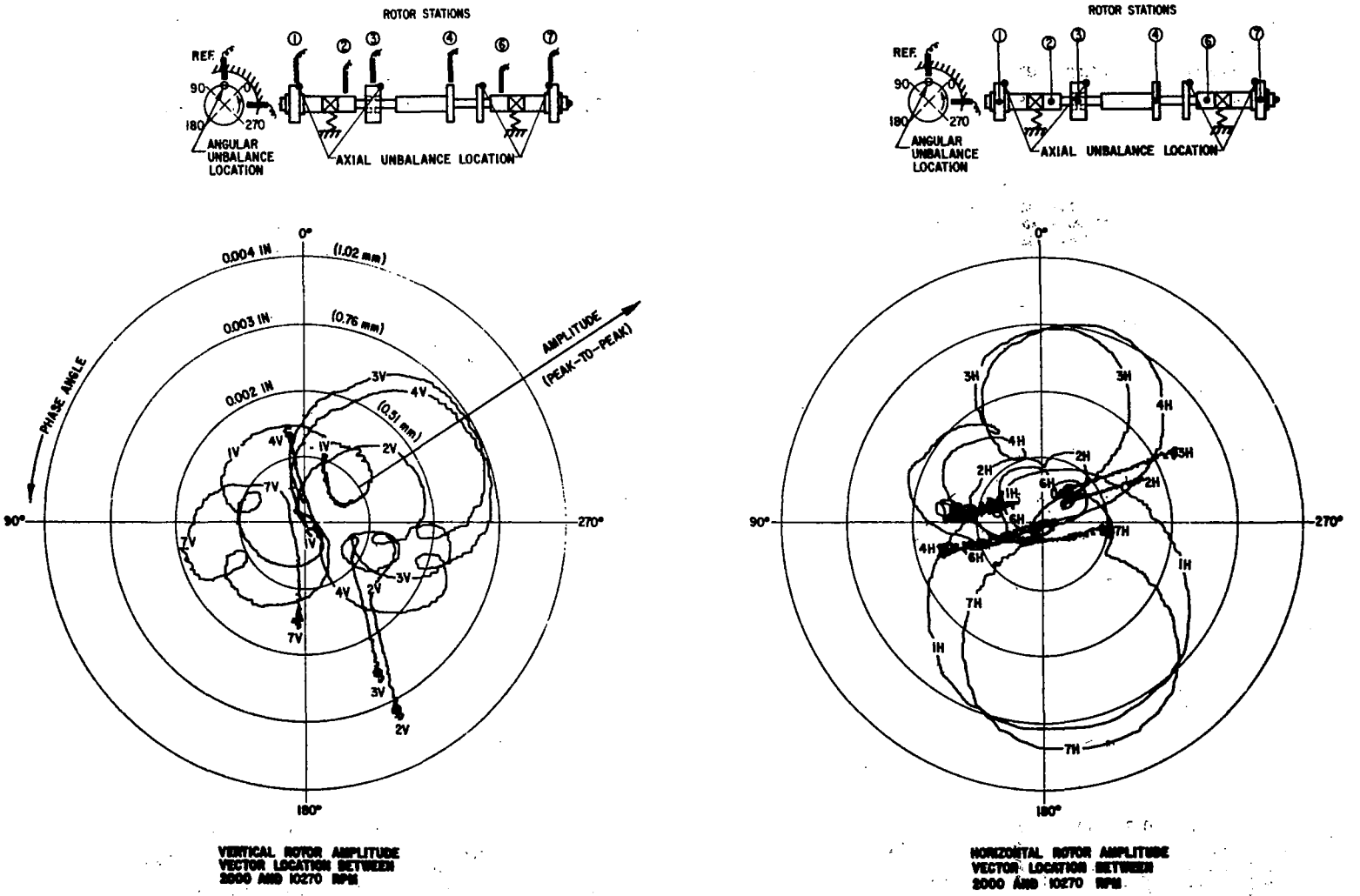

Fig. 98 Vertical and Horizontal Amplitude Vector Locations for Flexibly-Supported Rotor After Balancing For Passage Through One Bending Critical Speed (In-Line, In-Phase Unbalance)

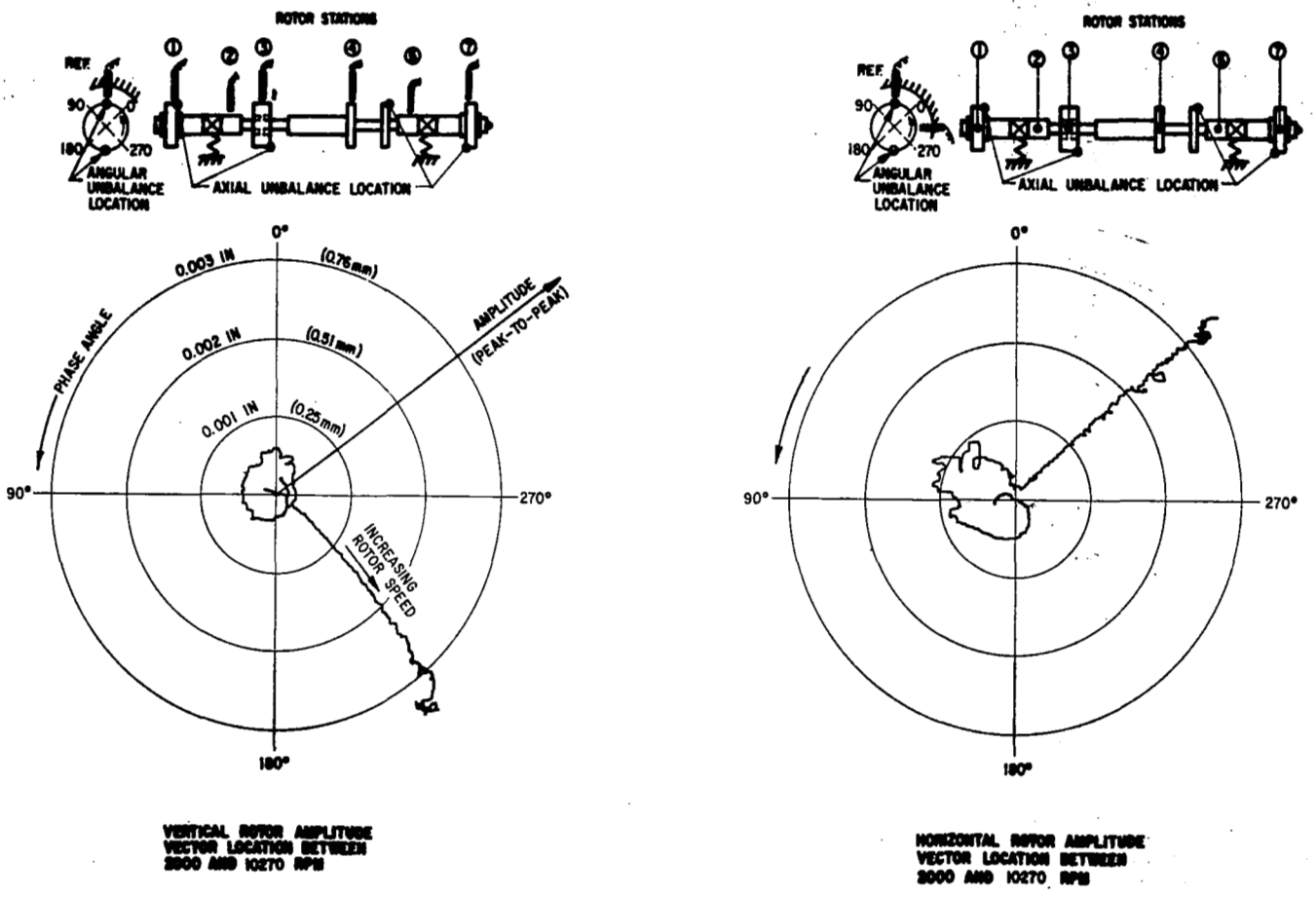

Fig. 99 Vertical and Horizontal Amplitude Vector Locations (At Station 3) For Flexibly-Supported Rotor After Balancing For Passage Through One Bending Critical Speed (In-Line, Alternating-Phase Unbalance)

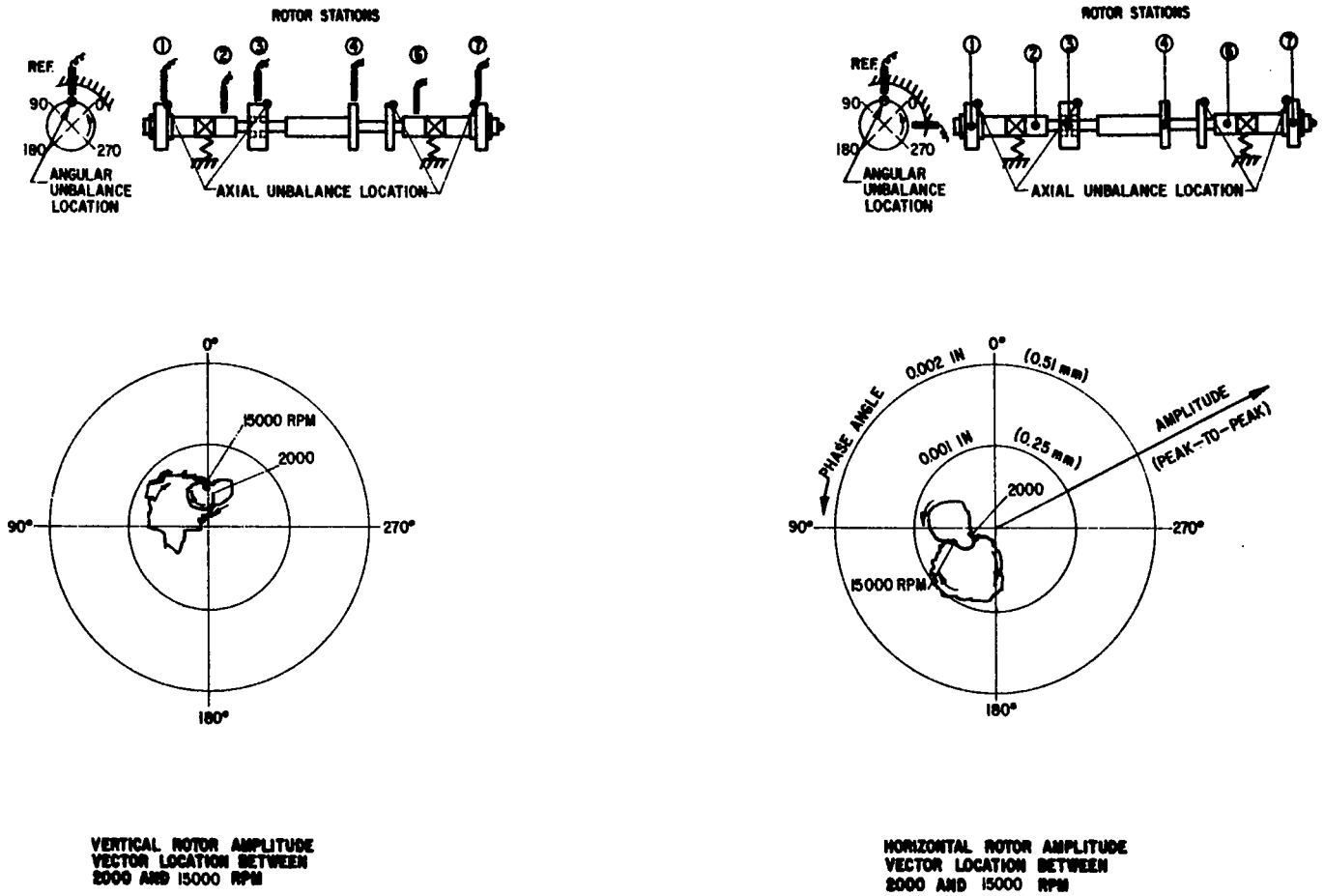

Fig. 100 Vertical and Horizontal Amplitude Vector Locations (At Station 3) For Flexibly-Supported Rotor After Balancing (In-Line, In-Phase Unbalance)

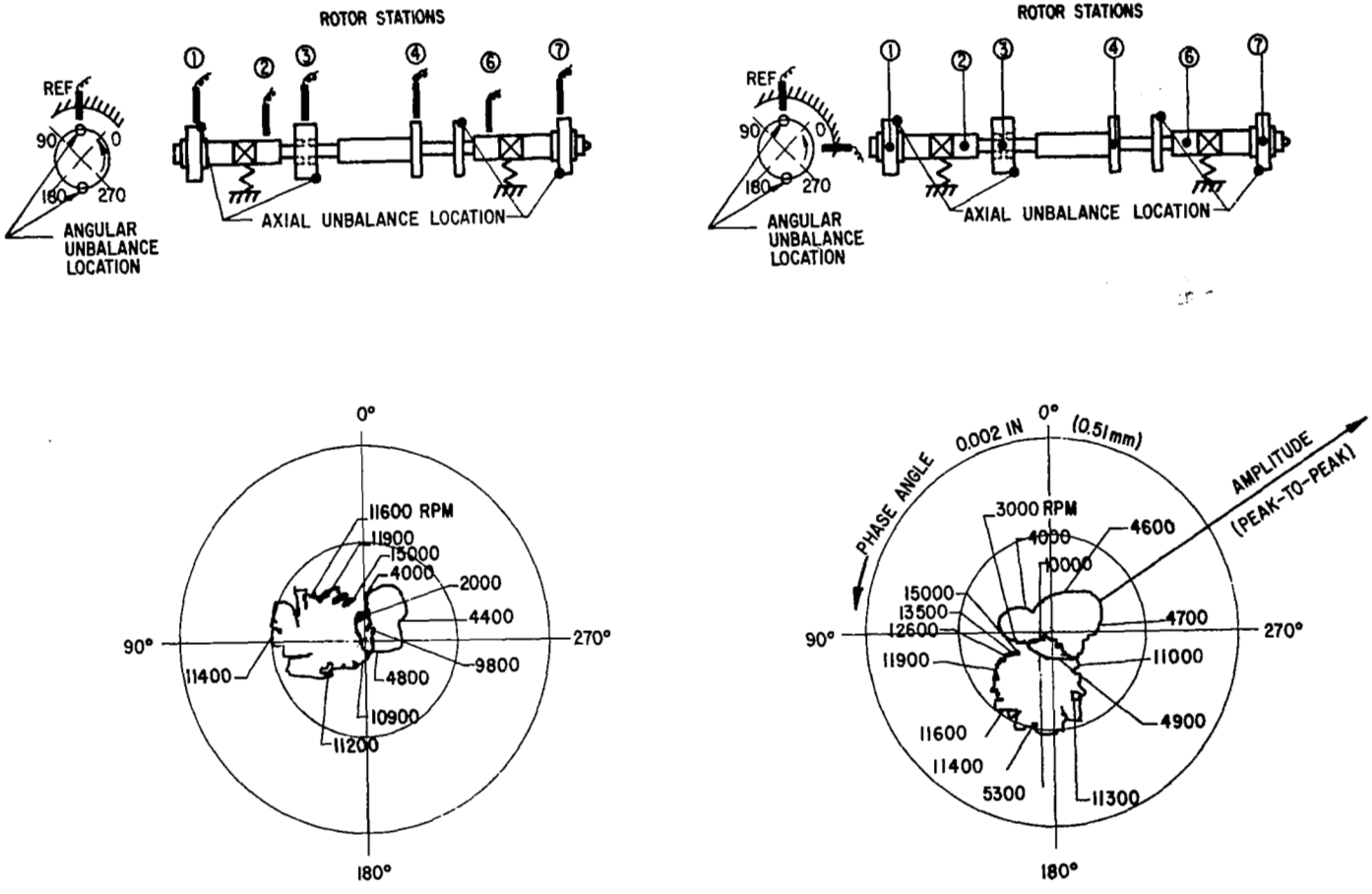

VERTICAL ROTOR AMPLITUDE VECTOR LOCATION BETWEEN 2000 AND 15000 RPM

HORIZONTAL ROTOR AMPLITUDE VECTOR LOCATION BETWEEN 2000 AND 15000 RPM

Fig. 101 Vertical and Horizontal Amplitude Vector Locations (At Station 3) For Flexibly-Supported Rotor After Balancing (In-Line, Alternating-Phase Unbalance)

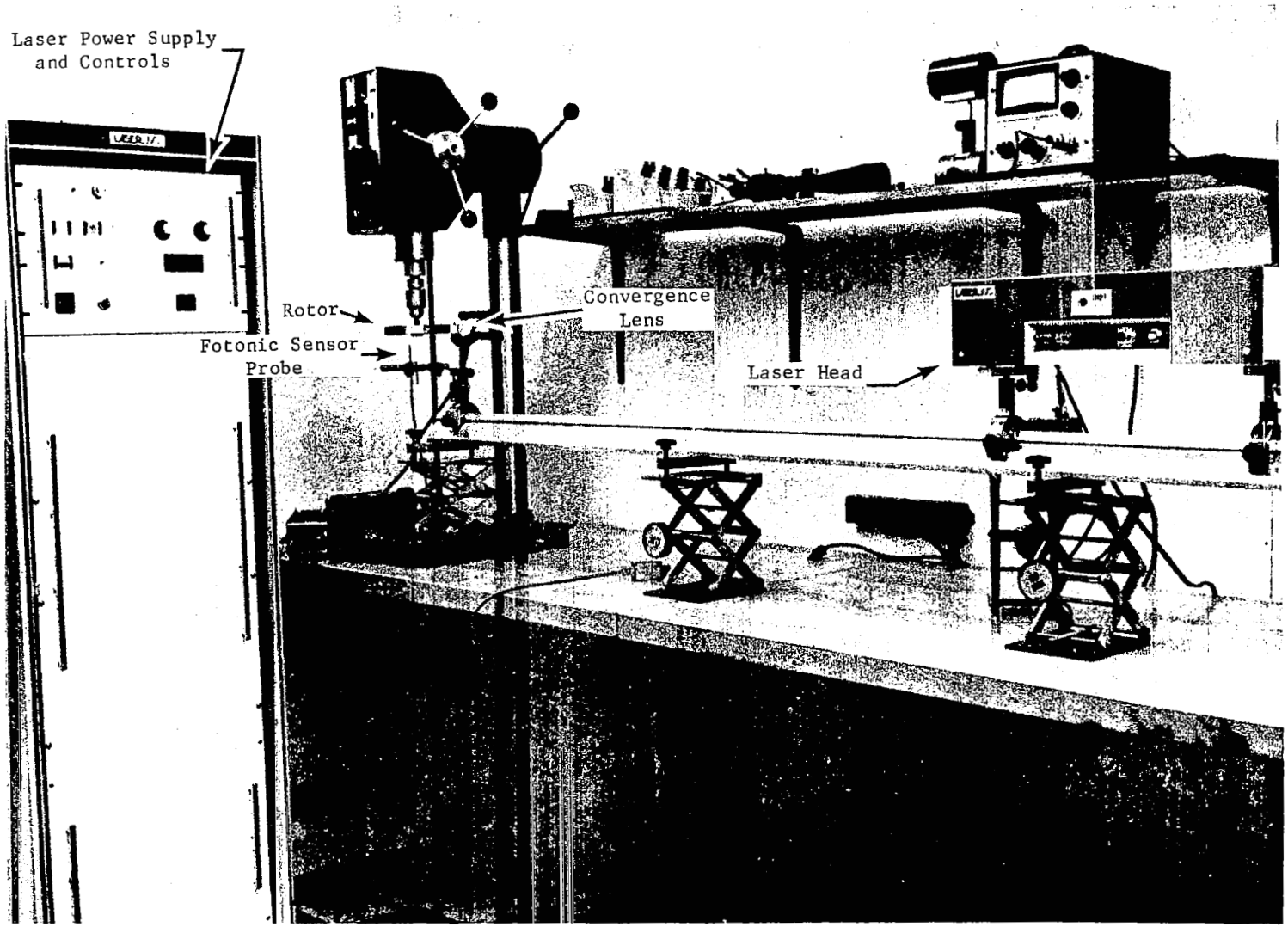

Fig. 102 Laser Setup For Material Removal From Rotating Disc

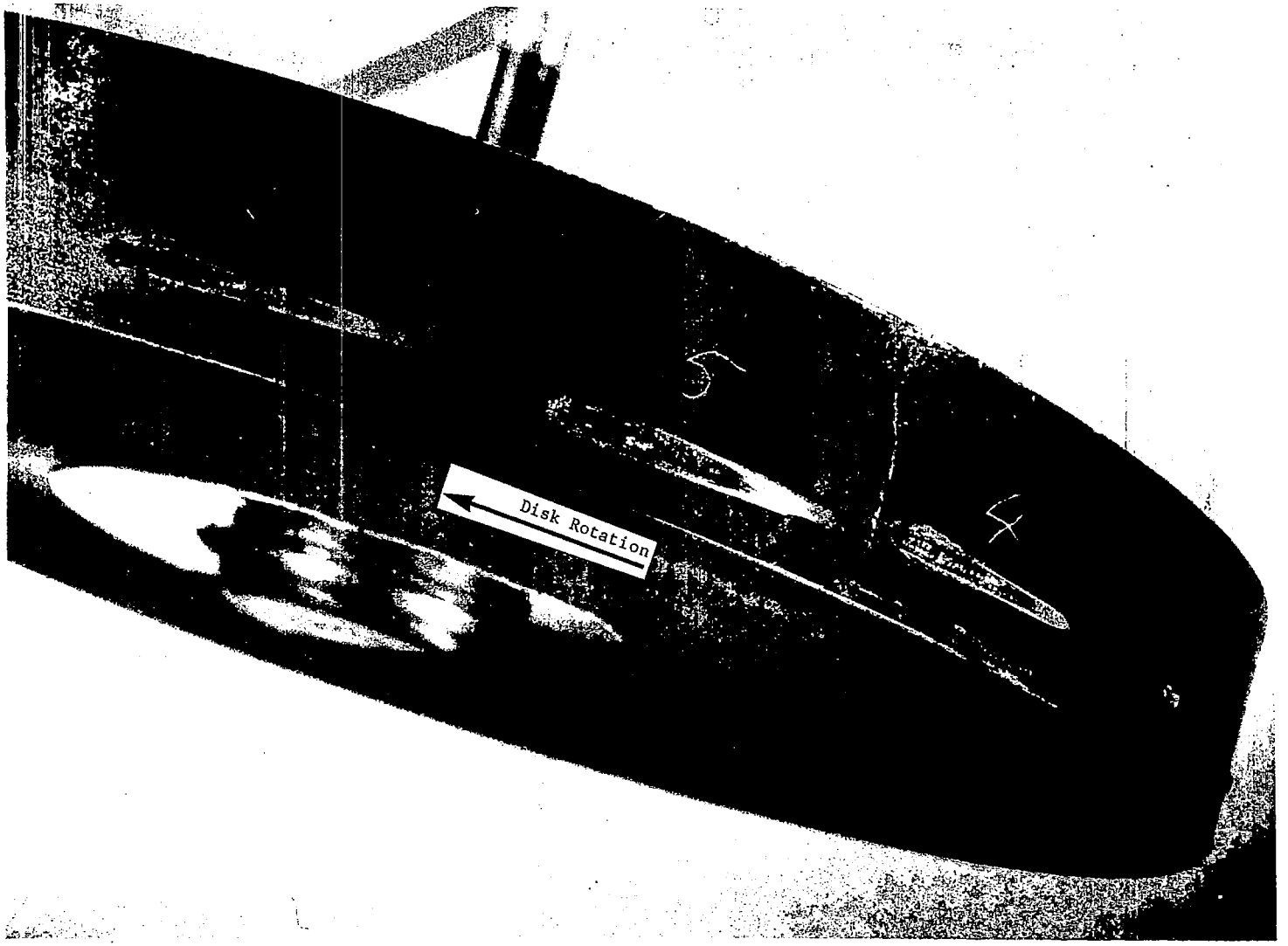

Fig. 103 Steel Disc With Laser-Removed Simulated Balance Corrections

Fig. 104 Uncoated Steel Disc With Laser-Removed Simulated Balance Corrections (Dynamic and Static Irradiation)

Fig. 105 Coated Steel Disc With Laser-Removed Simulated Balance Corrections in Multiple Axial Locations

Fig. 106 Steel Disc With Laser-Removed Simulated Balance Corrections and Fotonic Sensor Target

*U.S. GOVERNMENT PRINTING OFFICE: 1975 - 635-275/9